INVESTIGATION OF EFFECTS OF MICROSTRUCTURAL AND SURFACE PROPERTIES OF ULTRAFILTRATION / NANOFILTRATION CERAMIC MEMBRANES ON THEIR PERFORMANCE

A Thesis Submitted to
The Graduate School of Engineering and Sciences of
İzmir Institute of Technology
in Partial Fulfillment of the Requirements for the Degree of

DOCTOR OF PHILOSOPHY

in Chemical Engineering

by
İlker ERDEM

October 2009
İZMİR

We approve the thesis of **İlker ERDEM**

Prof. Muhsin ÇİFTÇİOĞLU
Supervisor

Assoc. Prof. Fehime ÖZKAN
Committee Member

Prof. Serdar ÖZÇELİK
Committee Member

Assoc. Prof. Yekta GÖKSUNGUR
Committee Member

Prof. Devrim BALKÖSE
Committee Member

23 September 2009

Prof. Devrim BALKÖSE
Head of the Chemical Engineering Department

Assoc.Prof. Talat Yalçın
Dean of the Graduate School of Engineering and Sciences

ACKNOWLEDGMENTS

I would like to express my special thanks to my advisor Prof. Muhsin Çiftçioğlu not only for his guidance and supervision and also for his encouragement and support throughout this study.

I am grateful to the staff in the Material Research Center (MAM) for their devoted performance in characterization experiments.

I would like to thank to my colleagues (in alphabetical order) Dr. Ö. Çağlar Duvarcı, A.E. Çetin, R. Çiftçioğlu, Dr. S. Özcan, E. Şahin, D. Şimşek, Dr. B. Topuz and other members of the Chemical Engineering Department for their priceless contribution during this work.

I want to express my thanks to Prof. Şebnem Harsa, head of the Food Engineering Dept., for her support and for kindly permitting analysis via digital refractometer. I also want to thank to members of the Food Engineering Dept. welcoming me to their lab.

I also would like to thank to the members of the Chemical Engineering Dept. with whom we have worked together for a long period and from whom I learned a lot.

Finally, I am grateful to my parents, my brother, relatives and friends, for their endless support, patience and encouragement. I am indebted to them for their trust and love.

İlker Erdem

ABSTRACT

INVESTIGATION OF EFFECTS OF MICROSTRUCTURAL AND SURFACE PROPERTIES OF ULTRAFILTRATION / NANOFILTRATION CERAMIC MEMBRANES ON THEIR PERFORMANCE

The ceramic membranes with their superior chemical, thermal, mechanical and microbiological properties and long service lives are gaining importance in pressure driven filtration processes. The diverse requirements of different applications enforce preparation of tailor-made ceramic membranes with specific characteristics. This dissertation focused on the preparation and characterization and filtration performance of asymmetric multilayer ceramic membranes. Support is the layer responsible for mechanical stability while top layer is mainly responsible for separation and intermediate layer is balancing the microstructural difference between these two layers. The permeability of alumina support could be increased over 100 L / m^2 h by 15% starch addition. The intermediate layer was prepared by coating fine alumina or zirconia powders and / or colloidal sols with thicknesses between 0.2-70 μ. The top layer was formed from pure or mix of zirconia or titania polymeric sols with average particle sizes in the range of 3 – 50 nm with a thickness smaller than 1μ. The physicochemical properties of these mixed oxides were modified by changing the composition and calcination temperature enabling preparation of top layers with varying Donnan exclusion capacities. The membranes prepared could reject sugar, PEG 1000 and PEG 4000 up to 10, 60 and 19%, respectively, that which can be increased via further optimization of parameters in coating / heat treatment processes.

ÖZET

ULTRAFİLTRASYON / NANOFİLTRASYON SERAMİK MEMBRANLARIN MİKROYAPISAL VE YÜZEYSEL ÖZELLİKLERİNİN PERFORMANSLARI ÜZERİNE ETKİLERİNİN İNCELENMESİ

Seramik membranlar sahip oldukları üstün kimyasal, ısıl, mekanik ve mikrobiyolojik özellikler ve uzun hizmet ömürleri ile basınç itici gücüyle çalışan pek çok sınai süzme işlemlerinde önem kazanmaktadır. Farklı uygulamaların değişen gereksinimleri belirli özelliklere sahip özel membranların hazırlanmasını gerektirmektedir. Bu tez çalışması bakışımsız çok katmanlı bir yapıya sahip seramik membranların hazırlanması ve karakterize edilmesi ve süzme başarımı üzerinedir.

Destek mekanik dayanımdan sorumlu katman, üst tabaka genel anlamda ayrıştırmadan sorumlu katmanken ara tabaka bu iki katman arasında mikroyapısal geçişi (dengeyi) sağlayan katmandır. Alumina desteğin geçirgenliği %15 nişasta ilavesiyle 100 L / m^2 saat' in üzerine çıkartılmıştır. Ara tabaka alumina veya zirkonya ince seramik tozları ya da kolloidal solleri kullanılarak 0.2-70 μ kalınlığında hazırlanmıştır. Üst tabaka saf veya karışım halinde 3 – 50 nm ortalama parçacık boyutuna sahip zirkonya ve titanya polimerik sollerinden 1μ' dan daha düşük bir kalınlıkta hazırlanmıştır. Bu karışık oksitlerin fizikokimyasal özellikleri bileşimlerinin ve ısıl işlem sıcaklıklarının değiştirilmesiyle düzenlenerek farklı Donan ayrım yeteneklerine sahip üst tabakaların hazırlanması mümkün kılınmıştır. Hazırlanan membranlar şeker, PEG 1000 ve PEG 4000'i sırasıyla %10, 60 ve 20 seviyelerinde tutabilmişlerdir ki bu değerler kaplama / ısıl işlem süreçlerindeki değişkenlerin iyileştirilmesiyle arttırılabilir.

TABLE OF CONTENTS

LIST OF FIGURES ix

LIST OF TABLES xxii

CHAPTER 1. INTRODUCTION 1

CHAPTER 2. STRUCTURE AND PREPARATION OF CERAMIC MEMBRANES 10

2.1. Processing of Porous Ceramics 11

2.1.1. Preparation of Supports 11

2.1.2. Preparation of Intermediate and Top Layers 14

CHAPTER 3. IMPORTANT PARAMETERS OF SOL-GEL PROCESSING 17

3.1. Precursors (Raw Materials) 17

3.2. Additives 18

3.3. Coating and Further Processes 20

CHAPTER 4. RECENT RESEARCH ON CERAMIC MEMBRANES AND FILTRATION 21

4.1. Membrane Coupled Bioreactors for Production of Organic Acids 21

4.2. Desalination 24

4.3. Fractionation and Concentration of Extracts 28

4.4. Water Treatment 30

CHAPTER 5. EXPERIMENTAL 31

5.1. Preparation and Characterization of Asymmetric Ceramic Composite Membranes 31

5.1.1. Supports 31

5.1.1.1. Supports with double layers 32

5.1.2. Intermediate Layers 32

5.1.2.1. First Intermediate Layer 33
5.1.2.2. Second Intermediate Layer 34
5.1.3. Top Layers 35
5.2. Filtration Experiments 38
5.2.1. Clean Water Permeability (CWP) 38
5.2.2. Retention Tests 38

CHAPTER 6. RESULTS AND DISCUSSION 41
6.1. Preparation and Characterization of Asymmetric Ceramic Composite Membranes 41
6.1.1. Supports 41
6.1.1.1 Supports prepared via higher solid content suspensions 48
6.1.1.2 Supports with double layers 49
6.1.2. Intermediate Layers 63
6.1.2.1. Preparation and Characterization of First Intermediate Layer 63
6.1.2.1.1. Dip-coating 63
6.1.2.1.2. Wet-coating 64
6.1.2.1.3. Spin-coating 72
6.1.2.2. Second Intermediate Layer 73
6.1.3. Preparation and Characterization of Top Layer 79
6.1.3.1. Sol Preparation 79
6.1.3.2. Thermal characterization 83
6.1.3.3. Crystallinity 87
6.1.3.4. Surface charge (zeta potential) 91
6.1.3.5. Addition of some elements 103
6.1.3.6. Coating 105
6.1.3.6.1 Aging of Sol and Simultaneous Coating 113
6.1.3.7. Modification of heat treatment regime 118
6.2. Filtration Experiments 124
6.2.1. Clean Water Permeability (CWP) 124
6.2.2. Retention Tests 124
6.2.2.1. Neutral Organic Solutions (Sugar, PEG) 125

6.2.2.1.1. The effect of modification of sols by ethylene glycol (EG) addition 132

CHAPTER 7. CONCLUSIONS AND RECOMMENDATIONS 144

REFERENCES 147

LIST OF FIGURES

Figure **Page**

Figure 1. The streams before and after the membrane 1
Figure 2. Filtration spectrum for pressure driven membrane processes 4
Figure 3. Surface charge values of anatase (TiO_2) suspensions with varying NaCl molarity and pH values 7
Figure 4. Electrophoretic mobility values as a function of pH for magnesia doped zirconia (13mol 8
Figure 5. Rejection of anions in a NaCl/Na_2SO_4 mixture by magnesia doped zirconia membrane as a function of pH 9
Figure 6. Zeta potential of alumina solutions as a function of pH and KNO_3 or $LiNO_3$ concentration 9
Figure 7. Electron microscopy images of a supported microporous zirconia layer formed by nanocrystallites of less than 10 nm 11
Figure 8. The microstructures of alumina supports prepared by using starch from different sources 13
Figure 9. The possible simultaneous reactions in sol preparation 14
Figure 10. The two alternative routes in sol-gel procedure 16
Figure 11. Schematic representation of core-shell stabilization method 20
Figure 12. The molecular structures of sucrose and lactose 22
Figure 13. Bioreactor coupled with a membrane unit 22
Figure 14. The productivity for batch reactor and bioreactor with continuous product removal by using a membrane 23
Figure 15. Cross-flow filtration of a lactic acid fermentation broth on a 0.1 mm Kerasep membrane 24
Figure 16. NaCl retention for k-NF-new (TiO_2 top layer) as a function of pH 26
Figure 17. Zetapotential of k-NF-new (TiO_2 top layer) for NaCl, KCl, Na_2SO_4 (10^{-3} M) 27
Figure 18. Na_2SO_4 (10^{-2} M) retention for k-NF-new (TiO_2 top layer) at different pH values 27
Figure 19. General scheme of grape proanthocyanidins 29
Figure 20. A dimer of proanthocyanidin ; procyanidin B_1 29

Figure 21. The diagram of filtration set-up 39
Figure 22. The Brix vs. concentration calibration curve for PEG 1000 and 4000 40
Figure 23. The photographs of two different starches taken at the same magnification by using optic microscope 42
Figure 24. The SEM micrographs of potato (a) and wheat starches (b) 43
Figure 25. The change in porosity with respect to additive amount and heat treatment temperature 44
Figure 26. The change in open (interconnected) porosity with respect to additive amount and heat treatment temperature 44
Figure 27. The clean water permeability (CWP) values vs. trans-membrane pressure (TMP) for supports prepared with different amounts of pore-forming additives (starch mixture) and heat treated at 1300°C 45
Figure 28. The SEM image of cross-section of alumina support prepared by using 10 % wheat starch as pore-forming agent 46
Figure 29. The SEM image of cross-section of alumina support showing the pores formed by air bubbles left in the ceramic slip during casting and / or decomposition of starch 46
Figure 30. The SEM image of cross-section of alumina support showing the microstructure and gaps left by decomposition of starch 47
Figure 31. The SEM image of cross-section of alumina support showing the microstructure and interconnected pores between partially sintered particulates 47
Figure 32. The SEM image of surface of alumina support prepared via 53 vol. % Alcoa alumina suspension (ht 1300° C /2h) 48
Figure 33. The SEM image of surface of alumina support prepared via 53 vol. % Alcoa alumina suspension (ht 1300° C /2h) 49
Figure 34. The SEM micrograph showing the surface of starch- free alumina layer after heat treating at 1300° C / 2h 50
Figure 35. The SEM micrograph showing the surface of starch- free alumina layer after heat treating at 1300° C / 2h 51
Figure 36. The SEM micrograph showing the surface of with-starch alumina layer after heat treating at 1300° C / 2h with whiskery formations 51
Figure 37. The SEM micrograph showing the surface of with-starch alumina layer after heat treating at 1300° C / 2h with whiskery formations 52

Figure 38. The SEM micrograph showing the surface of with-starch alumina layer after heat treating at 1300° C / 2h with glassy formations..... 52
Figure 39. The SEM micrograph showing the surface of with-starch alumina layer after heat treating at 1300° C / 2h with glassy formations..... 53
Figure 40. The SEM micrograph showing the surface and cross-section of with-starch alumina layer after heat treating at 1300° C / 2h with whiskery formation on surface 53
Figure 41. The SEM micrograph showing the cross-section of with-starch alumina layer after heat treating at 1300° C / 2h 54
Figure 42. The SEM micrograph showing the cross-section of with-starch and starch-free alumina layer after heat treating at 1300° C / 2h 54
Figure 43. The surface of the AKP-50 alumina support (starch-free layer) facing the die after heat treatment at 1100° C / 2h 55
Figure 44. The SEM micrograph showing the cross-section of the double layer AKP-50 alumina support (1100° C / 2h) with more porous layer (10% corn starch) and denser and thinner layer (starch-free)..... 56
Figure 45. The SEM micrograph showing the cross-section of more porous part of the double layer AKP-50 alumina support (1100° C / 2h) formed via 10% corn starch 56
Figure 46. The SEM micrograph showing the surface of more porous part of the double layer AKP-50 alumina support (1100° C / 2h) formed via 10% corn starch 57
Figure 47. The SEM micrograph showing the surface of denser part of the double layer AKP-50 alumina support (1100° C / 2h) formed via double casting of starch-free suspension 58
Figure 48. The SEM micrograph showing the surface of denser part of the double layer AKP-50 alumina support (1100° C / 2h) formed via double casting of starch-free suspension 59
Figure 49. The SEM micrograph showing the cross-section of denser part of the double layer AKP-50 alumina support (1100° C / 2h) formed via double casting of starch-free suspension and casting 10% corn starch suspension for once..... 59
Figure 50. The SEM micrograph showing the surface of more porous part of the double layer AKP-50 alumina support (1100° C / 2h) formed via

casting 10% corn starch suspension for once 60
Figure 51. The SEM micrograph showing the surface of the denser layer of the AKP-50 support (1100° C / 2h) (S (+)) cast after 10% corn starch containing porous layer..... 60
Figure 52. The SEM micrograph showing the cross-section of the double layer AKP-50 support (1100° C / 2h) (S (+)) cast via starch-free (2 mL) and 10% corn starch containing suspensions 61
Figure 53. The SEM micrograph showing the surface of the more porous layer of the double layer AKP-50 support (1100° C / 2h) (S (+)) cast via 10% corn starch containing suspension (facing die)..... 61
Figure 54. The SEM micrograph showing the surface of the denser layer of the AKP-50 support (1100° C / 2h) (S (-)) cast after 10% corn starch containing porous layer..... 62
Figure 55. The SEM micrograph showing the surface of the more porous layer of the AKP-50 support (1100° C / 2h) (S (-)) cast via 10% corn starch containing suspension facing die 62
Figure 56. The SEM micrograph of dip-coated support (11% starch, 1300°C / 2 hours) surface with a suspension of finer alumina particles (10 vol. %) and heat treated at 1100°C / 2 hours..... 65
Figure 57. The SEM micrograph of dip-coated support (11% starch, 1300°C / 2 hours) surface with a suspension of finer alumina particles (10 vol. %) and heat treated at 1100°C / 2 hours..... 66
Figure 58. The SEM micrograph of the intersection of first intermediate layer formed by dip-coating 1.5 vol. % zirconia suspension (heat treated at 1100° C)..... 66
Figure 59. The SEM micrograph of the intersection of first intermediate layer formed by dip-coating 1.5 vol. % zirconia suspension (heat treated at 1100° C)..... 67
Figure 60. The SEM micrograph of first intermediate layer formed by dip-coating the support by using 1.5 vol. % zirconia suspension heat treated at 1100° C..... 67
Figure 61. The SEM micrograph of first intermediate layer formed by dip-coating the support by using 1.5 vol. % zirconia suspension heat treated at 1150° C..... 68

Figure 62. The SEM micrograph showing the pinhole on a support (10 % wheat starch, 1350° C / 2 h) wet-coated twice: 1st; 2.5 mL 1.5 vol.% AKP-50 suspension (3%PVA), 950° C / 2 h, 2nd; 1 mL 1 vol.% AKP-50 suspension (3%PVA), 950° C / 2 h 68
Figure 63. The SEM micrograph showing the microstructure of AKP-50 heat treated at 950° C / 2 h which was cast via wet-coating of 1 vol.% AKP-50 (3%PVA) 69
Figure 64. The SEM micrograph showing a crack on the AKP-50 layer formed via wet-coating 1 vol.% AKP-50 (3%PVA), 950° C / 2 h 70
Figure 65. The SEM micrograph showing depth of the crack in Figure 64 on the AKP-50 layer formed via wet-coating 1 vol.% AKP-50 (3%PVA), 950° C / 2 h 70
Figure 66. The SEM micrograph showing the thickness of the layer wet-coated (w-c) on a support (10% wheat starch, Alcoa alumina, 1300° C / 2h) via 1st w-c: 2mL 1.5 vol% AKP-50 (3%PVA), 950° C / 2h, 2nd w-c: 1mL 1 vol% AKP-50 (3%PVA), 950° C / 2h 71
Figure 67. The SEM micrograph showing the thickness of the layer wet-coated as described for Figure 66 on a different part of the support 71
Figure 68. The SEM micrograph of surface of Alcoa support (10% wheat starch, 1300° C / 2h), wet-coated (wc) via 2 mL AKP-50 (3%PVA) suspension, heat treated (ht) 900° C / 2h, [spin coat (sc) (Regime 5) 2 mL AKP-50 (3%PVA) suspension] x 2, heat treated (ht) 900° C / 90 min, sc via 1 vol% AKP-50 (3% PVA), Regime 6 Mod-2, ht 900° C / 90 min, sc via 1 vol % AKP-50 (3%PVA) suspension and Regime 6 mod-2, ht 900° C / 120 min. 72
Figure 69. The volumetric particle size distribution of alumina sol (A08) determined via Zetasizer 74
Figure 70. The average particle size of colloidal zirconia sol with respect to increasing initial water:alkoxide molar ratio 75
Figure 71. The volumetric particle size distribution of two colloidal sols; alumina (A08): continuous line, zirconia: dashed line 76
Figure 72. Alcoa alumina support (10% wheat starch, 1300° C / 2 hours), double wet coated (1.5 and 1 vol.% AKP-50 alumina, (3% PVA), 950° C / 2 hours), dip-coated via Zr colloidal sol (15 sec., 450° C / 2 hours) 77

Figure 73. Alcoa alumina support (10% wheat starch, 1300° C / 2 hours), double wet coated (1.5 and 1 vol.% AKP-50 alumina, (3% PVA), 950° C / 2 hours), dip-coated via Zr colloidal sol (15 sec., 450° C / 2 hours) 77
Figure 74. Alcoa alumina support (10% wheat starch, 1300° C / 2 hours), double wet coated (1.5 and 1 vol.% AKP-50 alumina, (3% PVA), 950° C / 2 hours), dip-coated via Zr colloidal sol (15 sec., 450° C / 2 hours) 78
Figure 75. Alcoa alumina support (10% wheat starch, 1300° C / 2 hours), double wet coated (1.5 and 1 vol.% AKP-50 alumina, (3% PVA), 950° C / 2 hours), dip-coated via Zr colloidal sol (15 sec., 450° C / 2 hours) 78
Figure 76. The average particle size values for mixed sols determined by using laser light scattering 80
Figure 77. The volumetric particle size distribution of polymeric Full Ti sol..... 81
Figure 78. The volumetric particle size distribution of polymeric TiZr 7525 sol 81
Figure 79. The volumetric particle size distribution of polymeric TiZr 5050 sol 82
Figure 80. The volumetric particle size distribution of polymeric TiZr 2575 sol 82
Figure 81. The volumetric particle size distribution of polymeric Full Zr sol 83
Figure 82. The TGA results for Ti / Zr sol system 84
Figure 83. The TGA result for Full Ti 84
Figure 84. The TGA result for Ti.Zr 7525 85
Figure 85. The TGA result for Ti.Zr 5050 85
Figure 86. The TGA result for Ti.Zr 2575 86
Figure 87. The TGA result for Full Zr 86
Figure 88. The XRD result for Full Ti 88
Figure 89. The XRD result for Ti.Zr 7525 89
Figure 90. The XRD result for Ti.Zr 5050 89
Figure 91. The XRD result for Ti.Zr 2575 90
Figure 92. The XRD result for Full Zr 90
Figure 93. The crystallite sizes of Full Ti and Full Zr calculated via Expert Plus with varying calcination temperature 91
Figure 94. The zeta potential (mV) values of dried / ground / calcined Ti / Zr

sols with different Ti ratios (%) and varying calcination temperature 92
Figure 95. The zeta potential measurement (n=10) results for dried / ground / calcined Ti / Zr sols in 10^{-3} M KCl solution with initial pH 3.5 93
Figure 96. The zeta potential measurement (n=10) results for dried / ground / calcined Ti / Zr sols in 10^{-3} M KCl solution with initial pH 7.2 94
Figure 97. The zeta potential measurement (n=20) results for dried / ground / calcined Ti / Zr sols in 10^{-3} M KCl solution with initial pH 9.8 96
Figure 98. The zeta potential of zirconia dispersed in 10^{-3}M KCl solution with initial pH value of 7.4 and the final pH values of the solution 97
Figure 99. The XRD analysis for zirconia powders calcined at three different temperatures 98
Figure 100. The crystallite sizes of pure Zr calcined at different temperatures calculated via XRD instrument software 98
Figure 101. The volumetric particle size distribution of Zr sol 99
Figure 102. The SEM micrographs of the zirconia sol uncalcined (a) and calcined at 400° (b), 450° (c) and 500° C (d) 99
Figure 103. The zeta potential values of Zr sol dried, ground and calcined at varying temperatures for 150 minutes, measured in 10^{-3} M KCl solution with varying initial pH values 101
Figure 104. The zeta potential values of Zr sol dried, ground and calcined at varying temperatures for 150 minutes, measured in 10^{-3} M KCl solution with varying initial pH values 101
Figure 105. The zeta potential of titania calcined at varyng temperatures dispersed in 10^{-3}M KCl solution with initial pH value of 7.4 102
Figure 106. The XRD analysis for titania powders calcined at different temperatures 102
Figure 107. The crystallite sizes of titania (prepared via TiAcac 1-2) calcined at varying temperatures 103
Figure 108. The zeta potential values for pure anatase and rutile titania measured in 10^{-3} M KCl solution with varying initial pH values 104
Figure 109. The average particle sizes of the Full Zr polymeric sol (alkoxide : alcohol molar ratio of 1 : 15) with iron and boron addition of 0.1 or 0.2 mole per mole of alkoxide 104
Figure 110. The zeta potentials of the dried-calcined Full Zr polymeric sol

(alkoxide : alcohol molar ratio of 1 : 15) with iron or boron addition of 0.2 mole per mole of alkoxide 105
Figure 111. The zeta potentials of the dried-calcined (500° C / 2 hours) Full Zr polymeric sol (alkoxide : alcohol molar ratio of 1 : 15) with iron or boron addition of 0.2 mole per mole of alkoxide at varying pH values ... 106
Figure 112. SEM micrograph of the die facing starch-free surface of AKP-50 double layer alumina support (10% corn starch, 1100° C / 2 h), dip-coated via 1:4 diluted polymeric Zr sol (NOR) (400° C / 2 h) 107
Figure 113. SEM micrograph of the air facing starch-free surface of AKP-50 double layer alumina support (10% corn starch, D(-), 1100° C / 2 h), dip-coated via 1st 1:4 diluted polymeric Zr sol (NOR), 2nd and 3rd undiluted polymeric Zr sol (NOR) (400° C / 2 h, after each dip-coating) 107
Figure 114. SEM micrograph of the air facing starch-free surface of AKP-50 double layer alumina support (10% corn starch, D(-), 1100° C / 2 h), dip-coated via 1st 1:4 diluted polymeric Zr sol (NOR), 2nd and 3rd undiluted polymeric Zr sol (NOR) (400° C / 2 h, after each dip-coating) 108
Figure 115. SEM micrograph of the air facing starch-free surface of AKP-50 double layer alumina support (10% corn starch, D(-), 1100° C / 2 h), dip-coated via 1st 1:4 diluted polymeric Zr sol (NOR), 2nd and 3rd undiluted polymeric Zr sol (NOR) (400° C / 2 h, after each dip-coating) 108
Figure 116. SEM micrograph of the air facing starch-free surface of AKP-50 double layer alumina support (10% corn starch, D(+), 1100° C / 2 h), dip-coated via polymeric Zr sol containing 0.2 mole Fe per mole of Zr (400° C / 2 h, after each dip-coating) 109
Figure 117. SEM micrograph of the air facing starch-free surface of AKP-50 double layer alumina support (10% corn starch, D(+), 1100° C / 2 h), dip-coated via polymeric Zr sol containing 0.1 mole Fe per mole of Zr (400° C / 2 h, after each dip-coating) 109
Figure 118. SEM micrograph of the air facing starch-free surface of AKP-50 double layer alumina support (10% corn starch, D(-), 1100° C / 2 h), dip-coated (10+1 sec.) via dispersion of AKP-50 alumina in in polymeric Zr sol (~0.5 vol. %) (400° C / 2 h) 110
Figure 119. SEM micrograph of the air facing starch-free surface of AKP-50 double layer alumina support (10% corn starch, D(-), 1100° C / 2 h),

dip-coated (10+1 sec.) via dispersion of AKP-50 alumina in polymeric Zr sol (~0.5 vol. %) (400° C / 2 h) 111
Figure 120. SEM micrograph of the air facing starch-free surface of AKP-50 double layer alumina support (10% corn starch, D(-), 1100° C / 2 h), dip-coated (10+1 sec.) via dispersion of AKP-50 alumina in polymeric Zr sol (~0.5 vol. %) (400° C / 2 h) 111
Figure 121. SEM micrograph of the air facing starch-free surface of AKP-50 double layer alumina support (10% corn starch, D(-), 1100° C/2h), dip-coated several times (10 sec.) via dispersion of AKP-50 alumina in polymeric Zr sol (~0.5 vol. %) (400° C / 2 h) 112
Figure 122. SEM micrograph of the air facing starch-free surface of AKP-50 double layer alumina support (10% corn starch, D(-), 1100° C / 2 h), dip-coated (several times for 10 sec.) via dispersion of AKP-50 alumina in polymeric Zr sol (~0.5 vol. %) (400° C / 2 h) 112
Figure 123. SEM-EDX micrograph of the air facing starch-free surface of AKP-50 double layer alumina support (10% corn starch, D(-), 1100° C/2h), dip-coated several times (10 sec.) via dispersion of AKP-50 alumina in polymeric Zr sol (~0.5 vol. %) (400° C / 2 h..... 113
Figure 124. The change in average particle size (PS) of the 1 wt. % Zr sol (with 25 vol. % EG) at room temperature (RT) 114
Figure 125. The change in average particle size (PS) of the 0.5 wt. % Full Zr sol (with 25 vol. % EG) at room temperature (RT) 115
Figure 126. The change in average particle size (PS) of the 0.5 wt. % TiZr 2575 sol (with 25 vol. % EG) at room temperature (RT) 116
Figure 127. The change in average particle size (PS) of the 0.5 wt. % TiZr 5050 sol (with 25 vol. % EG) at room temperature (RT) 117
Figure 128. The change in average particle size (PS) of the 0.5 wt. % TiZr 7525 sol (with 25 vol. % EG) at room temperature (RT) 117
Figure 129. The change in average particle size (PS) of the 0.5 wt. % Full Ti sol (with 25 vol. % EG) at room temperature (RT) 118
Figure 130. SEM micrograph of surface of multilayer membrane composed of: i) Alcoa alumina support (43 vol. % suspension, 1300° C / 2h), ii) AKP-50 alumina intermediate layer (1, 4, 2 vol. % suspensions, 10 sec. d-c, 1000° C / 30 min. after each coating), iii) Zr Sol NOR,

20 sec. d-c, 400° C / 2h (3° C / min. heating and cooling rate 119
Figure 131. SEM micrograph of coating on the surface of multilayer membrane composed of: i) Alcoa alumina support (43 vol. % suspension, 1300° C / 2h), ii) AKP-50 alumina intermediate layer (1, 4, 2 vol. % suspensions, 10 sec. d-c, 1000° C / 30 min. after each coating), iii) Zr Sol NOR, 20 sec. d-c, 400° C / 2h (3° C / min. heating and cooling rate)..... 120
Figure 132. SEM micrograph of surface of multilayer membrane composed of: i)AKP-50 support, ii) γ-alumina intermediate layer, iii) Zr Sol NOR, 1:8 diluted, 5 sec. d-c, 400° C / 2h (3° C / min. heating and cooling rate)..... 120
Figure 133. SEM micrograph of surface of multilayer membrane composed of: i) AKP-50 support, ii) γ-alumina intermediate layer, iii) Zr Sol NOR, 1:8 diluted, 5 sec. d-c, 400° C / 2h (3° C / min. heating and cooling rate)..... 121
Figure 134. SEM micrograph of surface of multilayer membrane composed of: i) Alcoa alumina support (43 vol. % suspension, 1300° C / 2h), ii) AKP-50 alumina intermediate layer (4, vol. % suspensions, 10 sec. d-c (twice), 1000° C / 30 min. and 1100° C / 2h), iii) Zr Sol NOR, 20 sec. d-c, 400° C / 2h (3° C / min. heating and cooling rate), cleaned via brushing, iv) 0.25 wt. % Zr + EG Sol, 10 sec. and 5 sec. d-c, 400° C / 2h (0.5° C / min. heating and cooling rate) (after each coating) 121
Figure 135. SEM micrograph of defect on multilayer membrane composed of: i) Alcoa alumina support (43 vol. % suspension, 1300° C / 2h), ii) AKP-50 alumina intermediate layer (4, vol. % suspensions, 10 sec. d-c (twice), 1000° C / 30 min. and 1100° C / 2h), iii) Zr Sol NOR, 20 sec. d-c, 400° C / 2h (3° C / min. heating and cooling rate),cleaned via brushing, iv) 0.25 wt. % Zr + EG Sol, 10 sec. and 5 sec. d-c, 400° C / 2h (0.5° C / min. heating and cooling rate) (after each coating) 122
Figure 136. SEM micrograph of surface of multilayer membrane composed of: i) Alcoa alumina support (50 vol. % suspension, 1300° C / 2h), ii) TZ-3Y zirconia intermediate layer (1 vol. % (+ EG) suspensions, 20 and 5 sec. d-c (twice), 1050° C / 1h (after each coating)), iii) Zr Sol 1-20-1 (+ EG), 20 sec. d-c, 400° C / 2h (3° C / min.

heating and cooling rate), cleaned via brushing,
iv) 1 and 0.1 wt. % Zr (1-20-1) + EG Sol, 10 sec. and 20 sec. d-c
(respectively), 400° C / 2h (0.5° C / min. heating and cooling rate)
(after each coating) 123
Figure 137. The CWP (L / m^2 hour) values for varying trans-membrane pressures
for the membrane consisting of i) a support prepared from alumina
with 10% starch addition and partially sintering at 1300°C for 2 hours,
ii) an intermediate layer formed by dip-coating alumina sol and
calcination at 600°C for 3 hours, iii) a top layer of formed
by dip-coating Full Zr and calcination at 400°C for 3 hours 125
Figure 138. The permeate flux (L / m^2 hour) values for membranes with varying
top layer consisting of i) a support prepared from alumina with 10% starch
addition and partially sintering at 1300°C for 2 hours, ii) an intermediate
layer formed by dip-coating alumina sol and calcination at 600°C
for 3 hours, iii) a top layer of formed by dip-coating Full Zr *or*
TiZr 5050 *or* Full Ti, and calcination at 400°C for 3 hours..... 126
Figure 139. The sugar retention (%) values for membranes with varying
top layer consisting of i) a support prepared from alumina with 10% starch
addition and partially sintering at 1300°C for 2 hours, ii) an intermediate
layer formed by dip-coating alumina sol and calcination at 600°C
for 3 hours, iii) a top layer of formed by dip-coating Full Zr *or*
TiZr 5050 *or* Full Ti, and calcination at 400°C for 3 hours..... 127
Figure 140. The SEM micrograph of intermediate layer formed by dip-coating
alumina sol and calcining at 600°C on the support (11% starch, 1300°C /
2 hours) showing the presence of pinholes..... 128
Figure 141. The SEM micrograph of one of the pinholes in Figure 140 129
Figure 142. The permeate flux (L / m^2 h) and sugar retention (%) values for the
membrane composed of i) a support prepared from alumina with
15% starch addition and partially sintering at 1300°C for
2 hours, ii) an intermediate layer formed by dip-coating alumina
sol and calcination at 600°C for 3 hours, iii) a top layer of formed
by multiple dip-coating by using TiZr 5050 and calcination
at 600°C for 2 hours 129
Figure 143. The permeate flux (L / m^2 h) and sugar retention (%) values for the

membrane composed of i) a support prepared from alumina with 10% starch (mix.) addition and partially sintering at 1300°C for 2 hours, ii) an intermediate layer formed by dip-coating alumina sol and calcination at 600°C for 3 hours, iii) a top layer of formed by dip & pour-coating by using TiZr 5050 and calcination at 600°C for 2 hours 130
Figure 144. The SEM micrograph of cross-section of a membrane consisting of: i)a support prepared from alumina with 7% starch addition and partially sintering at 1300°C for 2 hours, ii) an intermediate layer formed by dip-coating alumina sol and calcination at 600°C for 3 hours, iii) a top layer of formed by dip-coating TiZr 2575 and calcinations at 500°C for 3 hours..... 131
Figure 145. The SEM micrograph of cross-section of a membrane consisting of i)a support prepared from alumina with 11% starch addition and partially sintering at 1300°C for 2 hours, ii) an intermediate layer formed by dip-coating 10 vol. % AKP-50 and heat treatment at 1100°C for 2 hours, iii) an intermediate layer formed by dip-coating 1 % alumina sol and heat treatment at 600°C for 3 hours iv)a top layer of formed by dip-coating TiZr 5050 and calcination at 400°C for 3 hours 132
Figure 146. The viscosity values for propanol–ethylene glycol binary system at 25° C plotted from data excerpted from Pal & Sharma (1998) 133
Figure 147. The SEM micrograph of the surface of an Alcoa support prepared via a 53 vol.% suspension ht at 1300° C / 2h and dip-coated (10 sec.) via 0.5 wt.% Full Zr + EG (25 vol. %) sol with ave. PS of 1.9 nm (and ht at 400° C / 1h with 0.5° C / min heating / cooling rates) 134
Figure 148. The SEM micrograph of the surface of an Alcoa support prepared via a 53 vol.% suspension ht at 1300° C / 2h and dip-coated (10 sec.) via 0.5 wt.% Full Zr + EG (25 vol. %) sol with ave. PS of 6.7 nm (and ht at 400° C / 1h with 0.5° C / min heating / cooling rates) 135
Figure 149. The SEM micrograph of the surface of an Alcoa support prepared via a 53 vol.% suspension ht at 1300° C / 2h and dip-coated (10 sec.) via 1 wt.% TiZr 2575 + EG (25 vol. %) sol with ave. PS of 20 nm (and ht at 400° C / 1h with 0.5° C / min heating / cooling rates) 135
Figure 150. The SEM micrograph of the surface of an Alcoa support prepared via a 53 vol.% suspension ht at 1300° C / 2h and dip-coated (5 sec.) via

1 wt.% Full Zr + EG (25 vol. %) sol with ave. PS of 31.5 nm (and ht at 400° C / 1h with 0.5° C / min heating / cooling rates) 136
Figure 151. The SEM micrograph of the surface of an Alcoa support prepared via a 53 vol.% suspension ht at 1300° C / 2h and dip-coated (5 sec.) via 1 wt.% Full Zr + EG (25 vol. %) sol with ave. PS of 31.5 nm (and ht at 400° C / 1h with 0.5° C / min heating / cooling rates) 136
Figure 152. The permeate flux and sugar retention values for membranes prepared via sols with varying ave. PS (+ 25 vol. % EG) 138
Figure 153. The permeate flux and sugar retention values for membranes prepared via sols with 25 vol. % EG on supports with intermediate layers 140
Figure 154. The permeate flux and PEG 4000 retention values for membranes prepared via sols with 25 vol. % EG 143

LIST OF TABLES

Table **Page**

Table 1. A selection of applications for ceramic membranes 2

Table 2. Membrane processes according to driving forces and phases in contact 3

Table 3. Advantages and disadvantages for ceramic membranes 6

Table 4. Molecular weights of proanthocyanidin monomer (catechin) and its oligomers 29

Table 5. The parameters used in spin-coating procedure 34

Table 6. The molar ratios of elements in the sols 36

Table 7. The molar ratios of elements in the sols 80

Table 8. The average particle size values for mixed sols determined by using laser light scattering 80

Table 9. The zeta potential measurement (n=6) results (zeta: mV, width: standard deviation) of dried / ground / calcined Ti / Zr sols in 10^{-3} M KCl solutions with initial pH value of 8.4 92

Table 10. The zeta potential measurement (n=10) results for dried / ground / (un)calcined Ti / Zr sols in 10^{-3} M KCl solution with initial pH 3.5 93

Table 11. The zeta potential measurement (n=10) results for dried / ground / (un)calcined Ti / Zr sols in 10^{-3} M KCl solution with initial pH 7.2 94

Table 12. The zeta potential measurement (n=20) results for dried / ground / (un)calcined Ti / Zr sols in 10^{-3} M KCl solution with initial pH 9.8 95

Table 13. The membranes prepared via sols with EG addition (25 vol. %) with varying ave. PS 137

Table 14. The membranes prepared via sols with EG addition (25 vol. %) coating on supports with intermediate layers 139

Table 15. The membranes prepared via sols with EG addition (25 vol. %) with varying ave. PS 142

CHAPTER 1

INTRODUCTION

Membrane is a selective barrier enabling separation of materials in the feed stream into two new streams with different compositions as shown in Figure 1. This simple method have found many application areas along with the progress in the preparation techniques of the appropriate membranes mainly in food, beverage, pharmaceutical, biotechnology and chemical industries. Some of these applications of the ceramic membranes are tabulated in Table 1.

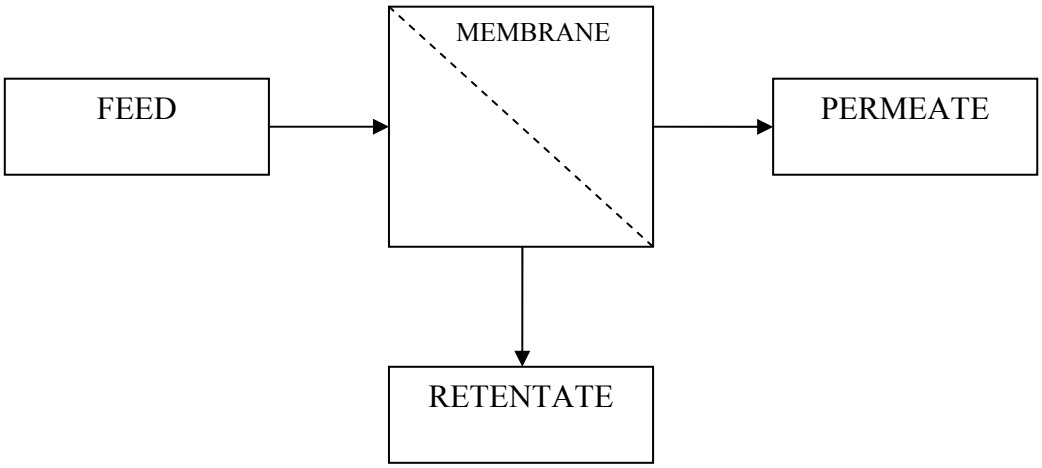

Figure 1. The streams before and after the membrane.

The membrane processes can be classified into subgroups with respect to the driving forces of the separation and the phases in contact as shown in Table 2. The pressure driven membrane processes are the most widely used applications with the advantage of increasing process efficiency to some extent simply by increasing the applied mechanical energy. The various application areas of pressure driven membrane processes are shown in Figure 2.

Table 1. A selection of applications for ceramic membranes (Source: Finley 2005).

Food & Beverage	Pharmaceutical & Biotechnology	Chemical & Industrial	Recovery & Recycling
Animal blood	Antibiotics, vaccines, additives	Catalyst recovery	Aqueous cleaner recycle system
Bacteria removal from milk or wastewater	Apyrogenic water & process water	Chemical baths	Cleaning of gas condensate
Brine regeneration	Biotechnological products from fermentation broths	Cleansing of photochemical developers	Cleaning of radioactive waste
Butter milk concentration	Blood plasma	Cleansing of pickling baths	Decreasing bath regeneration
Casein to seric protein separation	Cell separation after heavy-duty bio processes	Concentration of brick engobes	Dye penetrating effluent
Clarification & sterilization of fruit juices	Continuous fermentation	Depolluting paper pulp effluent	Effluent concentration
Clarification of soft drinks (juices, wines, beers)	Enzyme concentration	Filtration of cooling lubricants	Electro-deposition bath
Clarification of sugar syrup, vinegar	Extraction / clarification of amino acids	Filtration of drilling emulsions	Extraction of metallic particles
Eggs	Extraction / clarification of enzymes	Filtration of dye stuff	Industrial laundries
Filtration of bottom beer	Extraction / clarification of fermentation liquids	Ink wastewater treatment	Landfill leachate
Filtration of lactoferrin	Extraction / clarification of antibiotics	Mixed gas filtration in fertilizer industry	Oil/water emulsion separation
Glucose syrup clarification	Protein filtration	Paper: removing coating solutions	Phosphatation bath from water
Micro-filtration (MF) of milk	Pyrogen-free antibiotics	Purification & recovery of raw materials	Pretreatment of cleaners
Milk concentration		Recovery & recycling of solvents	Recovery of precious metals
Milk standardization		Recovery of black liquor (paper making)	Removal of brines
Mushroom juice clarification		Recycling of cleaning baths	Removal of contaminated glycol
Pretreatment for reverse osmosis (RO)		Recovery of dye & pigments (textile & leather)	Removal of water from PVC emulsions
Production & treatment of dairy products		Recycling of paints & lacquers	Swimming pool water
Protein extraction		Recovery of contaminated organic solvents	Treatment of nuclear effluent
Protein recovery from white water		Regeneration of baths	Treatment of paint effluent
Reduction of fat content in whey		Sizing recovery for textile industry	Washing machine tanks
Soy		Treatment of acids	Water recycling
Treatment of white water			
Water recovery & recycling			
Whey concentration			
Wine wastewater			

Table 2. Membrane processes according to driving forces and phases in contact (Source: Tsuru 2001).

Membrane Process	*Phase*		Driving Force	Pore Size	Note
	Feed	Permeate			
Micro-filtration	L	L	ΔP	0.1-10 μm	Removal of particles
Ultra-filtration	L	L	ΔP	2-100 nm	Separation of macromolecules
Nano-filtration	L	L	ΔP	1-2 nm	Separation of low MW solutes (MWCO 200-1000); electrolyte separation by surface charge
Reverse Osmosis (RO)	L	L	ΔP	< 1 nm	Reject electrolytes; solution-diffusion mechanism (polymeric membranes
Gas separation	G	G	ΔP	< 0.5-1 nm	
Vapour permeation	G	G	ΔP	0.5-2 nm	
Pervaporation	L	G	ΔP		
Electrodialysis	L	L	ΔΦ		
Dialysis	L	L	ΔC		
Membrane distillation	L	L	ΔT		

L: liquid phase, G: gas phase. ΔP: (partial) pressure difference, ΔΦ: electrical potential difference, ΔC: concentration difference, ΔT: temperature difference.

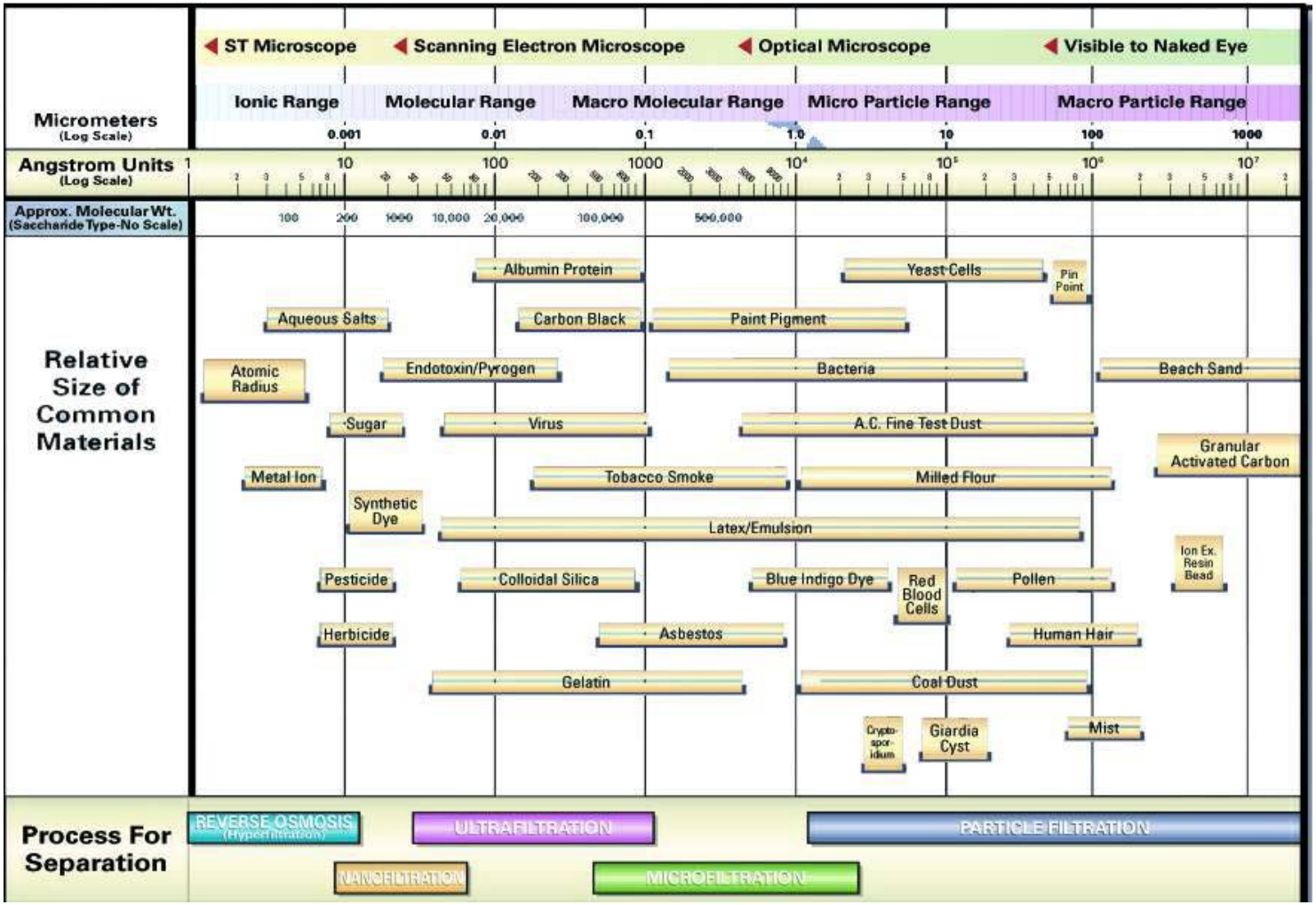

Figure 2. Filtration spectrum for pressure driven membrane processes
(Source: Osmonics 2009)

Ceramic membranes possess superior properties like high chemical, thermal, mechanical, microbiological stabilities, high separation efficiencies and long service life. They can be used in a wide pH range and can be sterilized either chemically or thermally. Organic materials can be filtered without any membrane deformation. They are resistant to microbiological attacks and degradation. Their shape and pore sizes are stable under high filtration pressures. Advantages of ceramic membranes are kept during lifetime for years in the absence of any mechanical failure. Their long service life overcomes high initial installation costs. The advantages and disadvantages of the ceramic membranes are summarized in Table 3. The ceramic membranes had about 12% of the market share according to the reported values in 1996 (Tsuru 2001), and their market share will probably increase with the introduction of new tailor-made ceramic micro-filtration (MF), ultra-filtration (UF), and nano-filtration (NF) membranes.

The main mechanisms effective in separation with ceramic membranes can be classified as size exclusion (steric hindrance) and Donnan exclusion (electrostatic hindrance). Materials which are larger than the pore size of the membrane are rejected by the membrane which is called size exclusion. The materials which have the same charge with the membrane surface are also rejected by the membrane with respect to the magnitudes of its charge. The magnitudes of the charges of both the membrane and the material to be separated are important in this mechanism.

Ceramic membranes are metal oxides like alumina (Al_2O_3), silica (SiO_2), titania (TiO_2) and zirconia (ZrO_2) which have amphoteric characteristics. They gain a surface charge when immersed in liquid medium with respect to the pH of the liquid medium. They generally have positive surface charge in low pH solutions and negative surface charge at high pH. The intersection point where the surface charge is zero is defined as the isoelectric point (iep). The isoelectric point varies for different oxide materials.

Table 3. Advantages and disadvantages of ceramic membranes
(Source: Tsuru 2001).

Advantages/Disadvantages	*Applications and Comments*
Thermal stability	Separation at high temperature, steam sterilization
Resistance to organic solvents	Separation of non aqueous systems, separation of oil
Resistance to chemicals, acidic and alkali pH	Chemical cleaning, recovery of acid/base
Resistance to peroxide	Chemical cleaning, application of textile processing
Mechanical strength	Back-washing
Long life time	
Uniform pore size	Dependent upon preparation method
Difficult sealing and module construction	
Cost	Expensive source materials, complex processing

The surface charges of amphoteric ceramic membranes change not only with respect to the type of metal oxide and pH of the liquid medium but also with respect to the type and concentration of ionic species in the liquid medium. Some ionic species with opposite charges are adsorbed on the metal-oxide layer specifically and depress the charge of the oxide layer. The surface charges of the ceramic membranes widely change with respect to the ion type and concentration in the liquid in contact with the membrane. Gustafsson, et al. (2000) investigated the effect of NaCl and pH on surface charge of anatase (TiO_2). They reported that the isoelectric point (iep) of anatase changed from ~5.8 to ~6.8 when the NaCl concentration was increased from 0 to 0.5 M and they found that the surface charge values were slightly positive in 1 M NaCl at all pH levels as shown in Figure 3. This indicates a specific cation adsorption which will affect the retention behaviour of the membrane made of this material.

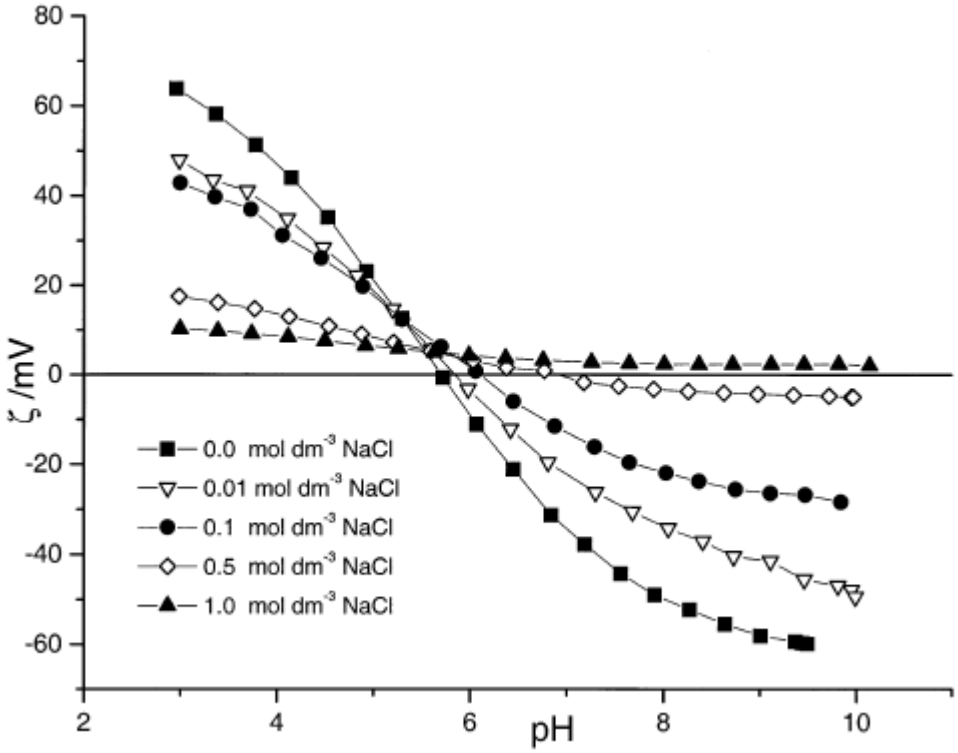

Figure 3. Surface charge values of anatase (TiO_2) suspensions with varying NaCl molarity and pH values (Source: Gustafsson, et al. 2000).

Vacassy, et al. (1998) reported specific adsorption of SO_4^{2-} on 13mol% MgO doped ZrO_2 ceramic membrane which suppressed the positive charge of the zirconia membrane at acidic pH range. They prepared and characterized zirconia NF membranes by measuring their zeta potential (i.e. electrophoretic mobility) values of zirconia powder in NaCl and Na_2SO_4 salt solutions (Figure 4). They performed filtration experiments with these solutions in order to monitor the effect of surface charge on salt retention (Figure 5). The ionic species (SO_4^{2-}) with negative charge was rejected at a larger extent by the membrane at high pH values. The rejection of monovalent species (Cl^-) was lower than divalent species (SO_4^{2-}) at all pH values showing the importance of charge on salt retention.

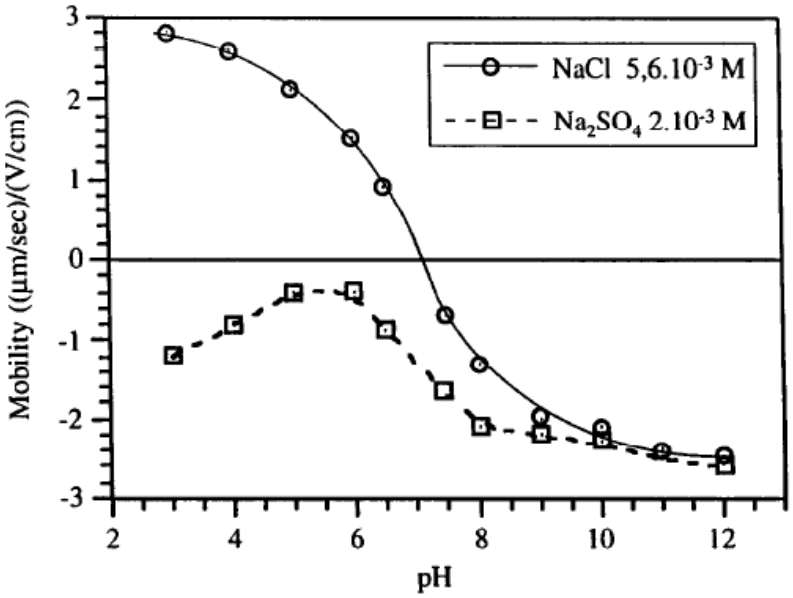

Figure 4. Electrophoretic mobility values as a function of pH for magnesia doped zirconia (13 mol %) (Source: Vacassy, et al. 1998).

Cations also can be adsorbed specifically and unspecifically on metal oxides. Experiments performed by using alumina and KNO_3 or $LiNO_3$ solutions showed that Li^+ was specifically adsorbed and change the isoelectric point of alumina while K^+ was not as shown in Figure 6. The effect of salt concentration on the surface charge is also shown in the figure. The magnitudes of zeta potential decreased as the salt concentration increased. This variation should also be considered to predict the extent of Donnan exclusion.

Both size exclusion and Donnan exclusion mechanisms are effective on pressure driven filtration applications. Their share in retention mechanism varies according to the application. The size exclusion is the dominant mechanism in the filtration of relatively larger materials (like in MF). The Donnan exclusion gains importance as the size of the material to be separated decreases (like in UF and NF).

The different requirements of different applications enforce preparation of tailor-made ceramic membranes with certain characteristics. The research reported in this dissertation focuses on the preparation and characterization of ceramic membranes with asymmetric multilayer structures by using different materials and possible improvement of surface characteristics of ceramic membranes during preparation / surface modification.

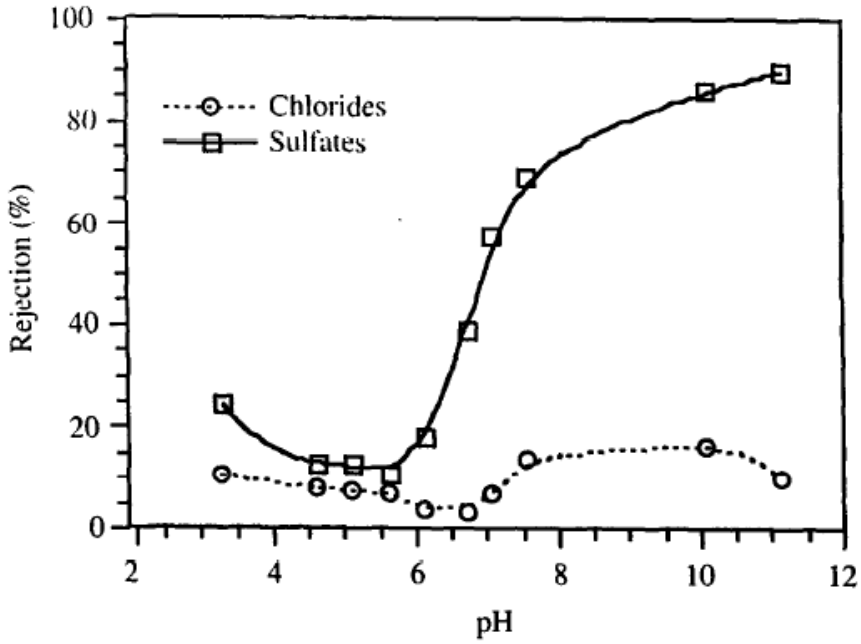

Figure 5. Rejection of anions in a $NaCl/Na_2SO_4$ mixture by magnesia doped zirconia membrane as a function of pH (Source: Vacassy, et al. 1998).

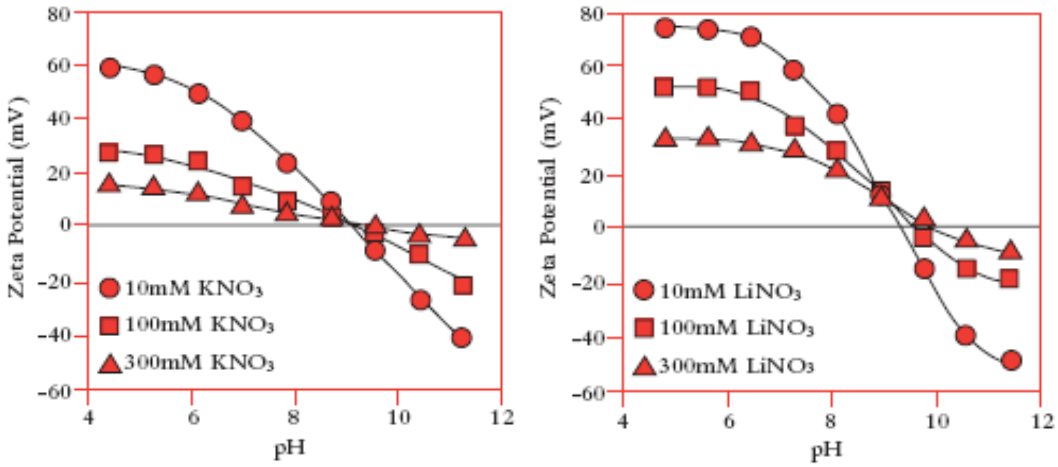

Figure 6. Zeta potential of alumina solutions as a function of pH and KNO_3 or $LiNO_3$ concentration (Malvern 2009).

CHAPTER 2

STRUCTURE AND PREPARATION OF CERAMIC MEMBRANES

Ceramic membranes are porous structures enabling passage of some constituents in the feed stream with sizes comparable or smaller than the pore sizes while rejecting others with sizes comparable or larger than the size of the pores. The resistance to the passage of carrying medium (the liquid in which the constituents are dissolved or dispersed) increases with the decreasing pore size. This causes higher energy i.e. higher driving force (pressure difference) requirements for separation applications by using membranes with smaller pores as shown in Table 2.

The removal of smaller particles is only possible by using membranes with smaller pores and will increase the energy consumption. The asymmetric membrane structure is an alternative to overcome this drawback. The asymmetric ceramic membranes are composed of two or three layers.

Bottom layer has relatively larger pores that have lower resistance to liquid flow but also little or no separation efficiency. This bottom layer has a considerable thickness and responsible for mechanical strength of the membrane and it is generally called as “support”. An intermediate layer can be formed over the support with smaller pores which is expected to regulate the pressure and micro-structural difference between support and top layer. The top layer over the intermediate layer has the smallest pore size and is responsible for separation. Its thickness is kept as small as possible to decrease the amount of needed energy for the separation process. An example to the asymmetric structure in membranes is shown in the SEM (Scanning Electron Microscope) image in Figure 7a. TEM (Transmission Electron Microscope) image of the top layer is given in the same figure (b).

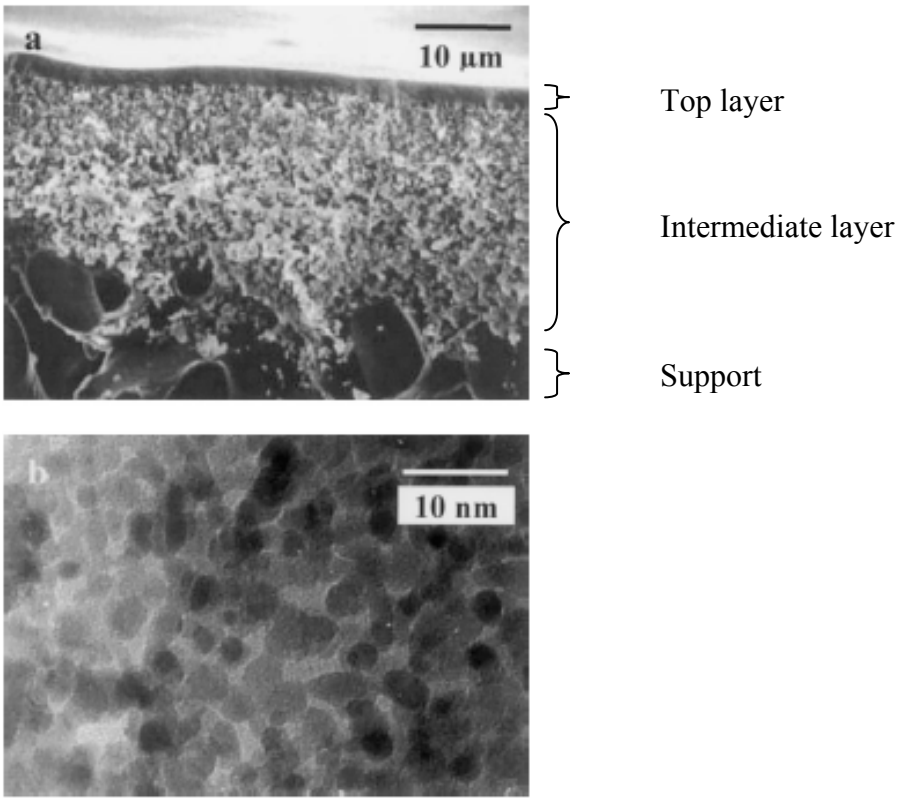

Figure 7. Electron microscopy images of a supported microporous zirconia layer formed by nanocrystallites of less than 10 nm (Source: Cot, et al. 2000).

2.1. Processing of Porous Ceramics

Preparation of an asymmetric membrane with desired microstructures is a challenging process including several steps. The preparation of the layers of an asymmetric structure is conducted progressively layer by layer.

2.1.1. Preparation of Supports

Support is the thickest part of the membrane with the largest pores and responsible for the mechanical strength of the membrane. It is expected to have low resistance to fluid flow and should have a homogeneous structure with sufficient

mechanical strength under working pressures. For this reason the support is prepared by packing of fine ceramic powders to have a three dimensional porous structure with interconnected open pores. The size and distribution of pores are influenced with the size and shape of the particles packed, the presence/absence and size of the pore forming agents (e.g. starch, PVA, other polymeric chains), heat treatment temperature and duration.

Previous research showed that there may be beneficial effects of addition of pore forming additives (e.g. starch) on increasing the porosity of the supports prepared from alumina powder (Erdem, et al. 2006). Researchers reported preparation of ceramic supports with different pore structures via using three different starches as pore forming agents (Gregorova and Pabst 2007). They reported that the pores formed by potato starch were larger (50μm) than wheat starch (20 μm) and rice starch (14 μm) as shown in Figure 8.

The initial particle size distribution of ceramic powders is important in the pore sizes of the resulting support. Larger pores are obtained with the packaging of larger particles and vice versa. The ceramic powders tend to form agglomerates either in dry form or in suspensions to decrease their surface potential. The packing of agglomerates with different sizes may result in non-uniform structures. Therefore, the agglomerates should be broken by using sonic or mechanical mixing and by using some additives (e.g. agglomeration blocking polymers, pH regulators, etc.).

The fine ceramic powders can be packed either by dry methods (die-pressing) or wet methods (slip-casting, impregnation of sponge with powder slurry) (Galassi 2006). Additives for controlled drying and/or pore forming can be used for both methods. Additives can also be used to stabilize the ceramic suspensions in wet forming methods for ensuring homogeneity of slips before consolidation. The homogeneous distribution of these additives is essential to prepare supports with uniform microstructures.

The temperature and duration of heat treatment are important parameters in support preparation. The heat treatment should provide the energy for partial sintering of powders to reach the desired mechanical strength and to burn out the additives leaving interconnected open pores. Excessive heat treatment will decrease the total porosity and open pore content. Heat treatment at lower temperatures/durations will result in supports with insufficient mechanical properties.

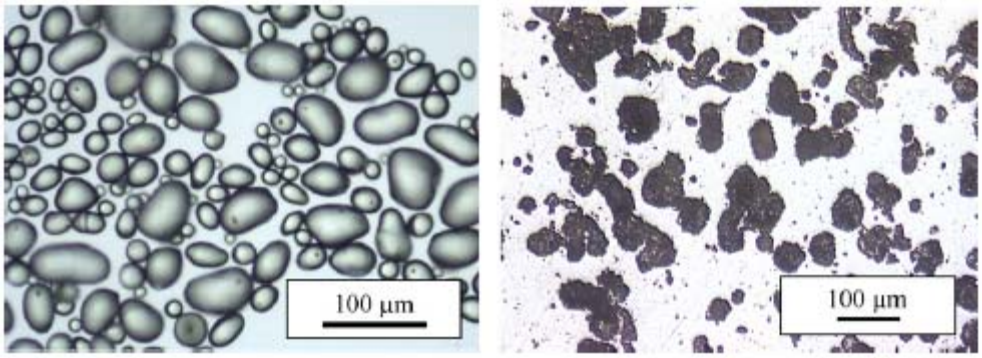

a) potato starch (left) and resulting oxide structure (right)

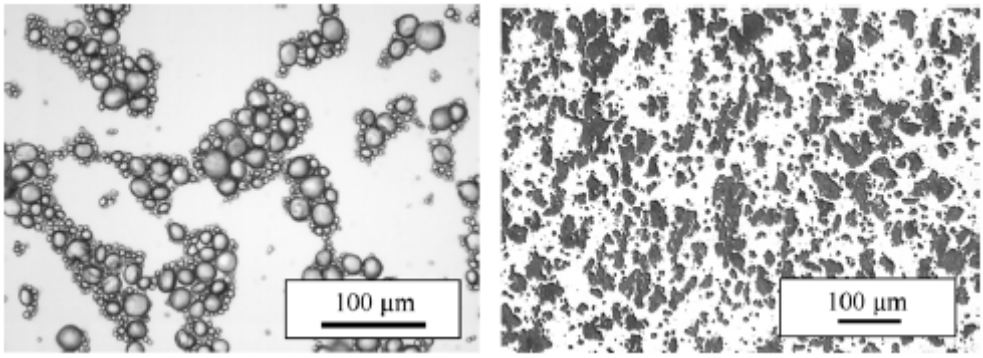

b) wheat starch (left) and resulting oxide structure (right)

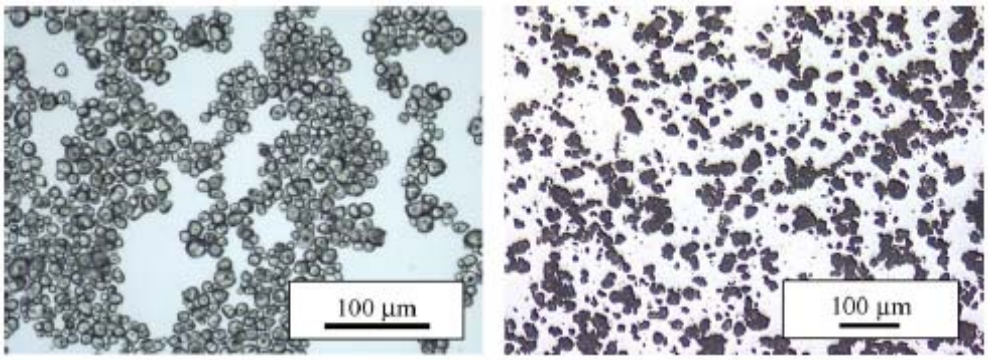

c) rice starch (left) and resulting oxide structure (right)

Figure 8. The microstructures of alumina supports prepared by using starch from different sources (Source: Gregorova and Pabst 2007).

2.1.2. Preparation of Intermediate and Top Layers

The intermediate layer can be prepared by consolidation of particles finer than the ceramic powders used in support preparation. These particles can be fine powders or some other precursors which will form stable intermediate layers after heat treatment.

The layer with the highest selectivity is the top layer which is relatively thinner than the other layers as shown in Figure 2. It has the smallest pores of the membrane. This thin layer with fine pores can be prepared by a number of techniques (e.g. CVD (Chemical Vapour Deposition), sol-gel procedure, etc.). The aim is to form a layer of fine interconnected open pores with a uniform pore size distribution.

The sol-gel processing is a versatile tool which enables controlling the formation via changing parameters in the procedure and can be performed only with simple laboratory facilities. The starting materials are metal salts or alkoxides in general (Pierre 1998). First a stable suspension of colloidal solid particles is prepared by using these precursors, which is called as a "sol". Two main reactions take place in the sol preparation from alkoxides namely hydrolysis and condensation. These two main reactions are schematically illustrated in Figure 9.

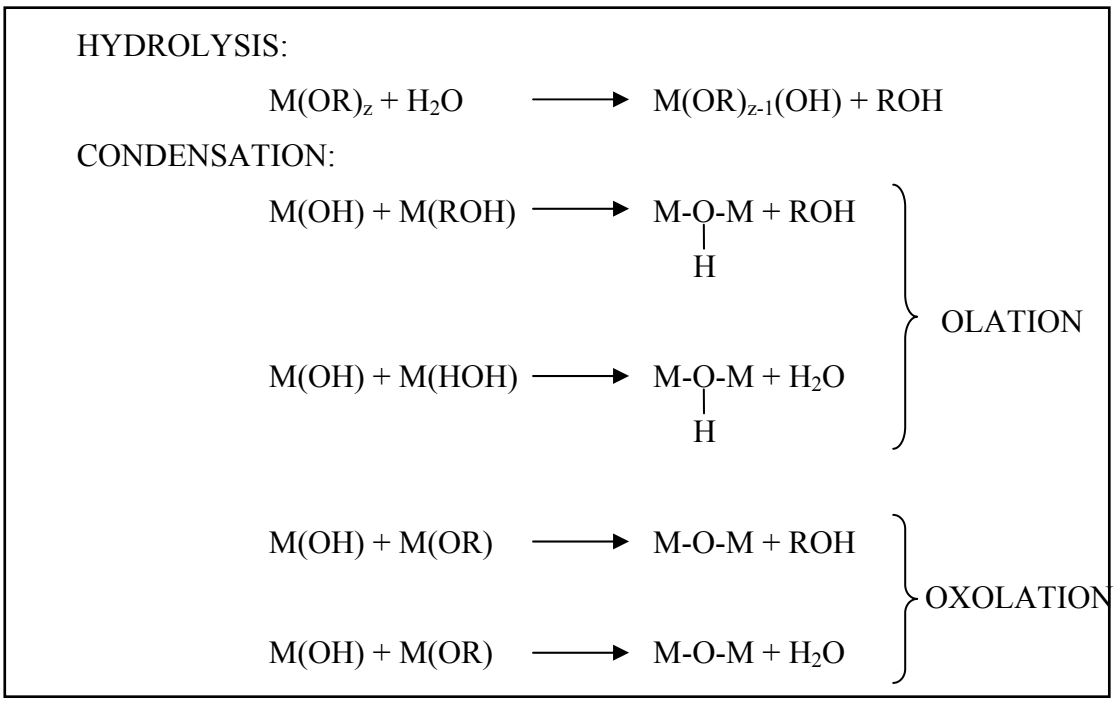

Figure 9. The possible simultaneous reactions in sol preparation (M: Metal, R: Alkyl group, O: Oxygen, H: Hydrogen)

Hydrolysis is a substitution reaction in which the organic side chain(s) (alkoxy group) (-OR) of metal alkoxide leaves it place to a hydroxyl (-OH) group coming from water molecule forming an alcohol molecule (ROH). The hydrolysis is facilitated with higher charge densities on the metal (M) and inhibited as the number of hydroxo ligands (M-OH) around the metal increases (Brinker and Scherer 1990). A detailed discussion on the substitution reactions of alkoxides with respect to their coordination number and environmental pH is given in the references (Brinker and Scherer 1990, Pierre 1998).

Hydrolysed alkoxide species are combined to form longer chains in condensation. Water or an alcohol molecule is also formed during reaction. The condensation reaction takes place as "olation" or "oxolation" and is susceptible to even atmospheric oxygen and carbon dioxide (Pierre 1998). It causes formation and elongation of precursor chains and is possible when there is still unreacted (-OH) groups around (in coordination sphere of) the metal (Brinker and Scherer 1990).

The rates of simultaneous hydrolysis and condensation reactions are important factors on the particle size distribution of the sol. The sol-gel route can proceed in two ways resulting either in polymeric or colloidal sols. These routes are schematically shown in Figure 10. The hydrolysis and condensation reaction is faster in the colloidal sol route, adjusted by changing reaction conditions (type of alkoxide, solvent, catalyst, composition of reactants, molar ratio of water, temperature, etc.), resulting in a fully hydrolyzed alkoxide (highly branched polymer). The rapid condensation reaction causes particulate growth and/or precipitation. Particulate sols can be formed via controlling the reaction conditions and precipitate peptization by acid addition.

In polymeric sol route limited amount of water is added, the hydrolysis reaction is kept slower and partial hydrolysis occur resulting in a linear organic polymer. The void spaces among the sol particles (for colloidal route) and the size of the gel network (for polymeric route) determine the pore size of the membrane. (Tsuru 2001)

The sols will form a three dimensional porous interconnected solid structure at the end of both polymeric and colloidal routes which is called a "gel". The gel contains liquid medium in its pores between the solid particles. The gel is called "aquagel" or "alcogel" if most of the liquid in its pores is water or alcohol, respectively. The gel is not stable mechanically or chemically. There is equilibrium between liquid medium in the pores and solid particles forming the network. The gel can be dried either classically to get "xerogel" or by using freeze drying to get "aerogel". (Pierre 1998)

Dried gels are brittle solid structures which should be heat treated to obtain mechanically and chemically stable microporous layers. Winkler and Baltus (2003) tried to modify surface characteristics of alumina membranes by using sol-gel method with titania and silica precursors but they were not successful due to the absence of a required heat treatment. The heat treatment temperature and duration for thin layers of dried gels are important parameters on resulting stable porous oxide structure as are in preparation of supports. The removal of organics and crystallization of oxides occur during the heat treatment. This transformation is very important and effective on the properties of the formed top layer.

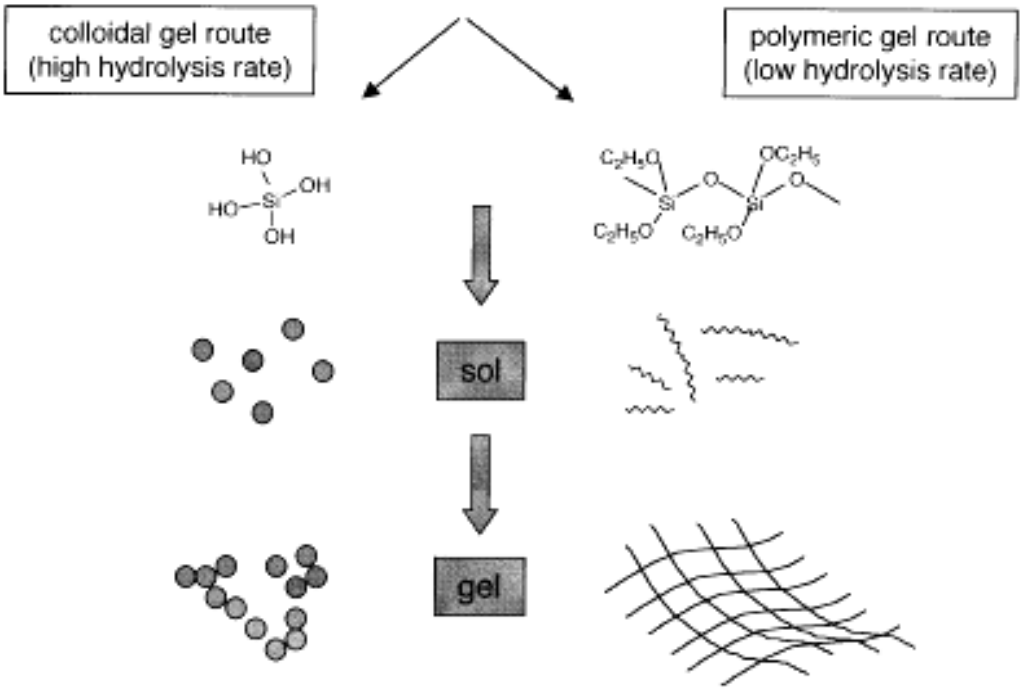

Figure 10. The two alternative routes in sol-gel processing
(Source: Tsuru 2001).

CHAPTER 3

IMPORTANT PARAMETERS OF SOL-GEL PROCESSING

3.1. Precursors (Raw Materials)

The raw materials as metal sources could be either salts or alkoxides. The widely used alkoxides are generally very hydrophilic and must be used carefully to prevent uncontrolled gelation. Alkoxides can be used solely or they can be mixed in certain ratios to obtain mixed sols. Using sols of one alkoxide will result in a homogeneous oxide structure with uniform properties. Mixed sols are generally prepared to enhance or change the properties of the resulting oxide structure. Aust, et al. (2006) worked with ZrO_2/TiO_2 system to obtain gas separation membranes with higher chemical and hydrothermal resistance in comparison to commonly used silica membranes. Their research was focused on membrane preparation with a higher crystallization temperature to prevent the collapse of the microporous structure during heat treatment. They formed an intermediate layer of mixed oxide by using colloidal sol-gel route and formed a nanoporous top layer by using polymeric sol-gel route. Their precursors were tetraethyl-orto-titanate and zirconium (IV)-propoxide. Mixed oxide prepared with these precursors resulted in an oxide structure with a 100-300° C higher crystallization temperatures and smaller pore sizes when compared with the pure oxides. They also confirmed the chemical stability under mild acidic and severe basic conditions.

The ZrO_2/TiO_2 system was investigated by Van Gestel, et al. (2006). They reported high chemical resistance of ceramic NF membrane with a MWCO (molecular weight cut-off) in the range of 200-300. They used yittria as a dopant to stabilize zirconia in the tetragonal phase.

ZrO_2/SiO_2 mixed oxide top layers were prepared with tetraethoxysilane ($Si(C_2H_5O)_4$) and zirconium-tetra-propoxide ($Zr(C_3H_7O)_4$) and the transformation of zirconia from tetragonal to monoclinic phase was delayed to higher temperatures with the addition of SiO_2 (Agoudjil, et al. 2005).

Benfer, et al. (2001) prepared nanofiltration (NF) membranes by coating zirconia or titania ultrafiltration (UF) membranes with polymeric sols forming either pure zirconia or titania top layer. They tested the performance of these membranes and planned to scale-up for membrane production which would be used in textile industry.

Hao, et al. (2004) worked with ZrO_2/Al_2O_3 system and prepared nanoporous (4.3 nm average pore size) membranes with higher thermal stability than the pure oxides. The zirconia composite membrane preserved its tetragonal structure between 700-1100° C and was stated to be proper for high temperature catalytic reactions.

The resulting membranes could be alumina (Al_2O_3), silica (SiO_2), zirconia (ZrO_2), titania (TiO_2) or combination of these (mixed oxides). The silica system enables good pore size control but possesses low chemical stability in neutral or alkaline pH values. Alumina (γ-alumina) membranes were not stable at high acidic medium (pH<2) while titania and zirconia membranes were stable in both acidic and basic medium. (Tsuru 2001)

3.2. Additives

Additives are used in sol-gel processing with many purposes like:

- to initiate and control the rates of hydrolysis and condensation reactions:

Acids (e.g. HNO_3, HCl, organic acids), bases (e.g. NaOH, NH_3, NH_4OH) or other special chemicals like acetyl-acetone (acac) can be used for this. The amount of acid catalyst was effective on the particle size distribution of prepared sol (Erdem 2002). The average particle size of zirconia sol prepared by using zirconium propoxide in propanol and nitric acid decreased from 5.7 nm to 3.1 nm as the acid amount increased from 0.826 mL to 1.026mL per mL of propanol.

- to change the physicochemical properties of the resulting oxide structure:

Preparation of iron modified silica membranes were reported with high negative zeta potential values over a pH range and with enhanced mechanical stability by Skluzacek, et al. (2006). The aim was to increase the salt rejection efficiency by preparing a ceramic membrane with high magnitudes of zeta potential.

- to closely control the thickness and porosity of the top layer:

Gaudon, et al. (2006) used methylethylketone (MEK) in the dispersions of yittria stabilized zirconia (YSZ) for controlling the thickness of the dip-coated layer. The thickness of the coated layer was increased as the volumetric ratio of the MEK increased, possibly due to changes in rheological properties of the polymeric sol (i.e. increasing viscosity).

PVA (polyvinyl alcohol) or PEG (polyethylene glycol) can be used as a binder and viscosity modifier to enhance dip-coating of the sol on the support. Ahmad, et al. (2005) determined that 1 g PVA per 50 mL of water as the optimum binder level for dip-coating of alumina sols.

Sakka, et al. (2005) introduced two interesting methods to prepare oxide layers of uniform porosity with the addition of spherical PMMA (polymethyl methacrylate) beads with diameters of 300 nm and 1300 nm. In the first method they packed the polymeric spheres and filled the void space between them with the sol and formed a uniform porous structure after heat treatment at 550° C. In the second method they electrostatically stabilized the polymer solution and nanosized ceramic particles to have a well-dispersed mixture. TiO_2 particles were modified with PEI (polyethylene imine) to have positive surface charge at working pH (pH=6). The procedure for this method is illustrated in Figure 11. On the other hand an inorganic phase perovskite ($SrCo_{0.6}Fe_{0.4}O_3$) was added to alumina sol to retard γ to α-alumina phase transformation during heat treatment by Ahmad, et al. (2005) to control the pore structure.

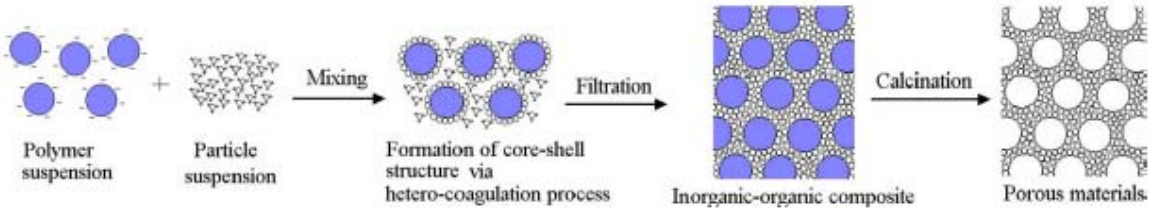

Figure 11. Schematic representation of core-shell stabilization method (Source: Sakka, et al. 2005).

3.3. Coating and Further Processes

Coating of the sol on the support is a critical process step. Its duration in combination with the viscosity of the sol along with the method utilized will determine the thickness of the coating. The thickness of the coated layer increases with the increasing sol viscosity and coating time. Dip-coating, spin coating or other coating methods with controlled parameters can be used.

Drying sequence of the sol can affect the properties of the resulting green body. Drying can be performed either classically to get "xerogel"s or by freeze drying to get "aerogel"s. These two will have different pore sizes and structures with the same starting.

Heat treatment is inevitable to maintain the stability of the coated layer and it can be used as a tool to modify the final characteristics of the coated layer. Ceramic materials go through some phase transformations with increasing temperature. These phase changes can result in crack-formation due to the differences between specific volumes of each phase. Overcoming possible crack-formation and preparation of ceramic membranes with different phase distribution may result in membranes with different physicochemical properties which may enhance their separation properties. Mixed oxides can be prepared or some additives can be added to have oxide structures with different characteristics after heat treatment at different temperatures.

The surface of ceramic membranes can be further modified by some polymeric species for enhancing/changing their selectivity to different components of the feed stream. The ion-implantation technique can be another alternative for surface modification.

CHAPTER 4

RECENT RESEARCH ON CERAMIC MEMBRANES AND FILTRATION

The wide application possibilities of ceramic membranes for different purposes like separation, concentration, purification, clarification, etc. in several industries enforce the research on preparation, characterization, optimization, modification and application of ceramic membranes. Nowadays ceramic NF membranes are currently produced for industrial scale applications which will replace polymeric *predecessor*s. The robust structure and higher stabilities of ceramic membranes in harsh working conditions will probably make them more preferable especially for applications where polymeric membranes tend to fail in time like highly acidic medium, or medium containing organic solvents. The ceramic membranes are shrinkage-free under high pressures and high solute concentrations which may be another problem when polymeric membranes are used especially for higher pressure applications like NF and RO. Freger, et al. (2000) reported that high salt concentrations caused skin shrinkage while filtering organic (lactic) and inorganic (sodium) salt mixtures with a commercial polyamide membrane at high salt concentrations and highly acidic medium.

4.1. Membrane Coupled Bioreactor for Production of Organic Acids

Lactose (milk sugar, a disaccharide; composed of two monosaccharides (glucose+galactse) as shown in Figure 12, MW: 342 g/mol) in whey is one of the main raw materials used in lactic acid production by fermentation. Lactic acid is a widely consumed organic acid (around 350 millions kg per year) and the worldwide growth of its consumption is believed by some observers to be 12–15% per year (Joglekar, et al. 2006).

The enriched fermentation medium with suitable nitrogen source (proteins, peptides, amino acids), carbon source (sugar, e.g. lactose) and minerals are used for the

production of lactic acid. The carbon source can be molasses (by product of sugar industry), protein-free (UF treated) whey (5 % lactose) or higher polymers of sugar (like starch) which are needed to be initially hydrolyzed to smaller sugars (disaccharides or monosaccharides) by enzymatic or acidic treatment. The yield of fermentation process can be increased by removing product (lactic acid, MW: 90 g/mol) from the reactor continuously to prevent product inhibition by a specially designed bioreactor as shown in Figure 13. The product (acid) should be removed while keeping the sugar (lactose) in the reactor to increase the productivity as shown in Figure 14. The membrane for this application must be capable of separating lactose and lactic acid. It should be resistant to acidic conditions (pH<5) for long operation times. These demands can be supplied by a specially prepared ceramic NF membrane.

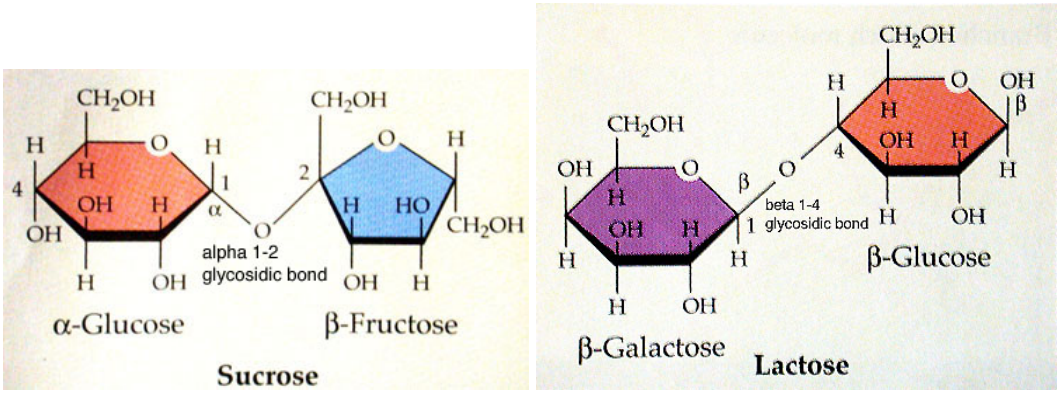

Figure 12. The molecular structures of sucrose (commonly consumed sugar) and lactose (sugar dominant in milk).

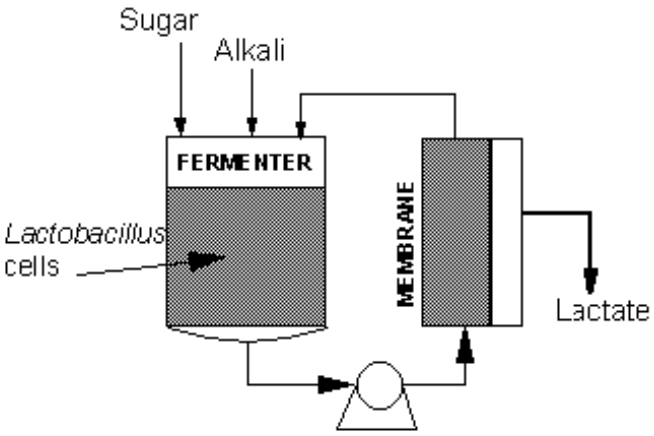

Figure 13. Bioreactor coupled with a membrane unit (Source: Cheryan 1998).

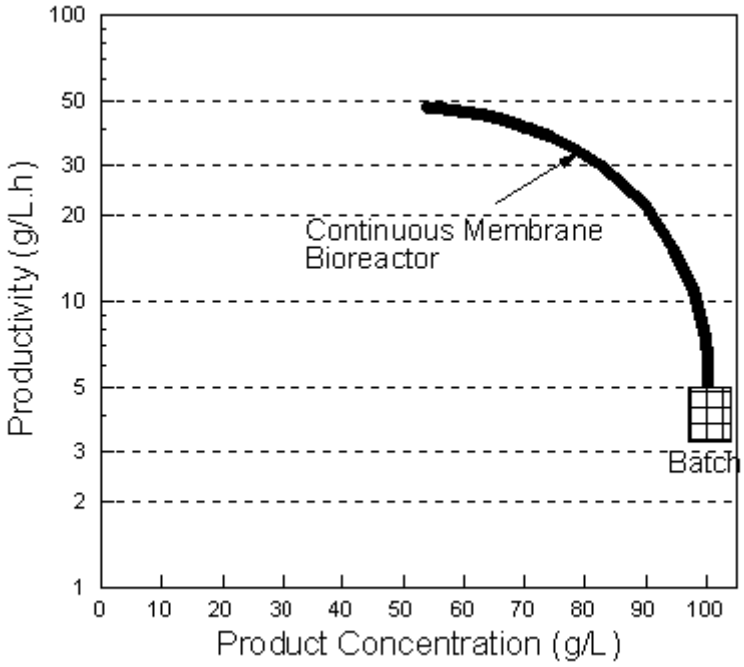

Figure 14. The productivity for batch reactor and bioreactor with continuous product removal by using a membrane (Source: Cheryan 1998).

Milcent and Carrere (2001) worked on lactic acid fermentation broth clarification by using three different commercial tubular ceramic MF membranes (Kerasep Al_2O_3 -TiO_2) with nominal pore sizes of 0.1 and 0.8 μm and third with a MWCO (molecular weight cut-off) value of 300 kDa. The filtration experiments were performed after batch fermentation was completed and influences of pore size, cross-flow velocity, temperature, medium pH on the filtration were investigated. They reported a higher steady-state permeate flux for ceramic membrane with 0.1μm nominal pore diameter. They showed the positive effects of transmembrane pressure (0.5-2.5 bars) on permeate flux and presence of irreversible fouling of some constituents probably from molasses preventing the increase in permeate flux when the cross-flow velocity (2-4 m/s) was increased. They regulated the pH between ~4.8 to 10.5 and reached a maximum permeate flux at around 7.5. The permeate fluxes at higher and lower pH values were considerably smaller indicating the importance of pH during such a filtration process. In this work there was not a challenge to separate lactose from lactic acid, since nearly all the lactose was consumed during batch fermentation. The decrease in pH was depressed by addition of alkali solutions (ammonium hydroxide, 32% vol / vol) continuously and operating pH was kept at 6.2. The product inhibition which

results in decreasing pH can be overcome by membrane coupled bioreactor design with a ceramic membrane with high resistance to acidity and capable of separation of lactose and lactic acid instead of alkali addition.

Another point about this research is the possible effect of monovalent and divalent ions on the separation efficiency of ceramic membranes. Researchers used sulphuric acid (95%) and ammonium hydroxide (32%) to alter the pH of the fermentation broth before filtration to investigate the effect of pH on filtration. They reported a decrease in permeate flux by decreasing the pH of the broth from 6.2 to lower values, but while increasing the pH, the permeate flux was first increased and then decreased giving an optimum pH value between 7 and 8 as shown in Figure 15. This behaviour can possibly be explained by investigating the adsorption of ammonium ions on the ceramic membranes affecting its surface charge.

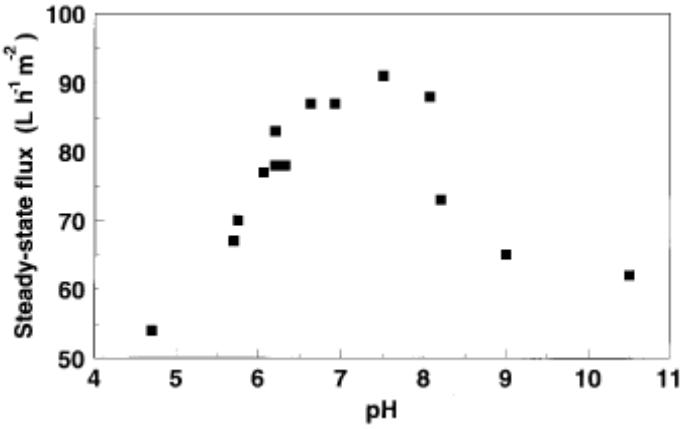

Figure 15. Cross-flow filtration of a lactic acid fermentation broth on a 0.1 mm Kerasep membrane: Steady-state permeate flux vs. broth pH (Source: Milcent and Carrere 2001).

4.2. Desalination

Desalination is an important application of filtration which is used in many industries. Narong and James (2006) worked on NaCl retention by using a composite ceramic UF membrane consisting of a titania (TiO_2) layer (5nm nominal pore size) on alumina support with 1.2µm nominal pore size. They reported the minimum rejection

was at around pH 4 which was reported to be isoelectric point (iep) of titania showing the importance of electrostatic interactions. The general rejection values were between 15-45% for varying NaCl concentrations in the 10^{-1}-10^{-3} M range.

Weber, et al. (2003) characterized the new ceramic NF membrane they prepared, which was composed of titania or zirconia top layer over alumina support, by performing filtration experiments with NaCl, KCl, Na_2SO_4, $CaCl_2$ and $NaNO_3$ solutions. The retention values for Na^+ and Cl^- were higher than the retentions reported by Narong and James (2006) as shown in Figure 16. The NaCl retention decreased to 5-35 % as the NaCl concentration was 10^{-1} M. They reported a higher iep for TiO_2 top layer as shown in Figure 17. The retention data for Na_2SO_4 as a function of pH had a different profile which increases with increasing pH reaching to 90% at pH 11 (and 15 bar TMP (trans-membrane pressure)) as shown in Figure 18. The retention values generally increased with increasing TMP slightly. They performed some other experiments to treat waste water from textile industry, alkaline solutions from bottle washing machines (pH=13-13.5) and pickling bath solutions (with high Cl concentration; 231 g/L, 3.86 M) from the metal-working industry. They concluded that the membrane they prepared fell into intermediate area between UF and NF. Another conclusion of the work was that the salt retention was controlled by the membrane charge and depends especially on the type of the salt, salt concentration and pH value of the solution. They also concluded that the composite ceramic membrane they prepared can be effectively used in the treatment of wastewaters from textile industry and alkaline solutions from bottle washing machines since it has high permeability rates (high permeate flux), good retention of organics and a low fouling tendency (Weber, et al. 2003). The membrane prepared was found to be not suitable for treatment of pickling bath solution since the salt retention decreases significantly as the electrolyte concentration increase during the filtration.

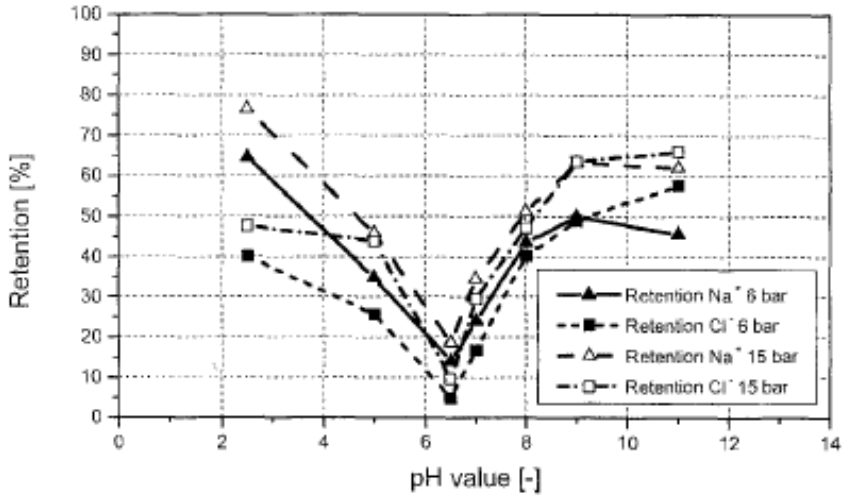

Figure 16. NaCl retention for k-NF-new (TiO_2 top layer) as a function of pH (Source: Weber, et al. 2003).

Tsuru, et al. (2002) prepared titania membranes with MWCO of 250, 400 and 2000 by sol-gel process and investigated the effects of mono- (Na^+, K^+) and divalent ions (Ca^{2+}, Mg^{2+}) and pH on permeate flux. They concluded that the divalent cations were adsorbed on the membrane and decreased the permeate flux at alkali pH by reducing the effective pore size.

Another example is demineralization of fermentation broths after antibiotic production. The fermentation broths should be first concentrated and demineralized for further purification of antibiotics by e.g. solvent extraction. Alves, et al. (2002) performed UF and NF to fermentation broth to separate clavulanic acid (an antibiotic). The UF membranes used were ceramic tubular membranes with MWCO (molecular weight cut off) of 15 and 150 kDa and a flat sheet polymeric membrane with MWCO of 20 kDa to separate microorganisms and the NF membrane was also polymeric with MWCO of 5 kDa. Tessier, et al. (2005) found the highest benzyl-penicillin recovery (97.4%) from the fermentation broth by using a UF followed by a NF step. The reduction of ionic strength in the fermentation product with NF (300 Da MWCO) was reported to be effective on the overall recovery yield.

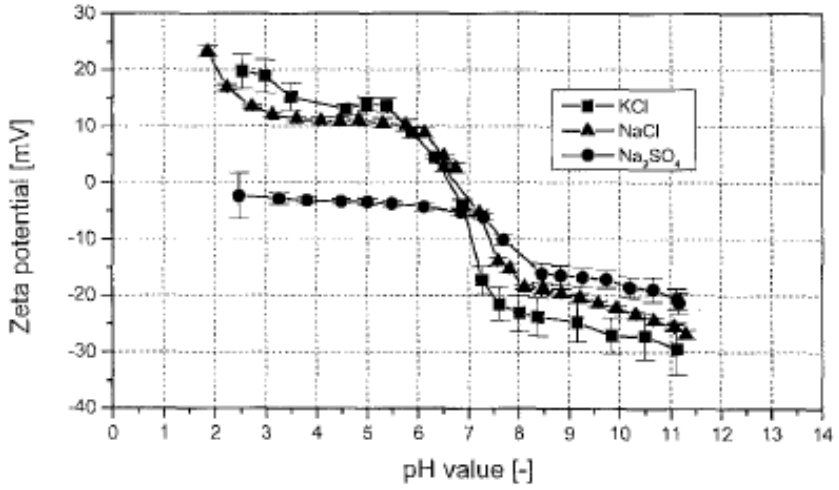

Figure 17. Zetapotential of k-NF-new (TiO_2 top layer) for NaCl, KCl, Na_2SO_4 (10^{-3} M) (Source: Weber, et al. 2003).

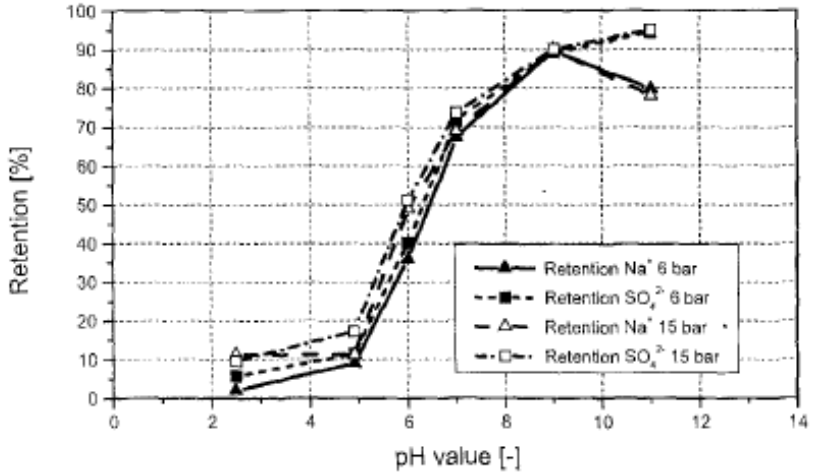

Figure 18. Na_2SO_4 (10^{-2} M) retention for k-NF-new (TiO_2 top layer) at different pH values (Source: Weber, et al. 2003).

Whey demineralization is another NF application where desalination yields a more valuable product. During cheese production sodium/potassium salts are added and calcium is naturally present. The excess salt should be removed for further processing of whey into value added products like protein concentrates to be used in food industry in special products for infants' and sportsmen's nutrition. These proteins are also used in food products like chocolate as emulsifying additive.

4.3. Fractionation and Concentration of Extracts

The antioxidants in grape seed extract are polymers of proanthocyanidines. The monomer structure of proanthocynidin is shown in Figure 19. The extract contains a complex mixture of antioxidants with different polymerization degree (Table 4). The antioxidant activity of antioxidant molecules with a lower degree of polymerization (i.e.monomers, dimmers) were found to be greater than molecules with higher degree of polymerization (Guendez, et al. 2005) especially the dimer procyanidin B_1 (Figure 20) showed the highest antioxidant capacity.

The fractionation of the antioxidant materials in the grape seed extract will result in the production of an antioxidant stream with a superior antioxidant capacity. The fractionation of these antioxidants is currently performed by using size exclusion columns. Utilization of a filtration process for separation will enhance the yield. There is only one reported research on the filtration fractionation of polyphenolic extracts from grape seed extract (Santamaria, et al. 2002). Several filtration experiments either with UF or NF polymeric membranes were conducted in this work. Oligomeric proanthocyanidins with high purities were obtained. They used methanol-water solution for extraction although acetone-water solutions can give a better extraction yield in order not to extract the highly polymerized species and also prevent the polymeric membrane damage which may occur in the presence of acetone. The presence of organic solvents in extracts would no longer be a problem when ceramic membranes were used.

The extraction of organics from natural sources can be performed by using supercritical fluid extraction instead of using organic solvents. There is a considerable research activity on this environmentally friendly extraction method. The permeate flux values are generally higher since the viscosities of supercritical fluids are 10 times lower and diffusivities are 10 to 100 times higher than liquids (Sarrade, et al. 1998). Sarrade, et al. (1998) combined ceramic membrane filtration and supercritical CO_2 extraction for extraction and fractionation of fish oil (triglycerides) with different fatty acids and extraction and purification of β-carotene from carrot oil and carrot seed. The membranes used were composed of either titania top layer on α-alumina or this composition plus a nafion (a sulfonated tetrafluorethylene copolymer) layer.

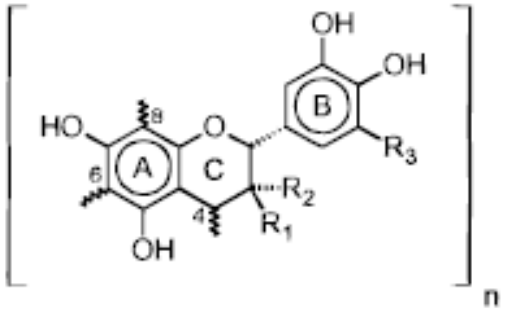

Figure 19. General scheme of grape proanthocyanidins (*n*: degree of polymerization), (R_1=OH, R_2=H, R_3=H), (+)-catechin; (R_1= H, R_2= OH, R_3= H), (-)-epicatechin; (R_1= H, R_2= *O*-galloyl, R_3= H), (-)-epicatechin-3-*O*-gallate; (R_1= H, R_2= OH, R_3= OH), (-)-epigallocatechin (Source: Labarbe, et al. 1999).

Table 4. Molecular weights of proanthocyanidin monomer (catechin) and its oligomers (Source: Santamaria, et al. 2002).

Polyphenolic compound	*MW (g/mol)*
Catechin	290
Dimer	578
Trimer	866

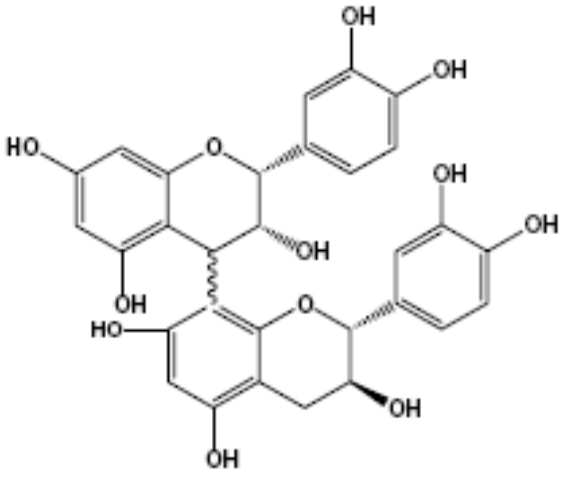

Figure 20. A dimer of proanthocyanidin ; procyanidin B_1 (Source: Guendez, et al. 2005).

4.4. Water Treatment

The global warming, unfortunately, is threatening the life in the "blue planet". The edible water sources which are only 0.01 % of all around the world (Walha, et al. 2007) are diminishing while the pollution of the present sources is increasing. One of the most important problems of survival of human beings on the world is the arising water deficiency. There is a huge research activity on recycling, cleaning and desalination of water (Gazagnes, et al. 2007, Duke, et al. 2007). The aim of these research activities is either cleaning the used potable water or producing potable water from sea or salty water sources. Gazagnes, et al. (2007) modified tubular ceramic membranes with given pore sizes (ZrO_2 (50 nm), Al_2O_3 (200 & 800nm) and aluminasilicate (400 nm)) to have hydrophobic ceramic membrane distillation units in order to investigate desalination of water. Edwards, et al. (1999) immobilized polyphenoloxidase enzyme on chitosan-coated poysulphone capillary membranes to improve wastewater bioremediation.

The phenol and its derivatives (e.g. with chlorine) are pollutants in several industrial waste waters like food, textile and paper industries (Ensuncho, et al. 2005). Rubia, et al. (2008) reported the difficulty of bioremediation of olive mill waste-water polluted by phenolic compounds since they are antibacterial and phytotoxic. The small sizes of these compounds make their separation from water by using membranes inefficient. Therefore, they should be oxidized to form more reactive species tending to get polymerized in order to have bigger sized pollutants. The oxidation reaction can be performed by using an oxidative enzyme as biocatalyst. Lante, et al. (2000) immobilized laccase from *Pyyricularia oryzae* on spiral wound asymmetric polyethersulphone membrane and investigated the phenol and its derivatives oxidation / transformation and reported different removal efficiencies for different phenolic substrates. The utilization of ceramic membranes in these environmental applications will be beneficial since the ceramic membranes have superior durability. They can be used directly or after immobilization / surface modifications of catalytic organic / inorganic materials.

CHAPTER 5

EXPERIMENTAL

5.1. Preparation and Characterization of Asymmetric Ceramic Composite Membranes

5.1.1. Supports

Supports were prepared from ceramic alumina powders (Alcoa CT3000SG, with D_{50}:0.7 μm or AKP-50, D_{50}:0.18 μm Sumitomo Co.) by slip-casting into polymeric dies. The slip was prepared by using ceramic powder, deionized water, dispersant (Darvan-C) and pore forming agent (starch). The amount of pore forming agent (PFA) was changed from 0 to 15%. The potato, wheat and corn starches were used to form a porous support with low resistance to water flow in the absence of mechanical failure. The suspensions with and without starch were prepared and cast separately or into same die to have porous and dense layers through the support. Since the solid content of the ceramic suspensions (slip) were high (40-57.5 vol. %) they were viscous. In some experiments the spreading of viscous slips was initiated via addition of drops of diluted surfactant solution. The aim was well-spreading of the slip by decreasing the tension of the slip-air surface in order to cast thinner support layers.

The cast green bodies were heat treated at 1300°C (1100°C for AKP-50) for 2 hours using high temperature furnaces (Carbolite RHF 1600, CWF 1300). The temperature was gradually increased to 700°C with 5°C/min up to 700°C and kept at that temperature for 20 minutes to prevent cracks due to the gases forming with oxidation of starch and dispersant. Till then the temperature was increased by 10°C/min to 1300°C (1100°C for AKP-50) and kept for 120 minutes at that temperature before cooling with a rate of 20°C/min (5°C/min for AKP-50) down to RT (room temperature).

5.1.1.1 Supports with double layers

Bilayered supports with different porosities were prepared in order to investigate the possibility of forming composite asymmetric structures with high permeate flux and a smooth defect free suitable surface for selective thin layer coating. Ceramic suspensions with and without pore forming additives were cast into dies successively. The relatively high viscosities of the suspensions (~50 vol. % solids content) caused difficulties in casting thin support layers with nonuniform die surface wetting and spreading. The membrane thickness is a dominant parameter in determining the resistance to fluid flow through the membrane. The surface tension of the suspension was decreased by using a dilute surfactant solution and thinner layers of well-spread suspensions were cast and undesired increases in membrane thickness was prevented.

5.1.2. Intermediate Layers

The intermediate layer regulates the huge structural difference between the support consisting of partially sintered micron-submicron particles and the top layer consisting of packing of nano particles with 3-10 nm ave. particle sizes. Formation of a nanoporous layer over the support by consolidation of nano-particles is relatively harder so that the asymmetric structure should be formed layer by layer.

Therefore, two intermediate layers were formed. First intermediate layer was formed by consolidation of a suspension of submicron ceramic particles which were smaller than the particles of the ceramic powder used in the support preparation. Second intermediate layer was formed by preparing and coating a sol with an average particle size between the average particle sizes of the particles forming first intermediate layer and top layer. The suspensions of the fine (submicron) ceramic powder in the sols were also used in the preparation of the intermediate layer.

5.1.2.1. First Intermediate Layer

There were two ceramic submicron powders used in preparation of first intermediate layer; alumina (AKP-50, Sumitomo Co.) and zirconia (TZ-3Y, Tosoh Co., 5.15 ± 0.20 wt% Y_2O_3, 16 ±3 m^2/g). Suspensions with different concentrations of these powders were prepared either with or without addition of PVA (poly vinyl alcohol, 80% hydrolyzed, MW: 9000-10000, 3 wt % in suspension) as drying control chemical additive (DCCA).

The suspensions prepared were either dip-coated (d-c) or spin-coated (s-c) or wet-coated (w-c) on the support discs. The suspensions of ceramic powder with varying volumetric ratio (1-20 vol. %) were prepared and the surfaces of the supports were coated via methods mentioned. Then the coated supports were dried and heat treated (ht) at 900-1150° C (Carbolite CWF 1300). The heating and cooling was performed gradually as 5° C / minute. For the coatings with PVA containing suspensions there was a dwelling period of 20 minutes at 450° C to burn out added binder organics.

Different methods of coating as mentioned above were used to benefit from their particular advantages. In fact, they also have particular disadvantages, too. The dip-coating is a practical way of coating. The suspensions of ceramic powder (1-20 vol. %) were prepared and the surfaces of the supports were dipped for 5-10 seconds. The main disadvantage of this method is the pinholes formed during the settling of the suspension on the porous support.

To overcome the pinhole problem another method inspired from a United States Patent (Patent Number: 4,810,273, date of patent: May, 7, 1989, “porous ceramic filter”, invented by Tadanori Komoda) was tried which may be called as “wet-coating”. The supports were first boiled in water for replacing the air in the pores with water. Then the sides of the supports were sealed by using parafilm and a piece of plastic tape was wrapped to form a cylindrical die in which the coating suspension will be added. In this method the pinhole formation was expected to be eliminated since it was due to the air bubble formation and detachment from the relatively bigger pores/inhomogeneities of the support.

The third method used for intermediate layer formation was spin-coating. The necessary amount of suspension (~2mL) was added on the support and the spinning was

initiated. The spinning procedure was tried with both dry and soaked supports. The spinning regime was varied for well-spreading of the suspension. The regimes used in spin-coating were as given in Table 5.

Table 5. The parameters used in spin-coating procedure.

	Regime 5	Regime 6	Regime 6 Mod-1	Regime 6 Mod-2
Acceleration time (sec)	10	3	10	20
RPM / sec	250 / 60	125 / 90	125 / 30	125 / 5
Acceleration time (sec)	20	10	10	10
RPM / sec	1250 / 10	1250 / 30	1250 / 20	1250 / 20

The absence or presence of cracks in the coated layer before and after heat treatment was determined by using optical microscope (Olympus BX-60M). The microstructure and the homogeneity of the formed layer after heat treatment was investigated by using SEM (scanning electron microscope, Philips XL30 SFEG).

5.1.2.2. Second Intermediate Layer

The sols used in the formation of the second intermediate layer were either prepared by using aluminium isopropoxide (98%) or zirconium propoxide (70% in propanol). The alumina precursor (boehmite) sol was prepared with molar ratios of alkoxide / nitric acid (65%) / water as 1: 0.25: 100. Hot water (80° C) was added on aluminium isopopoxide powder and stirred for a couple of hours. The acid solution was added and stirred for another couple of hours for peptization.

The zirconia sol was prepared by using zirconium propoxide, propanol, water and nitric acid. The molar ratios greater than stoichiometric hydrolysis ratio (4 for zirconium tetra propoxide) was used to prepare colloidal zirconia sol. Different

alkoxide / water ratios were investigated for the determination of stable sol preparation parameters and their effects on sol particle size. Alkoxide was first diluted to different concentrations by using propanol to which a mixture of acid, water and rest of the propanol was added drop-wise. Further acid addition was used for the clarification of the blurriness (if there was) and the sol was stirred for up to 2-3 days to get a clear colloidal sol. The prepared colloidal sols were kept in refrigerator in order to prevent uncontrolled hydrolysis-condensation reactions.

The sols were dip-coated on the supports coated by first top layer for 5-10 seconds, dried and heat treated at 500° C / 2 hours (Carbolite CWF 1300). The heating and cooling was performed gradually (3° C / minute).

The particle size distributions of both alumina and zirconia sols were determined by using laser light scattering technique (Zetasizer 3000 HSA, Malvern Co.). The structures of the layers formed by dip-coating with these sols were determined by using optical microscope (Olympus BX-60M) before and after heat treatment. The microstructure and the homogeneity of the formed layer after heat treatment was analysed by using SEM (scanning electron microscope, Philips XL30 SFEG).

5.1.3. Top Layers

Sols which will be used in forming top layers were prepared by using mainly two alkoxides: Zirconium IV propoxide (70% in propanol) and Titanium IV propoxide (98%). The sols were either prepared by using only one alkoxide or different ratios of these alkoxides. The ratios of the Ti / Zr in the prepared mixed sols are given in Table 6. The sols were prepared by polymeric sol route. This route was preferred in order to form smaller sol particles which will enable preparation of a thin layer with small pores. The molar ratios of the components in the polymeric sol for alkoxide / propanol / nitric acid were 1: 15 (or 20): 1, respectively (if other ratios are not mentioned). These ratios were determined after preliminary experiments performed to obtain clear and stable sols. No extra water was added to the sols to prevent uncontrolled hydrolysis (i.e. the water in the added nitric acid was enough even was excess to supply the necessary water amount). The sol preparation procedure consists of adding mixture of nitric acid and

propanol to the alkoxide-propanol mixture drop-wise while stirring. The sols were further diluted (e.g. 2, 1, 0.5 wt.%) to prevent the formation of thicker coatings which are prone to crack and peel out.

The sols were coated via dip-coating procedure for varying durations (2-180 sec) and sol concentrations (0.1-8 wt. %). The heat treatment (calcination) of the coated layers was performed at varying temperatures (400°-600° C) for 0.5-3 hours with different heating/cooling regimes (0.5-3° C / min.) (Carbolite CWF 1300). The coated layers were protected from direct radiation via ceramic shields during heat treatment.

Ethylene glycol (EG) was used to modify the viscosity and drying kinetics of the sol layers. EG has an eight times higher viscosity (16 cp) than propanol (2 cp), the main component of the sol media. Its boiling point (BP) is also higher (197 °C) than propanol (97 °C). The higher viscosity hinders the uncontrolled suction of the sol into the porous structure with capillary forces and higher BP results a slower drying (i.e. EG acts like a DCCA (drying control chemical additive)). The amount of EG added was 25-75 vol. %.

Table 6. The molar ratios of elements in the sols.

Name of the sol	**TiProX (titanium propoxide)**	**ZrProX (zirconium propoxide)**
Full Ti	100	0
TiZr 7525	75	25
TiZr 5050	50	50
TiZr 2575	25	75
Full Zr	0	100

The aging of the sols (either pure or mixed) were performed at room temperature (RT) or in the oven (at 39° C) for various solid contents (0.1-2 wt. %). The formation and growth kinetics of the nanoparticles in the sols were monitored via laser light scattering technique. During aging of the sols supports were dip-coated (d-c) via sols with increasing average particle size to see the effects of solid content and aging conditions on particle growth and membrane formation. The supports were dip-coated

(d-c) via sols with various average particle sizes. The supports coated were heat treated and the integrity (or presence) of the layers were determined via the optical microscope or SEM. The supports with cracked layers were re-coated. The membranes with almost crack free layers were subjected to filtration tests.

Some other elements like iron (Fe) and boron (B) were introduced into the sols to investigate possible effects of these elements to the surface characteristics (i.e. surface charge of the membrane formed by dip-coating, drying and calcination of the sol prepared). The iron was introduced as $Fe(NO_3)_3.9H_2O$ (Iron (III) hydrate nonahydrate, min. 98%) with molar ratios Fe / alkoxide as 0.1-0.3 : 1 during sol preparation. The boron was introduced as boric acid (H_3BO_3) with molar ratios 0.1-0.2 : 1 for B / alkoxide ratio. The propanol ratio was increased with increasing amount of Fe or B added and prepared sols were kept in refrigerator to prevent uncontrolled hydrolysis and condensation.

The particle size distributions of sols were determined by using laser light scattering technique (Zetasizer 3000 HSA, Malvern Co.). The surface charges of the dried-calcined sols were determined by electrophoretic mobility measurements (Zetasizer 3000 HSA, Malvern Co.). For this purpose a small amount of dried and ground sol powders which were calcined at varying temperatures (400° - 600° C) were dispersed in a dilute salt solution (e.g. 10^{-3} M KCl) and injected to the instrument.

The thermal characterization of the sols were performed by using TGA / DTA (thermogravimetric analysis) instrument (Perkin Elmer Diamond) using dried and ground powders of sols (i.e. unsupported membranes).

XRD (X-Ray Diffraction, Philips X'PERT PRO) instrument was used to determine the crystal structure of the unsupported membranes. The effect of heat treatment on phase change was monitored by performing XRD analysis of samples heat treated at different temperatures.

5.2. Filtration Experiments

5.2.1. Clean Water Permeability (CWP)

The permeate flux of the prepared asymmetric composite ceramic membranes were determined by determining permeate flux at different trans-membrane pressure (TMP) values while deionised water was being circulated in the filtration unit. The permeate flux (L permeate / m^2 hour) which is the amount of liquid passing through a certain area of the membrane at a certain time was determined by measuring the time at which permeate fills a container with known volume. The permeate flux of deionised water shows the clean water permeability (CWP).

A filtration set-up whose layout is shown in Figure 21 was used during these experiments which consisted of a feed tank, a piston pump with a frequency controller, stainless steel piping, a flow-meter, a membrane holder and pressure gauges. The temperature of the liquid in the feed tank can be kept constant by using a heater-stirrer and an immersed cooler. The pressure was controlled by the needle valve on the exit of the retentate from piping system to feed tank to get a trans-membrane pressure (TMP) up to 100 bars. The TMP was defined as the difference between both sides of the membrane, as shown in the formula in Figure 21.

5.2.2. Retention Tests

The separation performance of a membrane is described by using its retention characteristics. The retention of neutral organics like saccharides (e.g. sugar) or polyethylene glycol (PEG) with varying MW are determined to monitor size exclusion of the membranes. For this purpose sugar (~5%) or PEG (0.5-1 %, MW: 1000 or 4000) solutions were prepared. The filtration experiments were performed for 150-180 minutes and samples were collected from both permeate and retentate streams. The concentrations of the material in the samples were measured by using either hand-

refractometer or digital refractometer (Mettler Toledo RE50) in Brix (Bx: the soluble material amount wt. %).

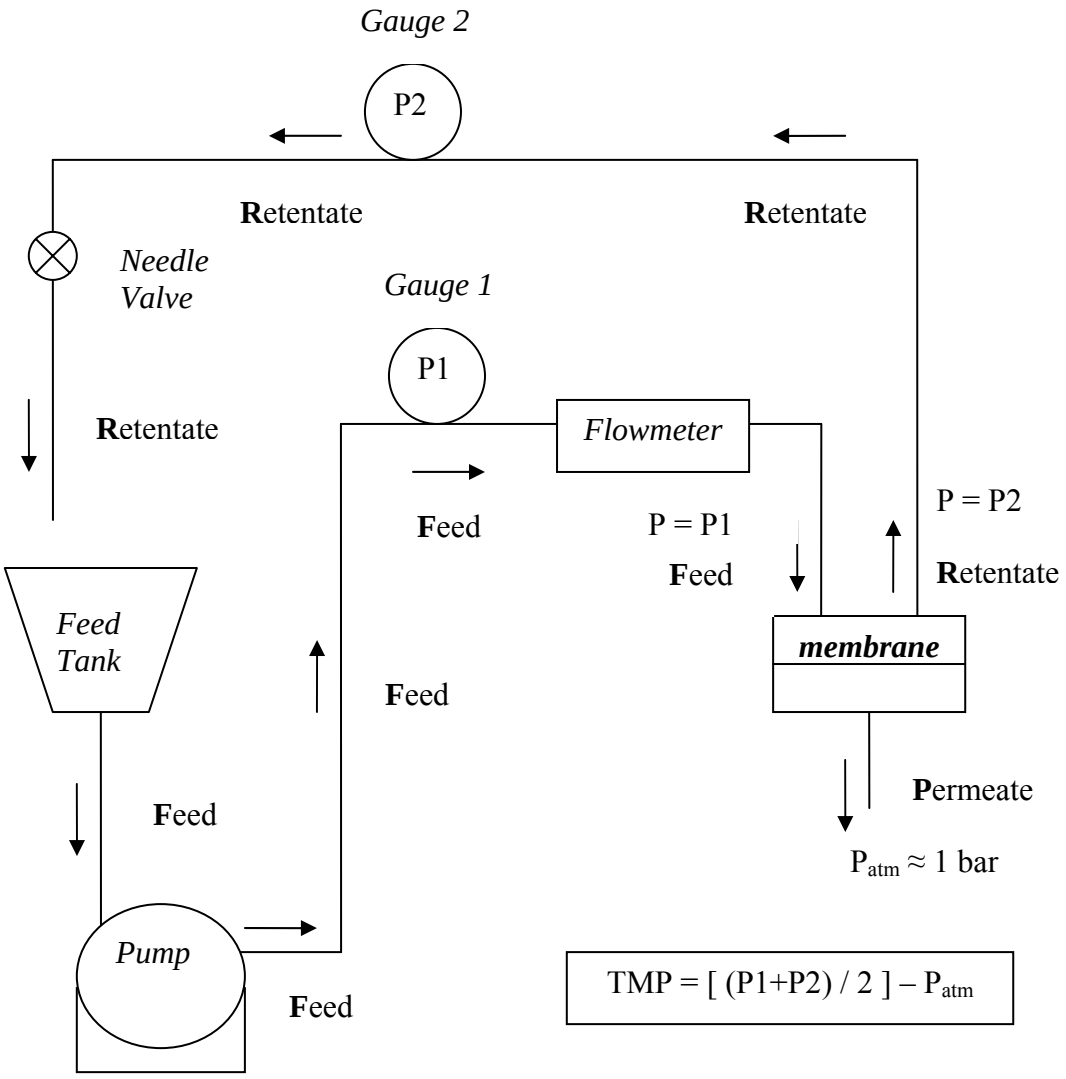

Figure 21. The diagram of filtration set-up.

The Bx values measured were converted into concentration by using a calibration curve (Figure 22) prepared by measuring Bx values of samples with known concentrations.

The retention (%) of a material was calculated as the difference between 1 and the ratios of the concentrations of the material in permeate and retentate streams i.e.;
$R\ (\%) = 100^* (1- (C_p / C_r))$.

The permeate flux was also measured during filtration experiments. The filtration experiments were performed at a TMP value of 5 bars mostly at room temperature without any temperature control unless otherwise stated.

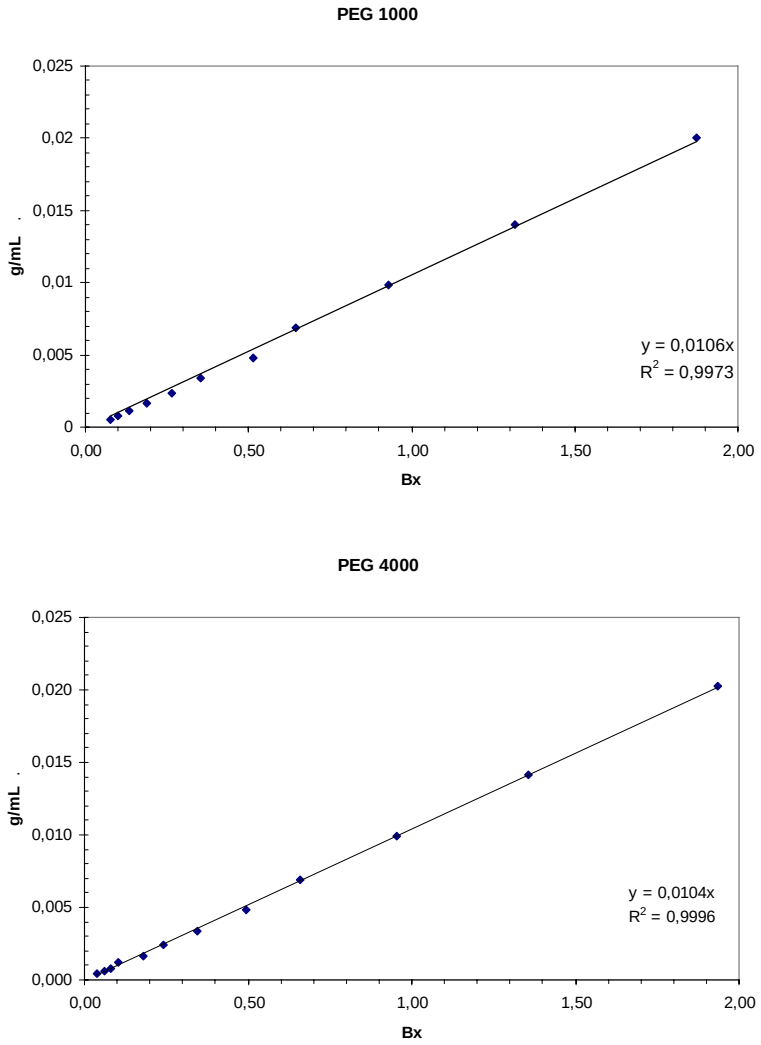

Figure 22. The Brix vs. concentration calibration curve for PEG 1000 and 4000.

CHAPTER 6

RESULTS AND DISCUSSION

6.1. Preparation and Characterization of Asymmetric Ceramic Composite Membranes

6.1.1. Supports

The supports were prepared by casting of alumina slips into polymeric dies. The suspensions were prepared with varying alumina / water volumetric ratios (up to 57.5 vol. % alumina). Different ratios of pore forming additives were used to investigate the possibility of increasing the CWP (i.e. decreasing the resistance to fluid flow) while preserving the mechanical integrity of the support under pressure.

A mixture of two starches (50 % Migros potato starch + 50 % Piyale wheat starch) or pure wheat or corn starch were used as pore forming additive. The mixture was expected to result in a more uniform interconnected porous structure since there is a considerable size difference between these two starches as shown in Figures 23 and 24.

The increase in amount of pore forming additives increased the porosity and also the CWP values as expected. The variation of the pore content with the additive level and heat treatment temperature is shown in Figure 25. An increment of starch addition from 5% to 10% resulted in 2-3% increase in porosity. Increasing heat treatment temperature from 1200°C to 1300°C caused nearly 5% lower porosity values (These results were obtained in the presence of 1.5% PVA in the slips).

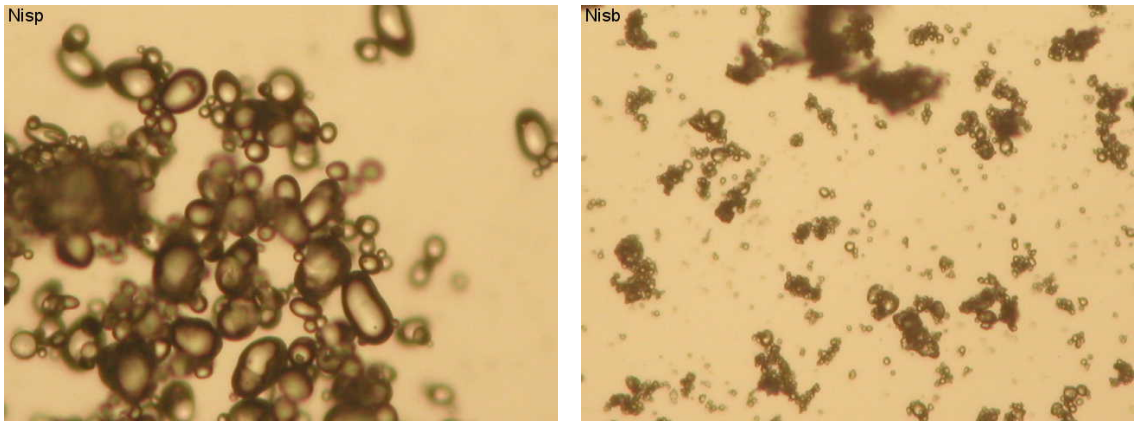

a) Potato starch, b) Wheat starch,

Figure 23. The photographs of two different starches taken at the same magnification by using optical microscope.

Another important criterion for membranes (or supports) is the interconnectivity of the pores since the closed pores will have no beneficial effect on increasing CWP. The change in amounts of open pores (i.e. interconnected porosity) is shown in Figure 26. The open porosity content for the 1200°C heat treated supports for two levels of additives were similar and was about 87-88% of the total porosity. There was about 5% decrease in open porosity most probably due to sintering of particles.

Higher values of total and open porosity will increase the permeate flux through the membrane. The membrane should also preserve its integrity while in use under high pressures and strikes of the high pressure pump. The heat treatment temperature was chosen as 1300°C for alumina supports prepared from Alcoa powder due to the frequent mechanical failures observed for the 1200°C heat treated supports.

The composition of the ceramic slips used to cast supports was also necessary to be regulated in order to prepare supports with desired dimensional stability. Especially the ceramic powder / water ratio was very effective on the uniform dimensional shrinkage. The increasing amounts of water (over 50 volume %) caused irregularities in the shape. The resulting supports were concave after heat treatment, probably due to slower sedimentation of finer particles in the slip in the presence of relatively higher water amounts. Some other irregularities on the surface of the supports were observed due to inhomogeneous casting when the viscosity of the slip was relatively high. The water, ceramic powder, dispersant (Darvan-C) and pore forming additive contents and the order of their addition were somehow regulated to overcome these irregularities, as

mentioned before. The pore forming additives were added to water and the ceramic powder was added slowly to this uniform starch suspension while stirring in an ultrasonic bath. Dispersant was partially added to the starch suspension before the ceramic powder addition while the rest was added during powder addition. The dies were coated with vaseline for easier release during forming.

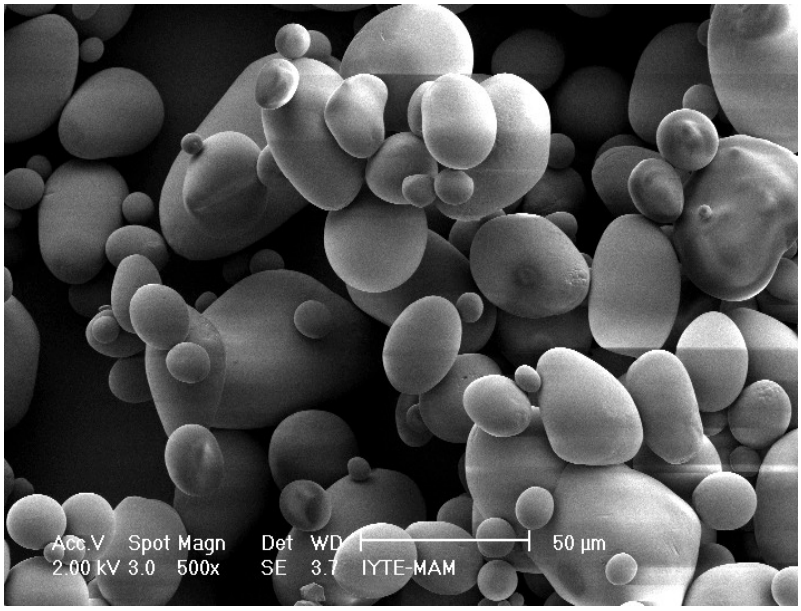

a) Potato starch

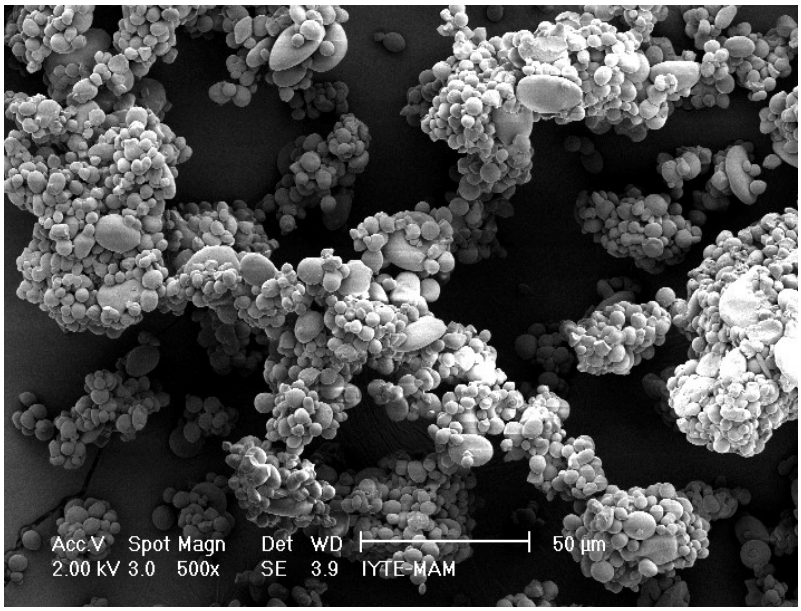

b) Wheat starch

Figure 24.The SEM micrographs of potato (a) and wheat starches (b).

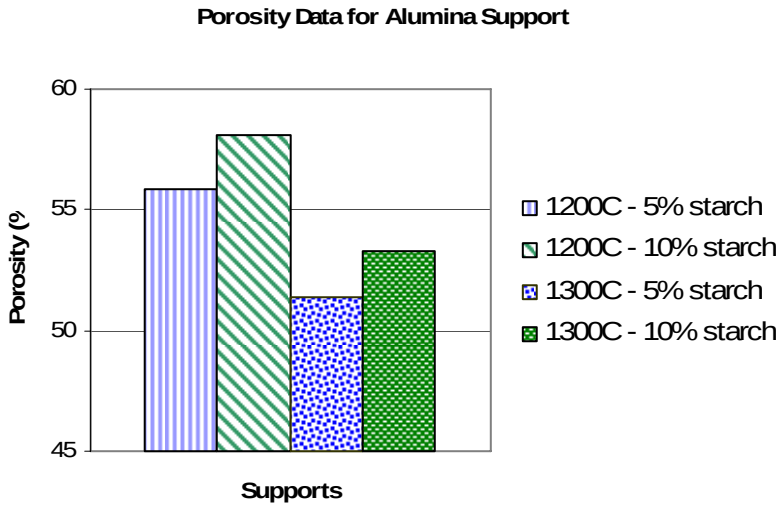

Figure 25. The change in porosity with respect to additive amount and heat treatment temperature.

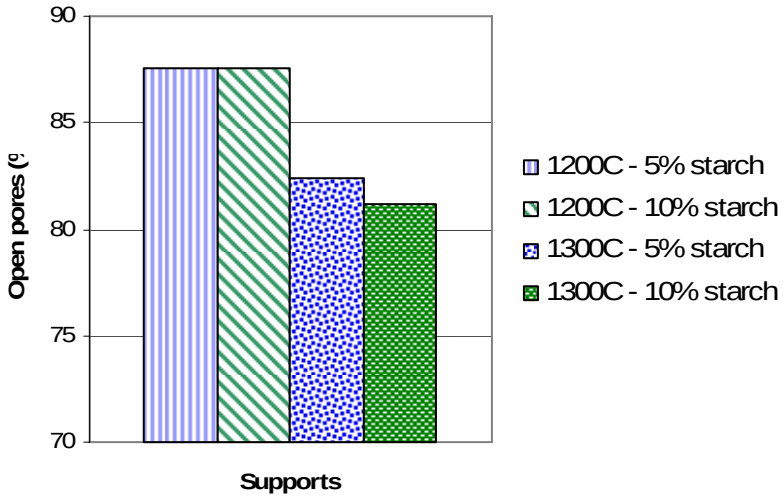

Figure 26. The change in open (interconnected) porosity with respect to additive amount and heat treatment temperature.

The change in the clean water permeability (CWP) values with respect to pore forming additive amount with varying trans-membrane pressure (TMP; the pressure difference between two sides of the membrane) is shown in Figure 27. The results for supports heat treated at 1300°C are given in L /m^2 hour. The permeate flux increased with increasing TMP values and this increase was more than expected for higher levels

of pore forming additives. This pronounced effect may be due to the swelling of the starch particles upon soaking.

The microstructures of the supports were investigated by using SEM (Scanning Electron Microscope, Philips XL30 SFEG). There were different types of pores with different sizes. These were formed by bubbles formed during casting, decomposition of the pore former and partially sintered alumina particles. Pores formed by air bubbles left in the slip resulted in the largest pores and the pores between partially sintered powder particles were the smallest pores in the support structure as shown in Figures 28-31.

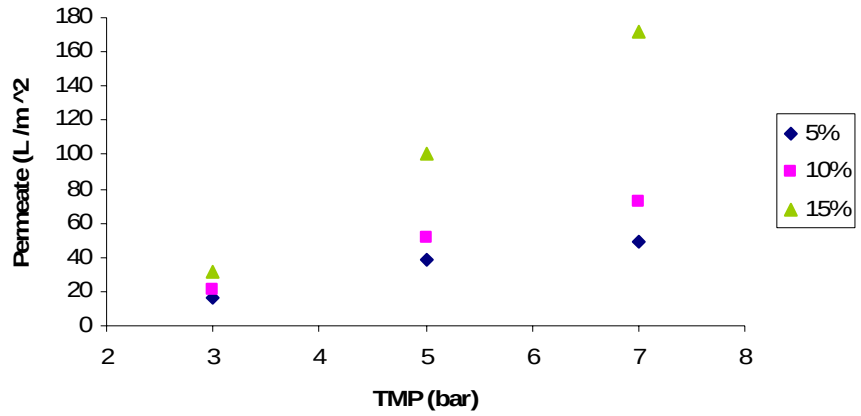

Figure 27. The clean water permeability (CWP) values vs. trans-membrane pressure (TMP) for supports prepared with different amounts of pore-forming additives (starch mixture) and heat treated at 1300°C.

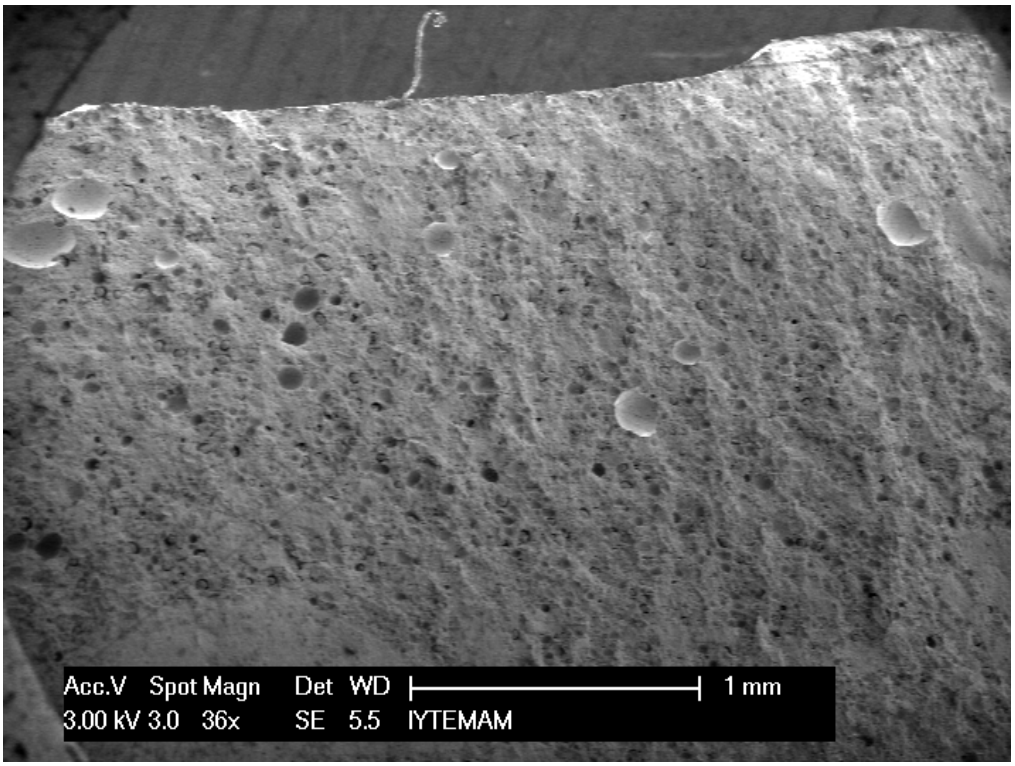

Figure 28.The SEM image of cross-section of alumina support prepared by using 10 % wheat starch as pore-forming agent.

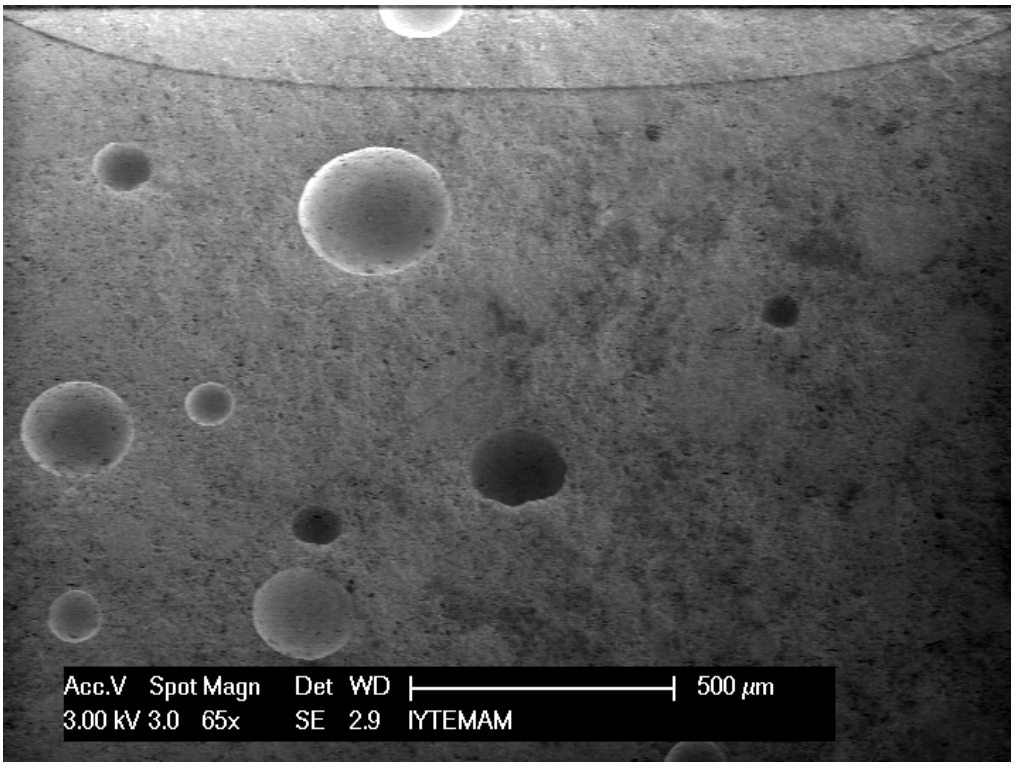

Figure 29. The SEM image of cross-section of alumina support showing the pores formed by air bubbles left in the ceramic slip during casting and / or decomposition of starch.

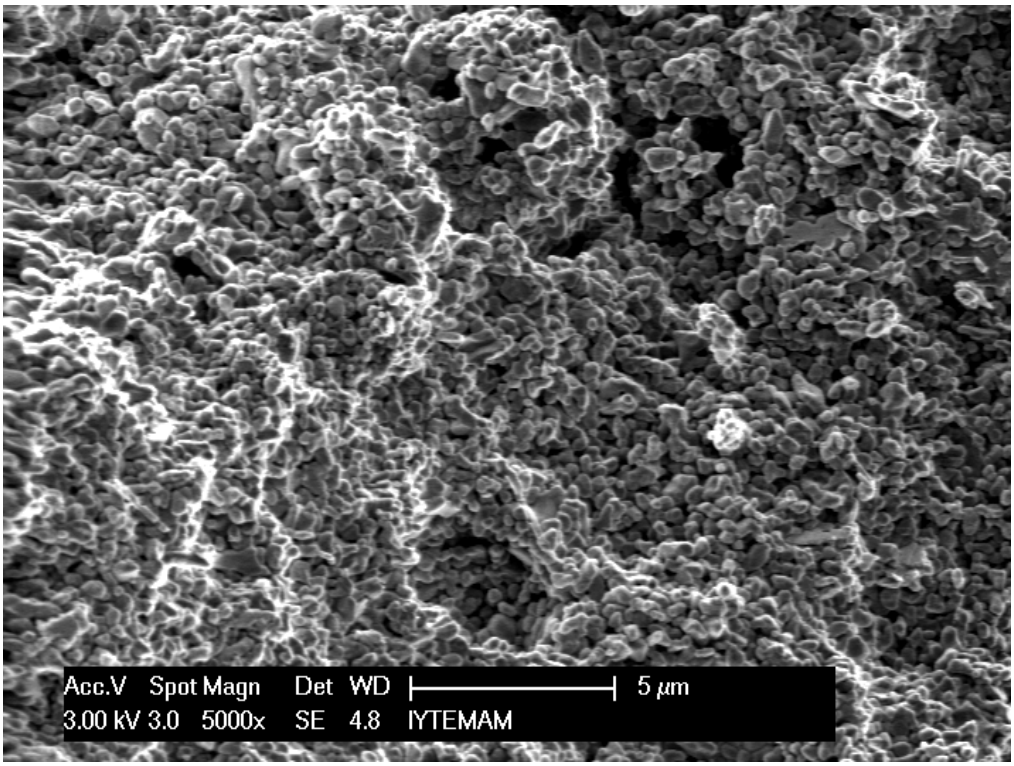

Figure 30. The SEM image of cross-section of alumina support showing the microstructure and pores left by decomposition of starch.

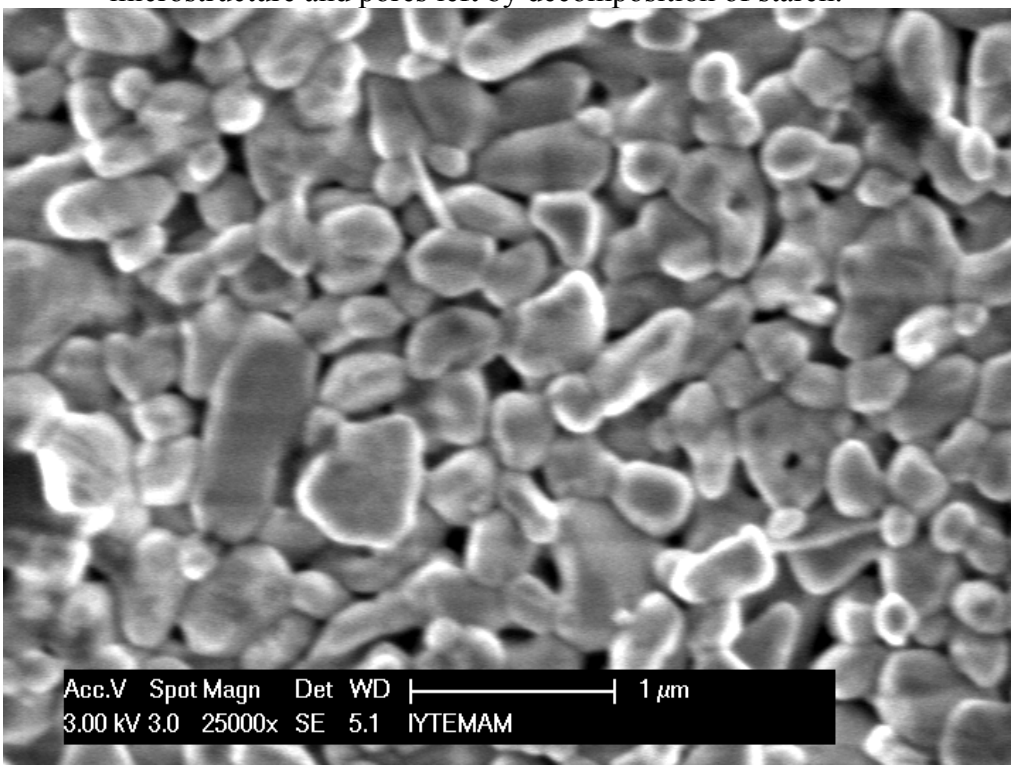

Figure 31. The SEM image of cross-section of alumina support showing the microstructure and interconnected pores between partially sintered particulates.

6.1.1.1 Supports prepared via higher solid content suspensions

Higher alumina content (e.g. 53-57 vol. %) slips were used for the casting of supports with a dense and homogeneous microstructure with defect free top surfaces. The top layer was formed on the surface of these supports without intermediate layers. Since the solids content of the suspension was increased the alumina particles were packed to a relatively higher density forming denser surfaces which could retain the coated sol to form the top layer without intermediate layers. The relatively denser surface of a ceramic support cast from a 53 vol. % Alcoa alumina suspension is shown in Figures 32 and 33.

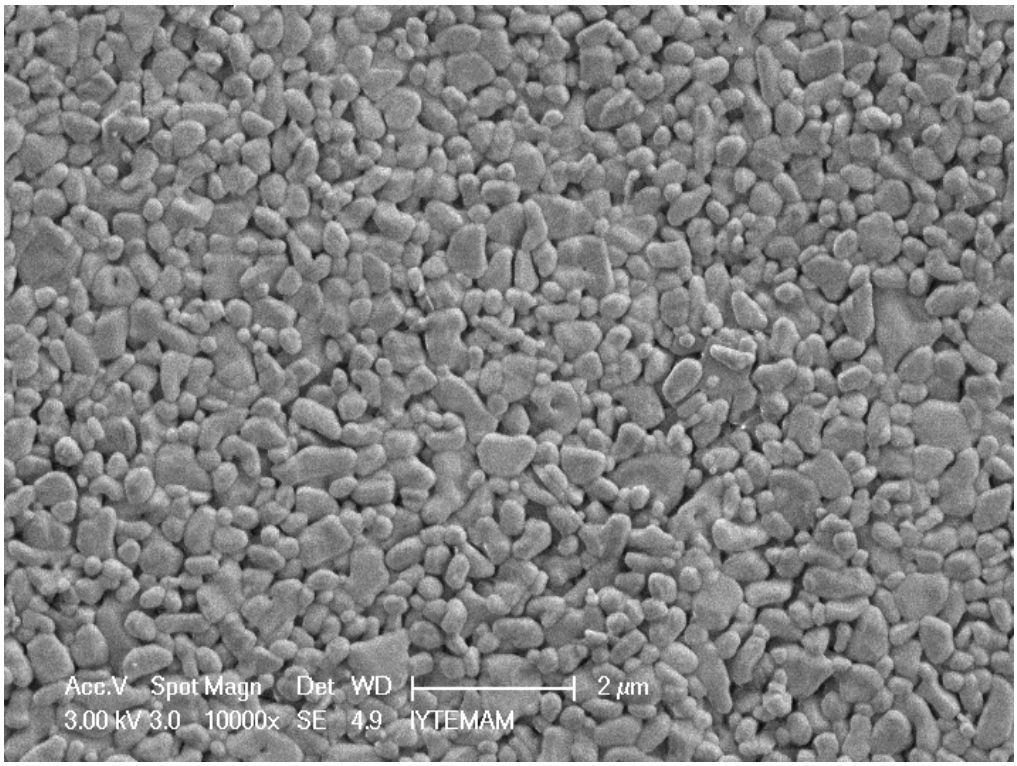

Figure 32. The SEM image of surface of alumina support prepared via 53 vol. % Alcoa alumina suspension (ht 1300° C /2h).

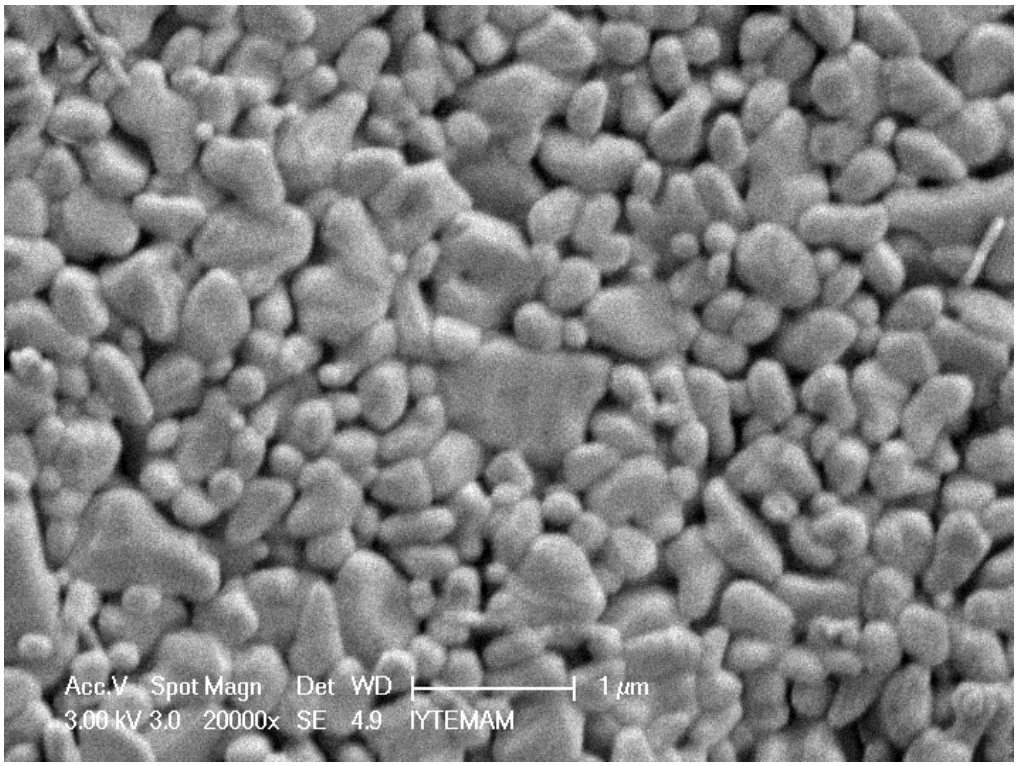

Figure 33. The SEM image of surface of alumina support prepared via 53 vol. % Alcoa alumina suspension (ht 1300° C /2h).

6.1.1.2 Supports with double layers

The double layer supports were prepared both by casting starch-free and starch containing alumina suspensions successively. The first layers were dried prior to second layer casting. In a typical support preparation procedure about 1 ml of starch-free Alcoa alumina suspension was pipetted into the die and upon the addition of one drop of surfactant immediate spreading of the suspension on the die surfaces was observed. Casting of the second porous layer was conducted by pipetting 4 ml of 7.5 % corn starch containing suspension on the semi-dried layer. The surface of the starch-free support layer facing the die after heat treatment at 1300°C for 2 hours can be seen in Figure 34. The dark regions in the pictures are most likely due to the cavities as seen in Figure 35.

The porous surface of the support facing air can be seen in Figures 36-39. This surface showed different characteristics. There were zones with whiskery formations as can be seen in Figures 36-38. These morphologically different phases may most likely

be due to the remnants of the surfactant anionic sodium containing compounds. There were also fully sintered (probably glassified) zones as can be seen in Figure 38-39 which may again be due to sodium containing liquid phases. Figure 40 shows the microstructure of both the cross-section and the surface.

The cross-section of the with-starch layer can be seen in Figure 41. The starch – free casting formed a denser layer as can be seen in Figure 42. The thickness of the denser layer without bigger pores due to absence of starch was ~50 μ. The further coatings would be on this denser layer. Therefore its homogeneity and thickness were important. The surface was homogeneous but with some stain like zones as can be seen in Figure 34 and 35 probably due to surface roughness. The thickness should be at least as thick as the immersion path length of the further coating material. The 50 μ thick denser layer could be considered sufficiently thick to stop the coating material to form a layer above it.

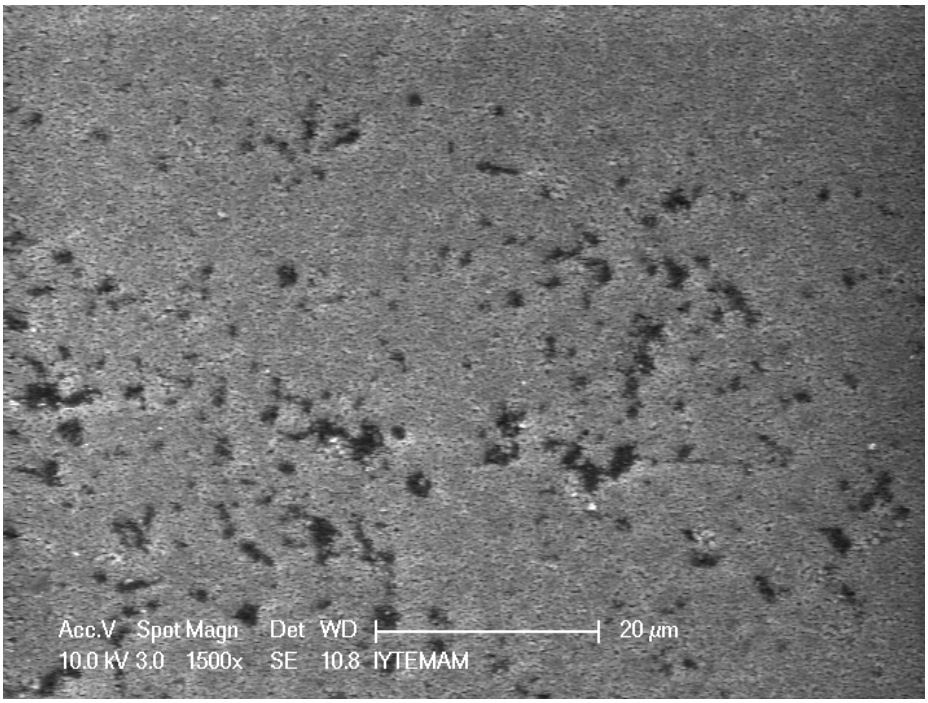

Figure 34. The SEM micrograph showing the surface of starch- free alumina layer after heat treating at 1300° C / 2h.

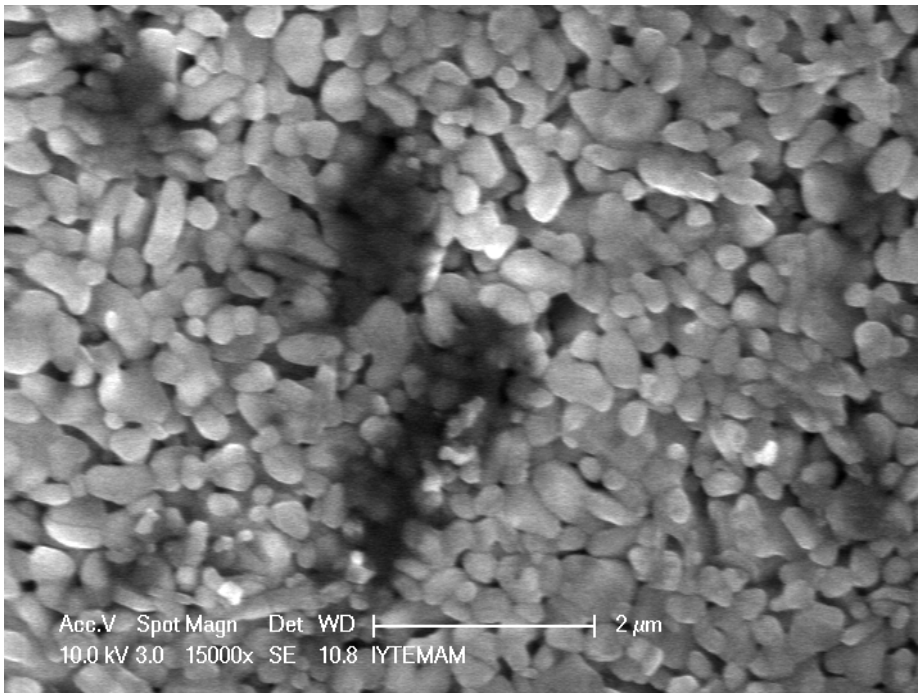

Figure 35. The SEM micrograph showing the surface of starch- free alumina layer after heat treating at 1300° C / 2h.

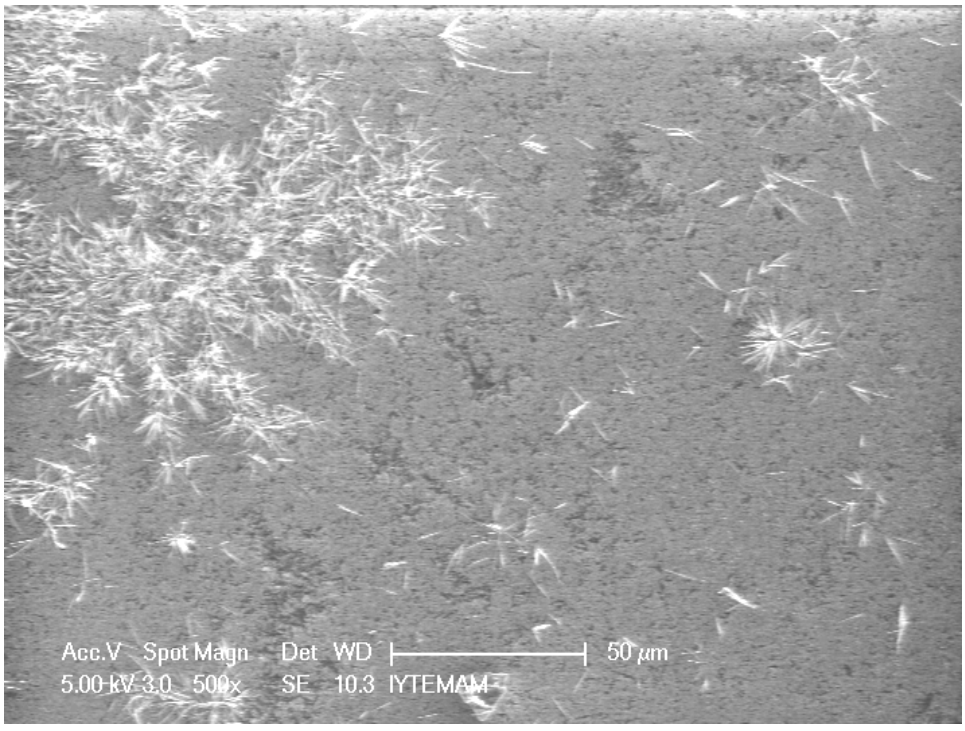

Figure 36. The SEM micrograph showing the surface of with-starch alumina layer after heat treating at 1300° C / 2h with whiskery formations.

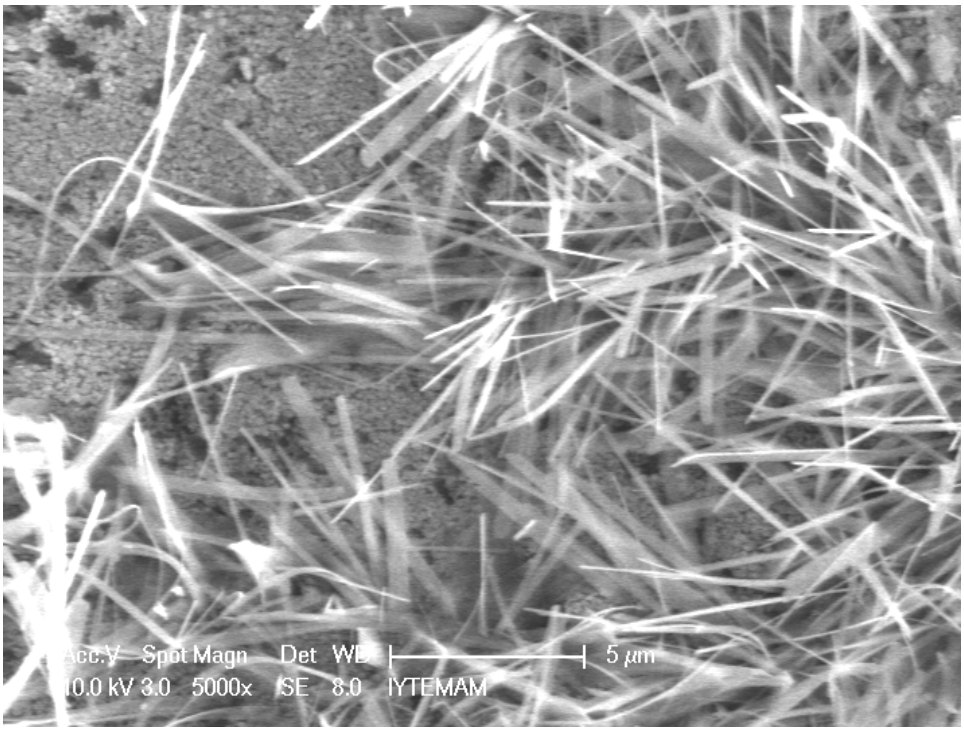

Figure 37. The SEM micrograph showing the surface of with-starch alumina layer after heat treating at 1300° C / 2h with whiskery formations.

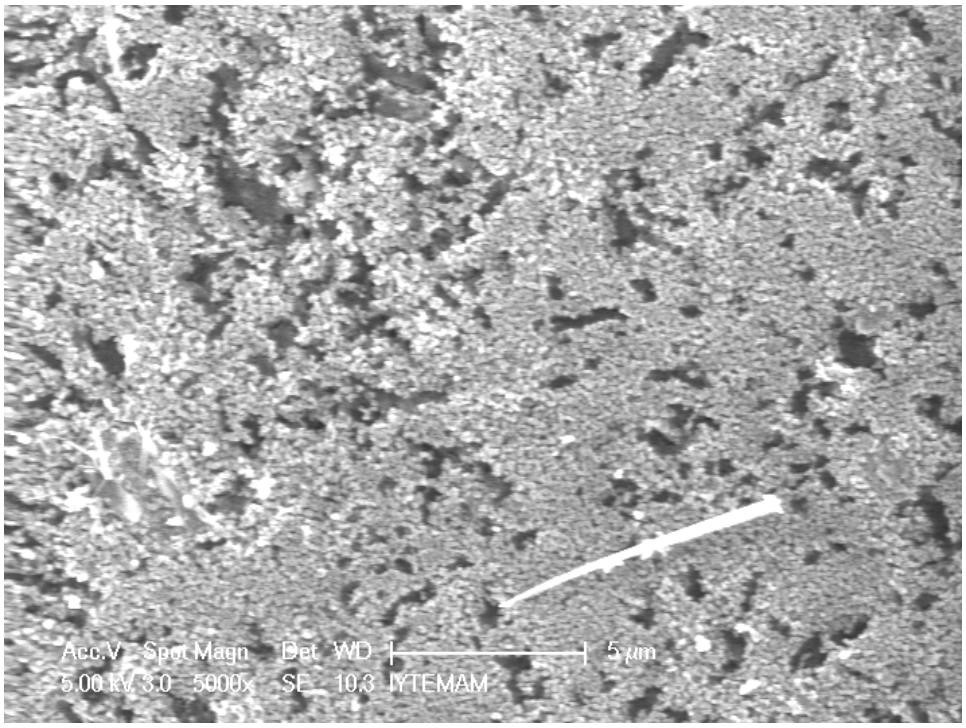

Figure 38. The SEM micrograph showing the surface of with-starch alumina layer after heat treating at 1300° C / 2h with glassy formations.

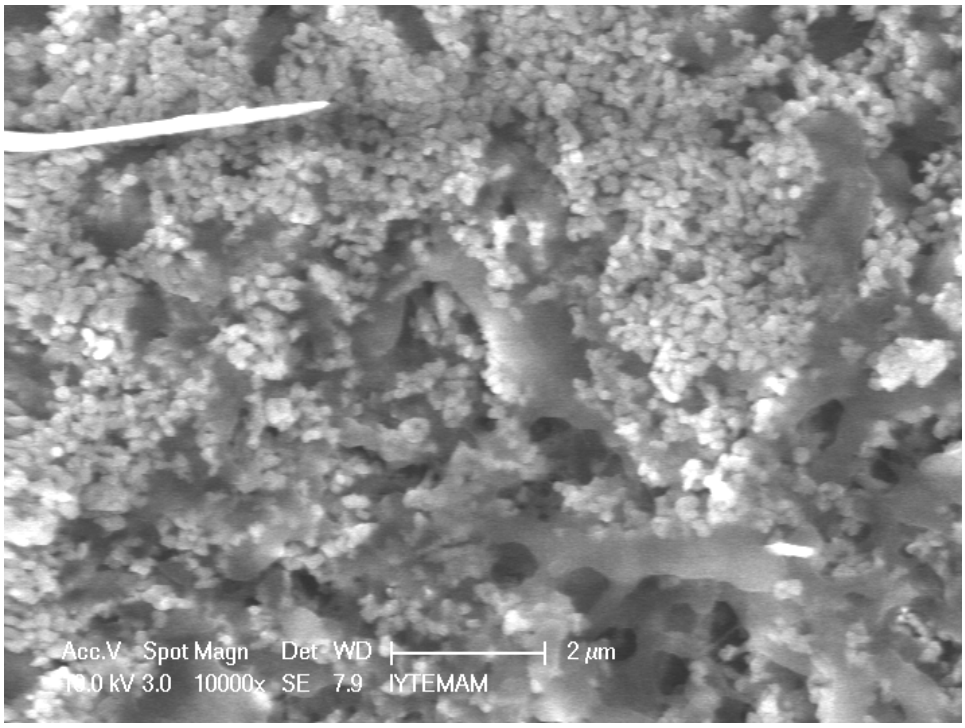

Figure 39. The SEM micrograph showing the surface of with-starch alumina layer after heat treating at 1300° C / 2h with glassy formations.

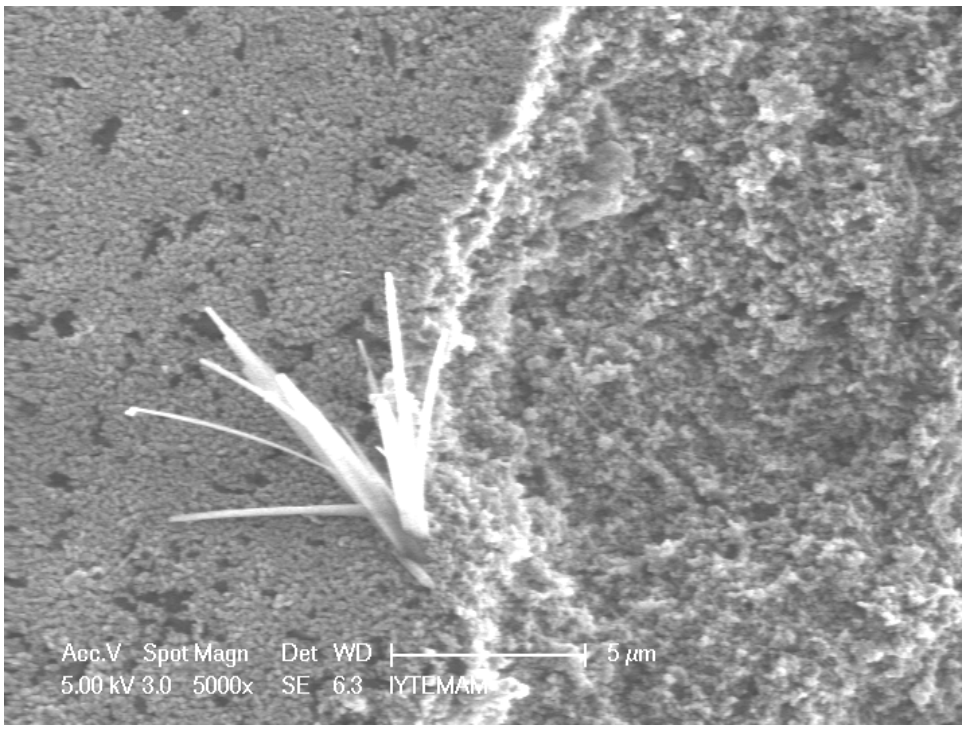

Figure 40. The SEM micrograph showing the surface and cross-section of with-starch alumina layer after heat treating at 1300° C / 2h with whiskery formation on surface.

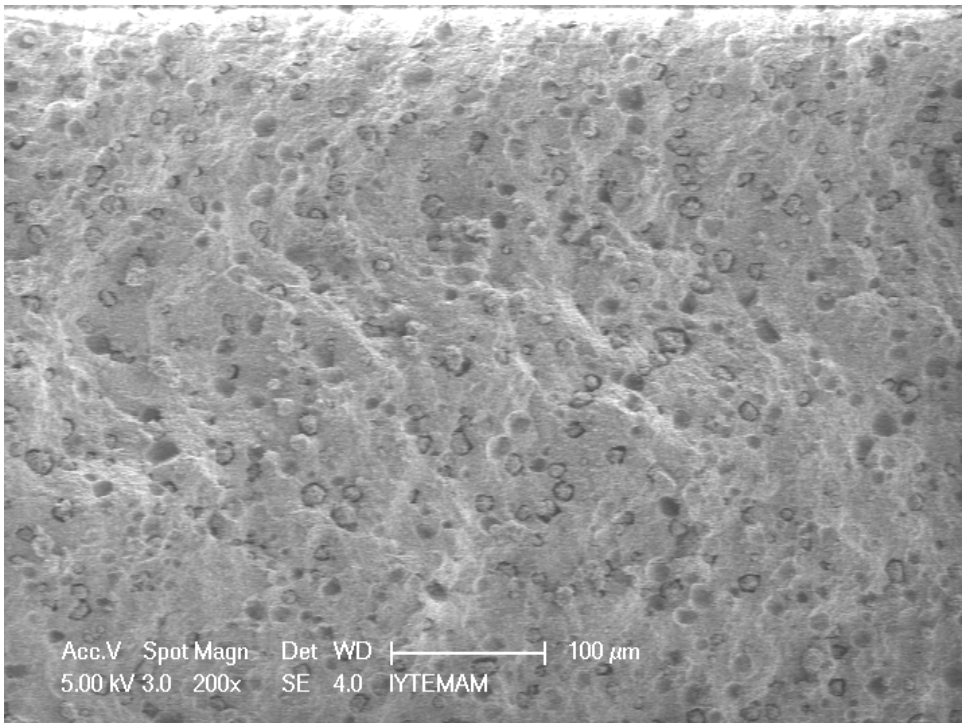

Figure 41. The SEM micrograph showing the cross-section of with-starch alumina layer after heat treating at 1300° C / 2h.

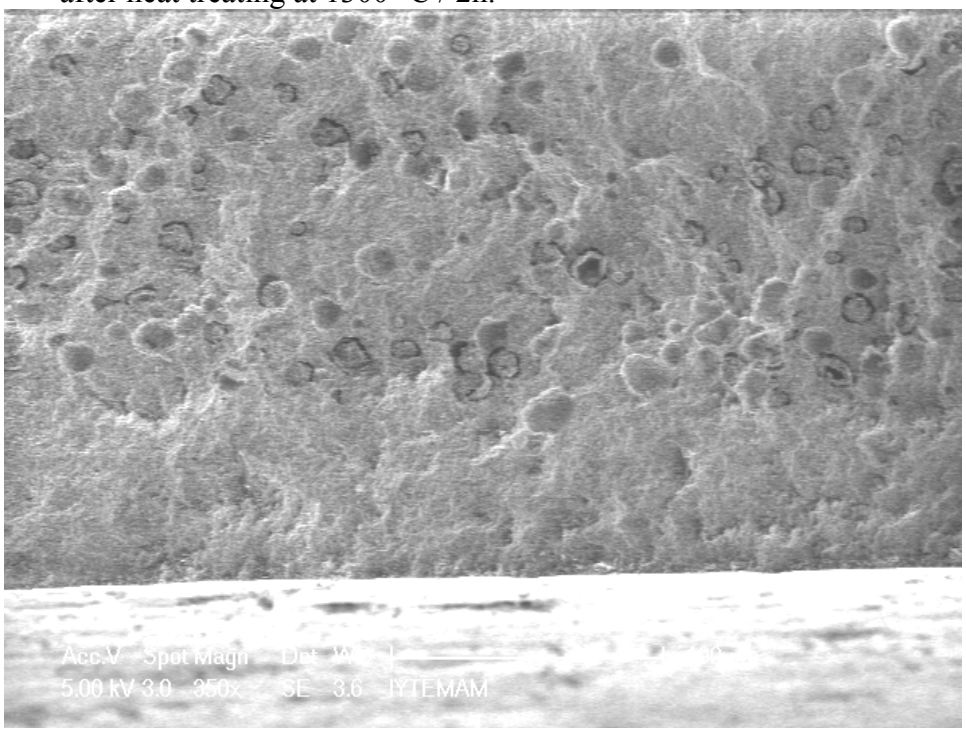

Figure 42. The SEM micrograph showing the cross-section of with-starch and starch-free alumina layer after heat treating at 1300° C / 2h.

Double layer supports were also prepared by using relatively finer ceramic powder (AKP-50 alumina). For this purpose, starch-free and 10% corn starch containing suspensions were cast on one another and heat treated at relatively lower temperatures (900°-1100° C instead of 1300°-1350° C as for Alcoa alumina, the coarser powder). The starch-free suspension was first poured and it was spread via addition of some drops of surfactant solution and mixing. There were some cracks after heat treatment on the surface as can be seen in Figure 43 formed probably due to inhomogeneous casting after addition of surfactant solution.

The thickness of the denser layer was ~50-100 μ as can be seen cross-section micrograph of this support in Figure 44 and th pores were homogeneously distributed in the more porous thicker layer as shown in Figure 45.

The other surface of the support (starch-free part) facing air instead of the die was free of cracks and was smoother as shown in Figure 46 again with some stain-like small zones.

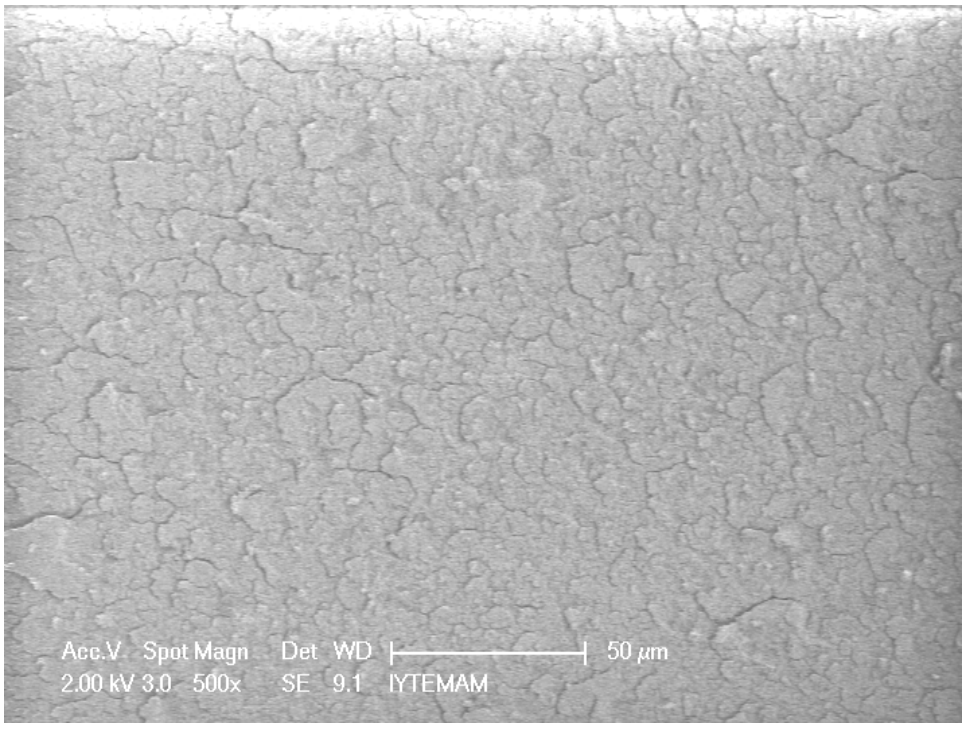

Figure 43. The surface of the AKP-50 alumina support (starch-free layer) facing the die after heat treatment at 1100° C / 2h.

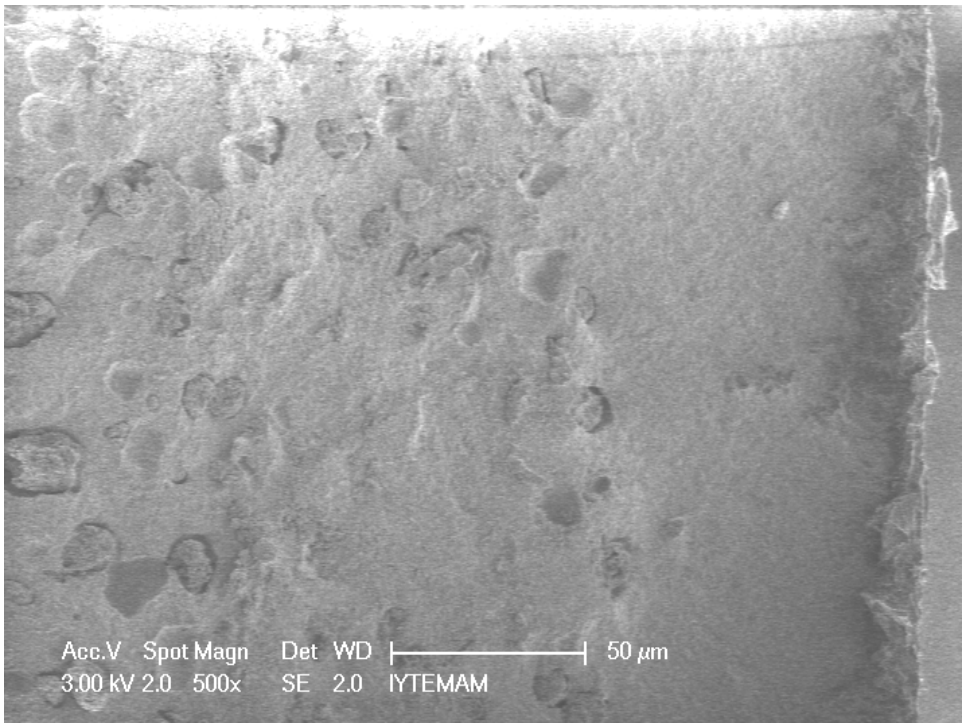

Figure 44. The SEM micrograph showing the cross-section of the double layer AKP-50 alumina support (1100° C / 2h) with more porous layer (10% corn starch) and denser and thinner layer (starch-free).

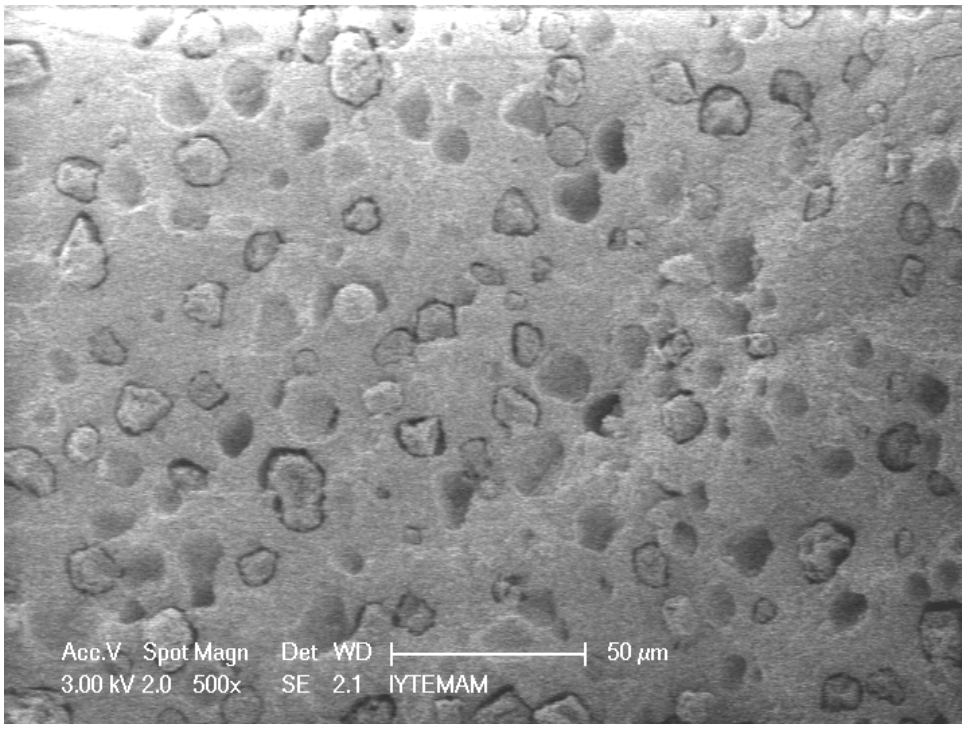

Figure 45. The SEM micrograph showing the cross-section of more porous part of the double layer AKP-50 alumina support (1100° C / 2h) formed via 10% corn starch.

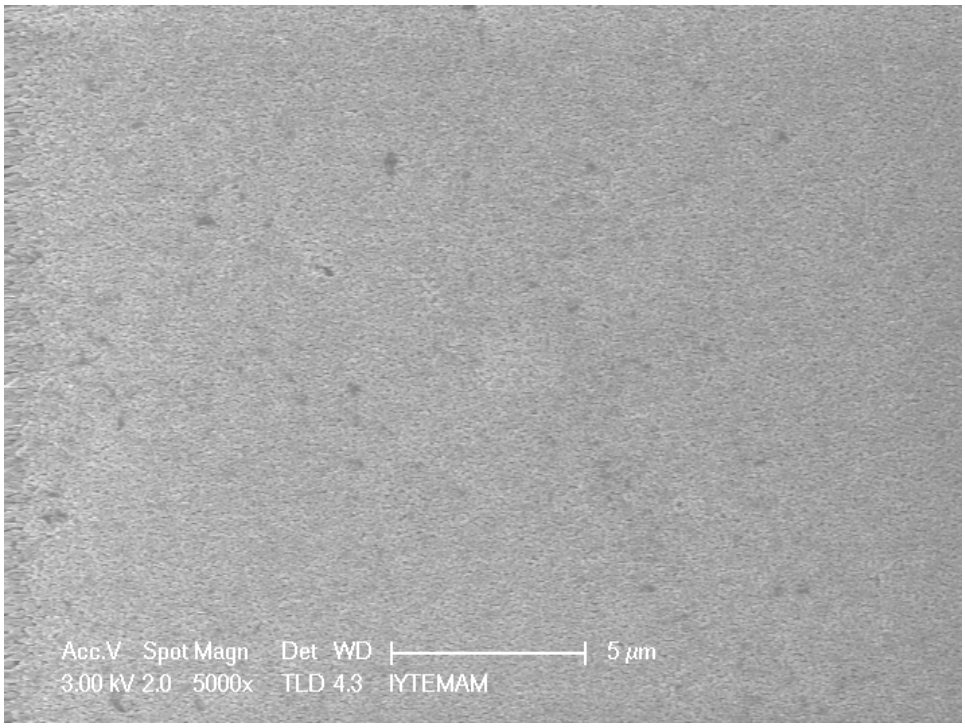

Figure 46. The SEM micrograph showing the surface of more porous part of the double layer AKP-50 alumina support (1100° C / 2h) formed via 10% corn starch.

There were cracks on the (die-facing) surface of the support prepared via (starch-free) AKP-50 alumina suspension and diluted surfactant solution as shown in Figure 47. This support was prepared by casting starch free suspension (~50 vol. %), drying and re-casting another thin layer via ~45 vol. % suspension to heal the cracks during drying of the first starch-free layer. The cracks were not totally healed as can be seen in Figure 48 since the healing suspension was too viscous to penetrate the cracks. This double coating of denser layer increased its thicknes to ~300-400 μ as can be seen in Figure 49. The surface of more porous layer (facing air) formed via 10% corn starch containing AKP-50 suspension was smooth as can be seen in Figure 50, even smoother than the surface of the denser layer (starch-free) facing the die. This smoother surface (facing air) could be used for further coatings since the smoothness of the surface to be coated was thought to affect the coating homogeneity positively. The casting order of the starch-free and starch containing suspensions were changed to have the denser layer (starch-free) over the more porous layer (i.e. facing air instead of facing die surface). For this purpose, the 10 % corn starch containing AKP-50 alumina suspension was poured first. 2 mL of the starch free suspension was pipetted on it after drying at ~43° C for 20-25 minutes and left drying at the same temperature. After pipetting the starch-

free suspension some surfactant solution was either added to spread the suspension on starch containing layer and cover the entire surface (S (+)) or more starch free suspension was used to cover the surface without surfactant addition (S (-)).

The surface of the S (+) support (of the denser layer, facing air) was smooth as can be seen in Figure 51, but there were some wavy zones. The thickness of the denser layer formed via 2 mL of ~50 vol. % suspension was ~800μ as can be seen in Figure 52.The surface of the more porous layer (10% corn starch containing) facing die was not very smooth as can be seen in Figure 53.

The surfaces of the samples prepared without surfactant solution addition (S (-)) were not as smooth as surfaces of surfactant added samples. There were some gap-like, stain-like zones on the surface of denser layer facing air as can be seen in Figure 54. The surface of the more porous layer (10% corn starch) facing the die was with relatively bigger pores due to decomposition of the starch touching the surface in the absence of surfactant as can be seen in Figure 55. These results show the possible beneficial effects of addition of surfactant to have a smoother surface at both sides of the support.

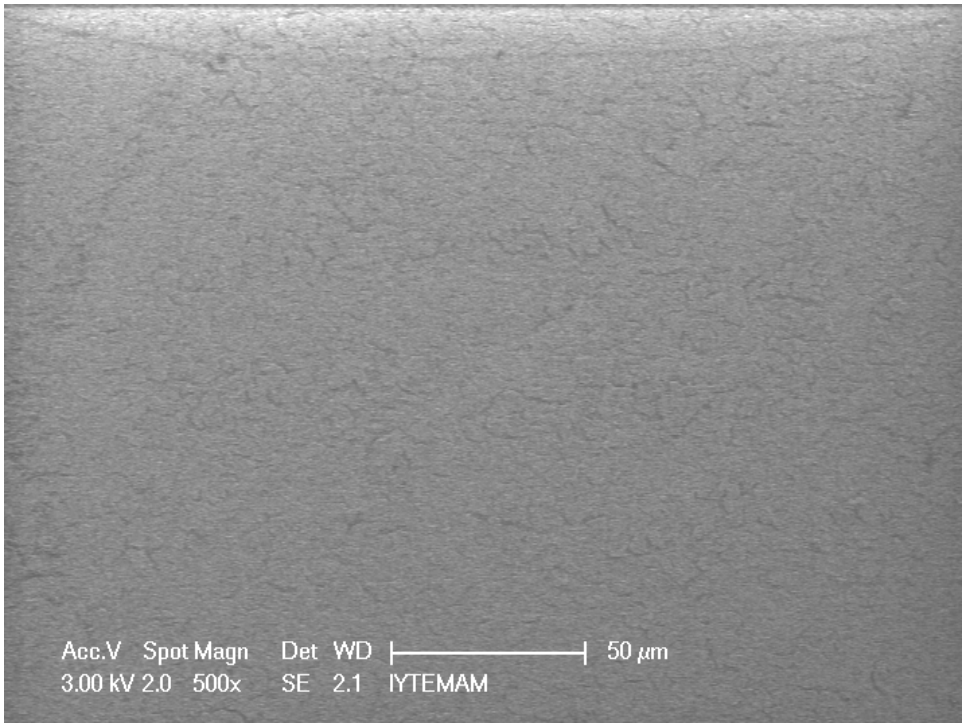

Figure 47. The SEM micrograph showing the surface of denser part of the double layer AKP-50 alumina support (1100° C / 2h) formed via double casting of starch-free suspension.

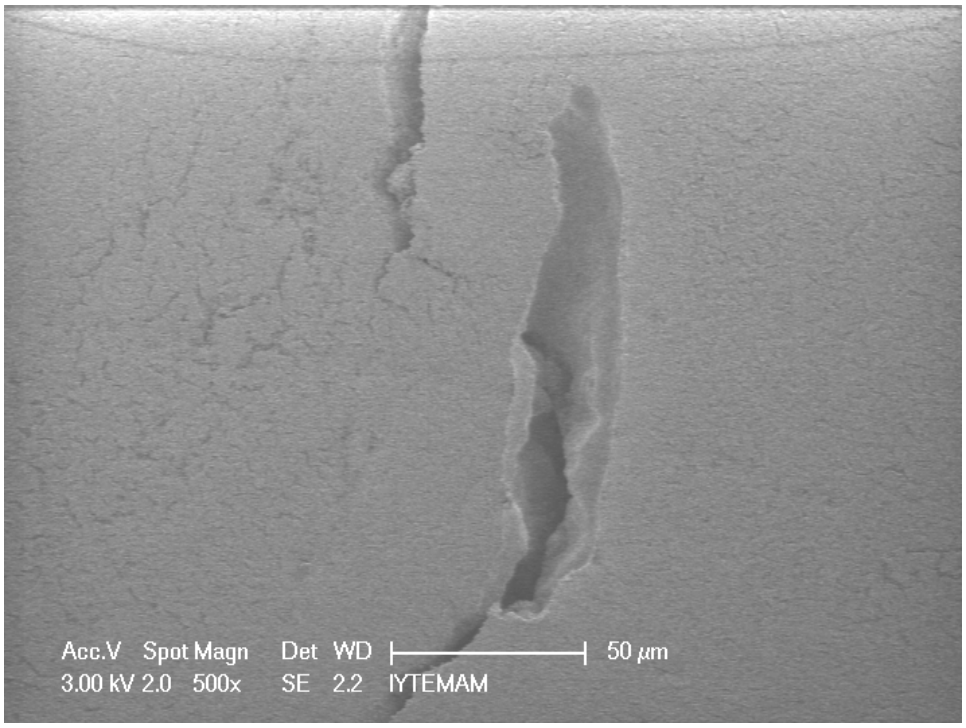

Figure 48. The SEM micrograph showing the surface of denser part of the double layer AKP-50 alumina support (1100° C / 2h) formed via double casting of starch-free suspension.

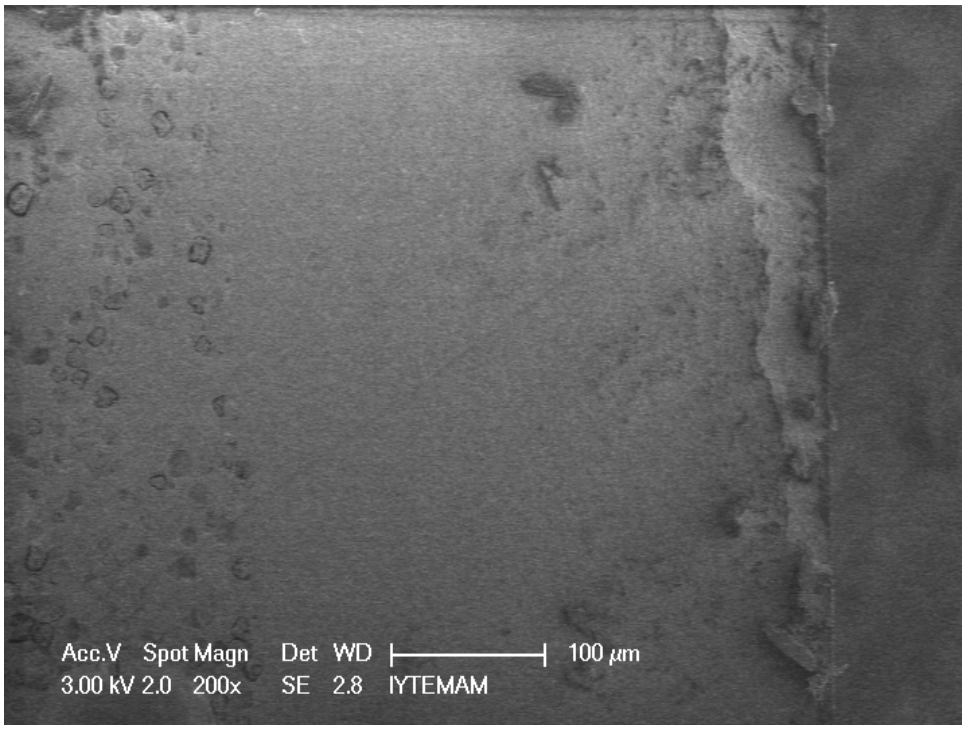

Figure 49. The SEM micrograph showing the cross-section of denser part of the double layer AKP-50 alumina support (1100° C / 2h) formed via double casting of starch-free suspension and casting 10% corn starch suspension for once.

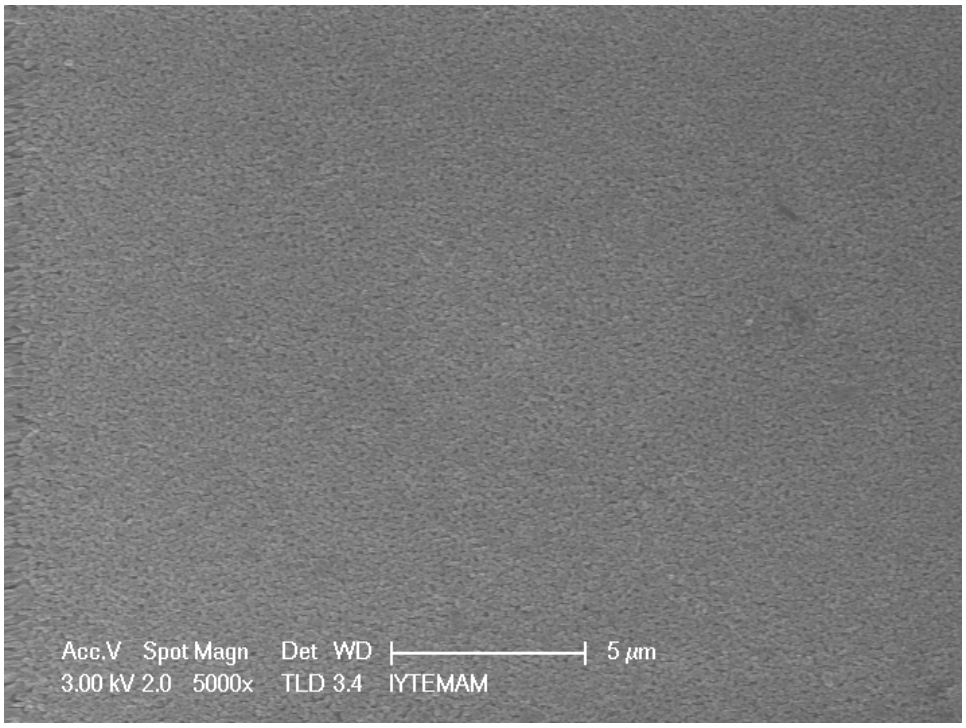

Figure 50. The SEM micrograph showing the surface of more porous part of the double layer AKP-50 alumina support (1100° C / 2h) formed via casting 10% corn starch suspension for once.

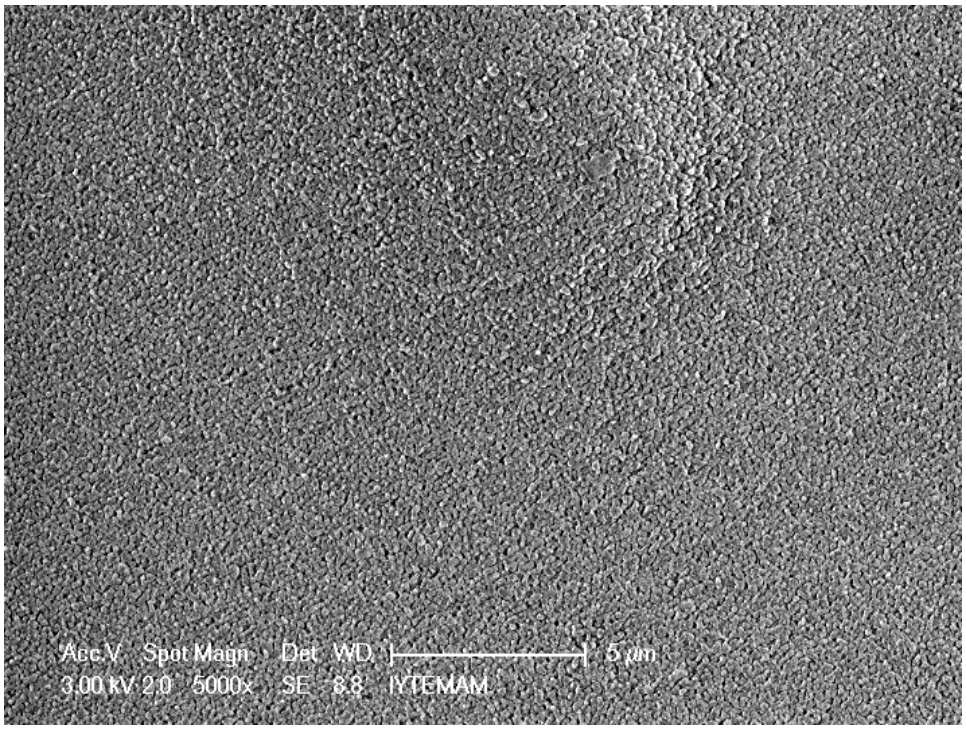

Figure 51. The SEM micrograph showing the surface of the denser layer of the AKP-50 support (1100° C / 2h) (S (+)) cast after 10% corn starch containing porous layer.

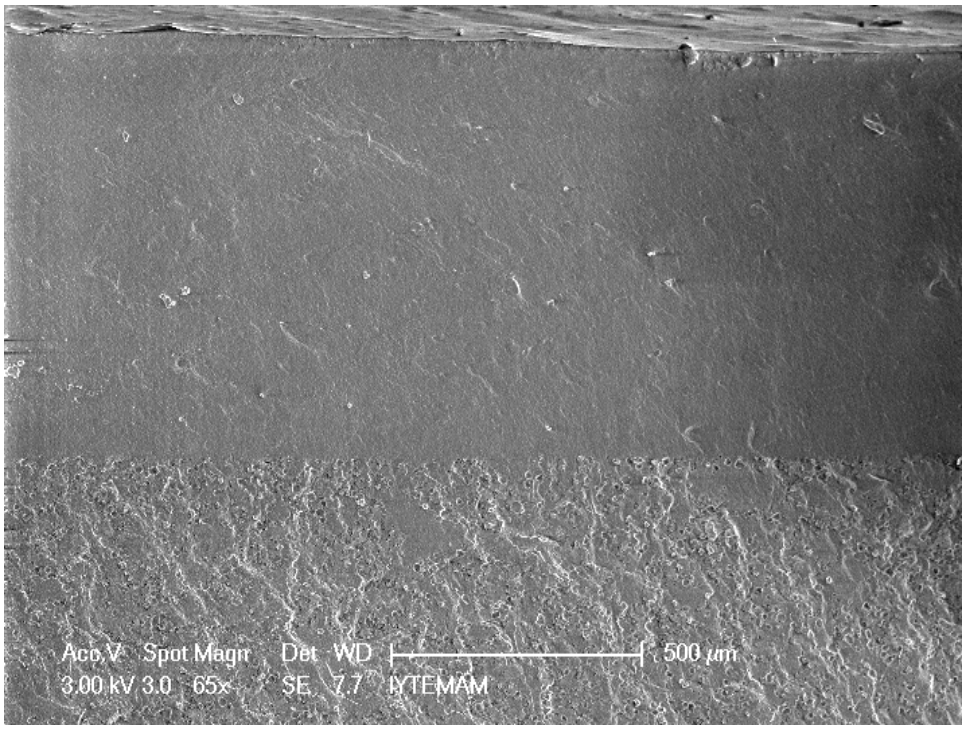

Figure 52. The SEM micrograph showing the cross-section of the double layer AKP-50 support (1100° C / 2h) (S (+)) cast via starch-free (2 mL) and 10% corn starch containing suspensions.

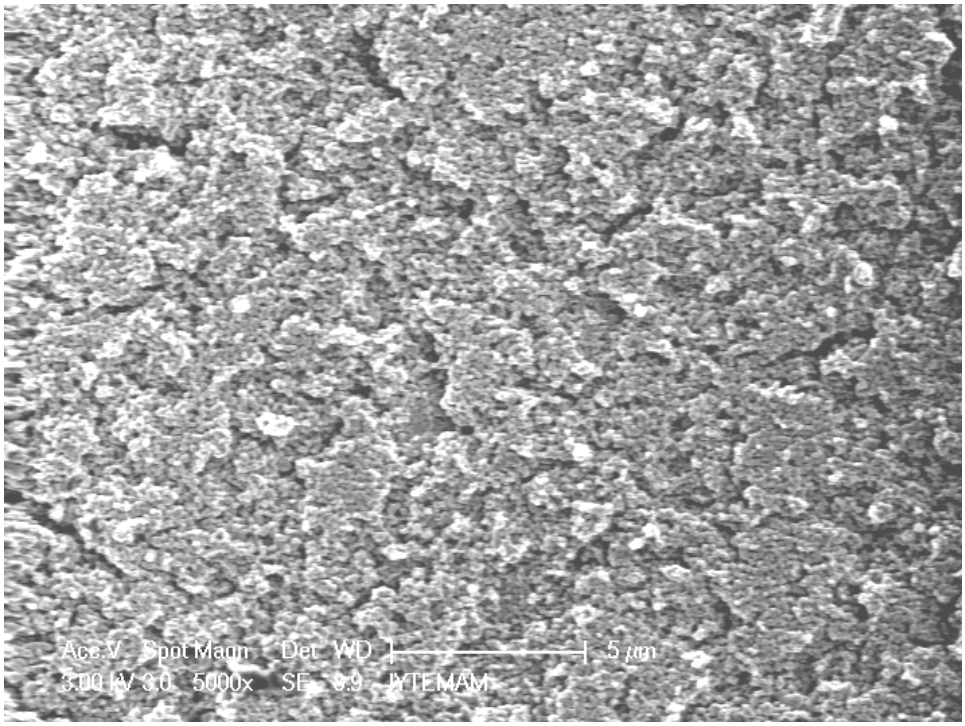

Figure 53. The SEM micrograph showing the surface of the more porous layer of the double layer AKP-50 support (1100° C / 2h) (S (+)) cast via 10% corn starch containing suspension (facing die).

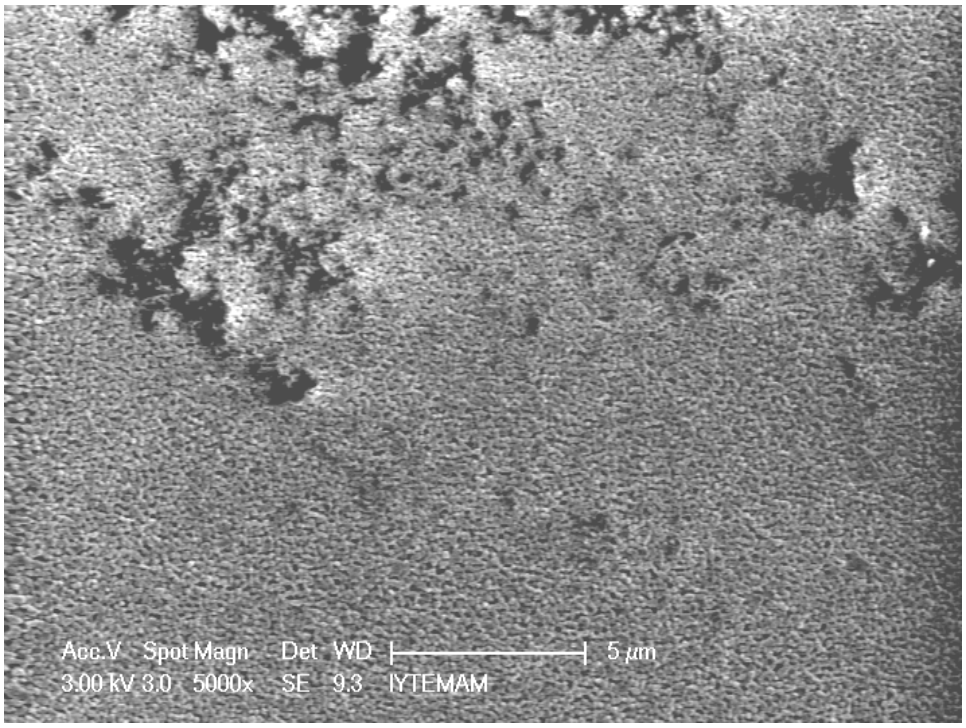

Figure 54. The SEM micrograph showing the surface of the denser layer of the AKP-50 support (1100° C / 2h) (S (-)) cast after 10% corn starch containing porous layer.

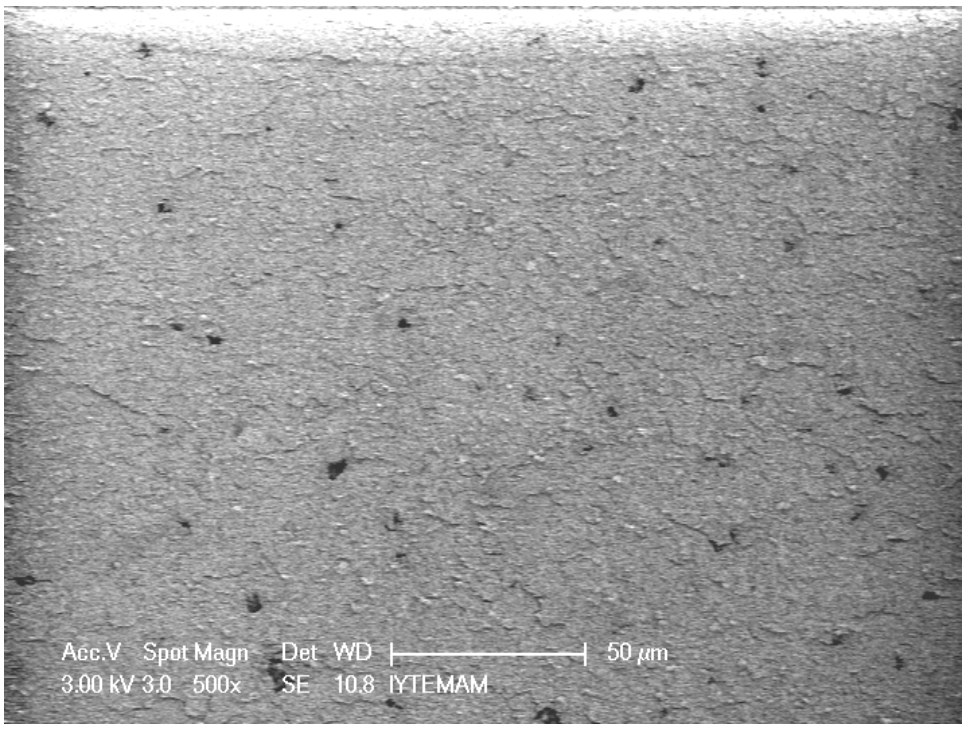

Figure 55. The SEM micrograph showing the surface of the more porous layer of the AKP-50 support (1100° C / 2h) (S (-)) cast via 10% corn starch containing suspension facing die.

6.1.2. Intermediate Layers

The intermediate layer was prepared in two layers to assemble the asymmetric structure of the ceramic composite membranes. The aim was to form a layer on the support with 50-55% porosity of which 80-85% was open pores. The partially sintered granules forming the support were in micron and submicron range in size. There were pores formed by decomposition of starch and also air bubbles formed during casting of the ceramic slip into the dies. Formation of a layer composed of nano particles on such a porous structure with pores several magnitudes larger than the nano particles was only possible by forming some intermediate layers composed of particles / granules with sizes between the particles forming the support and the nano particles which will form the top layer. For this purpose, an intermediate layer composed of two layers, one prepared by using submicron ceramic powders and second by using nano particles relatively bigger than the nano particles used in preparation of top layer was formed on the support.

6.1.2.1. Preparation and Characterization of First Intermediate Layer

The first intermediate layer was prepared by using suspensions of commercial submicron ceramic powders; either alumina (AKP-50, Sumitomo Co.) or zirconia (TZ-3Y, Tosoh Co.). The coatings were performed by using three methods: dip-coating, wet-coating and spin-coating. These methods have their own advantages and disadvantages affecting the coating efficiency.

6.1.2.1.1. Dip-coating

The suspensions of ceramic powders with varying compositions (1.5 to 20 %) were tested for dip-coating (d-c) the supports and the formed layer was partially sintered

by heat treating at 900-1150 °C for 2 hours. The main advantage of dip-coating method was that it results in a homogeneous coating even the support has some shape imperfectness (concave, wavy, rough surface). The main disadvantage is formation of pinholes during the suction and drying period. The air leaving the porous structure during this period resulted in pinholes which were hampering the efficiency of further coatings since the coated material was sucked in these pinholes instead of forming a thin layer on the surface.

Different concentrations for alumina powder (AKP-50) were tested as 5, 10 and 20 %. All of these concentrations were found to be sufficient to form a layer on the supports after 10 seconds dip-coating. Although the SEM analysis showed presence of some cracks and defects, support surface was covered with particulates of this finer ceramic powder as shown in Figure 54 and 55.

Zirconia powder (TZ-3Y) was also used in preparation of first intermediate layer. Its suspensions with varying concentrations (1-10 volume %) were tested. To prevent crack formation during drying 3% PVA (polyvinyl alcohol) was added in the suspension with 1.5 vol. %. The supports dip-coated by using this suspension for 10 seconds were heat treated at 1100 or 1150 °C for 2 hours. This procedure resulted formation of a layer with finer pores on the support with less cracks and defects compared to coatings without PVA addition. The thickness of the formed layer was around 10 μ as was observed in SEM images (Figure 58, 59).

Increasing the temperature of heat treatment from 1100° to 1150 °C resulted in growing in the sizes of particulates in the formed layer and some losses in porosity due to sintering as can be seen in Figure 60, 61. Higher porosity is more preferable for decreasing the resistance to fluid flow, that 1100 °C was selected for further experiments.

6.1.2.1.2. Wet-coating

Inspired from a US patent (Patent Number: 4,810,273, date of patent: May, 7, 1989, “porous ceramic filter”, invented by Tadanori Komoda) another coating procedure was formed. In this method the supports were first soaked (boiled in water)

and after sealing of the sides and formation of a cylindrical die the ceramic suspensions were pipetted on the surface to be coated. The main advantage of this method was preventing the formation of pinholes (as was in dip-coating). The elimination of pinhole formation was achieved up to some extent, but not totally. A pinhole on a support prepared via 10 % wheat starch and heat treating at 1350° C / 2 h and wet coated twice can be seen in Figure 62. The heat treatment at 950° C / 2 h resulted in a highly porous microstructure as shown in Figure 63.

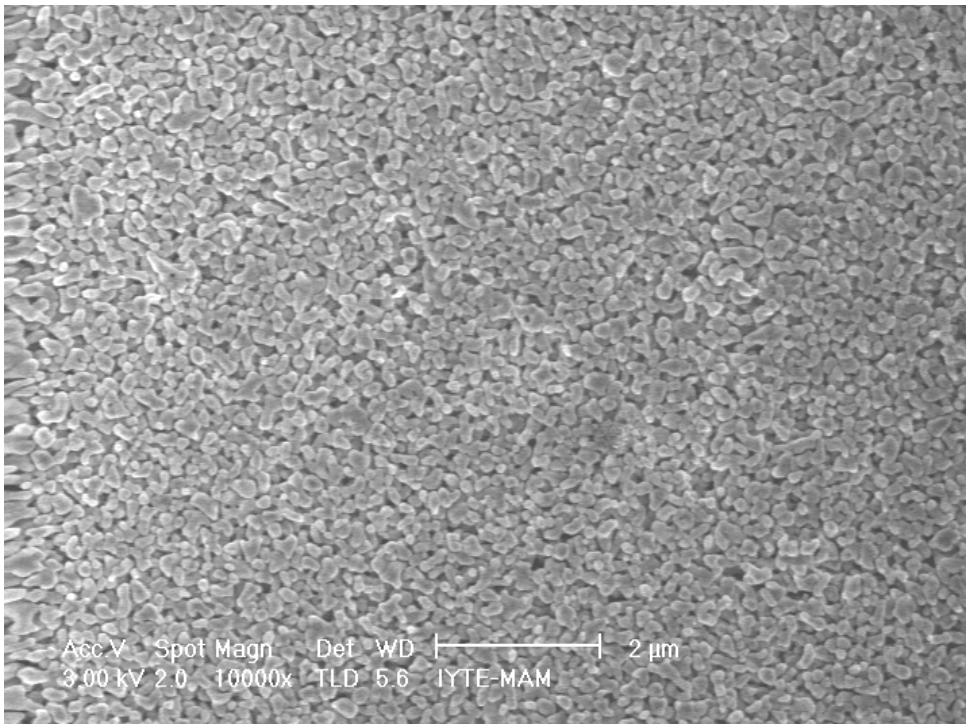

Figure 56. The SEM micrograph of dip-coated support (11% starch, 1300°C / 2 hours) surface with a suspension of finer alumina particles (10 vol. %) and heat treated at 1100°C / 2 hours.

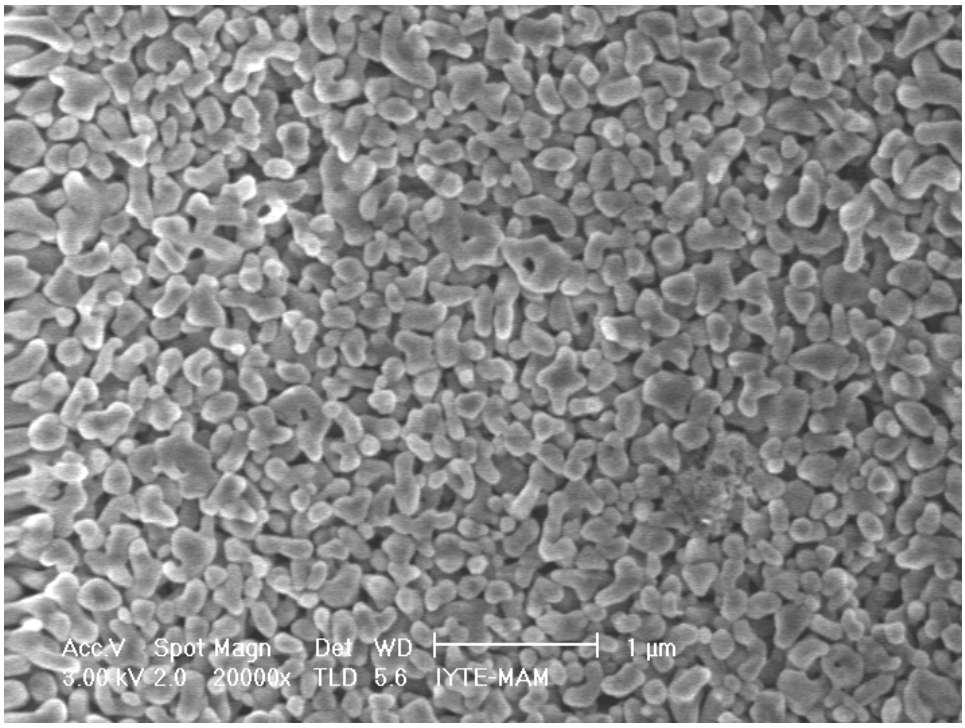

Figure 57. The SEM micrograph of dip-coated support (11% starch, 1300°C / 2 hours) surface with a suspension of finer alumina particles (10 vol. %) and heat treated at 1100°C / 2 hours.

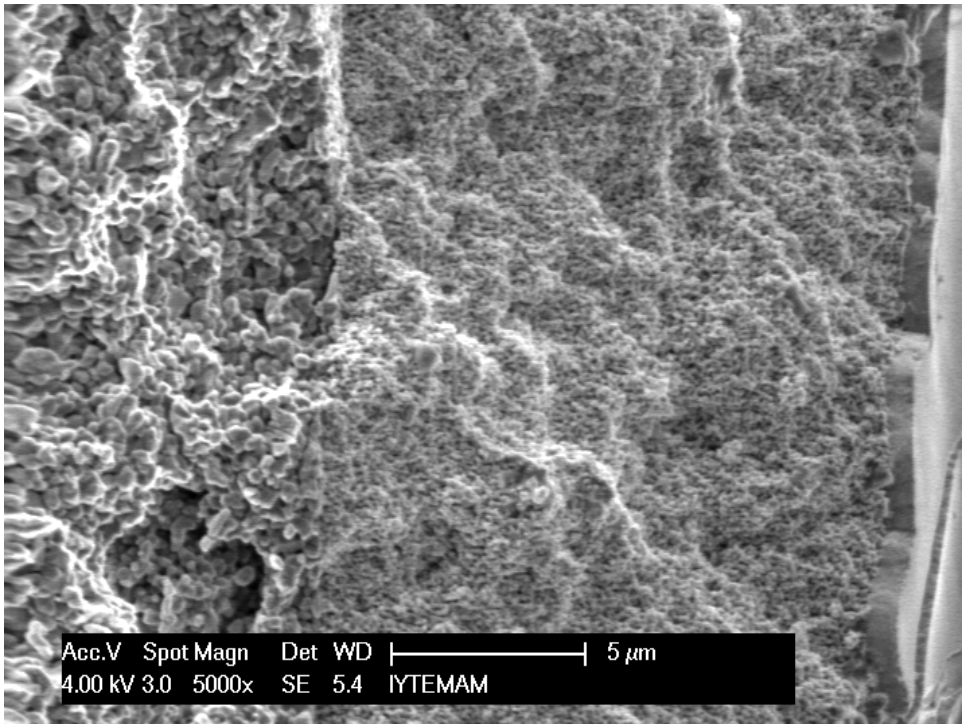

Figure 58. The SEM micrograph of the intersection of first intermediate layer formed by dip-coating 1.5 vol. % zirconia suspension (heat treated at 1100° C).

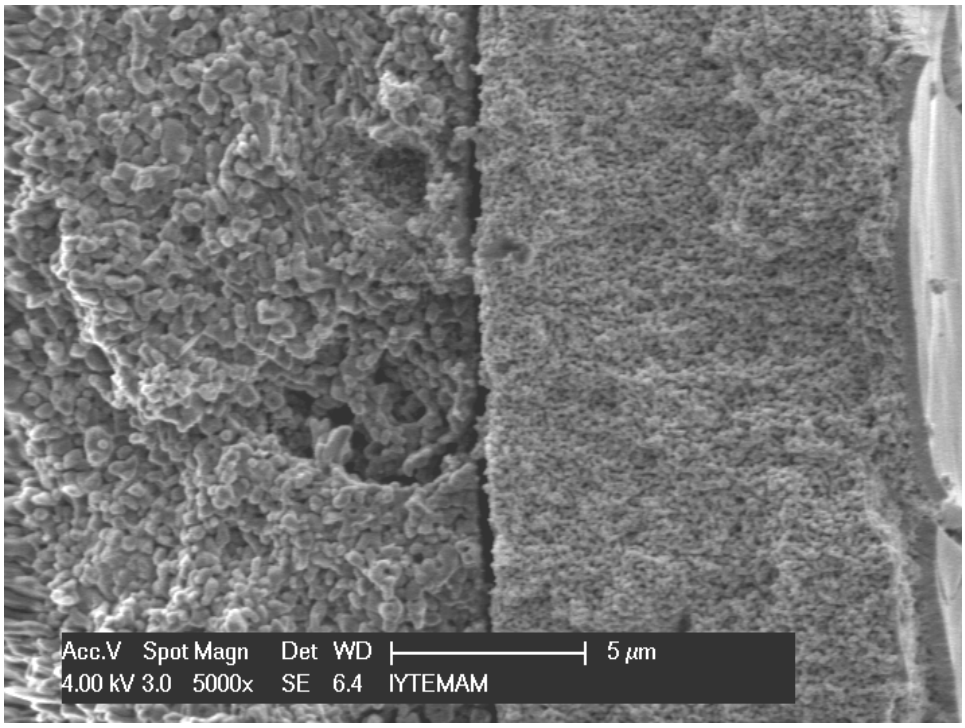

Figure 59. The SEM micrograph of the intersection of first intermediate layer formed by dip-coating 1.5 vol. % zirconia suspension (heat treated at 1100° C).

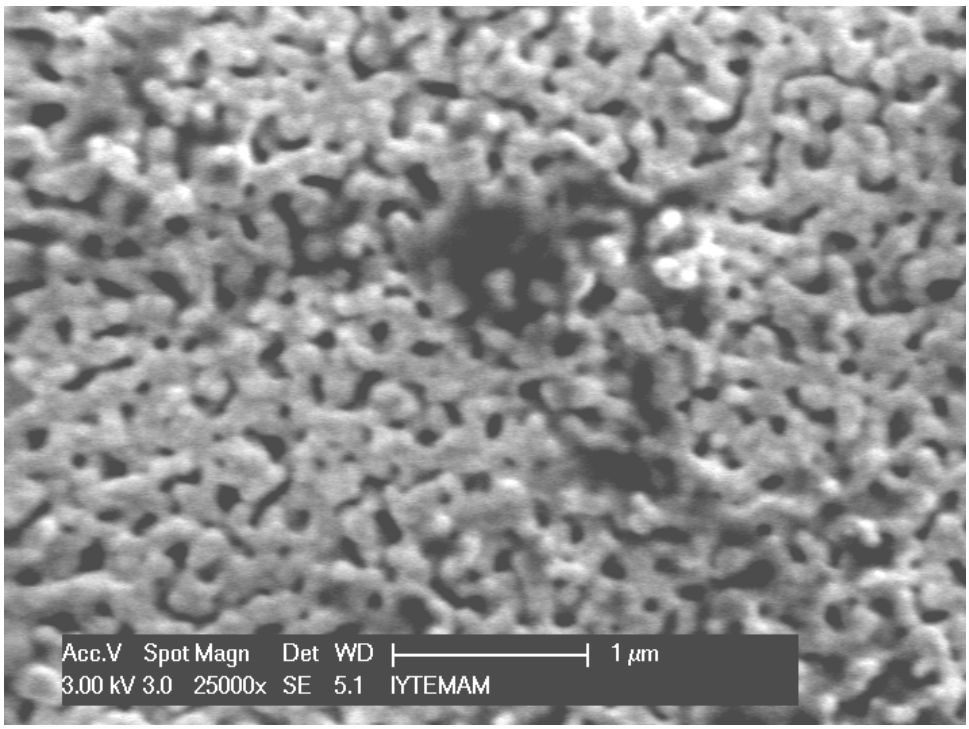

Figure 60. The SEM micrograph of first intermediate layer formed by dip-coating the support by using 1.5 vol. % zirconia suspension heat treated at 1100° C.

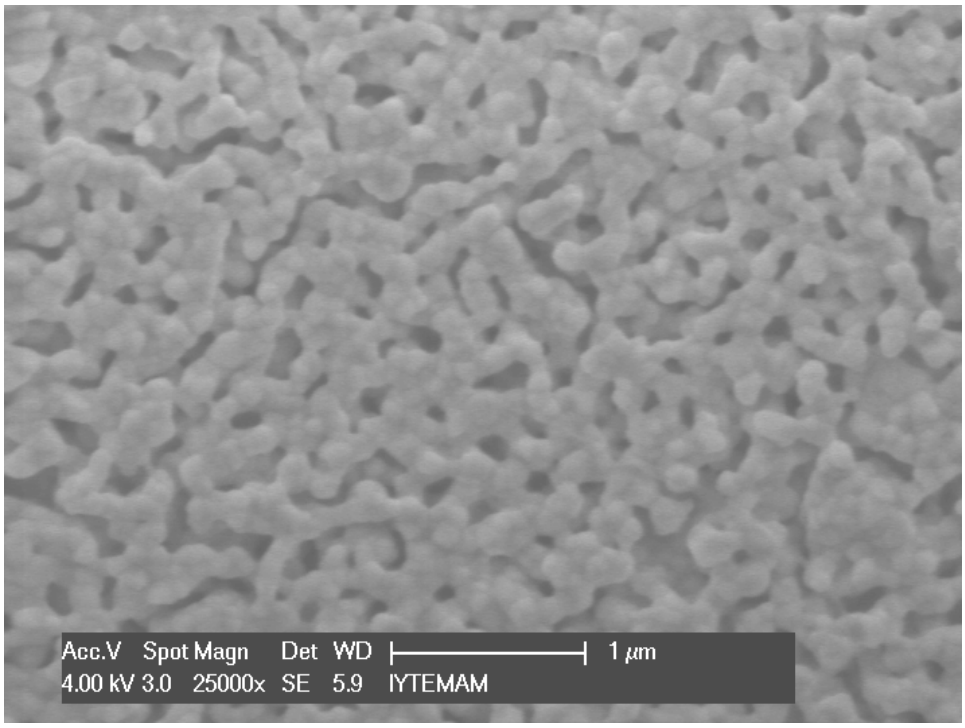

Figure 61. The SEM micrograph of first intermediate layer formed by dip-coating the support by using 1.5 vol. % zirconia suspension heat treated at 1150° C.

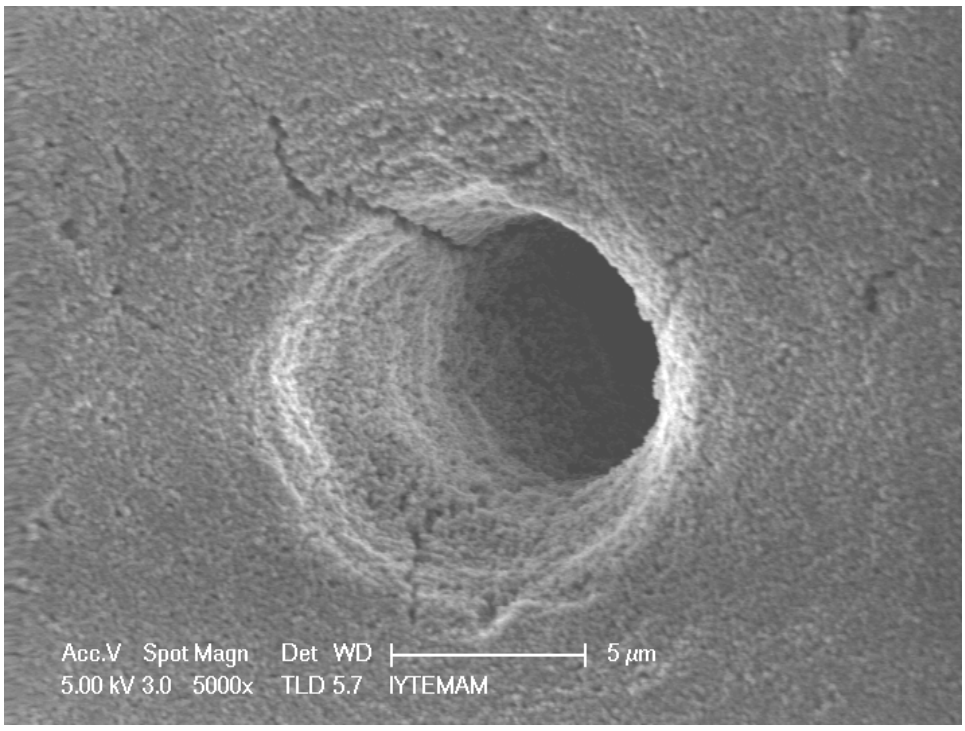

Figure 62. The SEM micrograph showing the pinhole on a support (10 % wheat starch, 1350° C / 2 h) wet-coated twice: 1st; 2.5 mL 1.5 vol.% AKP-50 suspension (3%PVA), 950° C / 2 h, 2nd; 1 mL 1 vol.% AKP-50 suspension (3%PVA), 950° C / 2 h.

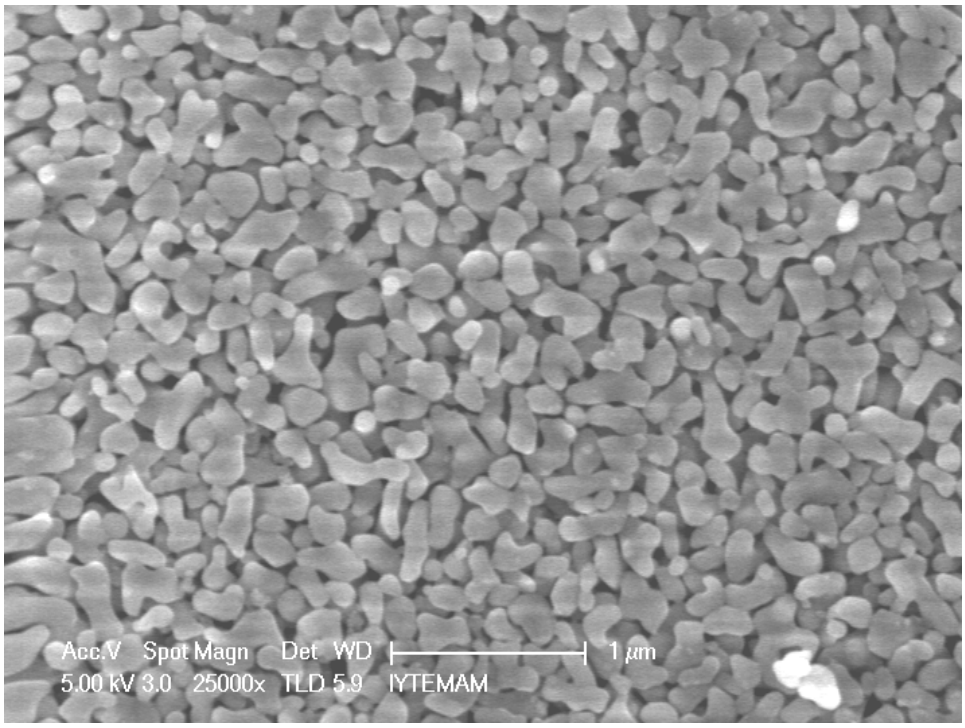

Figure 63. The SEM micrograph showing the microstructure of AKP-50 heat treated at 950° C / 2 h which was cast via wet-coating of 1 vol.% AKP-50 (3%PVA).

The varying concentration of the suspension was affecting the formed layer. Increasing the suspension concentration resulted in thicker layers which were prone to crack and peel out during drying or heat treatment. Low suspension concentration were resulting the increase in the number of point defects, determined via optical microscope, which were like tiny pinholes. This may be due to insufficient coating which would hamper the efficiency of further coatings with finer particles (i.e. sol). There were cracks observed on the layers formed via wet-coating like shown in Figure 64. The depth of the crack was also coated with AKP-50 as can be seen in Figure 65, but these cracks could still hamper the further coatings.

The main disadvantage of wet-coating (w-c) was observed on supports with imperfectness in shape (e.g. concave, wavy surfaces). Such imperfectness resulted in inhomogeneous thickness of coated layer at different parts of the surface. The zones with thicker coating were cracked and peeled out, while the zones with thinner coating were with point defects which possibly were tiny pinholes. The change of the cast layer via wet-coating across the cross-section of a support can be seen in Figures 66, 67.

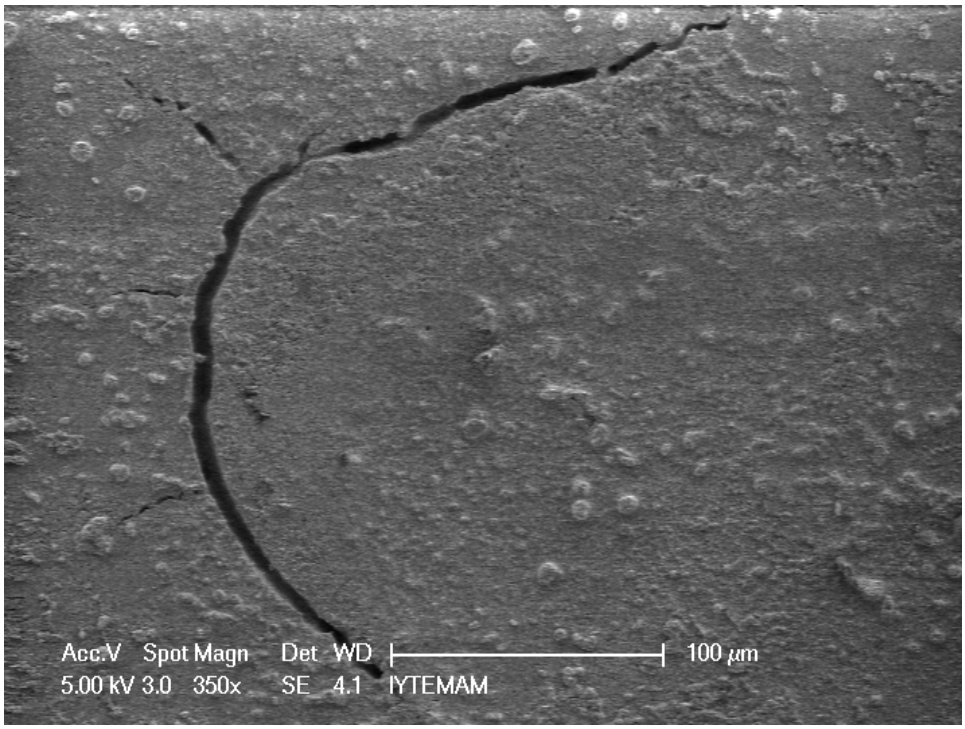

Figure 64. The SEM micrograph showing a crack on the AKP-50 layer formed via wet-coating 1 vol.% AKP-50 (3%PVA), 950° C / 2 h.

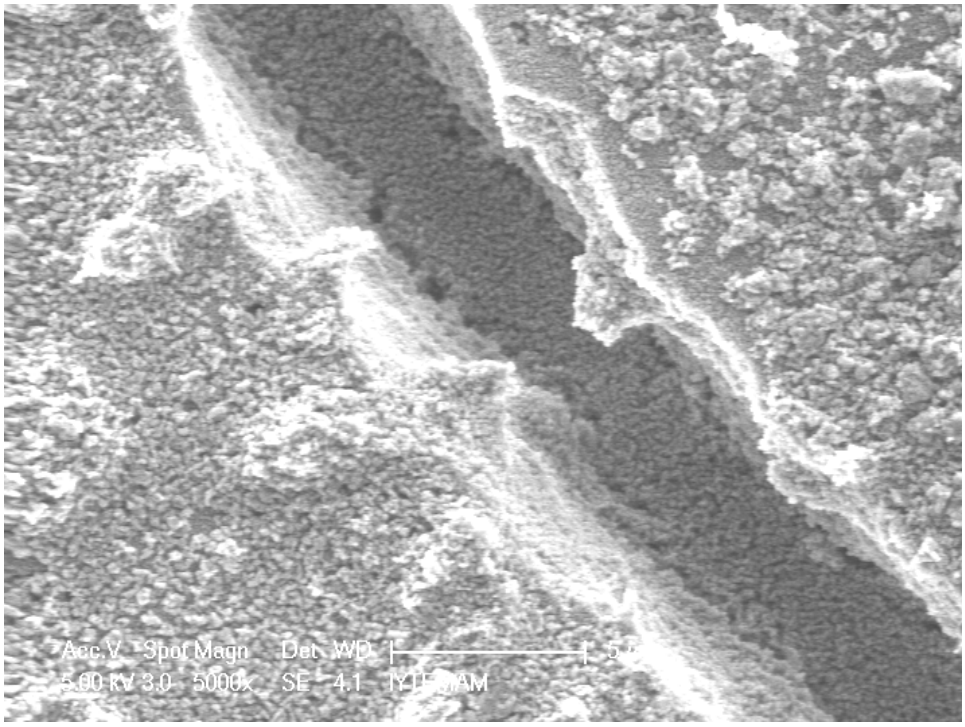

Figure 65. The SEM micrograph showing depth of the crack in Figure 64 on the AKP-50 layer formed via wet-coating 1 vol.% AKP-50 (3%PVA), 950° C / 2 h.

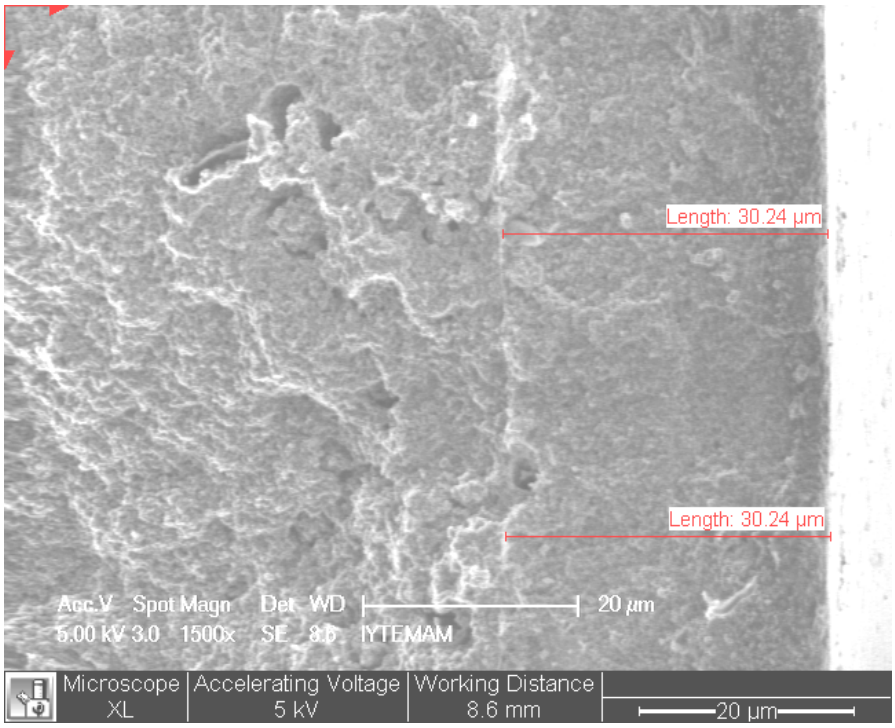

Figure 66. The SEM micrograph showing the thickness of the layer wet-coated (w-c) on a support (10% wheat starch, Alcoa alumina, 1300° C / 2h) via 1st w-c: 2mL 1.5 vol% AKP-50 (3%PVA), 950° C / 2h, 2nd w-c: 1mL 1 vol% AKP-50 (3%PVA), 950° C / 2h.

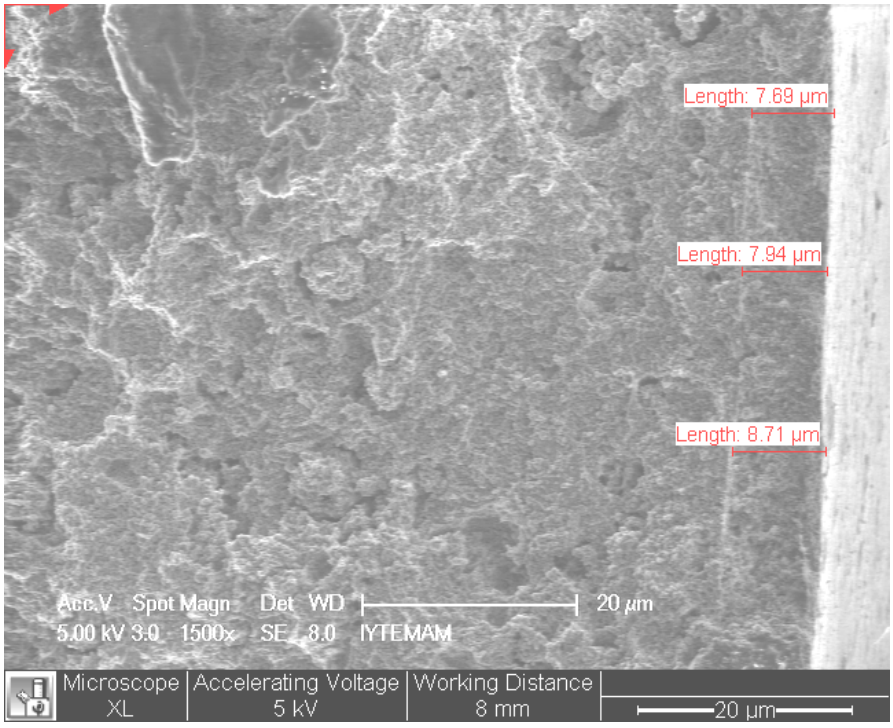

Figure 67. The SEM micrograph showing the thickness of the layer wet-coated as described for Figure 66 on a different part of the support.

6.1.2.1.3. Spin-coating

Spin-coating (s-c) was also used in forming the first intermediate layer. Submicron ceramic powder suspensions were prepared and necessary amount of these suspensions (2-3 mL) were pipetted on the spinning support. The spinning regime was adjusted to have the suspension spread over the surface totally then spinning at relatively lower rpm values (200-300 rpm) to present time for suction of the suspension on the surface and at higher rpm (1000-1250 rpm) to remove the excess suspension.

The spin-coating was performed by using either dry or soaked supports. The soaked supports were not coated since there was no suction of the suspension. The dry supports were coated but there were pinholes as were observed in dip-coating as can be seen in Figure 68. Therefore spin-coating was not able to present a layer without defects like pinholes.

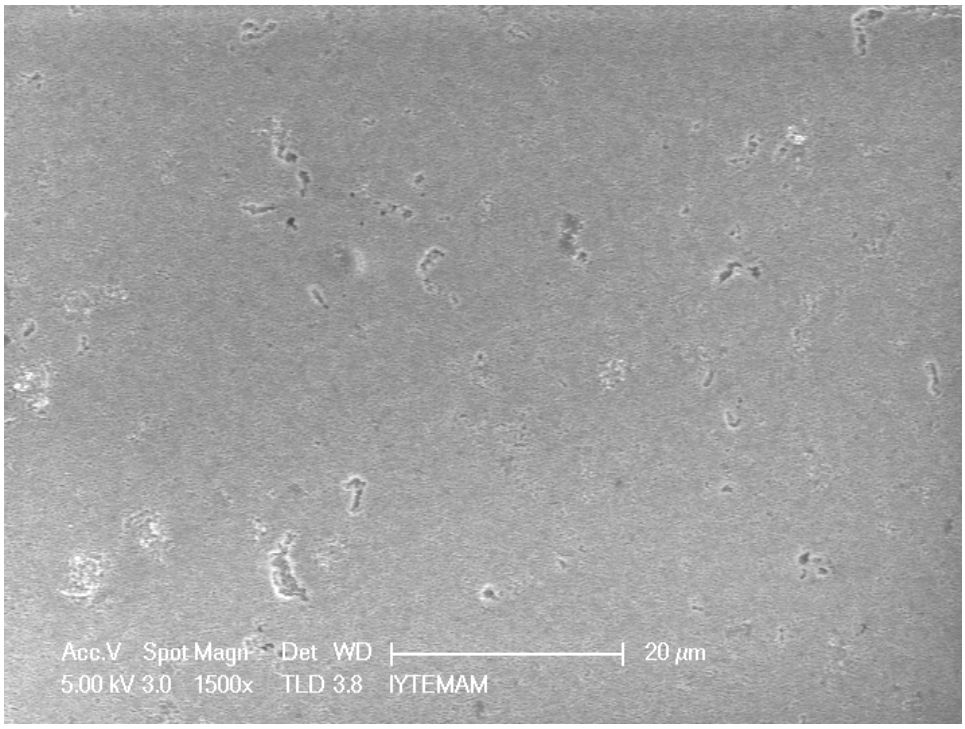

Figure 68. The SEM micrograph of surface of Alcoa support (10% wheat starch, 1300° C / 2h), wet-coated (wc) via 2 mL AKP-50 (3%PVA) suspension, heat treated (ht) 900° C / 2h, [spin coat (sc) (Regime 5) 2 mL AKP-50 (3%PVA) suspension] x 2, heat treated (ht) 900° C / 90 min, sc via 1 vol% AKP-50 (3% PVA), Regime 6 Mod-2, ht 900° C / 90 min, sc via 1 vol % AKP-50 (3%PVA) suspension and Regime 6 mod-2, ht 900° C / 120 min.

6.1.2.2. Second Intermediate Layer

A second intermediate layer was formed on the first to be able to form a top layer of nano particles with a few nano meters average particle size on top of it. For this purpose either alumina (A08-boehmite) or zirconia colloidal sols were prepared.

The alumina (boehmite) sol was prepared with molar ratios of alkoxide / nitric acid (65%) / water as 1: 0.25: 100 by using aluminium isopropoxide as alkoxide. The alumina sol was coded A08 and its average particle size was determined as 54.2 ± 0.6 nm (polydispersity index (PI): 0.562 ± 0.006) (on 25.07.2007) by using laser light scattering instrument (Zetasizer 3000HSA, Malvern Co.). The measurement was repeated 3 times which were all reported as acceptable results for the instrument's algorithm. The average particle size (PS) increased in time due to aging of the sol and was measured as 87.5 ± 0.6 nm (polydispersity index (PI): 0.663 ± 0.008) after a year (on 14.07.2008). The volumetric particle size distribution of the alumina sol determined in 2007 was as shown in Figure 69. As can be seen there were particles with varying sizes starting from 8 nm ending at 100 nm as the main fraction and there was another fraction of relatively bigger particles.

A colloidal zirconia sol was prepared by using zirconium (tetra) propoxide, nitric acid, propanol and water. The water in excess molar ratios than the stoichiometric hydrolysis ratio was tested to prepare a clear and stable colloidal sol with controlled particle size (PS). For this purpose, different molar ratios of alkoxide: acid: alcohol: water were tried. The initial molar ratio for acid: alkoxide was 0.5: 1 then it was changed to 1: 1 and kept at that value. Different alcohol: alkoxide initial molar ratios were tried as 20-75: 1. The initial molar ratios of water: alkoxide were also changed between 2 -25: 1.

The initial mixtures prepared with given initial molar ratios were not clear. There were fibres in the sols (mixtures) with relatively less water containing mixtures and the higher ratios of water resulted in gel formation. The mixtures were peptized by adding concentrated (65%) HNO_3 drop-wise and they were diluted by using propanol when necessary. The mixtures were left stirring after addition of acid and alcohol. The clear stable sol formation was observed after some days. The particle size (PS)

distributions of the sols were detected by using laser light scattering instrument (Zetasizer). This analysis gave information about the sol stability as well.

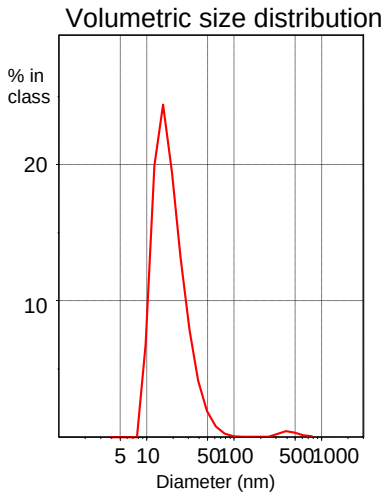

Figure 69.The volumetric particle size distribution of alumina sol (A08) determined via Zetasizer.

The average PS of the prepared colloidal sols increased by increasing initial water: alkoxide molar ratio. The average PS values were measured as 13, 17 and 24 nm for water: alkoxide molar ratios 4, 5 and 10, respectively, as shown in Figure 39.

The experiments showed that there was an optimum ratio of acid: alkoxide. For example for a colloidal sol with initial molar ratios of alkoxide: acid: propanol: water as 1: 1: 75: 25 addition of different amounts of acid for peptization resulted in different responses. Addition of 2 drops of acid was found insufficient to have a clear sol. Addition of 8 drops of acid resulted in a sol with particles having a wide particle size distribution (i.e. with a high polydispersity). Meanwhile addition of 4 drops of acid resulted in a clear stable sol with average PS of 49.2 ± 0.8 nm and a low polydispersity index (PI) as 0.589 ± 0.025.

In another batch a colloidal sol with initial molar ratios of alkoxide: acid: propanol: water as 1: 1: 30: 10 was prepared. It was diluted (1: 1) and necessary amount of acid was added on it for peptization. The resulting sol after stirring the mixture for a couple of days had an average PS comparable with the alumina sol as 54.2 ± 0.4 nm and

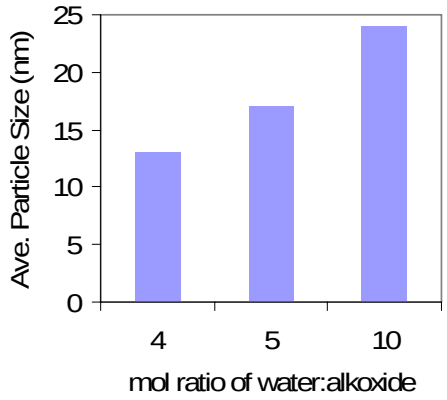

Figure 70. The average particle size of colloidal zirconia sol with respect to increasing initial water:alkoxide molar ratio.

its PI was 0.511 ± 0.007 (These values for alumina sol were 54.2 ± 0.6 nm and 0.562 ± 0.006.) The volumetric particle size distributions of two colloidal sols determined via Zetasizer are shown in Figure 71**.** The zirconia colloidal sol had nearly the same particle sizes of a couple of hundreds of nm which were present in the alumina sol in a small amount. The average particle sizes for alumina and zirconia sols with respect to volumetric distribution were 20 and 29 nm, respectively.

The alumina and zirconia sols were coated directly on the supports or on the first intermediate layer formed by using suspensions of fine ceramic alumina or zirconia particles. The coating was applied either by dipping the membrane in the sol for e.g. 10 seconds. Dip-coated membrane was left drying at room temperature and heat treated (calcined) at 500-600° C.

Direct coatings of the sol on the support did not result in a homogeneous layer formation. The nano particles in the sol couldn't deposit on the support with comparatively very big pores and sol was all sucked into the porous support. The SEM analysis showed that only local deposits were formed after several cycles of dip-coating procedure (coating-drying-calcination). The pores formed by decomposition of pore forming additives and air bubbles left in the ceramic slip during casting may be the reasons of local suction of the sol into the support. The first intermediate layer which was free of these huge pores could prevent the severe suction of the sol and help forming a more homogeneous and smooth surface for further coatings. The supports cast via 10% wheat starch containing Alcoa alumina (1300° C / 120 min.) were wet

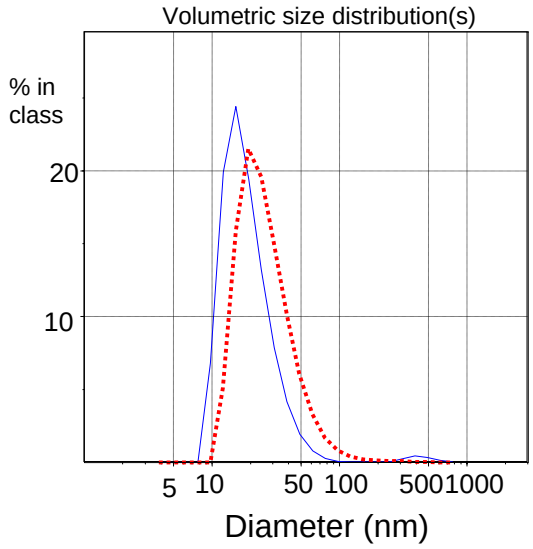

Figure 71. The volumetric particle size distribution of two colloidal sols; alumina (A08): continuous line, zirconia: dashed line.

coated by using 2 mL of 1.5 vol.% AKP-50 alumina suspension (3% PVA) and heat treated at 950° C for 120 min. Then these supports were re-wet coated via 1 mL of 1 vol.% AKP-50 alumina suspension (3% PVA) and heat treated as before. The second wet-coating was performed to eliminate possible defects in the first wet-coating. These double wet-coated supports were then dip-coated via undiluted Zr colloidal sol for 15 seconds, left drying and calcined at 450° C for 2 hours. The formed layer was investigated via SEM. The formed layer was not continuous. There were zones where sol was all sucked, some zones semi-coated and other zones where the formed layer was cracked as can be seen in Figures 72, 73, 74 and 75.

The alumina sol formed γ-alumina after calcination at 600° C as was also reported by Tsuru (2001) and Erdem (2002). This phase of alumina was chemically instable at very low (< 2) and high pH (> 11) values when compared with α-alumina, titania and zirconia (Tsuru, 2001, Van Gestel, et al. 2002). This difference may be a reason for preferring α-alumina, titania and zirconia to prepare the asymmetric ceramic membrane for aqueous applications where severe chemical conditions can be observed during the filtration or cleaning procedure.

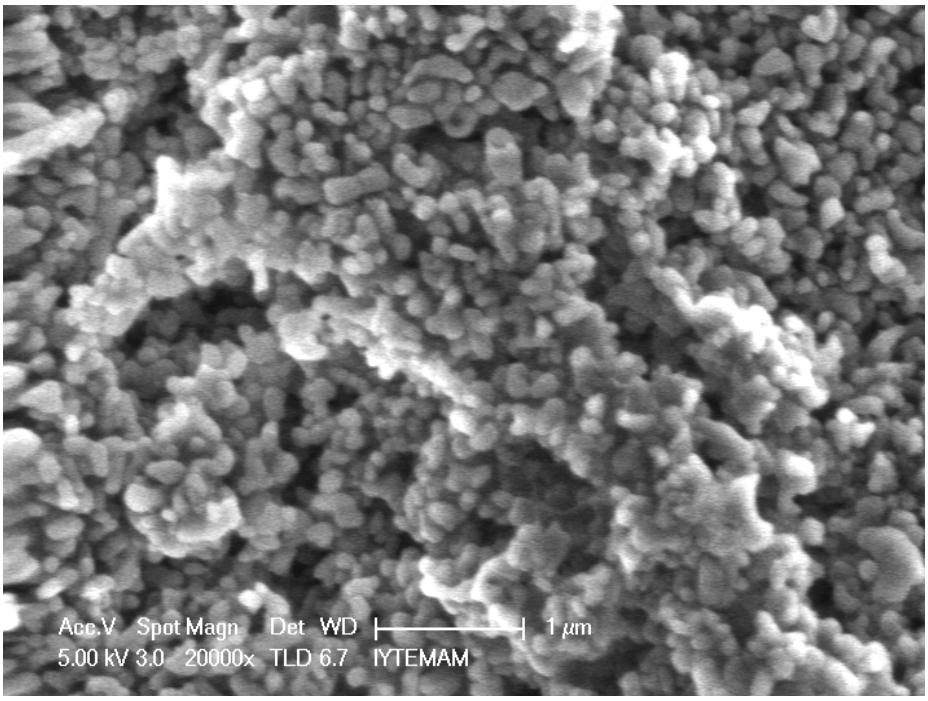

Figure 72. Alcoa alumina support (10% wheat starch, 1300° C / 2 hours), double wet coated (1.5 and 1 vol.% AKP-50 alumina, (3% PVA), 950° C / 2 hours), dip-coated via Zr colloidal sol (15 sec., 450° C / 2 hours).

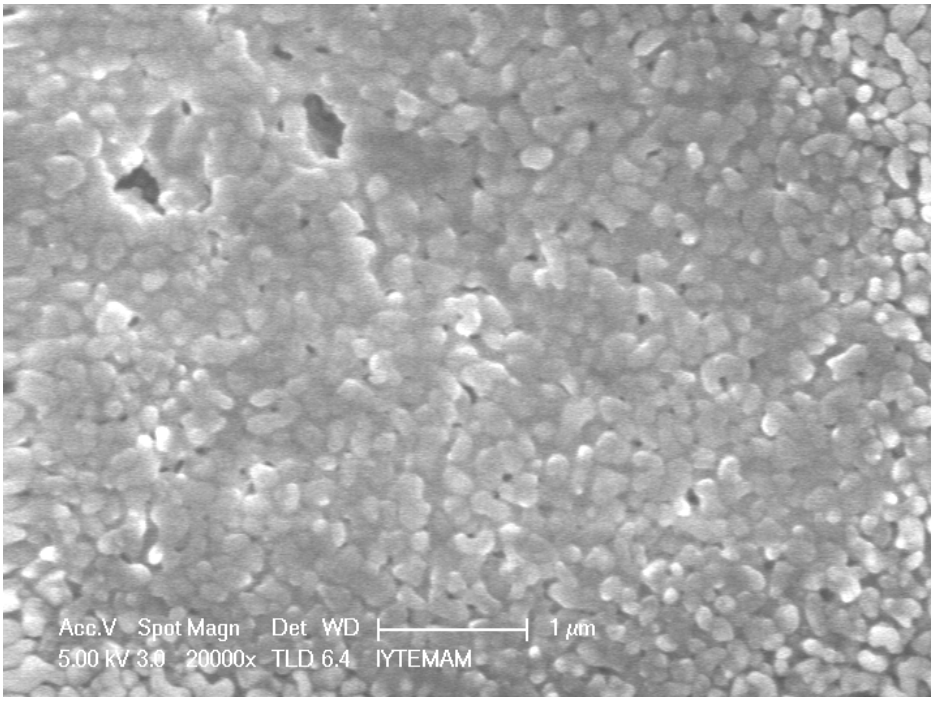

Figure 73. Alcoa alumina support (10% wheat starch, 1300° C / 2 hours), double wet coated (1.5 and 1 vol.% AKP-50 alumina, (3% PVA), 950° C / 2 hours), dip-coated via Zr colloidal sol (15 sec., 450° C / 2 hours).

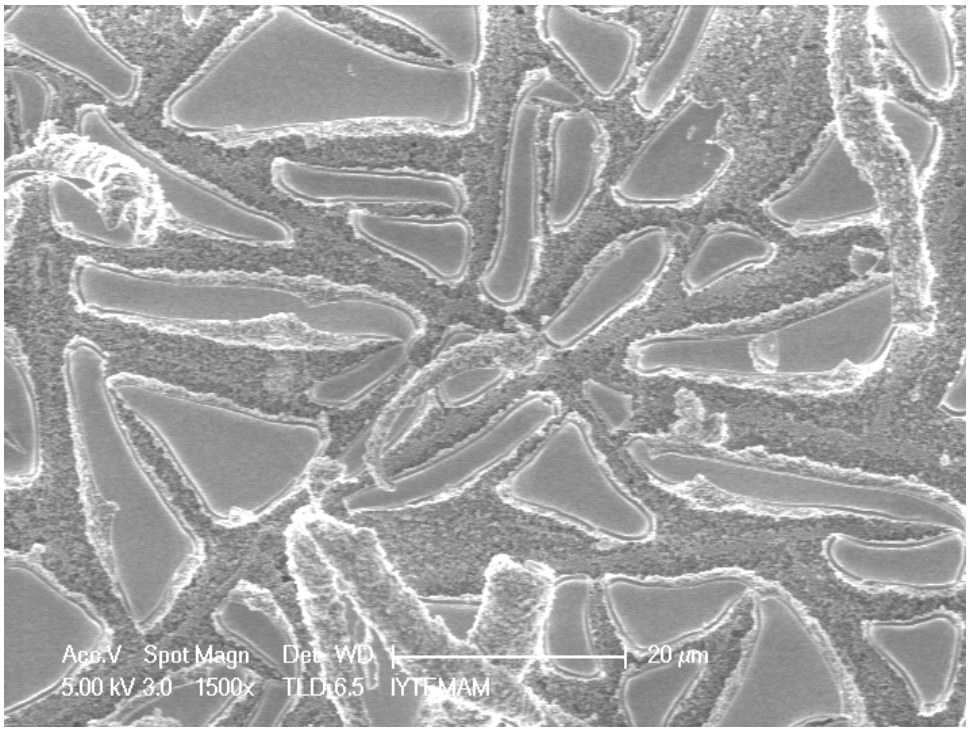

Figure 74. Alcoa alumina support (10% wheat starch, 1300° C / 2 hours), double wet coated (1.5 and 1 vol.% AKP-50 alumina, (3% PVA), 950° C / 2 hours), dip-coated via Zr colloidal sol (15 sec., 450° C / 2 hours).

Figure 75. Alcoa alumina support (10% wheat starch, 1300° C / 2 hours), double wet coated (1.5 and 1 vol.% AKP-50 alumina, (3% PVA), 950° C / 2 hours), dip-coated via Zr colloidal sol (15 sec., 450° C / 2 hours).

6.1.3. Preparation and Characterization of Top Layer

6.1.3.1. Sol Preparation

The top layer is the surface that faces the bulk fluid that will be filtered. It is almost totally responsible for separation due to size exclusion (steric hindrance) and mainly responsible for Donnan exclusion (electrostatic hindrance). Therefore, it plays a major role in the efficiency (or characteristics) of the membrane.

The top layer should have pores small enough to keep the materials to be separated. Its chemical stability should be as high as possible to have the opportunity to use it in different applications. Zirconia and titania were two ceramic materials used in formation of top layer. For this purpose polymeric sols of pure titania or zirconia or mixture of these two were prepared using zirconium IV propoxide (70% in propanol) and titanium IV propoxide (98%) with the molar ratios given in Table 7. These sols had nano particles composed of polymeric chains of alkoxides with average particle sizes of a few nano meters. After calcination they were oxidized and formed zirconia and titania porous structures with different characteristics.

The molar ratios of the constituents in the polymeric sol (alkoxide / propanol / nitric acid) were 1: 15 (or 20): 1, respectively. These ratios were reached after preliminary experiments performed to obtain clear stable mixed sols. No extra water was added to the sols to prevent uncontrolled hydrolysis. The average particle size of these sols were determined by using laser light scattering instrument (Zetasizer 3000HSA, Malvern Co.) as shown in Table 8 and Figure 76. The prepared sols contain particles with an average size of 3-6 nm and found to be promising precursors in preparation of top layers with nano-pores. The volumetric particle size distributions of these sols are given in Figure 77 - 80. They have a narrow particle size distribution (PSD) range as could be predicted from their low polydispersity index (PI; which can take values between 0 and 1, showing a narrower distribution if close to 0).

Table 7. The molar ratios of elements in the sols.

Name of the sol	TiProX (titanium propoxide)	ZrProX (zirconium propoxide)
Full Ti	100	0
TiZr 7525	75	25
TiZr 5050	50	50
TiZr 2575	25	75
Full Zr	0	100

Table 8. The average particle size values for mixed sols determined by using laser light scattering.

Code Of sol	*Ti molar ratio*	*Zr molar ratio*	*Average particle size (nm)*	*Polydispersity index*
Full Ti	100	0	2.8 ± 0.1	0.116 ± 0.032
TiZr 7525	75	25	3.9 ± 0.7	0.304 ± 0.071
TiZr 5050	50	50	3.0 ± 0.3	0.291 ± 0.016
TiZr 2575	25	75	3.6 ± 0.2	0.357 ± 0.091
Full Zr	0	100	5.2 ± 0.7	0.304 ± 0.079

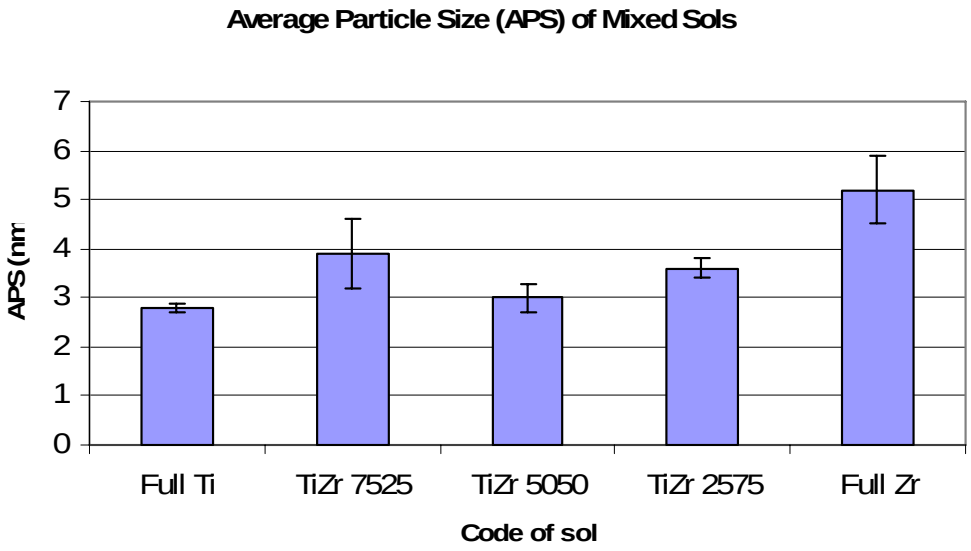

Figure 76. The average particle size values for mixed sols determined by using laser light scattering.

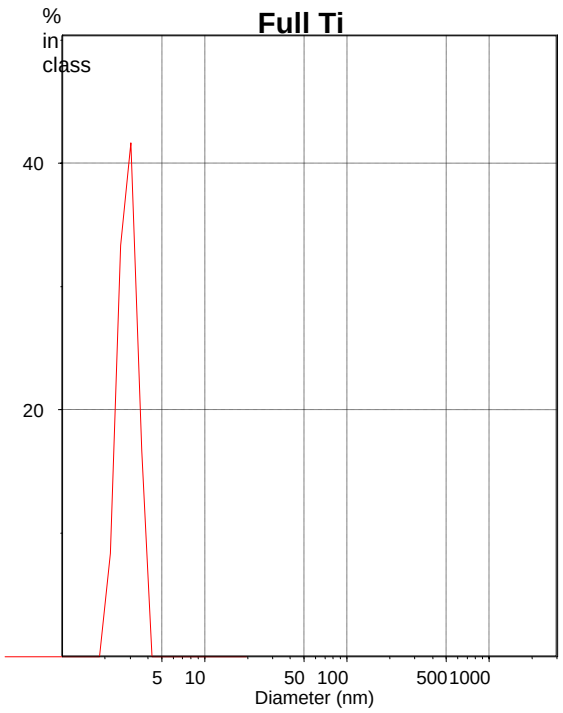

Figure 77. The volumetric particle size distribution of polymeric Full Ti sol.

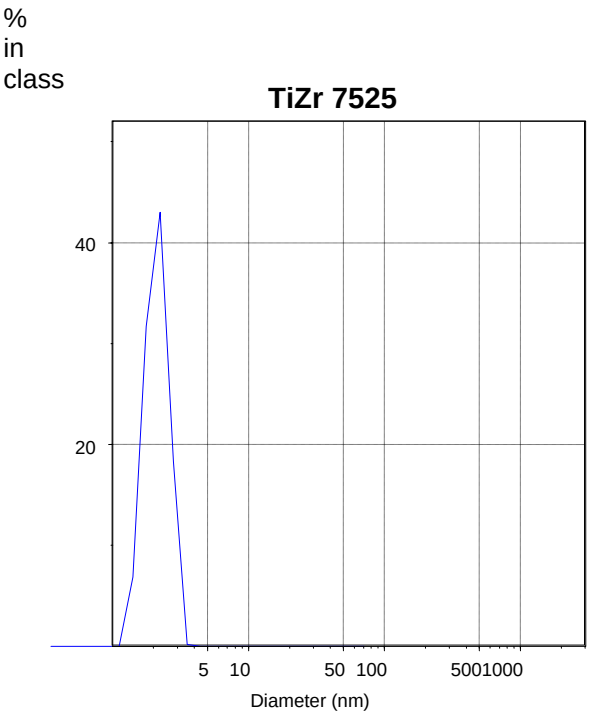

Figure 78. The volumetric particle size distribution of polymeric TiZr 7525 sol.

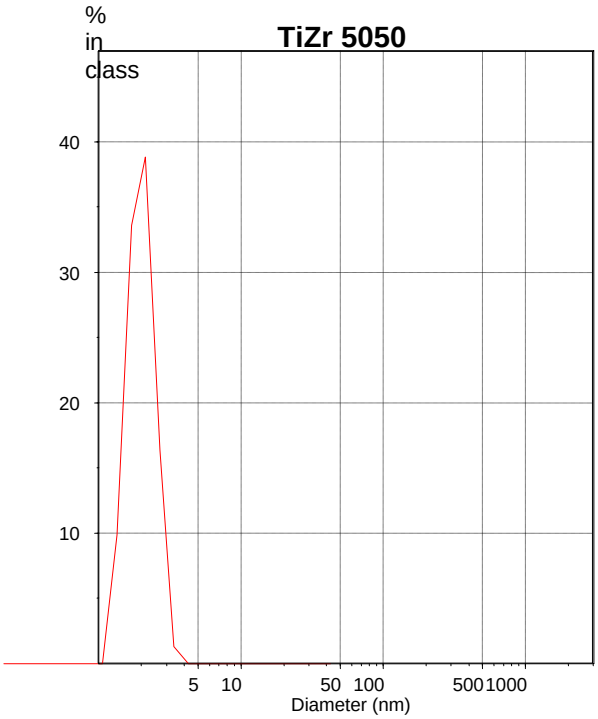

Figure 79. The volumetric particle size distribution of polymeric TiZr 5050 sol.

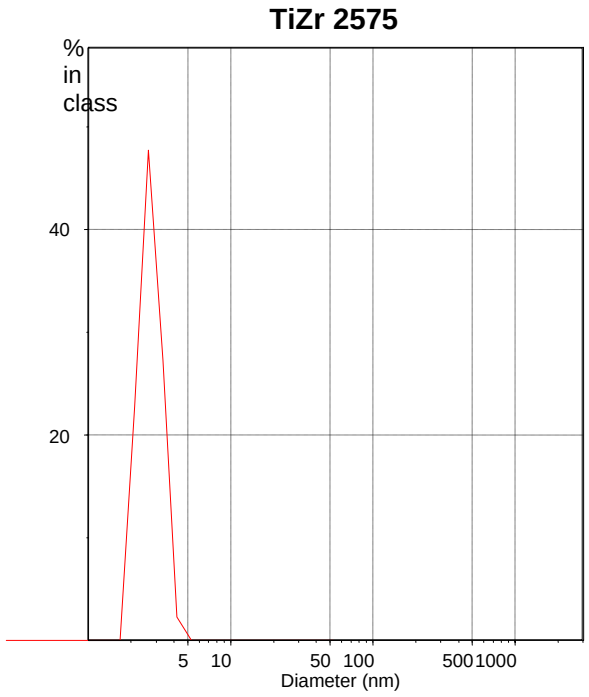

Figure 80. The volumetric particle size distribution of polymeric TiZr 2575 sol.

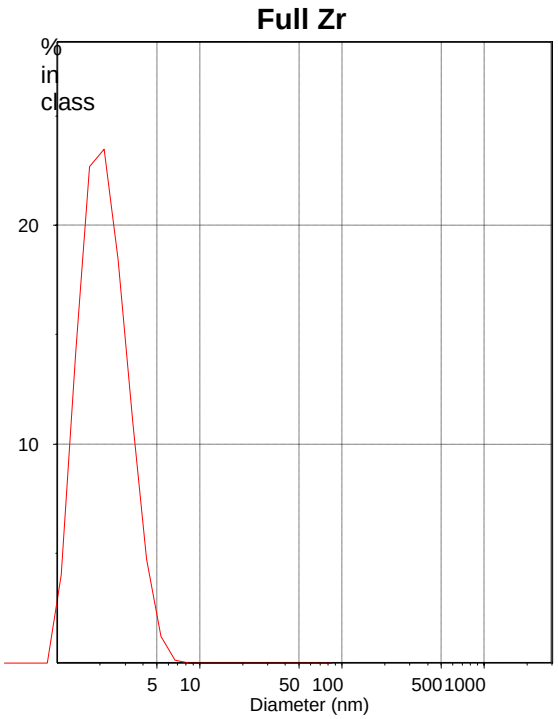

Figure 81. The volumetric particle size distribution of polymeric Full Zr sol.

6.1.3.2. Thermal characterization

The heat treatment temperature is an important parameter on ceramic processing. The mechanical, thermal and chemical stability of the membrane is related to its thermal history. Another important criterion for membranes, the porosity, is also affected from heat treatment. The severity of this effect increases as the particle sizes forming the green body decreases i.e. the green bodies formed by relatively smaller particles are more prone to get sintered and lose their porosity during heat treatment. Therefore, the calcination temperature for the top layer (and also intermediate layer) should be chosen appropriately. For this purpose some thermal characterization experiments (TGA/DTA) were performed (Perkin Elmer Diamond). The TGA results for Ti / Zr sols are given in Figure 82 - 87. Full Ti has reached thermogravimetric stability at around 400°C with only a 30% gravimetric loss, while Full Zr has reached to stability after reaching 500°C and it lost 45% of its weight. There is a sharp decrement in weight between 400-500°C for Full Zr. TiZr 5050 showed the highest weight loss (~53%) and reached the stability

only after 625°C. TiZr 7525 lost 43% of its weight and reached the stability at around 550°C. TiZr 2575 also lost the same % of its weight but its loss between 475-575°C was steeper like the loss observed between 400-500°C for Full Zr.

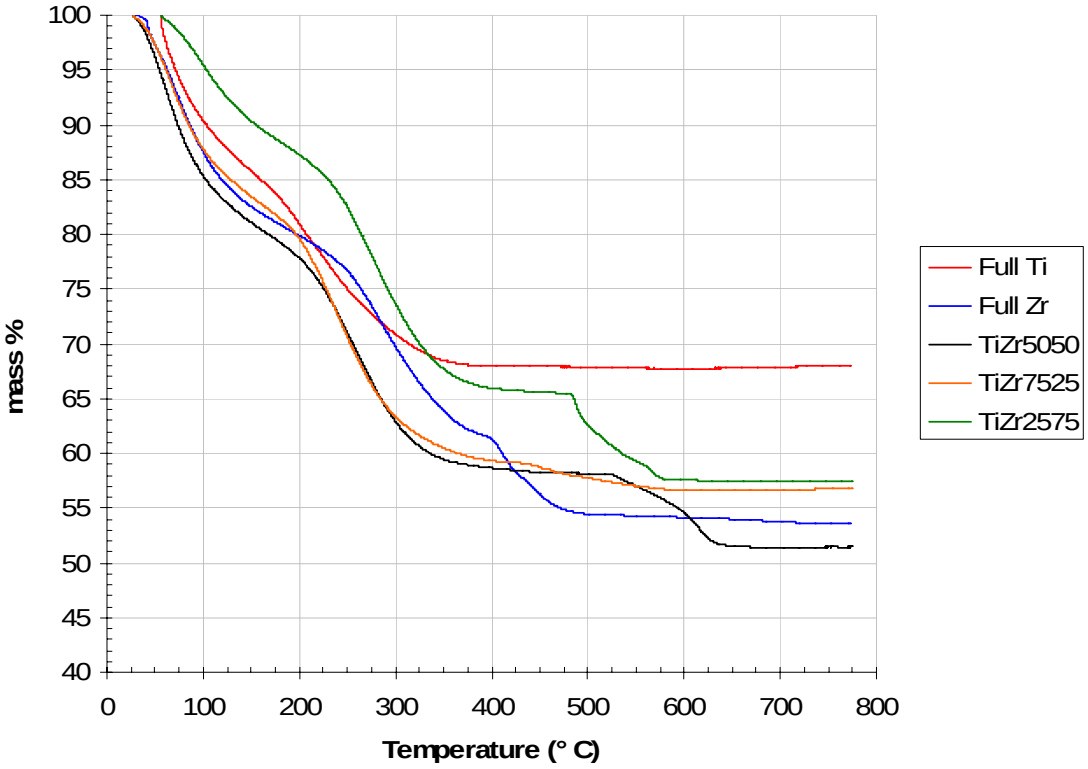

Figure 82. The TGA results for Ti / Zr sol system.

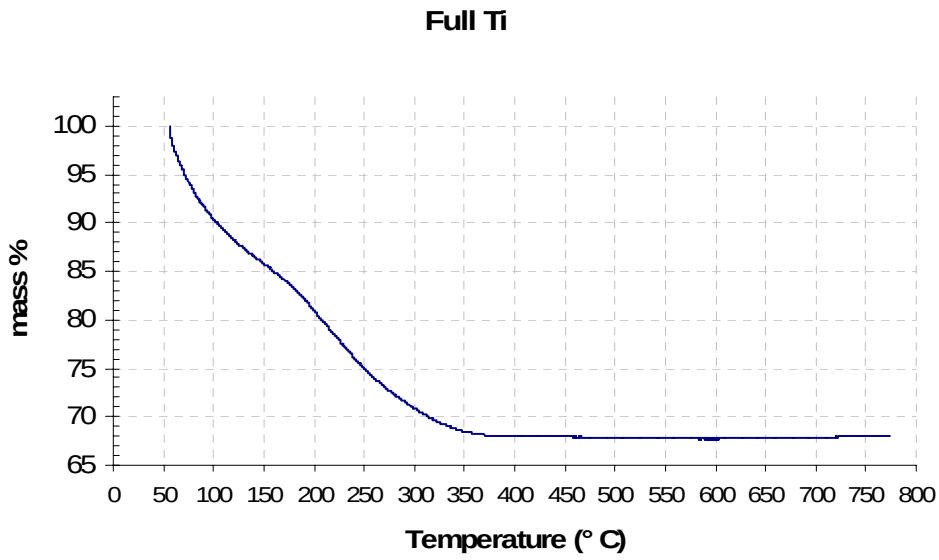

Figure 83. The TGA result for Full Ti.

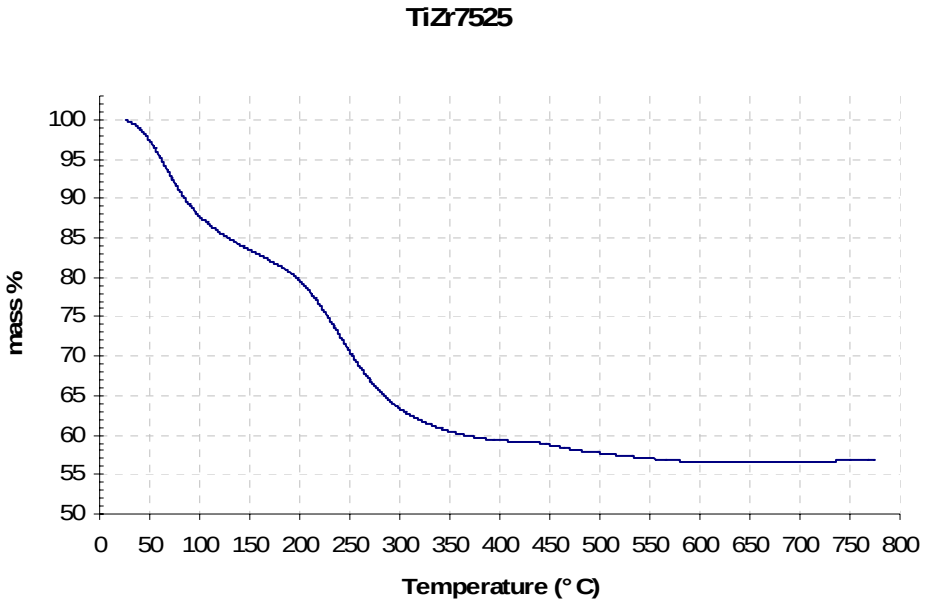

Figure 84. The TGA result for Ti.Zr 7525.

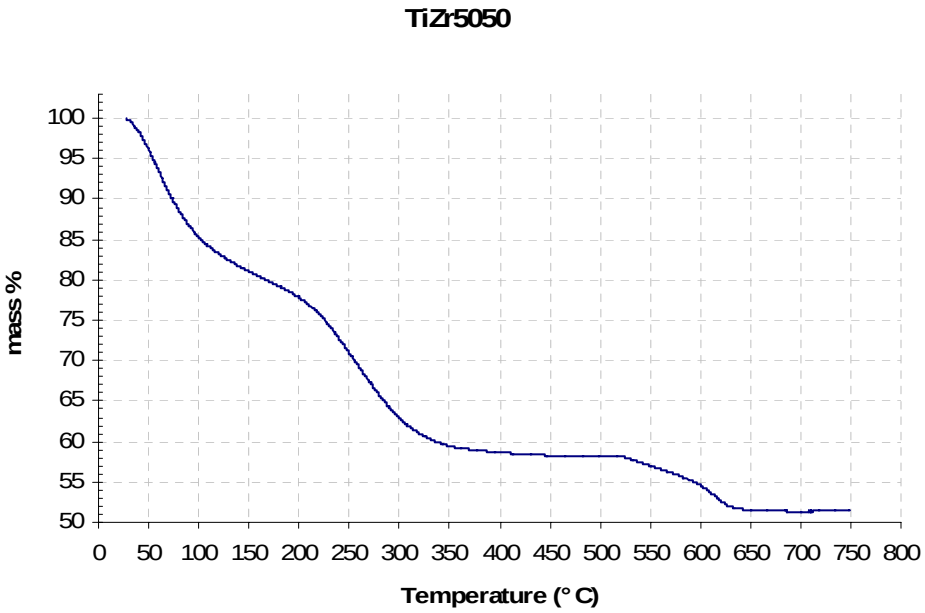

Figure 85. The TGA result for Ti.Zr 5050.

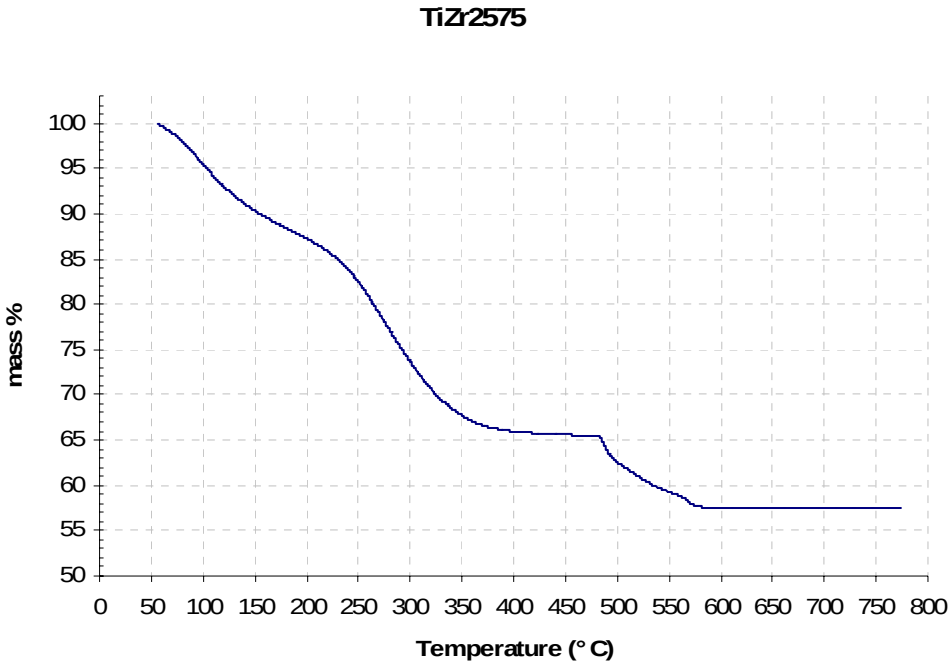

Figure 86. The TGA result for Ti.Zr 2575.

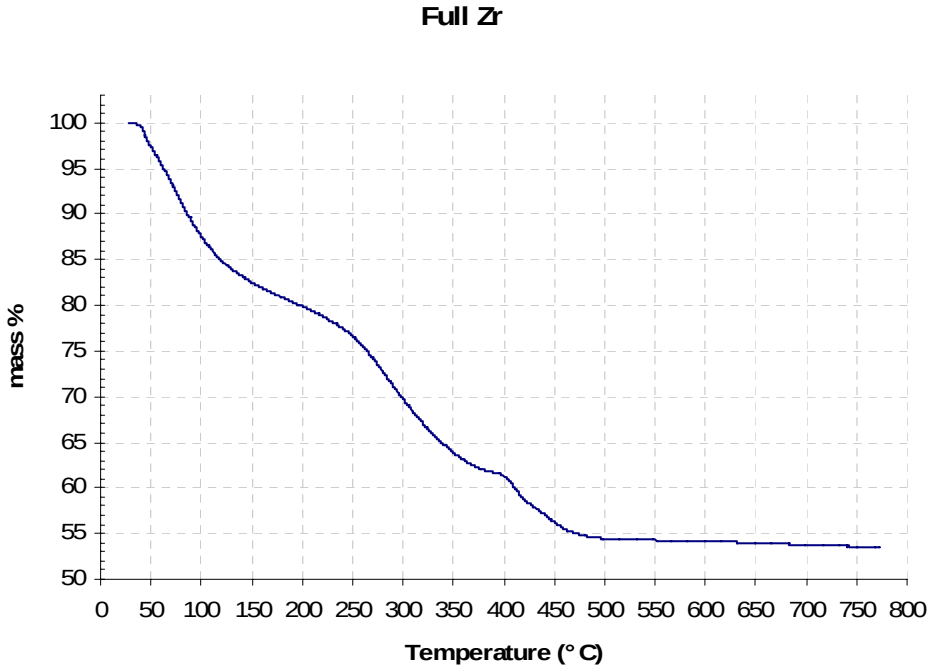

Figure 87. The TGA result for Full Zr.

There are two main weight loss regions for Ti-rich sols and three for Zr-reach sols in the thermogravimetric analysis profiles. These weight decrement regions were shifted to higher temperatures for mixed sols when compared to pure sols, Full Ti and Full Zr (i.e. the thermal stability was achieved at relatively higher temperatures by the mixed oxides when compared to pure oxides). The slopes of the decrements in these regions showed also differences indicating different susceptibilities to heat treatment.

6.1.3.3. Crystallinity

The heat treatment causes oxidation of organic constituents and formation of oxides (TiO_2, ZrO_2). The titania (TiO_2) has two crystal phases; anatase (A) and rutile (R), and zirconia (ZrO_2) has three phases; monoclinic (M), tetragonal (T) and cubic (C). These crystal structures occur after heat treatment of amorphous precursors (coated layers in our case). The heat treatment mainly affects the change of amorphous structure to crystalline structure. The crystallization behaviour of different materials (e.g. pure oxide or mixed oxide) may be different as is their thermogravimetric behaviour. A number of XRD analyses were performed to identify the crystallization behaviour of layers formed by using Ti / Zr mixed sols. Five different sols were calcined at temperatures 400 / 500 / 600°C for 3 hours for this purpose. The temperature range was selected as 400-600 °C, since this range was thought to contain the weigh loses not due to the removal of free or bound water but phase transformations. Further heat treatment temperatures may result losses in porosity and/or increases in pore sizes. The results of XRD analysis for five sols uncalcined and calcined at three different temperatures are given in Figure 88 - 92. The crystallization of the oxides was retarded when they are in mixed form. The common phase for zirconia was tetragonal (T), some monoclinic (M) formation occurred at higher temperatures. Titania is generally either amorphous or in anatase (A) phase. Anatase to rutile transformation started at elevated temperatures.

The crystallite sizes of pure Ti and Zr oxides were calculated via software (Expert Plus) of the XRD instrument. The crystallite sizes were increasing with increasing calcination temperature as shown in Figure 93. The crystallite sizes

calculated via Scherrer calculator were higher for Full Zr but the increase in crystallite size was steeper for Full Ti.

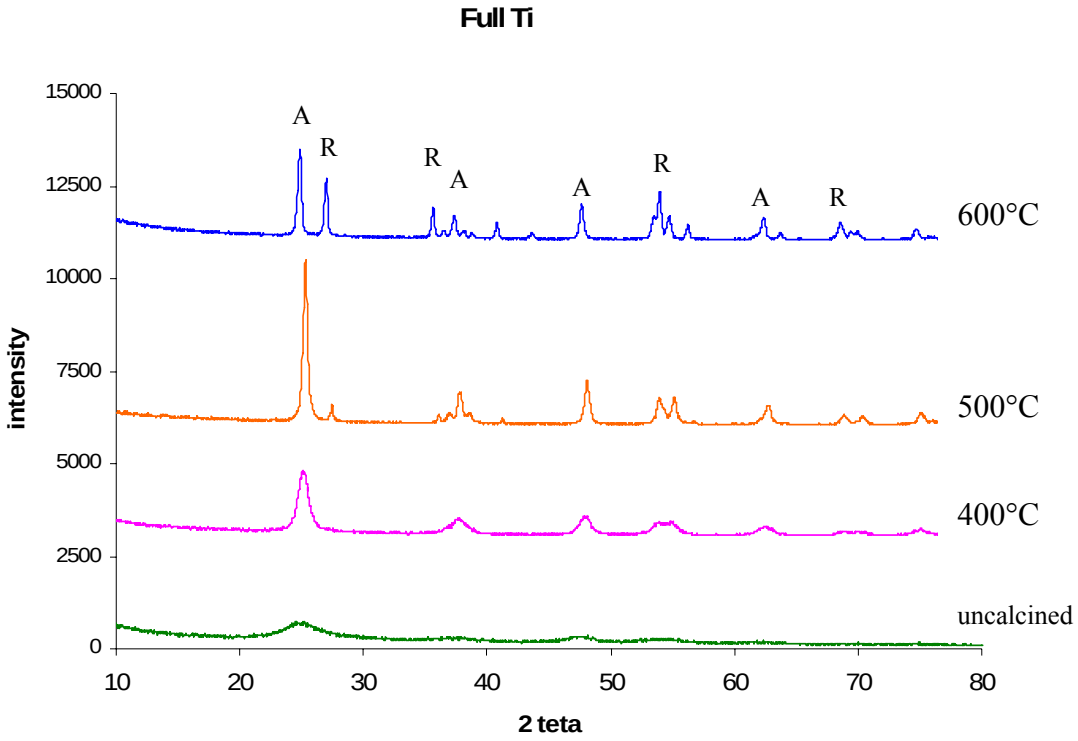

Figure 88. The XRD result for Full Ti.

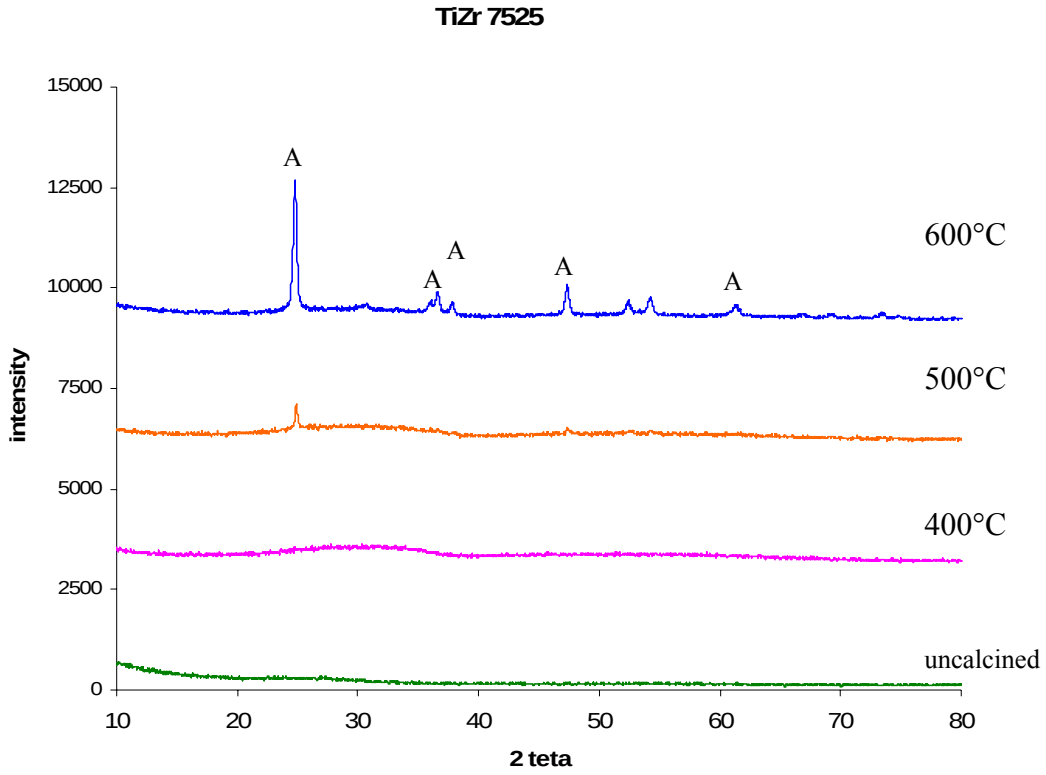

Figure 89. The XRD result for Ti.Zr 7525.

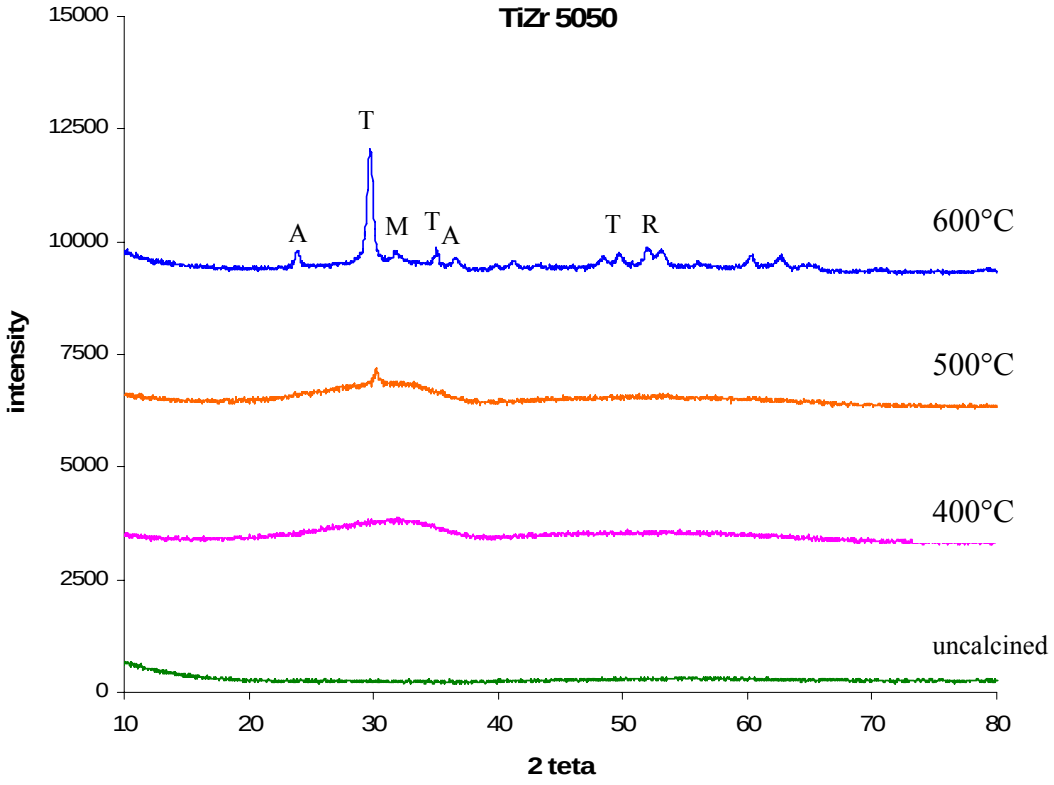

Figure 90. The XRD result for Ti.Zr 5050.

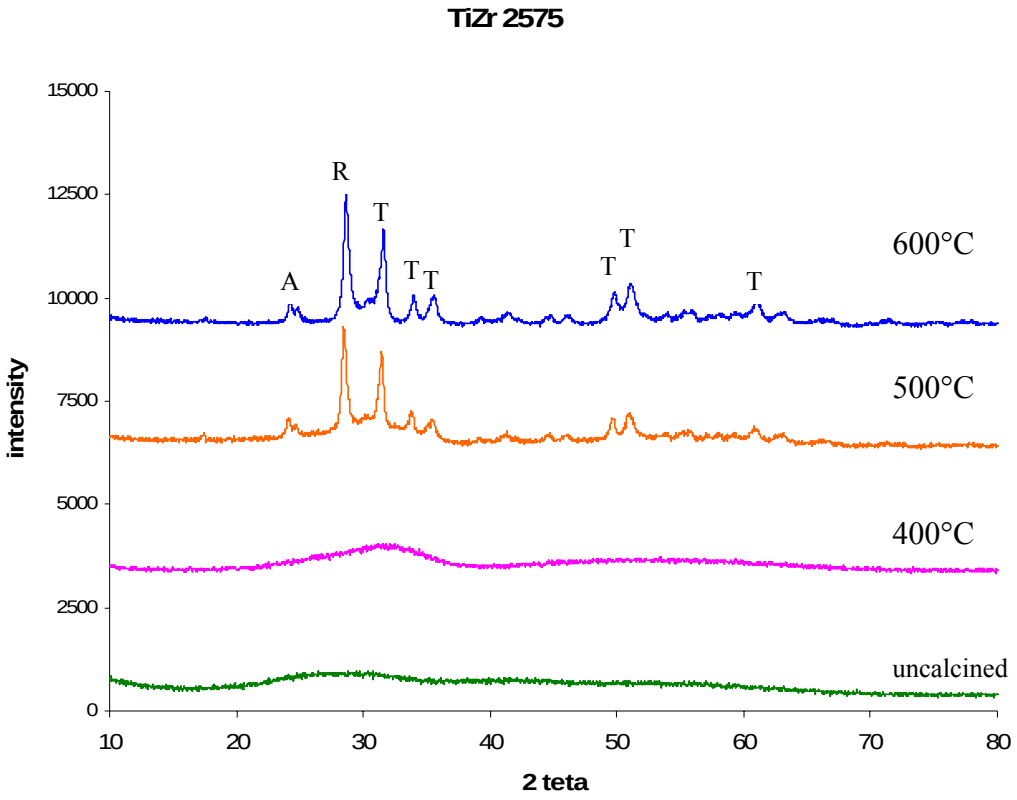

Figure 91. The XRD result for Ti.Zr 2575.

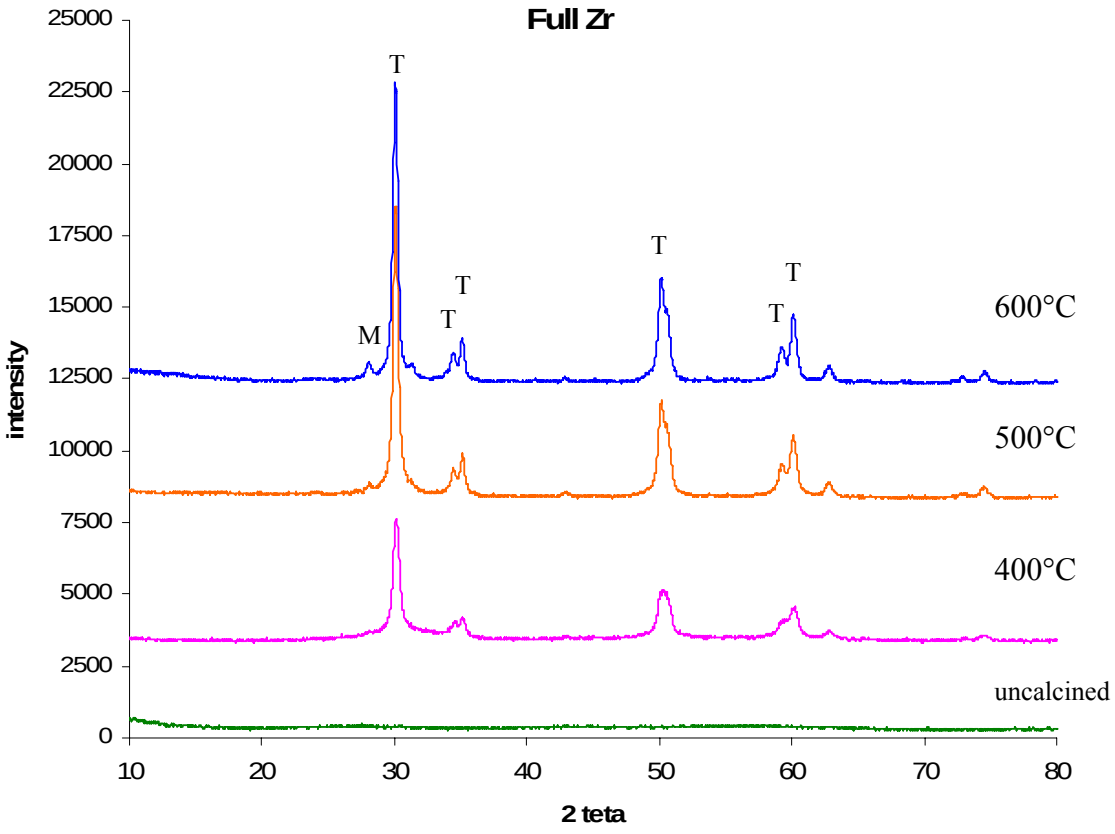

Figure 92. The XRD result for Full Zr.

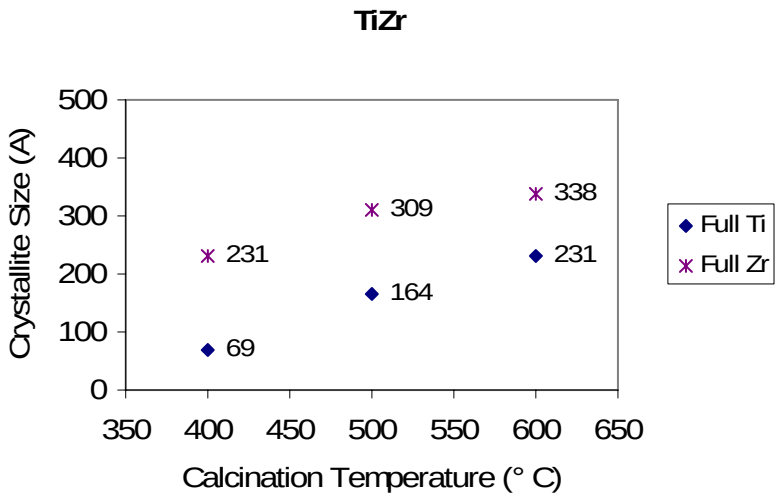

Figure 93. The crystallite sizes of Full Ti and Full Zr calculated via Expert Plus with varying calcination temperature.

6.1.3.4. Surface charge (zeta potential)

The phase transformations during heat treatment may be beneficial to prepare membranes with different physicochemical properties (e.g. zeta potential). Some zeta potential measurements were performed with the suspensions of ground calcined oxides. The measurements were carried out in 10^{-3} M KCl solutions with varying initial pH values (3.5 - 9.8). The measured zeta potentials were all negative, but with different magnitudes. The results of first measurements for initial pH value of 8.4 are given in Table 9 and Figure 94. The TiZr 5050 calcined at 500°C showed the highest zeta potential in magnitude. The differences in the magnitudes of zeta potential values may be beneficial in filtration experiments where surface charge is an effective parameter. This difference may be beneficial for some other applications besides membrane filtration, too (e.g. HPLC column packings, etc.). The zeta potential measurements should be repeated to have results with less standard deviation (width). The high standard deviations might be the result of sample preparation procedure or sample instability due to low ionic strength. There was a significant difference between zeta potentials of Full Ti calcined at 600° C and calcined at lower temperatures for KCl solution with an initial pH of 8.4.

Table 9. The zeta potential measurement (n=6) results (zeta: mV, width: standard deviation) of dried / ground / calcined Ti / Zr sols in 10^{-3} M KCl solutions with initial pH value of 8.4.

	400° C		500° C		600° C	
	Zeta (mV)	Width	**Zeta** (mV)	Width	**Zeta** (mV)	Width
Full Ti	-29.4 ± 5.4	21.5 ± 15	-30.1 ± 4	36.5 ± 23.3	-10.3 ± 10.6	22.1 ± 22.8
TiZr7525	-28.2 ± 10.4	33.9 ± 24.1	-44.2 ± 4.6	68.7 ± 33.5	-32.2 ± 10.2	60.7 ± 26.4
TiZr5050	-38.1 ± 8.1	7.4 ± 5	-47 ± 4.8	54.2 ± 22.1	-25.4 ± 7.1	21.8 ± 13.4
TiZr2575	-36 ± 6.5	50 ± 29.3	-36 ± 11.8	3.8 ± 4.4	-28.8 ± 3.5	42.7 ± 13.1
Full Zr	-19.2 ± 8.3	35.8 ± 26	-27.9 ± 7.4	42.6 ± 53	-18 ± 7.3	24.5 ± 49.6

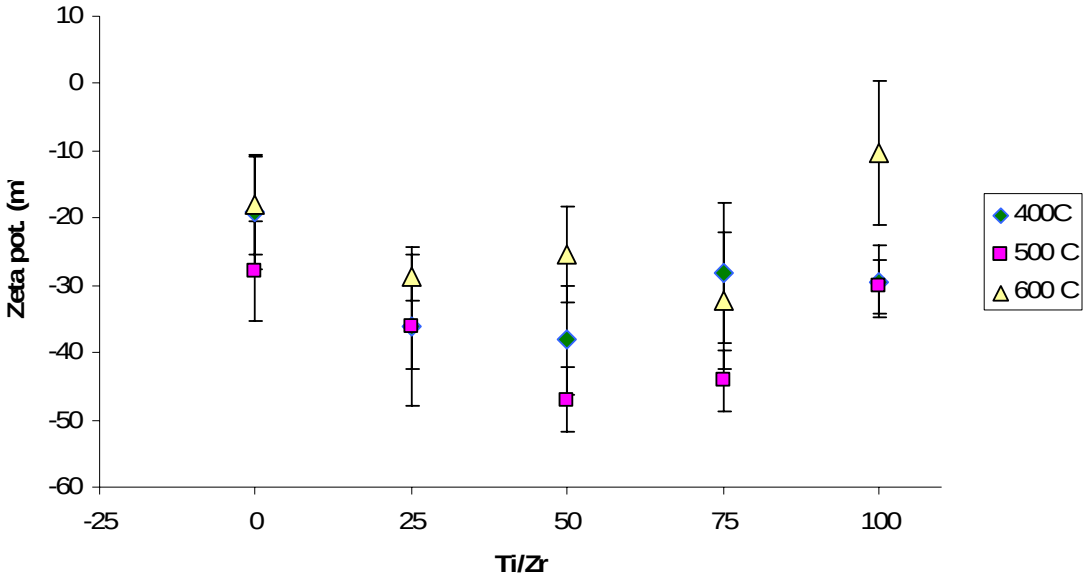

Figure 94. The zeta potential (mV) values of dried / ground / calcined Ti / Zr sols with different Ti ratios (%) and varying calcination temperature.

The zeta potential values of the Ti-Zr mixd oxide system were further measured at varying pH values: 3.5, 7.2 and 9.8, as mentioned above. The changes in zeta potential values measured in 10^{-3} M KCl solution with initial pH values 3.5, 7.2 and 9.8 were as shown in Table 10 / Figure 95, Table 11 / Figure 96**,** Table 12 / Figure 97, respectively.

At acidic pH (~3.5) (as shown in Table 9 / Figure 95) Full Ti calcined at 400° C had a high positive zeta potential (~46 mV) but at elevated calcinations temperatures it had very lower surface potential (~6 mV). The change in zeta potential values of Full Zr was not that severe. The data show a small decrement at 500° C calcination temperature. The trends for TiZr2575 and TiZr 5050 were similar and their surface potential were increasing with increasing calcination temperature which was greater for TiZr 5050. The zeta potential of TiZr 7525 did not change considerably with increasing calcination temperature, there was a slight decrease.

Table 10. The zeta potential measurement (n=10) results for dried / ground / (un)calcined Ti / Zr sols in 10^{-3} M KCl solution with initial pH 3.5.,

	400° C		500° C		600° C		Uncalcined	
	final pH	Zeta (mV)	final pH	Zeta (mV)	final pH	Zeta (mV)	final pH	Zeta (mV)
Full Ti	3.56	46.2 ± 4.3	3.53	5.1 ± 8.7	*3.5*	7.7 ± 7.5	*3.4*	45.1 ± 1.7
TiZr 7525	3.5	14.4 ± 15.7	3.5	9 ± 14.6	3.52	8.2 ± 13.5	3.4	33.2 ± 8.1
TiZr 5050	3.52	5.6 ± 9	3.5	32 ± 4.3	3.52	31.8 ± 8.9	3.3	11.8 ± 14.5
TiZr 2575	3.51	3.2 ± 11.8	3.52	43.3 ± 3.9	3.51	41.4 ± 5	3.43	19.3 ± 17.2
Full Zr	3.51	35 ± 11.2	3.52	22.9 ± 10.4	3.54	38.6 ± 15.3	3.25	31.4 ± 13.1

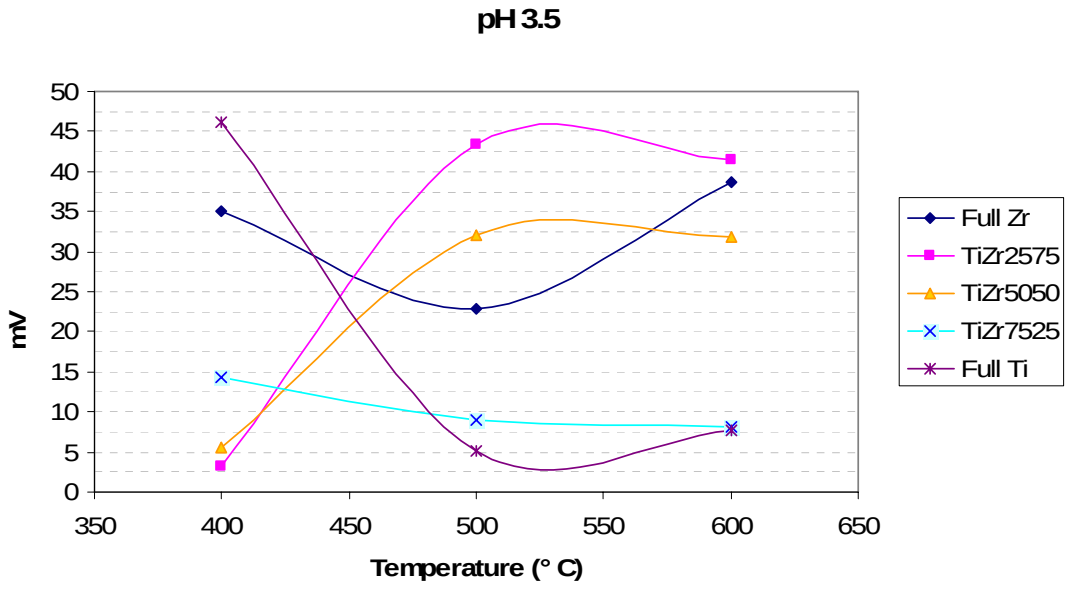

Figure 95. The zeta potential measurement (n=10) results for dried / ground / calcined Ti / Zr sols in 10^{-3} M KCl solution with initial pH 3.5.

For initial pH 7.2 the surface potentials for all samples were negative and had relatively low values in magnitude showing that the pH values were close to isoelectrical points of the oxides as can be seen in Table 10 / Figure 96. The zeta potential values for Full Ti were decreasing (in magnitude) with increasing calcination temperature while they were increasing for Full Zr. TiZr 5050 showed a similar trend with Full Ti while the profiles for TiZr 7525 and TiZr 2575 were more similar to Full Zr except the fact that after 500° C the change was not steep. TiZr 7525 had the lowest zeta potential values for varying calcination temperatures among three while Full Zr had the highest values.

Table 11. The zeta potential measurement (n=10) results for dried / ground / (un)calcined Ti / Zr sols in 10^{-3} M KCl solution with initial pH 7.2.

	400° C		500° C			600° C			Uncalcined		
	final pH	Zeta (mV)	final pH	Zeta (mV)	(+/-)	final pH	Zeta (mV)	(+/-)	final pH	Zeta (mV)	(+/-)
Full Ti	*7*	-17 ± 6.8	*6.4*	-6.7 ± 12.5		7.2	-3 ± 9.6		*3.9*	47 ± 1.8	
TiZr 7525	7.1	-2.4 ± 7.4	7.8	-7.1 ± 13.4		7.7	-9 ± 13.9		3.5	39 ± 2.2	
TiZr 5050	7.2	-24 ± 5.9	6.4	-14 ± 11.2		6.7	0.6 ± 2.8		3.6	24 ± 18.3	
TiZr 2575	7.7	-14 ± 9.7	7.4	-21 ± 9.7		7.1	-21 ± 14.5		3.6	25 ± 17.2	
Full Zr	7.9	-20 ± 14.3	7.2	-25 ± 10.9		6.7	-30 ± 14.3		3.9	15 ± 17.4	

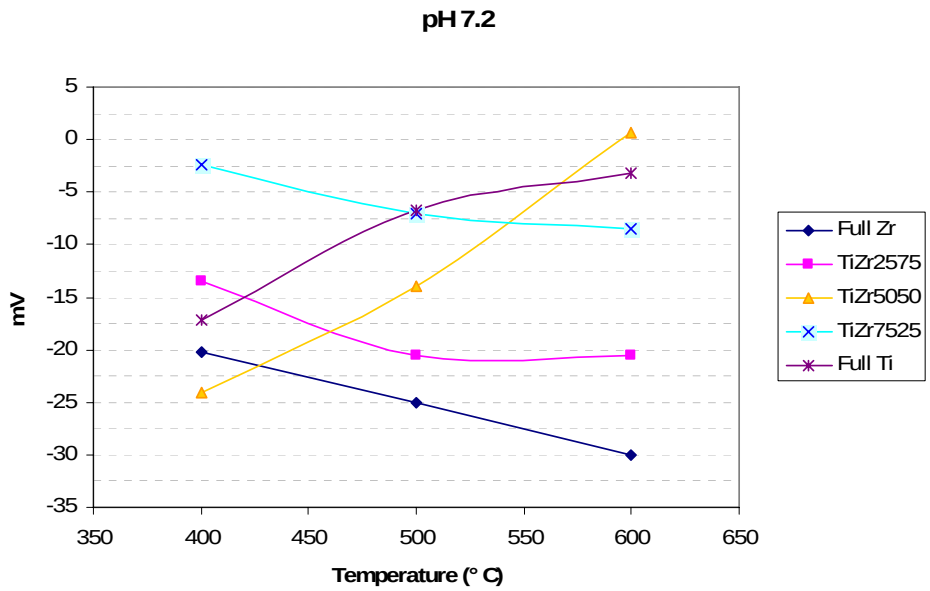

Figure 96. The zeta potential measurement (n=10) results for dried / ground / calcined Ti / Zr sols in 10^{-3} M KCl solution with initial pH 7.2.

For basic pH (~9.8) the zeta potential values were generally relatively higher in magnitude since the pH values reached were higher than the isoelectric points (pI) of the oxides as can be seen in Table 12 and Figure 97. The zeta potential of Full Ti was the highest among five for 400° C in magnitude but it decreased drastically at elevated calcination temperature (600° C). The Ti-rich sample TiZr 7525 showed a similar trend like Full Ti. The zeta potential of other three samples slightly increased with increasing calcination temperature. The highest zeta potential values were measured for TiZr 7525 among three.

The effect of calcination temperature on pure zirconia sol and its characteristics was further investigated. Zirconia unsupported layers were prepared from a zirconia sol with average particle size of 9.6 nm and calcined at three different temperatures (400°, 450° and 500° C). The zeta potential values of these samples were determined after dispersing in KCl solution (10^{-3} M, initial pH: 7.4) for surface characterization. The magnitudes of zeta potential values were found to be increasing with the increasing calcination temperature, -21.4, -25.1, -28.2 mV, respectively as shown in Figure 98.

Table 12. The zeta potential measurement (n=20) results for dried / ground / (un)calcined Ti / Zr sols in 10^{-3} M KCl solution with initial pH 9.8.

	400° C		**500° C**		**600° C**		**Uncalcined**	
	final pH	Zeta (mV)	final pH	Zeta (mV)	final pH	Zeta (mV)	final pH	Zeta (mV)
Full Ti	*7.6*	-46 ± 11.5	*7,5*	-43 ± 13	*7,6*	-9 ± 13	*5*	22 ± 0.5
TiZr 7525	9.2	-43 ± 11.7	9,1	-46 ± 9.8	9,1	-30 ± 23	3,7	41 ± 5.1
TiZr 5050	9.2	-38 ± 24.5	9,2	-49 ± 14	9,2	-50 ± 9.1	4	44 ± 6.2
TiZr 2575	9.3	-40 ± 22.4	9,4	-53 ± 8.8	9,4	-51 ± 6.7	3,3	37 ± 12.1
Full Zr	9,4	-37 ± 19.1	9	-40 ± 11	9,2	-45 ± 14	3,9	37 ± 13.1

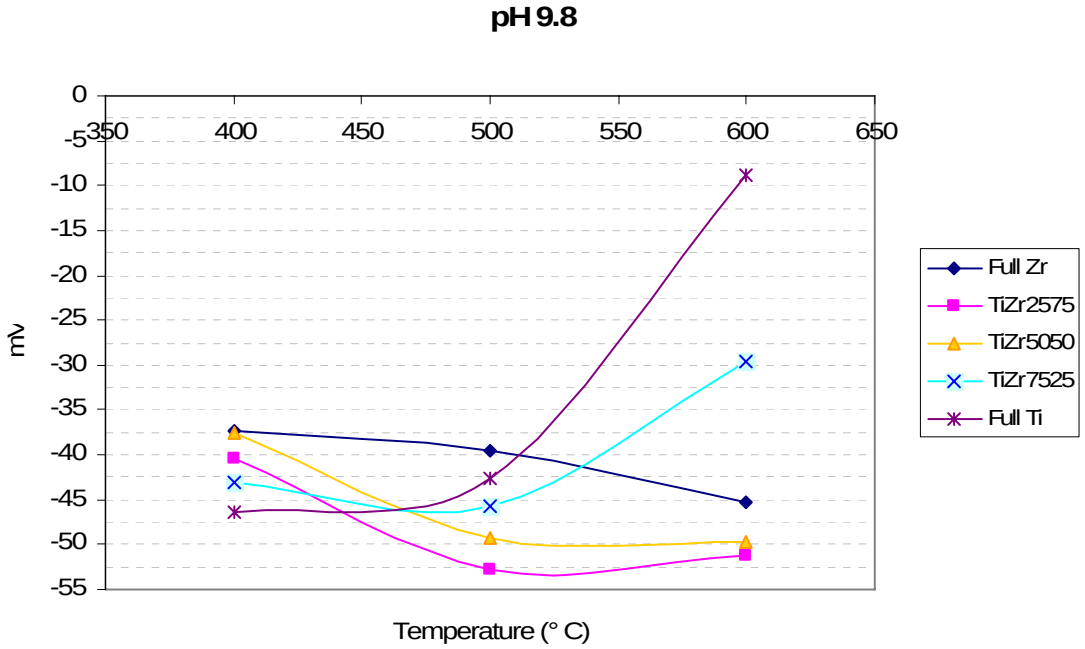

Figure 97. The zeta potential measurement (n=20) results for dried / ground / calcined Ti / Zr sols in 10^{-3} M KCl solution with initial pH 9.8.

This slight increase in the zeta potential magnitudes may be due to the change of crystal morphology which was determined by XRD analysis of which results are given in Figure 99. There was an increasing tetragonal to monoclinic phase transformation with increasing calcination temperature (i.e. zirconia has a polymorphic structure in between the temperature range investigated). Benfer, et al. (2001) reported ZrO_2 prepared with diethanolamine as a hydrolysis-condensation reactions regulator in sol preparation was in metastable tetragonal phase after calcination at 500° C and there were no peaks for monoclinic phase in the XRD patterns of that sample. Van Gestel, et al. (2006) prepared zirconia sols with acetylacetone to prevent rapid hydrolsis-condensation reactions. They calcined the unsupported layer formed by this sol at 400° and 450° C. The XRD patterns indicate the presence of monoclinic phase in the sample calcined at 450° C. They pointed the tetragonal to monoclinic phase transformation may increase the risk of crack–formation. The crystallite sizes with varying calcination temperatures calculated via software of the XRD instrument (Expert Plus, Scherrer calculator tool) are given in Figure 100. There were no big differences between the calculated crystallite sizes for samples calcined at 400° and 450° C but the crystallite size slightly increased when the sample was calcined at 500° C.

The average particle size of the zirconia sol forming these microstructures was 4.9 (± 0.4) nm (with respect to volumetric distribution) as shown in Figure 101. The microstructure of the layers formed by coating and calcination of the zirconia sol was analyzed by using SEM. The SEM micrographs for varying calcination temperatures are given in Figure 102. The micrographs showed that the microstructure after calcinations at different temperatures were all fine and formed by nanoparticulates with sizes around 20-50 nm. A sol with a smaller initial average particle size would probably result in an even finer microstructure.

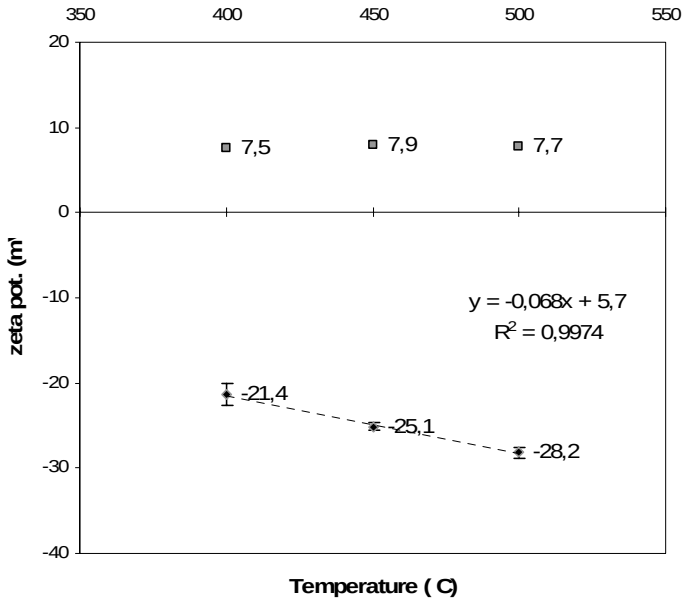

Figure 98. The zeta potential of zirconia dispersed in 10^{-3}M KCl solution with initial pH value of 7.4 and the final pH values of the solution.

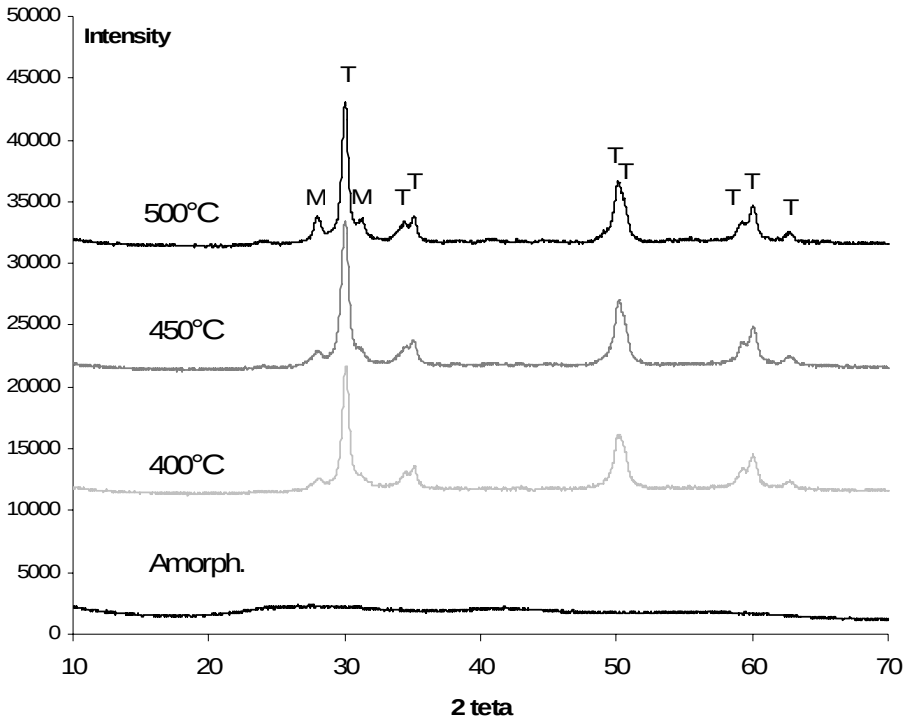

Figure 99. The XRD analysis for zirconia powders calcined at three different temperatures (M: monoclinic, T: tetragonal).

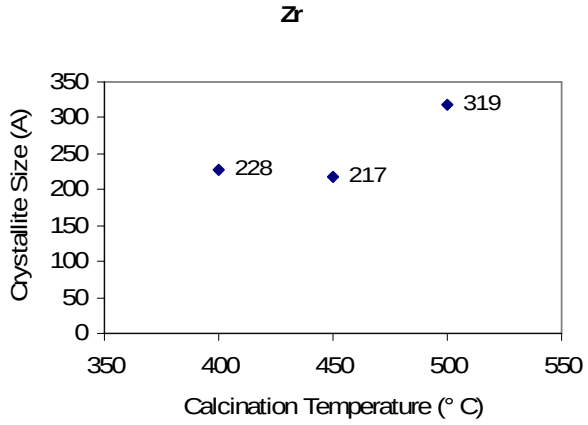

Figure 100. The crystallite sizes of pure Zr calcined at different temperatures calculated via XRD instrument software.

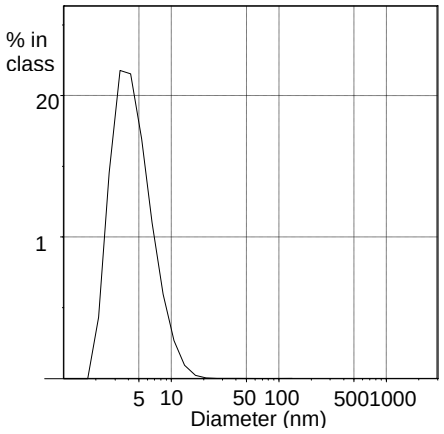

Figure 101. The volumetric particle size distribution of Zr sol.

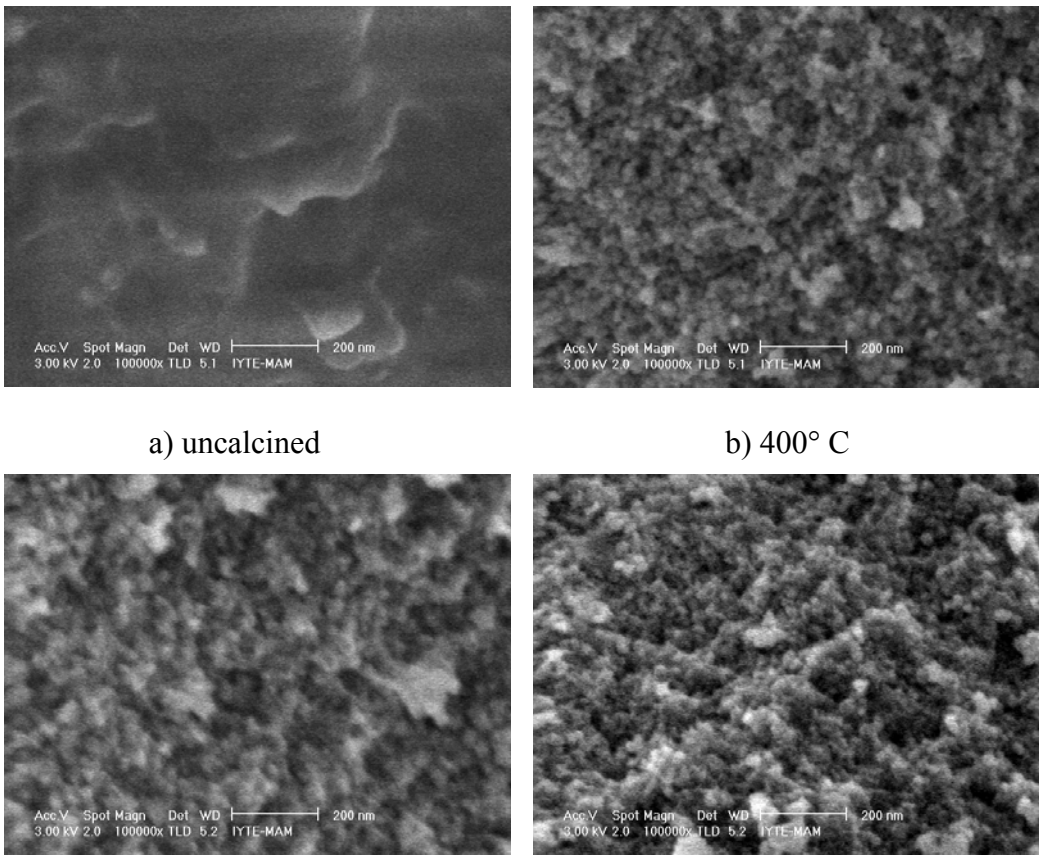

a) uncalcined b) 400° C

c) 450° C d) 500° C

Figure 102. The SEM micrographs of the zirconia sol uncalcined (a) and calcined at 400° (b), 450° (c) and 500° C (d).

The changes in zeta potential of zirconia calcined at varying temperatures for 150 minutes were measured by dispersing the ground oxide (coded 27-12-5) in 10^{-3} M KCl solution with initial pH values of 3.5, 4.4, 7.2 and 9.8. The results are shown in Figure 103. The differences between zeta potential of zirconia calcined at varying temperature are clearer at more acidic and basic pH values. Zirconia calcined at 400° C had the highest zeta potential value at acidic pH (~3.5) and zirconia calcined at 500° C had the lowest zeta potential value in magnitude at basic pH (~9.4). The increasing calcinations temperature resulted in a decrease in the magnitudes of zeta potential on acidic and basic side.

The data can be rearranged as shown in Figure 104 using the final pH values of the oxide dispersions. The isoelectric point of zirconia was increasing slightly with increasing calcination temperature.

The effect of calcination temperature on crystallinity and surface properties of titania sol was investigated. The titania sol was prepared by using molar ratios of alkoxide : propanol : acetyl acetone : nitric acid : water as 1 : 13.19 : 2 :0.0572 : 2, titanium propoxide as alkoxide and acetyl acetone (acac) as reaction rate controlling agent. The average particle size of the sol was measured as 2.9 ± 0.1 nm (PI: 0.231 ± 0.055, n=6, accepted runs=5). This sol was dried, ground and calcined at varying temperatures.

The zeta potential of calcined titania powders were measured in 10^{-3} M KCl with initial pH of 7.4. The results are given in Figure 105. The zetapotential values decreased by increasing calcination temperature and even reached negative values for 550° C.

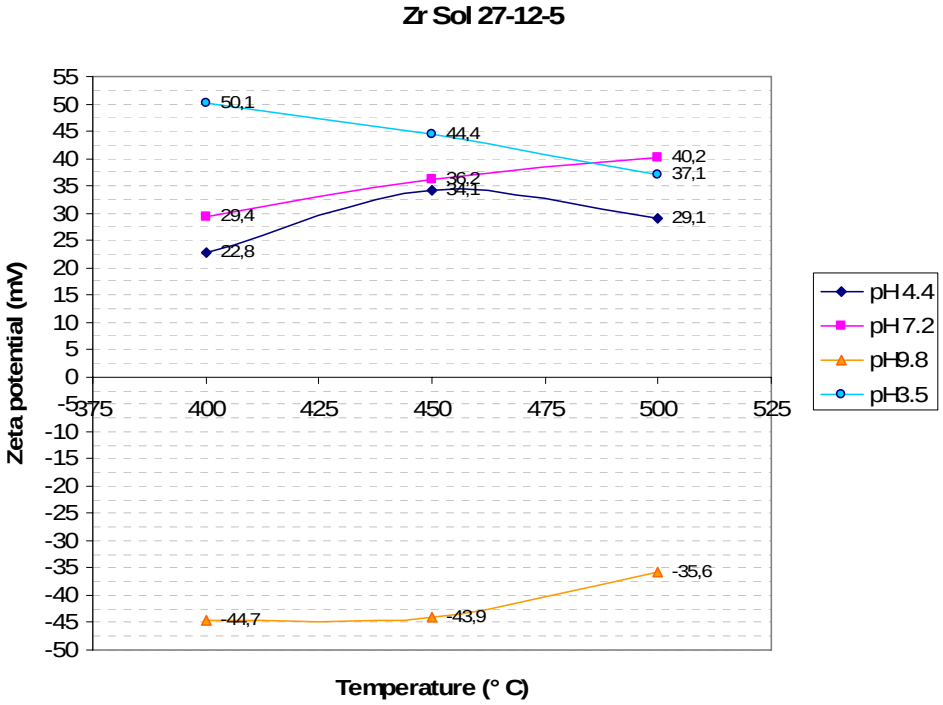

Figure 103. The zeta potential values of Zr sol dried, ground and calcined at varying temperatures for 150 minutes, measured in 10^{-3} M KCl solution with varying initial pH values.

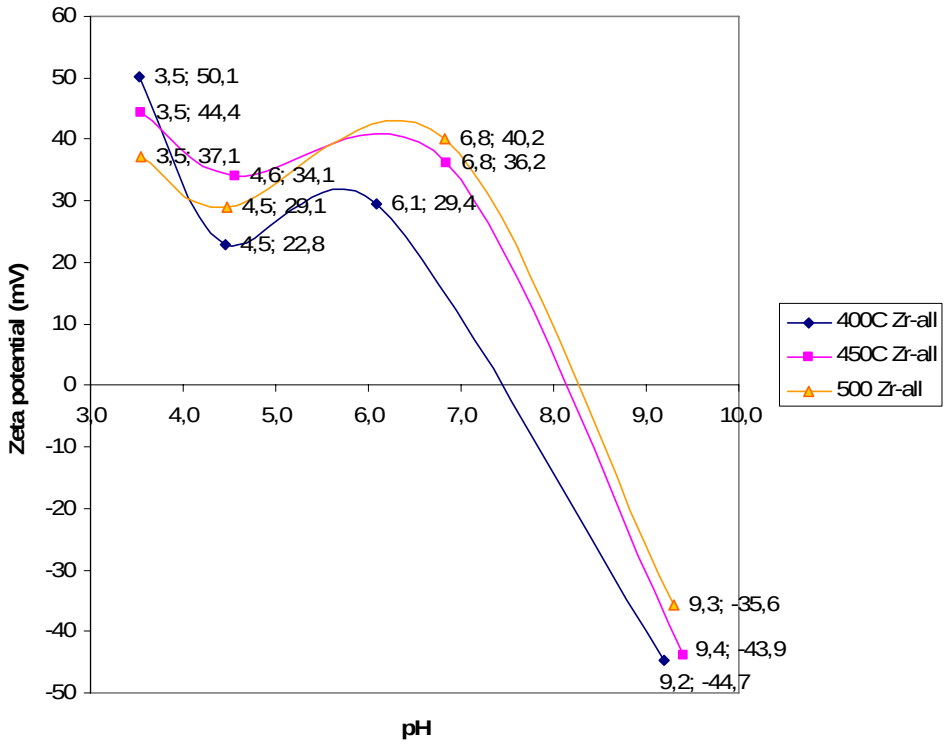

Figure 104. The zeta potential values of Zr sol dried, ground and calcined at varying temperatures for 150 minutes, measured in 10^{-3} M KCl solution with varying initial pH values.

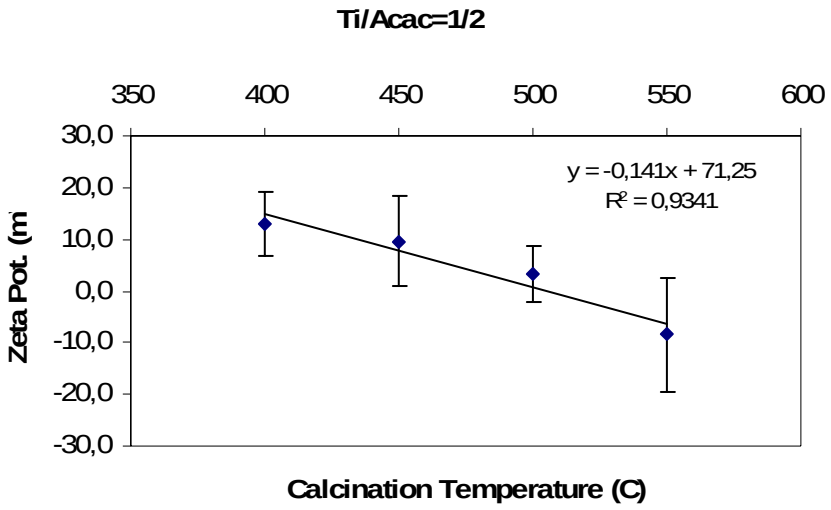

Figure 105. The zeta potential of titania calcined at varyng temperatures dispersed in 10^{-3} M KCl solution with initial pH value of 7.4.

The changes in crystallinity of the calcined titania was determined by using XRD. The phase transformation from anatase to rutile increased with increasing calcination temperature as can be seen in Figure 106. There may be a relationship between this phase transformation and change in surface charge of titania.

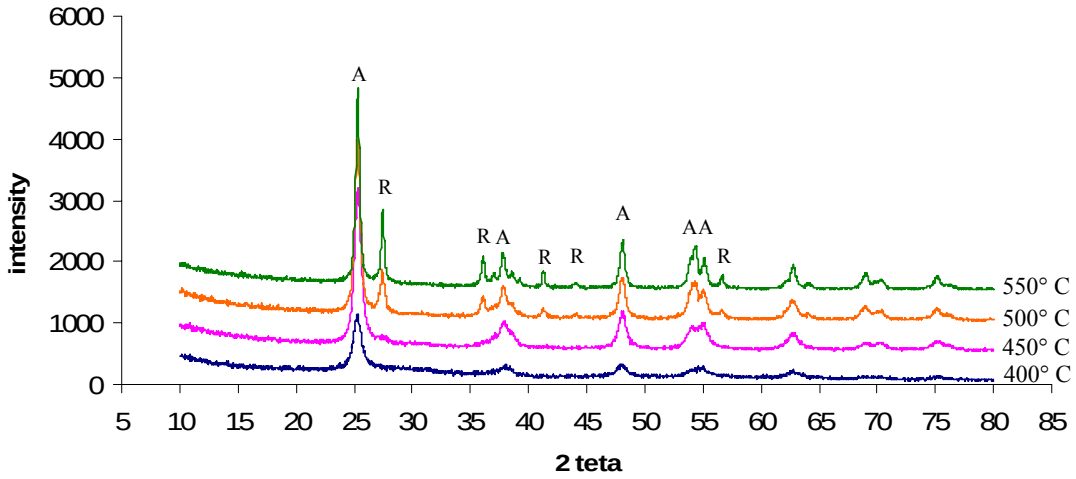

Figure 106. The XRD analysis for titania powders calcined at different temperatures (A: Anatase, R: Rutile).

The crystallite sizes of the titania calcined at different temperatures were calculated via software introduced with the XRD instrument (Expert Plus) using the Scherrer calculator tool. The crystallite sizes calculated from the peak with the highest intensity were found to increase with increasing calcination temperature as shown in Figure 107.

Two titania sols dried and calcined at 475° C and 800° C were characterized to have pure anatase and rutile phase, respectively, were kindly supplied from another researcher (Özlem Çağlar Duvarcı). The zeta potential values of these pure anatase and rutile titania were measured at varying initial pH values and the results are given in Figure 108. The isoelectric point was decreasing as the phase turned from anatase to rutile with increasing calcination temperature.

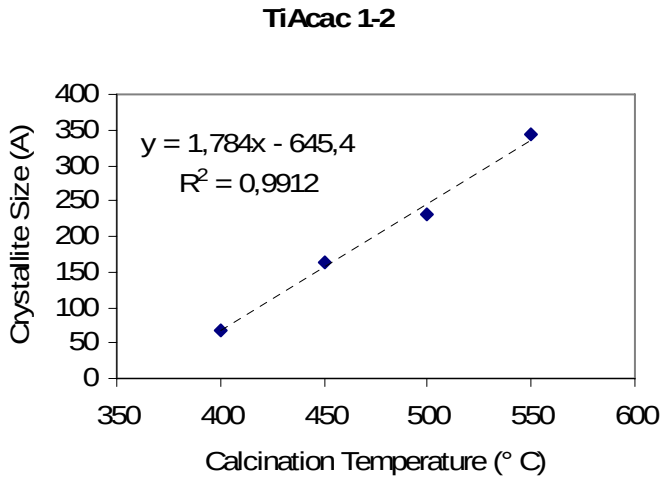

Figure 107. The crystallite sizes of titania (prepared via TiAcac 1-2) calcined at varying temperatures.

6.1.3.5. Addition of some elements

The effects of addition of some elements into the zirconia sol on its stability and on the surface formed by coating and calcining these sols were analyzed. For this purpose 0.1, 0.2 and 0.3 moles of iron (Fe) and 0.1 and 0.2 moles of Boron (B) were added into the sols. The molar ratio of propanol in the sols was 15 or 20 per mole of alkoxide. The average particle size of the sols prepared were > 11 nm as shown in

Figure 109 for sols with 15 moles of propanol per mol alkoxide. The average particle size increased with increasing Fe addition which was due to the water in the iron nitrate nona hydrate. The effect of this water decreased in a more diluted sol with higher alcohol : alkoxide ratio (i.e. with a more dilute sol). The average particle size for the sol with molar ratios of alkoxide : alcohol : Fe as 1 20 : 0.3 was 7.4 nm ± 0.2 nm.

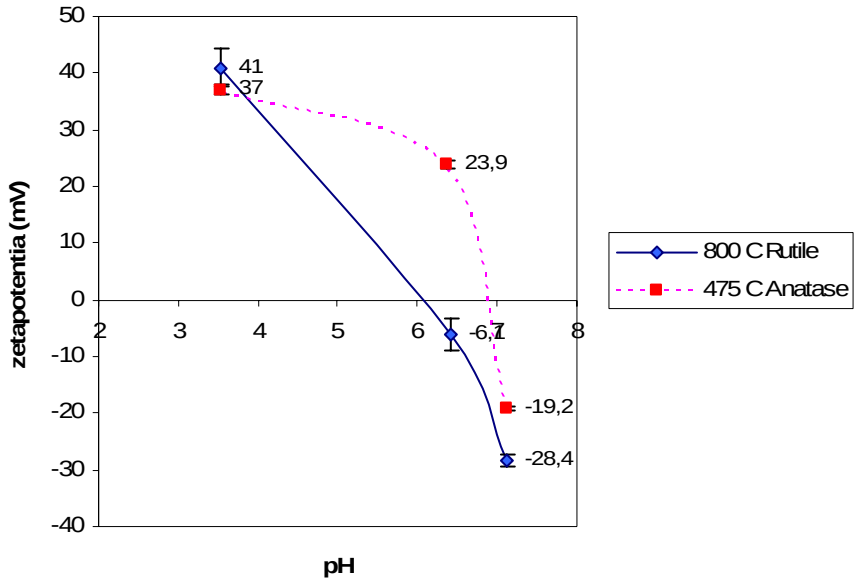

Figure 108. The zeta potential values for pure anatase and rutile titania measured in 10^{-3} M KCl solution with varying initial pH values.

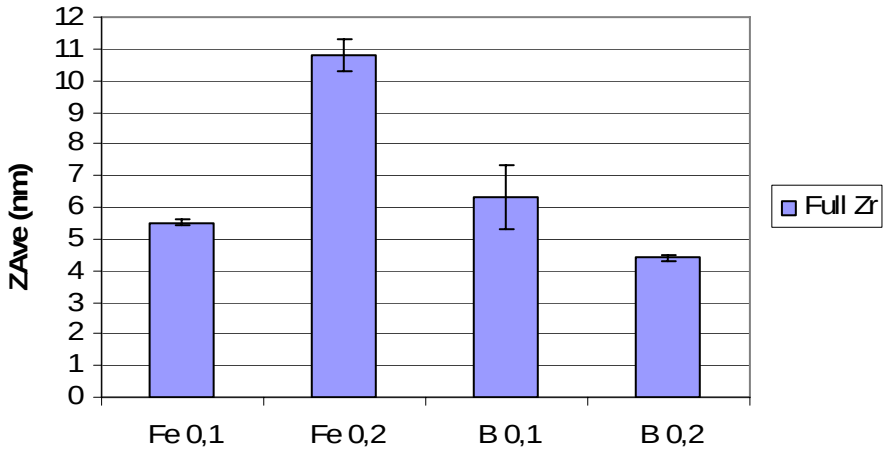

Figure 109. The average particle sizes of the Full Zr polymeric sol (alkoxide : alcohol molar ratio of 1 : 15) with iron and boron addition of 0.1 or 0.2 mole per mole of alkoxide.

The zeta potentials of the dried and calcined (500° C / 2 h) sols with 0.2 mole Fe or B per mole alkoxide addition were measured in 10^{-3} M KCl with initial pH of 7.91. The addition of Fe decreased the magnitude of the zeta potential of the oxide while B addition did not change the value as shown in Figure 110. The data of similar measurements at varying initial pH values can be seen in Figure 111. The iron addition resulted in decrease in zeta potential at acidic pH values and decreased the isoelectric point slightly. The iron-added zirconia showed the highest zeta potential (in magnitude) close to neutral pH.

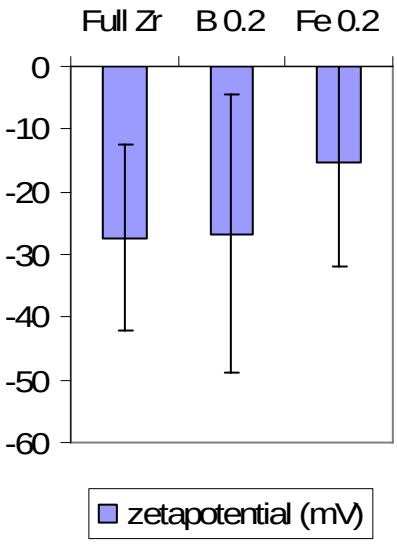

Figure 110. The zeta potentials of the dried-calcined (500° C / 2 hours) Full Zr polymeric sol (alkoxide : alcohol molar ratio of 1 : 15) with iron or boron addition of 0.2 mole per mole of alkoxide in 10^{-3} M KCl solution with initial pH value of 7.9.

6.1.3.6. Coating

The top layer was formed via dip-coating of pre-coated (or uncoated) supports via polymeric sols or dispersion of fine ceramic powder (AKP-50 alumina) in polymeric sols. After dip-coating the supports were left drying and heat treated at varying temperatures (400°-500° C). There were some coating problems, observed in formation of top layer as were for formation of intermediate layer. The polymeric sol was sucked into the pre-coated supports, preventing formation of a layer. There were zones where

there were small amounts of deposits of particulates in the polymeric sol as can be seen in Figure 112.

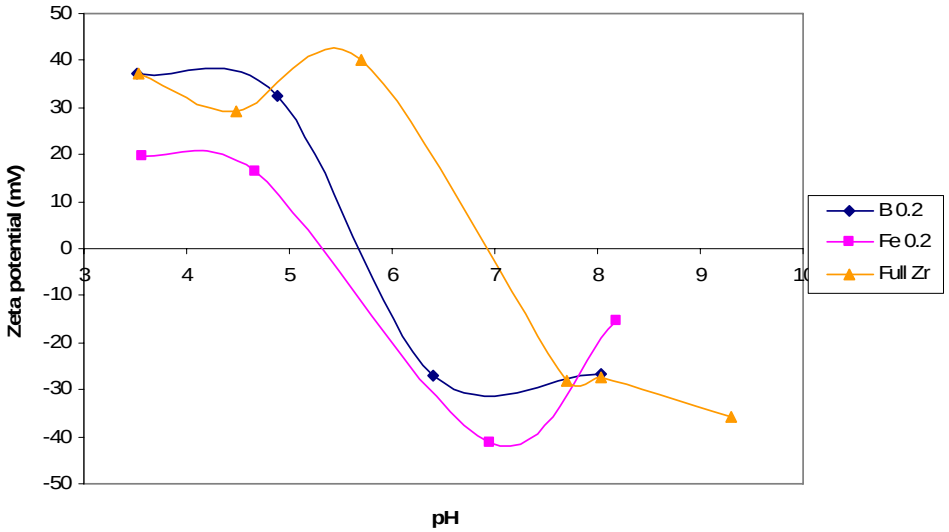

Figure 111. The zeta potentials of the dried-calcined (500° C / 2 hours) Full Zr polymeric sol (alkoxide : alcohol molar ratio of 1 : 15) with iron or boron addition of 0.2 mole per mole of alkoxide at varying pH values.

Increasing the number of polymeric sol dip-coating / heat treatment cycle did not enhance the layer formation. There were darker zones which were probably semi-coated as can be seen in Figure 113. There were small zones where the coating formed a layer as shown in Figure 114 and 115 but not so many.

The dip-coating by using more viscous polymeric sols (e.g. polymeric Zr sol with 0.2 mol Fe / mol Zr (Fe 0.2), with an average particle size of 9.3 nm in volumetric distribution, Fe 0.1 (8.3 nm) or boron containing B 0.2 (7.3 nm)) which has probably lost some of its propanol during storage formed thicker coated layers on the supportswhich were peeled out during drying. There were residues of these peelings as can be seen in Figure 116 and some semi-coated zones as can be seen in Figure 117. These results show the viscosity of the sol coated should not be too high to prevent formation of an excessively thick layer which will peel out during drying / heat treatment.

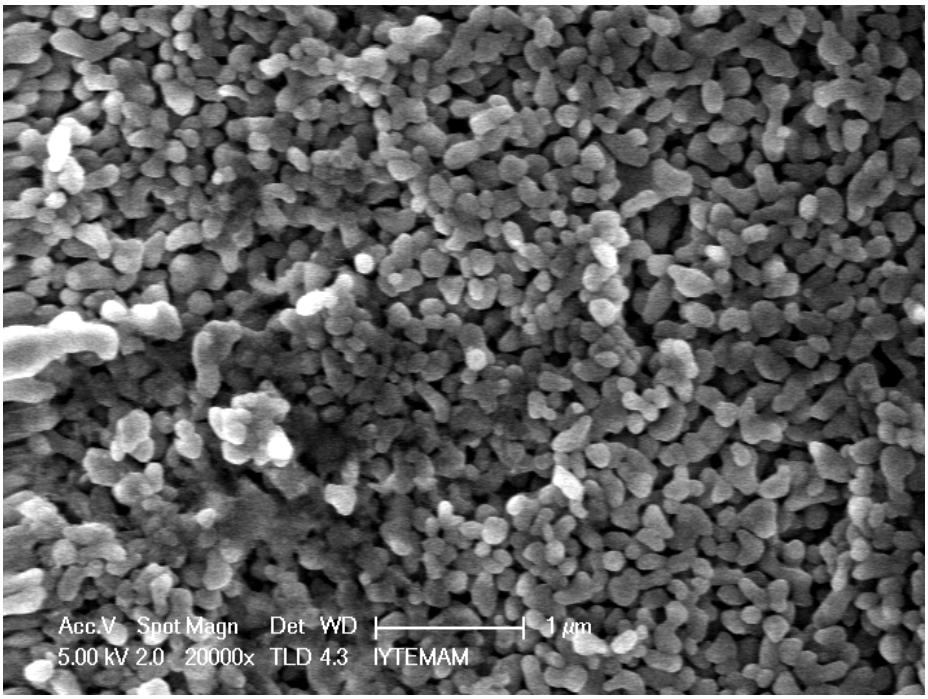

Figure 112. SEM micrograph of the die facing starch-free surface of AKP-50 double layer alumina support (10% corn starch, 1100° C / 2 h), dip-coated via 1:4 diluted polymeric Zr sol (NOR) (400° C / 2 h).

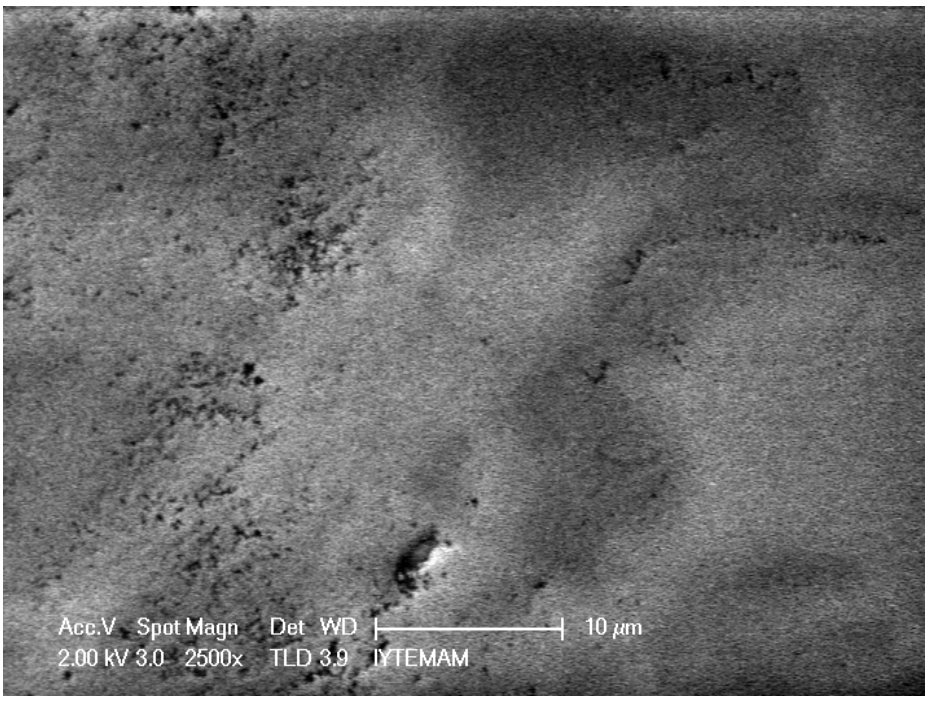

Figure 113. SEM micrograph of the air facing starch-free surface of AKP-50 double layer alumina support (10% corn starch, D(-), 1100° C / 2 h), dip-coated via 1st 1:4 diluted polymeric Zr sol (NOR), 2nd and 3rd undiluted polymeric Zr sol (NOR) (400° C / 2 h, after each dip-coating).

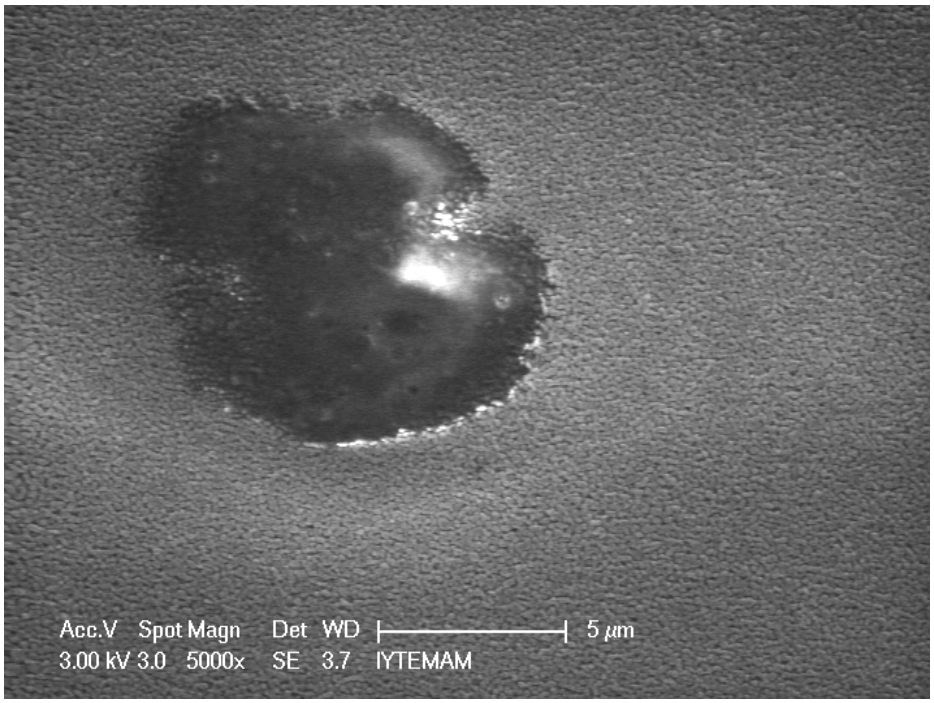

Figure 114. SEM micrograph of the air facing starch-free surface of AKP-50 double layer alumina support (10% corn starch, D(-), 1100° C / 2 h), dip-coated via 1st 1:4 diluted polymeric Zr sol (NOR), 2nd and 3rd undiluted polymeric Zr sol (NOR) (400° C / 2 h, after each dip-coating).

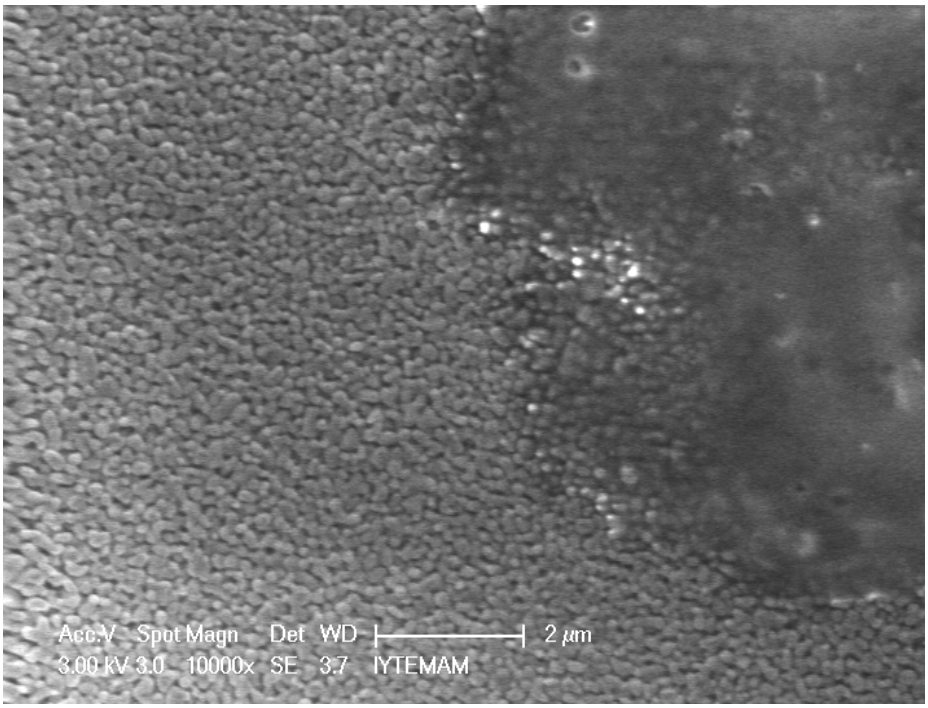

Figure 115. SEM micrograph of the air facing starch-free surface of AKP-50 double layer alumina support (10% corn starch, D(-), 1100° C / 2 h), dip-coated via 1st 1:4 diluted polymeric Zr sol (NOR), 2nd and 3rd undiluted polymeric Zr sol (NOR) (400° C / 2 h, after each dip-coating).

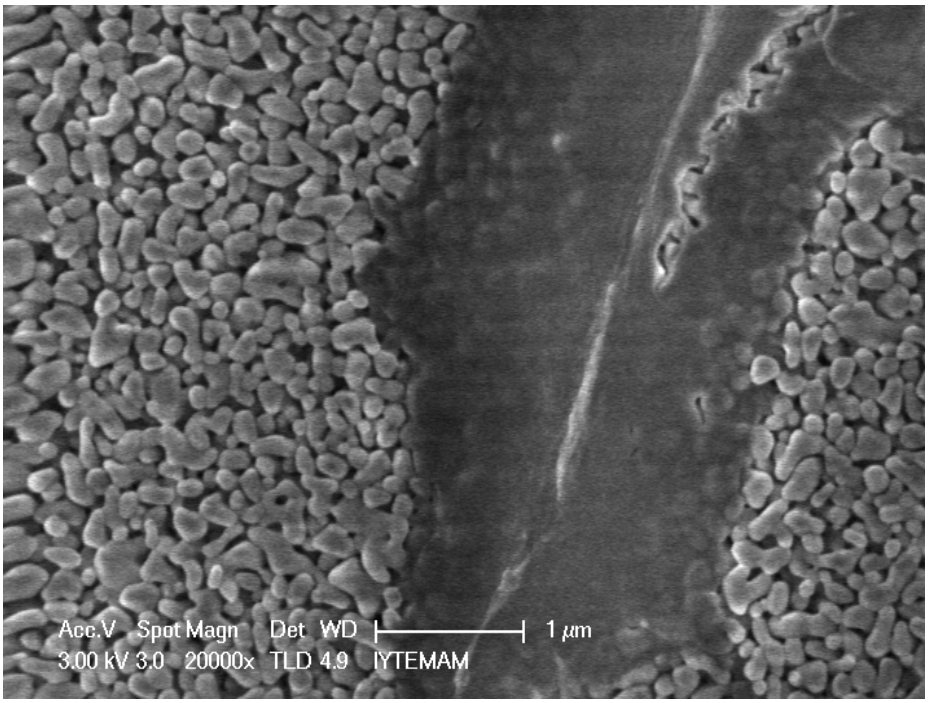

Figure 116. SEM micrograph of the air facing starch-free surface of AKP-50 double layer alumina support (10% corn starch, D(+), 1100° C / 2 h), dip-coated via polymeric Zr sol containing 0.2 mole Fe per mole of Zr (400° C / 2 h, after each dip-coating).

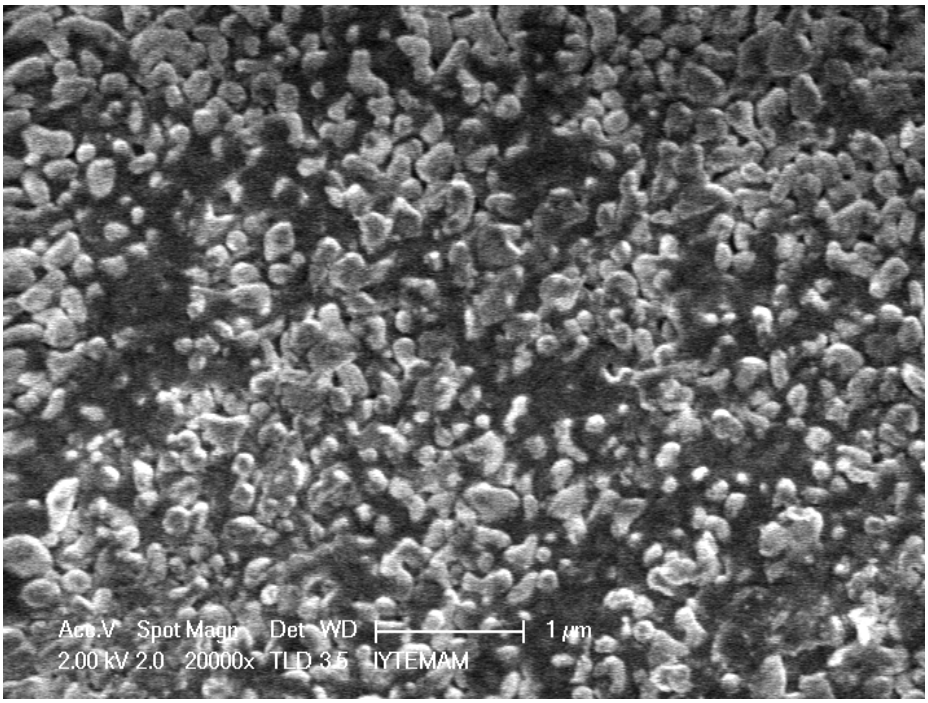

Figure 117. SEM micrograph of the air facing starch-free surface of AKP-50 double layer alumina support (10% corn starch, D(+), 1100° C / 2 h), dip-coated via polymeric Zr sol containing 0.1 mole Fe per mole of Zr (400° C / 2 h, after each dip-coating).

The polymeric sol was mixed with submicron alumina powder (AKP-50) to have a ~0.5 vol. % dispersion and this dispersion was used for dip-coating the supports to see probable enhancement on forming a layer of polymeric sol particulates. The dispersed fine powder was thought to fill the gaps on the surface while hampering the suction of the sol in the support by providing an alternative surface. The sediments of the fine alumina particles on the surface can be seen in Figure 118, 119 and 120. The layer formed via AKP-50 and polymeric sol was not continuous.

Increasing the number and duration of dip-coating resulted in a continuous layer of AKP-50 and polymeric sol as can be seen in Figure 121 but the sol was again sucked into the support only leaving some residues between submicron alumina particles (Figure 122), which was confirmed via SEM-EDX analysis (Figure 123).

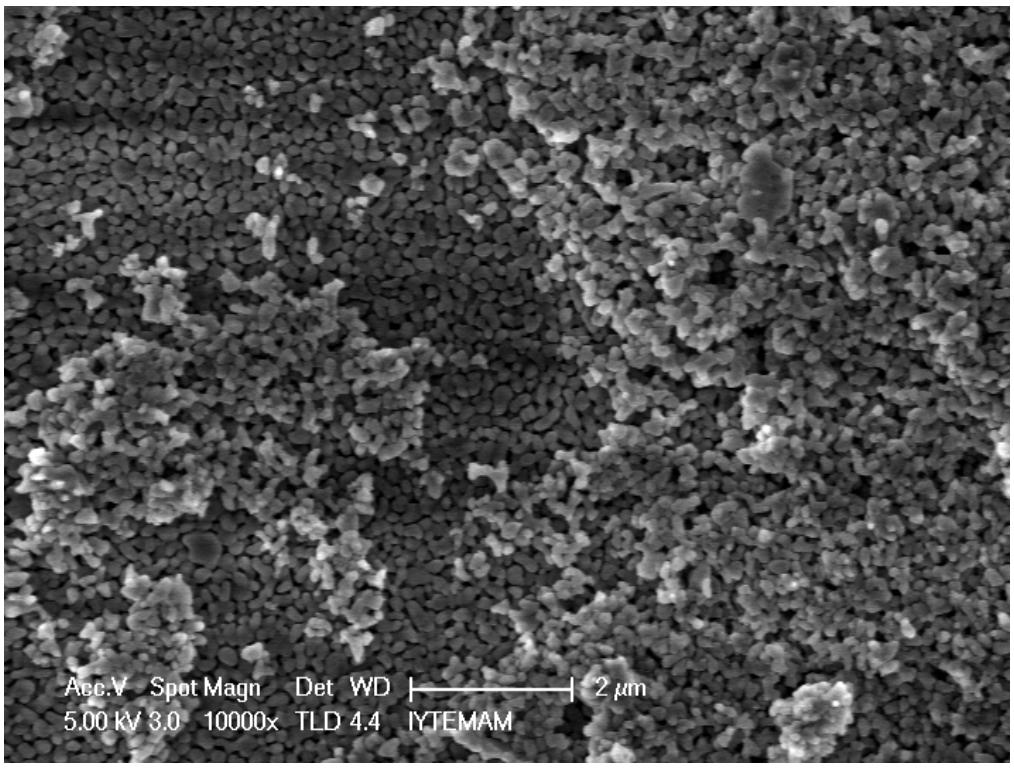

Figure 118. SEM micrograph of the air facing starch-free surface of AKP-50 double layer alumina support (10% corn starch, D(-), 1100° C / 2 h), dip-coated (10+1 sec.) via dispersion of AKP-50 alumina in in polymeric Zr sol (~0.5 vol. %) (400° C / 2 h).

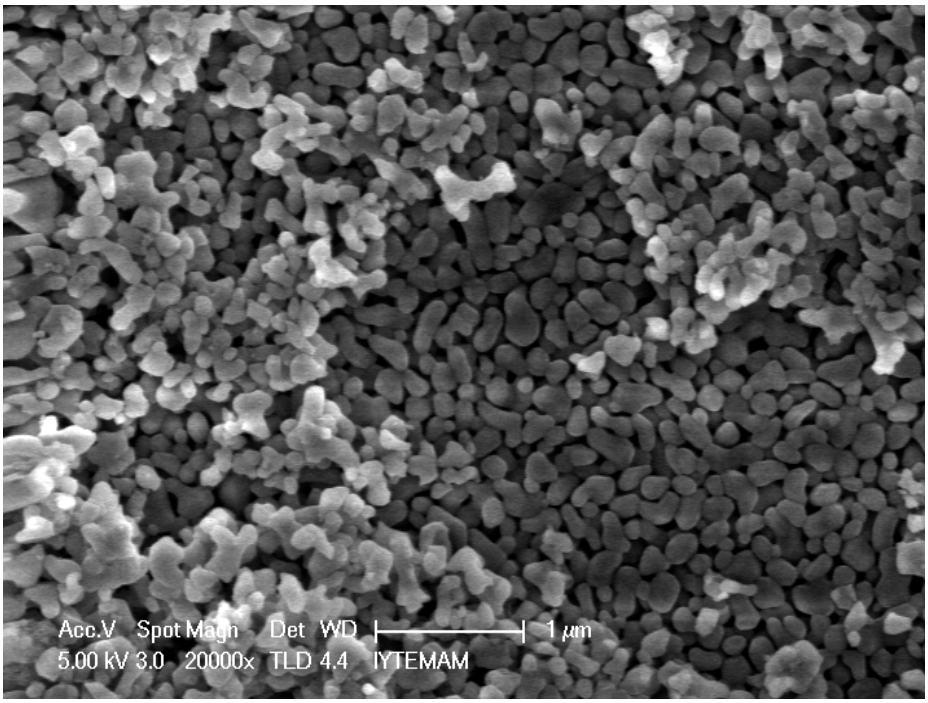

Figure 119. SEM micrograph of the air facing starch-free surface of AKP-50 double layer alumina support (10% corn starch, D(-), 1100° C / 2 h), dip-coated (10+1 sec.) via dispersion of AKP-50 alumina in polymeric Zr sol (~0.5 vol. %) (400° C / 2 h)

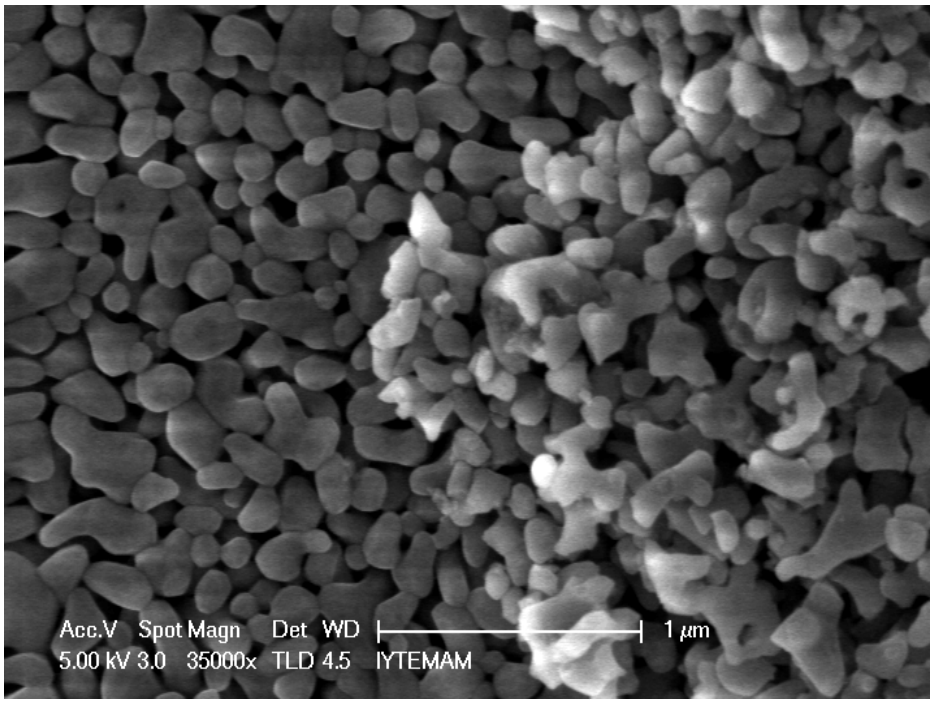

Figure 120. SEM micrograph of the air facing starch-free surface of AKP-50 double layer alumina support (10% corn starch, D(-), 1100° C / 2 h), dip-coated (10+1 sec.) via dispersion of AKP-50 alumina in polymeric Zr sol (~0.5 vol. %) (400° C / 2 h).

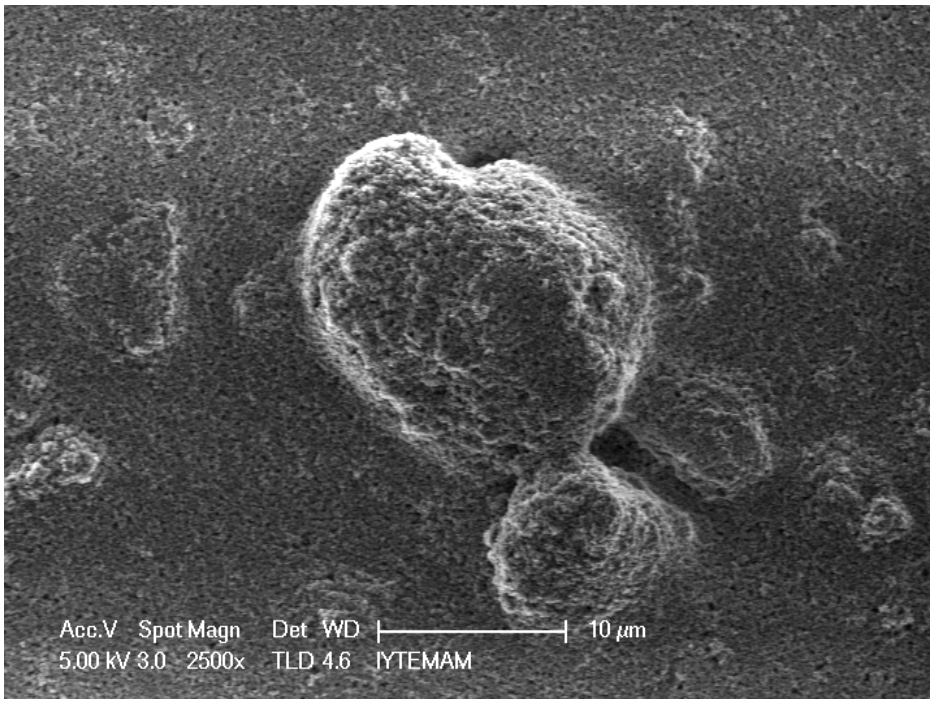

Figure 121. SEM micrograph of the air facing starch-free surface of AKP-50 double layer alumina support (10% corn starch, D(-), 1100° C/2h), dip-coated several times (10 sec.) via dispersion of AKP-50 alumina in polymeric Zr sol (~0.5 vol. %) (400° C / 2 h)

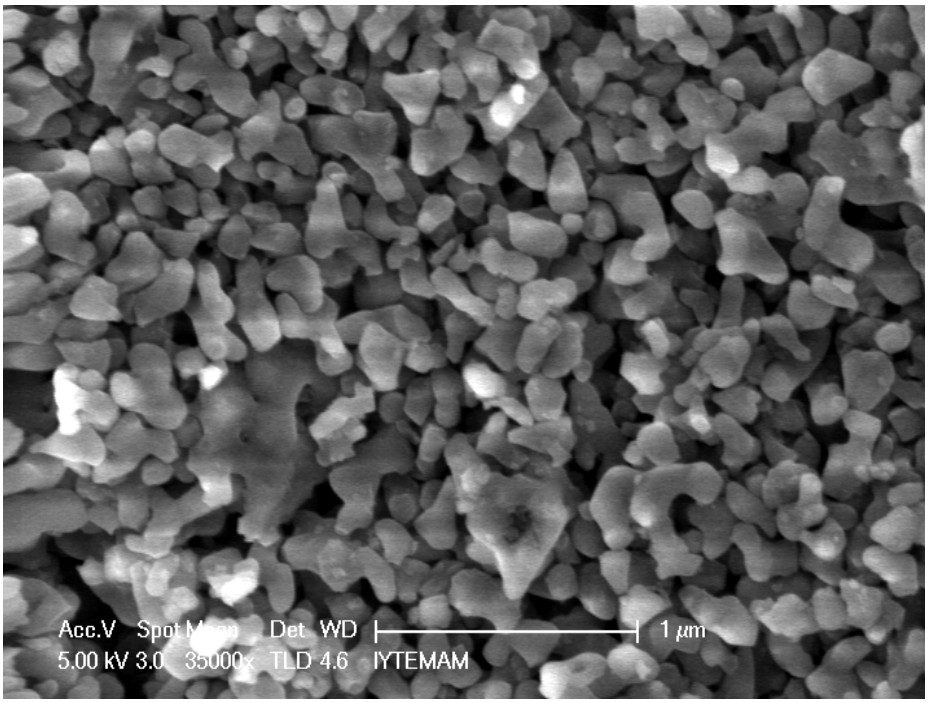

Figure 122. SEM micrograph of the air facing starch-free surface of AKP-50 double layer alumina support (10% corn starch, D(-), 1100° C / 2 h), dip-coated (several times for 10 sec.) via dispersion of AKP-50 alumina in polymeric Zr sol (~0.5 vol. %) (400° C / 2 h).

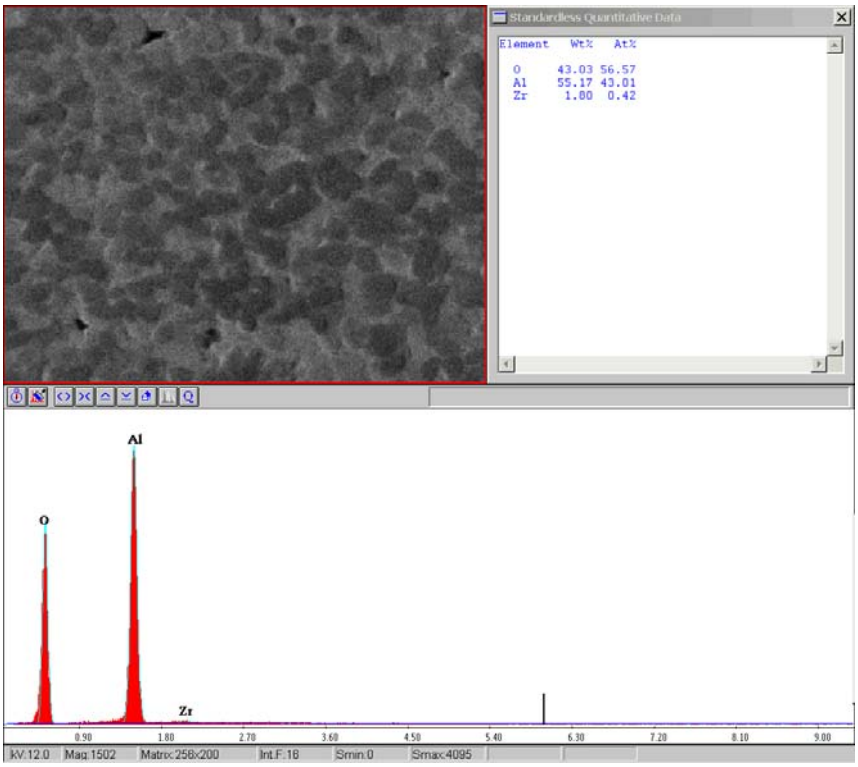

Figure 123. SEM-EDX micrograph of the air facing starch-free surface of AKP-50 double layer alumina support (10% corn starch, D(-), 1100° C/2h), dip-coated several times (10 sec.) via dispersion of AKP-50 alumina in polymeric Zr sol (~0.5 vol. %) (400° C / 2 h).

6.1.3.6.1 Aging of Sol and Simultaneous Coating

The viscosity and the drying kinetics of the sols were modified via addition of ethylene glycol (EG) (25-33 vol%). Since EG has a higher viscosity than Propanol the main media of the sol, the sol prepared with EG addition would have a higher viscosity and it would hardly be sucked by the porous surface. The vapour pressure of EG is lower than propanol that the drying of the sol with EG would dry more slowly which would probably prevent crack formations during drying. These predictions were investigated and it was observed that the EG addition has beneficial effects on crack prevention during drying. But a continuous layer formation on uncoated supports prepared via higher solid content (50-57 vol. %) suspensions was not possible. The sols were diluted from initial stocks and some EG was added to them. Then they were aged at room temperature (RT) or in an oven (39° C). The aging kinetics (i.e. the formation

and growth of nanoparticulates in the sols) were investigated via determining the particle size distribution of the sols in time using laser light scattering technique.

The growth kinetics of the Zr sol (1wt. %, with 25 vol. % EG) at RT was as shown in Figure 124. The changes in average PS of volumetric and number distributions and also change in Stoke's diameter can be seen in the figure. The average particle size (PS) of the Zr sol was increased 10 folds in 48 hours while it was kept at RT (~0.88 nm / h).

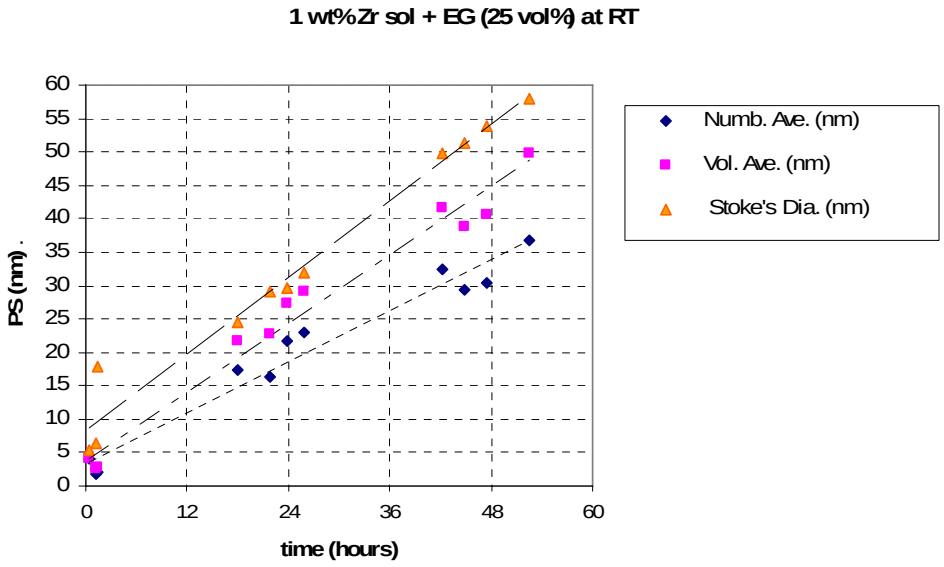

Figure 124. The change in average particle size (PS) of the 1 wt. % Zr sol (with 25 vol. % EG) at room temperature (RT).

The changes in the average particle size (PS) of the sol particulates were also investigated for other sols containing Zr and Ti in varying molar ratios. Simultaneously the supports prepared via suspensions with higher solid contents were dip-coated (d-c) by using these sols with varying in ave. PS. The sols were diluted to 0.5 or 1 wt. % and EG was added on them (25 vol%). The addition of EG was considered as the initial time. The aging kinetics were first determined at RT. The changes in the average PS of the sols were as shown in Figures 125, 126, 127, 128, 129.

The growth of the ave. PS in time was linear for 0.5 wt.% Full Zr sol which was ~0.4 nm / h with respect to volumetric PS distribution (PSD) (and ~0.44 nm / h with respect to Stoke's diameter). The ave. PS of TiZr 2575 was also increasing in time and

its rate was relatively higher ~0.56 nm / h with respect to volumetric PSD (and ~0.81 nm / h with respect to Stoke's diameter).

The sol particulate formation was relatively faster for Full Zr and Zr-rich TiZr 2575 sol. (i.e. the sol reached a stable form with monodisperse PSD relatively faster) which was not the case for TiZr 5050, TiZr 7525 and Full Ti. TiZr 5050 sol was stable (with a monodisperse PSD) only after 20 h. The increase in ave. PS of it was slow for first 24 hours. Afterwards the ave. PS increased faster (~2.3 nm / h) as shown in Figure 127.

For Ti-rich 0.5 wt. % sols (with 25 vol. %EG) there was no stability in 28 h (i.e. it was not possible to determine a monodisperse PSD (low poly dispersity) with detectable concentration). The changes in ave. PS for these sols are given in Figure 128, 129. The reason may be low solid content (0.5 wt. %) and / or lower reactivity of Ti species at the presence of EG.

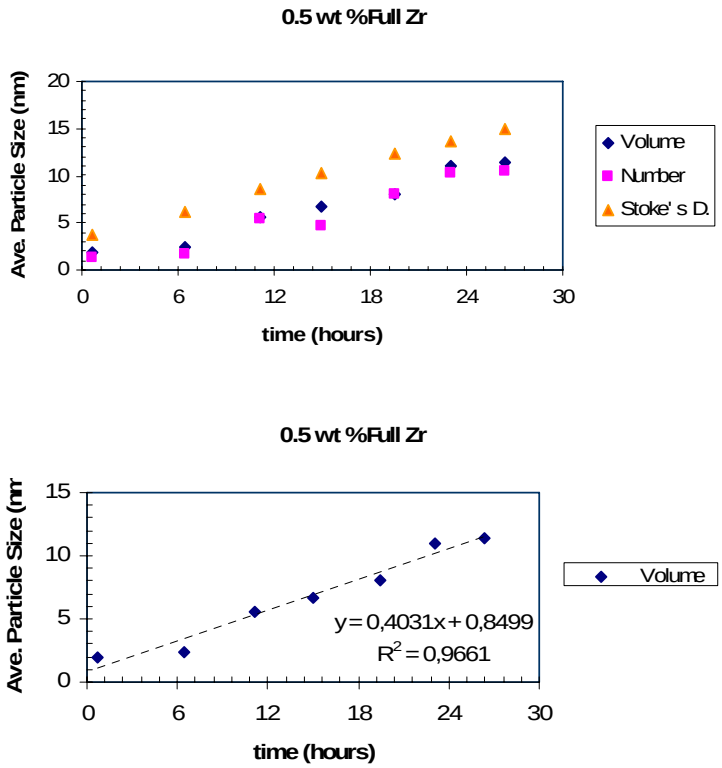

Figure 125. The change in average particle size (PS) of the 0.5 wt. % Full Zr sol (with 25 vol. % EG) at room temperature (RT).

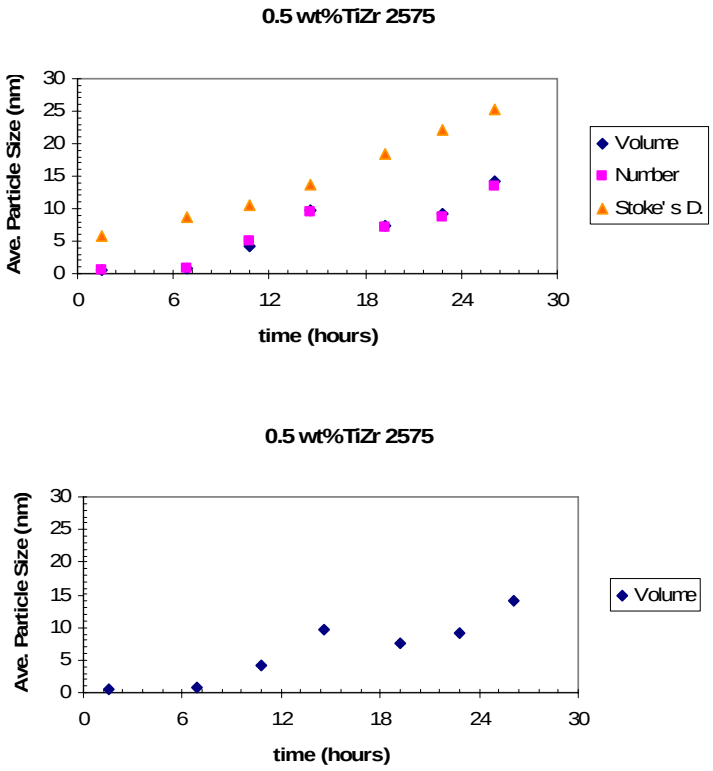

Figure 126. The change in average particle size (PS) of the 0.5 wt. % TiZr 2575 sol (with 25 vol. % EG) at room temperature (RT).

The sols aged were dip-coated on supports prepared by using suspensions with relatively higher alumina content (50-57 vol. %) during aging process to determine the layer formation capabilities of different sols with varying average particle size (ave. PS). The formation of the layer and its continuity were determined via visual determination, or examined by using stereo or electron microscope. The colourfulness on the supports was the evidence of presence of a coated layer. The coated surfaces were further examined via optic stereo microscope to determine the absence or presence of cracks which were not possible to determine by bare eyes. Some selected membranes were taken for SEM analysis to determine the continuities, thicknesses and microstructures of the formed layers.

It was determined that the sols with ave. PS smaller than 30-40 nm could not form a layer on the supports but sucked into the porous support although there was 25 vol% ethylene glycol (EG) in the sols.

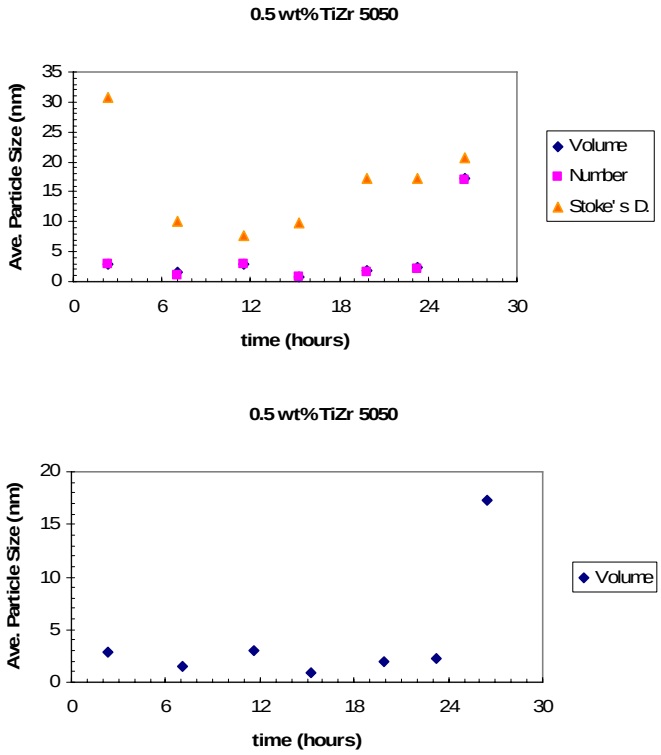

Figure 127. The change in average particle size (PS) of the 0.5 wt. % TiZr 5050 sol (with 25 vol. % EG) at room temperature (RT).

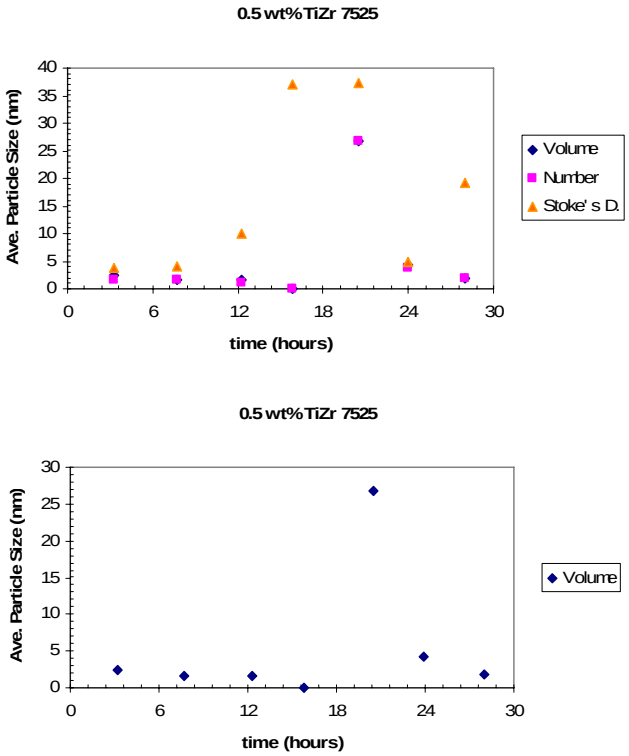

Figure 128. The change in average particle size (PS) of the 0.5 wt. % TiZr 7525 sol (with 25 vol. % EG) at room temperature (RT).

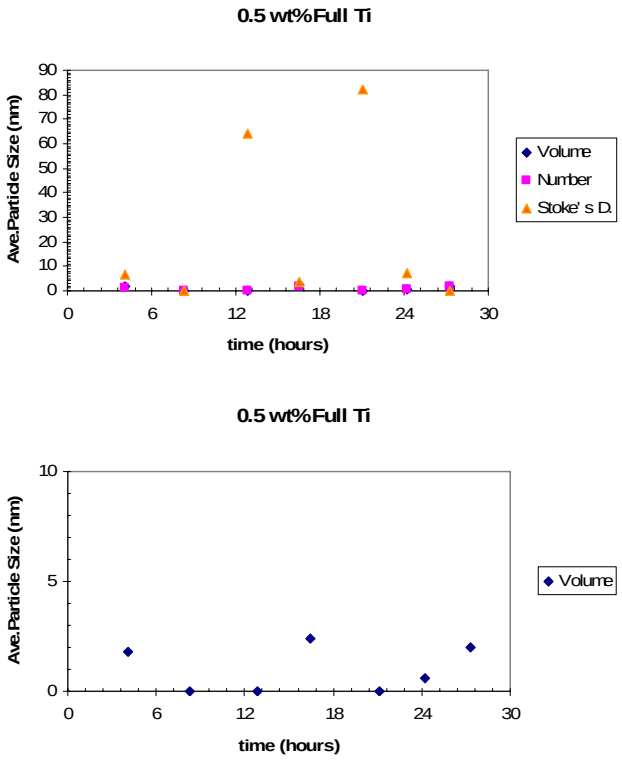

Figure 129. The change in average particle size (PS) of the 0.5 wt. % Full Ti sol (with 25 vol. % EG) at room temperature (RT).

6.1.3.7. Modification of heat treatment regime

The heat treatment of the coated layers (and also the support) is an important step. It determines both physical properties like porosity and mechanical strength. Besides it is effective on the physicochemical properties of the formed oxide layer as was presented for surface charge (zeta potential). The main parameters in the heat treatment are the temperature of the treatment and rates of increment and decrement of temperature. The thermal expansion/shrinkage coefficients of materials used in support and coated layer. These values also change for the same oxide with varying temperature. Hence, a fast heating / cooling will trigger crack formation in the coated layer.

The coated layers on different intermediate layers heat treated 3° C /minute were with cracks and there were severe peelings as can be seen in Figure 130 and 131. The coated layer peeled out after cracking and it tore off some particulates from the

intermediate AKP-50 layer. The torn off alumina particulates under the ~0.4 μ thick zirconia coating can be seen in Figure 131.

The same cracking/peeling problem was observed for zirconia coated γ-alumina intermediate layer as can be seen Figure 132 and 133. The peeling was not as severe as for AKP-50 intermediate layer, probably due to higher mechanical stability of γ-alumina layer.

Decreasing the heating/cooling rate to 0.5 °C / min. instead of 3°C / min. resulted in decrease in cracking and peeling. The coated layers were more continuous and defect-free after slower heat treatment at the same temperature as can be seen in Figure 134, 135 and 136 (a, b).

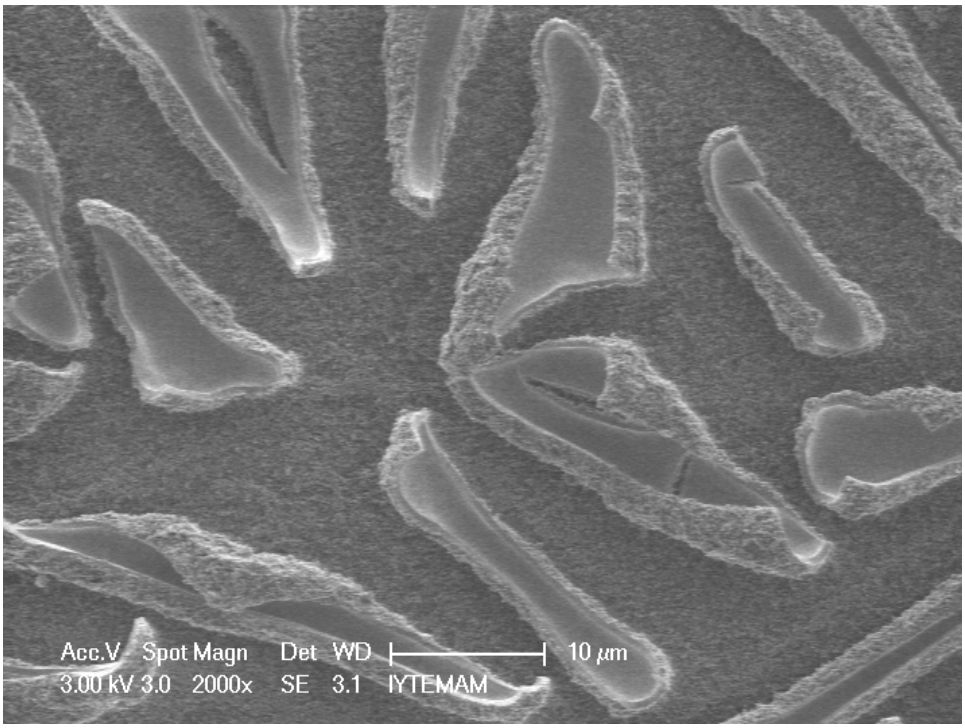

Figure 130. SEM micrograph of surface of multilayer membrane composed of: i) Alcoa alumina support (43 vol. % suspension, 1300° C / 2h), ii) AKP-50 alumina intermediate layer (1, 4, 2 vol. % suspensions, 10 sec. d-c, 1000° C / 30 min. after each coating), iii) Zr Sol NOR, 20 sec. d-c, 400° C / 2h (3° C / min. heating and cooling rate).

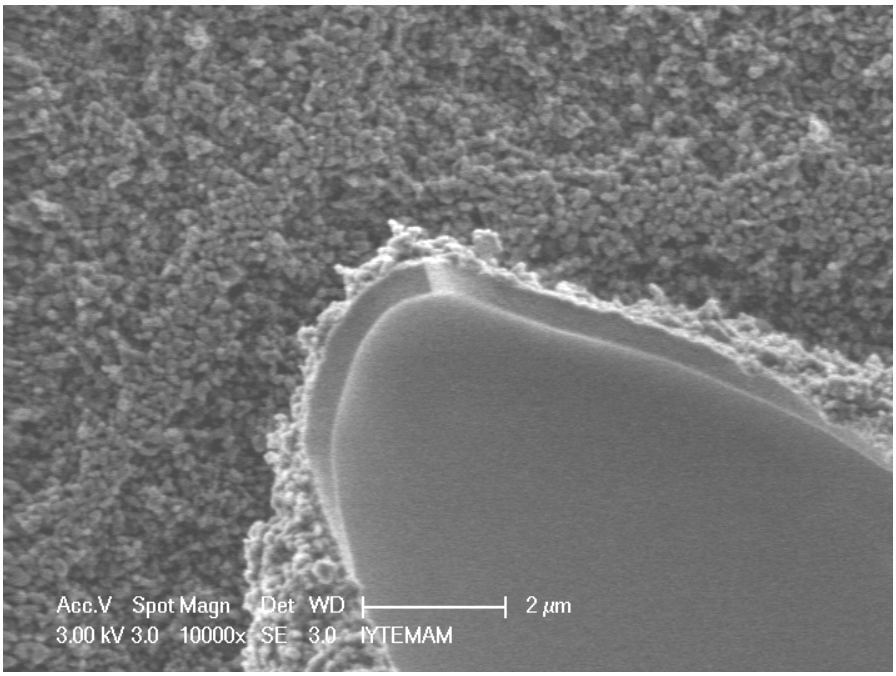

Figure 131. SEM micrograph of coating on the surface of multilayer membrane composed of: i) Alcoa alumina support (43 vol. % suspension, 1300° C / 2h), ii) AKP-50 alumina intermediate layer (1, 4, 2 vol. % suspensions, 10 sec. d-c, 1000° C / 30 min. after each coating), iii) Zr Sol NOR, 20 sec. d-c, 400° C / 2h (3° C / min. heating and cooling rate).

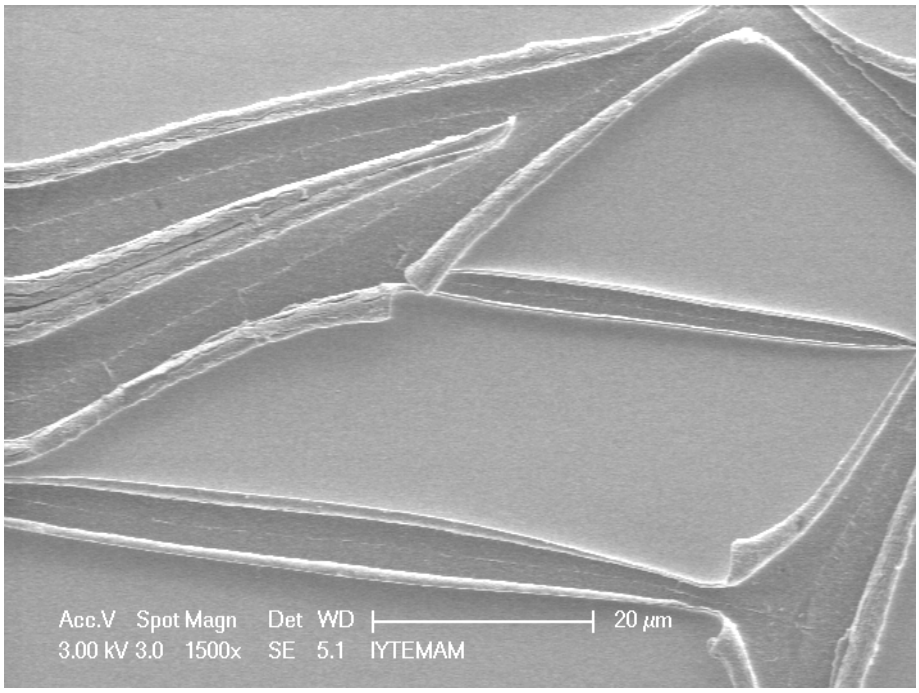

Figure 132. SEM micrograph of surface of multilayer membrane composed of: i) AKP-50 support, ii) γ-alumina intermediate layer, iii) Zr Sol NOR, 1:8 diluted, 5 sec. d-c, 400° C / 2h (3° C / min. heating and cooling rate).

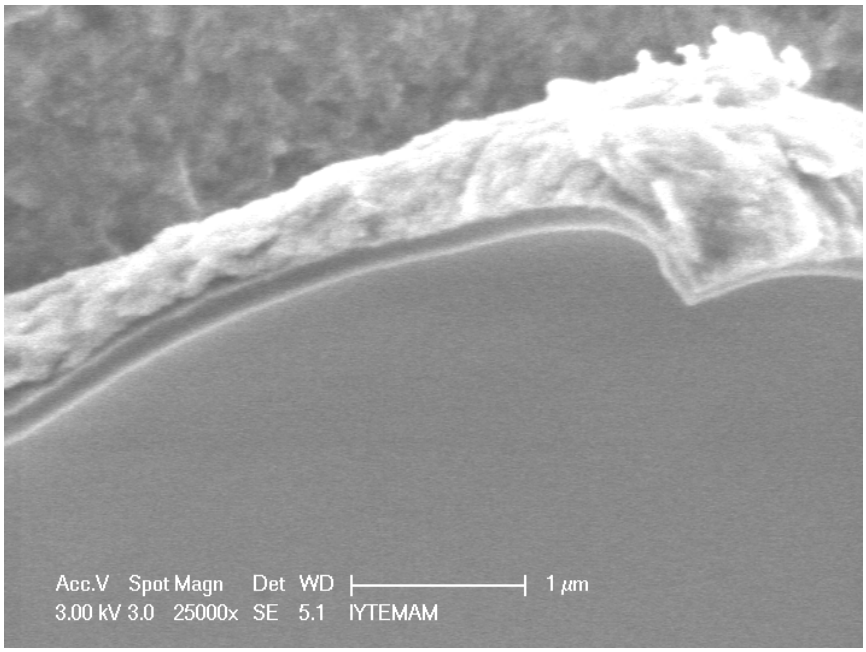

Figure 133. SEM micrograph of surface of multilayer membrane composed of: i) AKP-50 support, ii) γ-alumina intermediate layer, iii) Zr Sol NOR, 1:8 diluted, 5 sec. d-c, 400° C / 2h (3° C / min. heating and cooling rate).

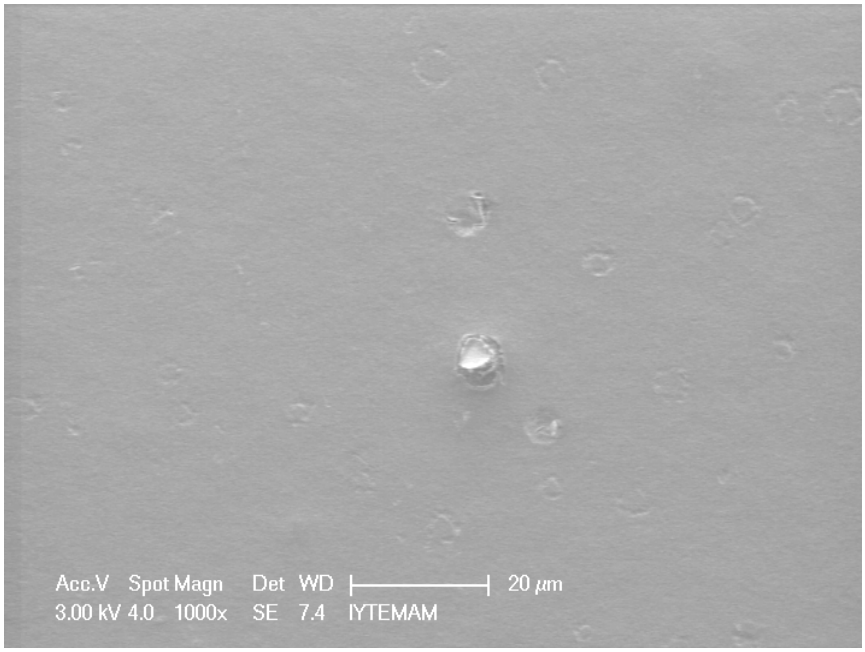

Figure 134. SEM micrograph of surface of multilayer membrane composed of: i) Alcoa alumina support (43 vol. % suspension, 1300° C / 2h), ii) AKP-50 alumina intermediate layer (4, vol. % suspensions, 10 sec. d-c (twice), 1000° C / 30 min. and 1100° C / 2h), iii) Zr Sol NOR, 20 sec. d-c, 400° C / 2h (3° C / min. heating and cooling rate),cleaned via brushing, iv) 0.25 wt. % Zr + EG Sol, 10 sec. and 5 sec. d-c, 400° C / 2h (0.5° C / min. heating and cooling rate) (after each coating) .

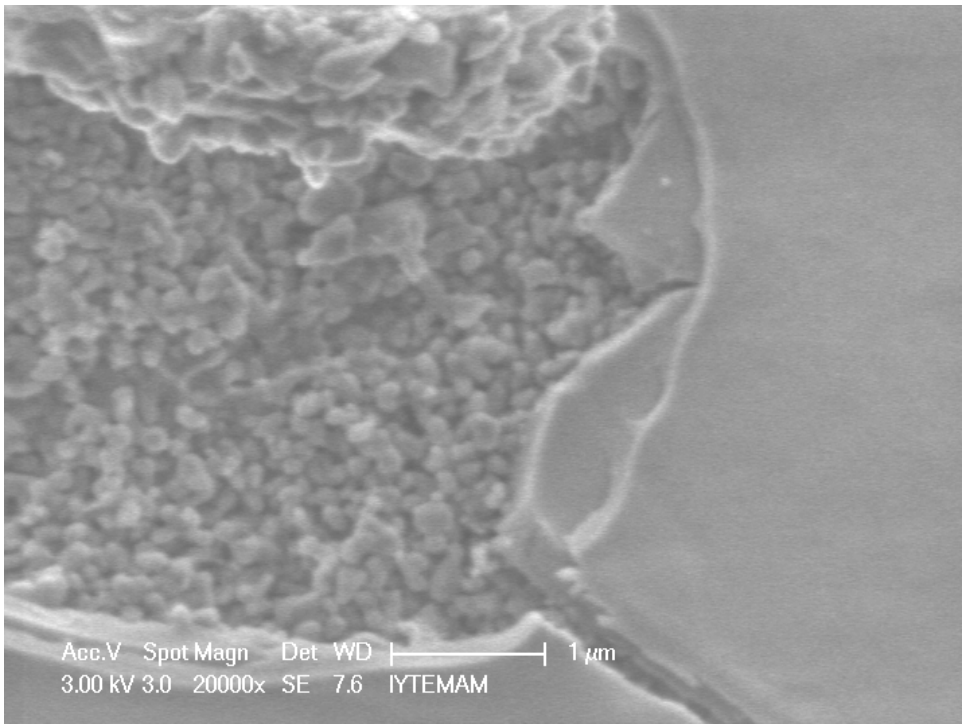

Figure 135. SEM micrograph of defect on multilayer membrane composed of: i) Alcoa alumina support (43 vol. % suspension, 1300° C / 2h), ii) AKP-50 alumina intermediate layer (4, vol. % suspensions, 10 sec. d-c (twice), 1000° C / 30 min. and 1100° C / 2h), iii) Zr Sol NOR, 20 sec. d-c, 400° C / 2h (3° C / min. heating and cooling rate),cleaned via brushing, iv) 0.25 wt. % Zr + EG Sol, 10 sec. and 5 sec. d-c, 400° C / 2h (0.5° C / min. heating and cooling rate) (after each coating) .

a)

b)

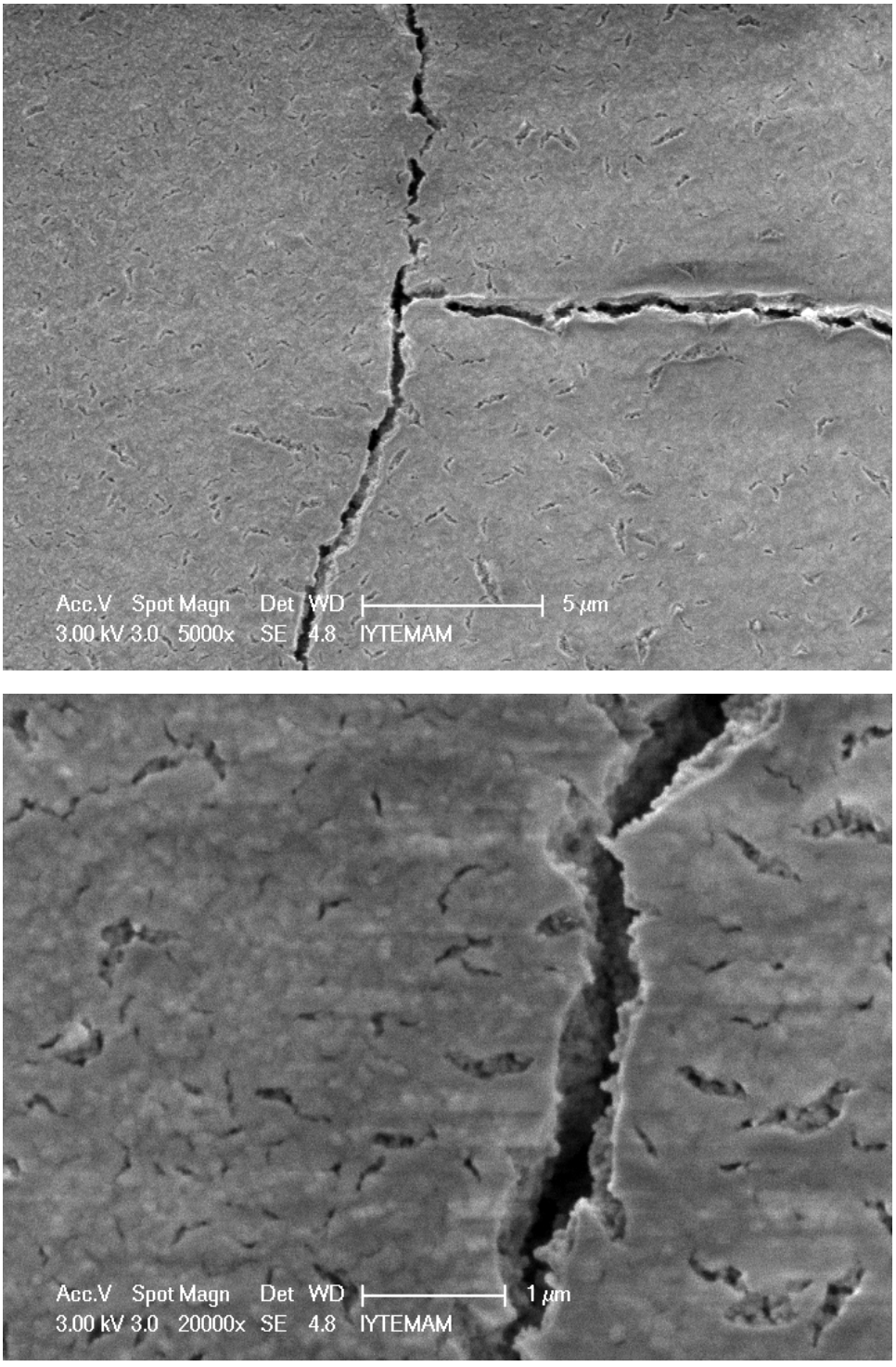

Figure 136. SEM micrograph of surface of multilayer membrane composed of: i) Alcoa alumina support (50 vol. % suspension, 1300° C / 2h), ii) TZ-3Y zirconia intermediate layer (1 vol. % (+ EG) suspensions, 20 and 5 sec. d-c (twice), 1050° C / 1h (after each coating)), iii) Zr Sol 1-20-1 (+ EG), 20 sec. d-c, 400° C / 2h (3° C / min. heating and cooling rate), cleaned via brushing, 1 and 0.1 wt. % Zr (1-20-1) + EG Sol, 10 sec. and 20 sec. d-c (respectively), 400° C / 2h (0.5° C / min. heating and cooling rate) (after each coating) .

6.2. Filtration Experiments

The different aspects of efficiency of membranes were tested by performing experiments. The important criteria for membrane efficiency are different with respect to the targeted application. However a number of parameters can be highlighted which are retention capacity and permeate flux for separation-concentration applications.

6.2.1. Clean Water Permeability (CWP)

The permeate flux is an important parameter during filtration applications. For separation-concentration applications higher the permeate flux, higher the efficiency of the membrane. The permeate flux of the membranes are determined by using water free of impurities and this characterization test is called clean water permeability (CWP) test. Deionized water was used for CWP analysis during the experiments. The permeate flux is determined by resistances to the fluid flow. These resistances are combination of resistances on and through the membrane. The structure of the membrane has a significant effect on permeate flux. The layers formed on support introduced new resistances and the permeability of the membrane would decrease. The CWP values for a prepared membrane with coatings on the support are shown in Figure 137. The CWP values decreased when compared to the values of the uncoated support (Figure 38) as expected and it was nearly 38 L / m^2 hour at a TMP of 5 bars instead of 51 L / m^2 hour which was the value for uncoated support.

6.2.2. Retention Tests

The retention capacity of the membrane can be described in different ways and probably the most popular one is molecular weight cut-off (MWCO) value which may be described as the molecular weight of the substance of which retention by membrane

is equal or higher than 90%. The MWCO value of the appropriate membrane decreases as the size of the target material (to separate or concentrate) decreases. This definition of retention only considers size exclusion but not charge effects on separation. The MWCO values of the membranes are determined by using uncharged polymers with known molecular weight (MW) (e.g. PEG (polyethylene glycol)).

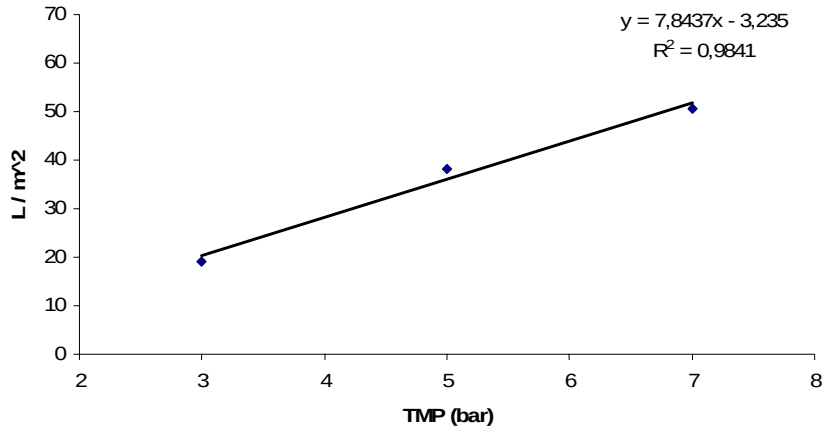

Figure 137. The CWP (L / m^2 hour) values for varying trans-membrane pressures for the membrane consisting of i) a support prepared from alumina with 10% starch addition and partially sintering at 1300°C for 2 hours, ii) an intermediate layer formed by dip-coating alumina sol and calcination at 600°C for 3 hours, iii) a top layer of formed by dip-coating Full Zr and calcination at 400°C for 3 hours.

6.2.2.1. Neutral Organic Solutions (Sugar, PEG)

The retention capacity of the prepared membranes were determined by using suspensions of PEG (MW: 1000 or 4000) or sugar in deionized water. The amount of sugar or PEG in permeate and retentate streams were measured by using refractometer (handheld and/or desktop digital (MettlerToledo RE-50)) and the retention (R (%)) was calculated by using the formula: R (%) = 100* (1- (C_p / C_r)) where C_p and C_r are material concentrations in the permeate and the retentate streams, respectively. The permeate fluxes were also measured. The sugar concentration of feed solution was ~50 g / L (i.e. ~5 Bx) and PEG concentration was ~10 g / L.

The sugar retention test was performed by using a membrane consisted of;

- support: Alcoa alumina, 5% wheat starch & 5% potato starch, 1300° C / 2 h,
- intermediate layer: Alumina sol (1%), 10 seconds dip-coating, 600° C / 3 h,
- top layer: either Full Zr or TiZr 5050 or Full Ti sol, 10 seconds dip-coating, 400° C / 3 h.

The permeate fluxes during these experiments were as shown in Figure 138 and the retention (%) values are shown in Figure 139. The sugar concentrations were only 9-11% higher in the retentate streams, indicating an insufficient retention of sugar for concentration or membrane reactor applications.

The possible reasons of low sugar retention were probably the defects in the coated layers either formed by suction of coated sol into the relatively huge void spaces in the support left by decomposition of starch or some cracks formed during drying or heat treatment. The other reason might be insufficient coating thickness (i.e. coating time, since the coating thickness is proportional to coating time).

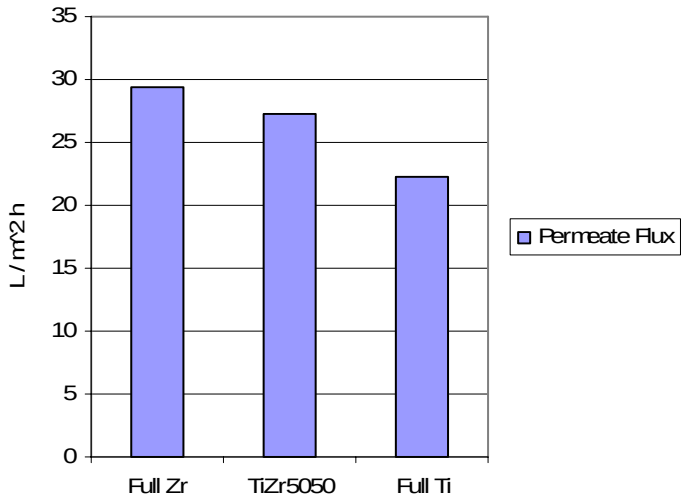

Figure 138. The permeate flux (L / m^2 hour) values for membranes with varying top layer consisting of i) a support prepared from alumina with 10% starch addition and partially sintering at 1300°C for 2 hours, ii) an intermediate layer formed by dip-coating alumina sol and calcination at 600°C for 3 hours, iii) a top layer of formed by dip-coating Full Zr *or* TiZr 5050 *or* Full Ti, and calcination at 400°C for 3 hours.

The SEM micrographs taken during preparation gave some clues supporting these predictions. The SEM micrographs of alumina sol coating after calcinations at

600°C showed the presence of pinholes in the formed layer as can be seen in Figure 140 and 141. Some of the pinholes in Figure 140 might be semi-coated as the one in Figure 141, but there might be none coated pinholes, too, which would adversely affect the retention values during filtration experiments. A second coating and calcination procedure might cover these pinholes and help reaching better retention values.

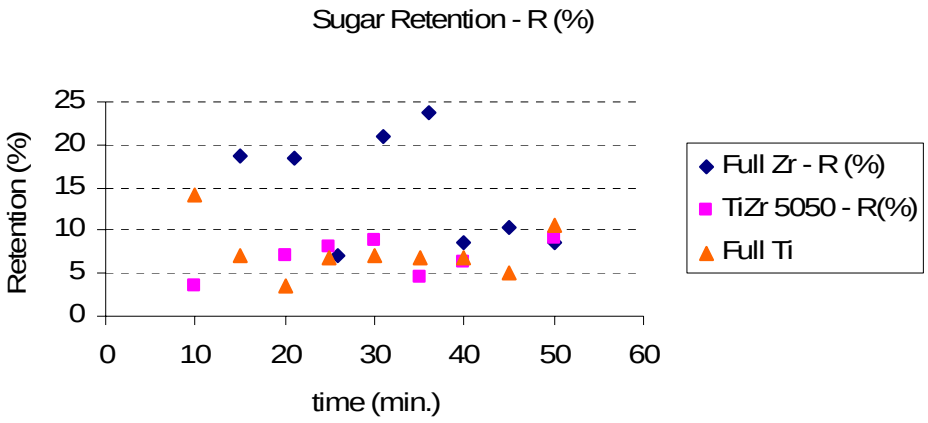

Figure 139. The sugar retention (%) values for membranes with varying top layer consisting of i) a support prepared from alumina with 10% starch addition and partially sintering at 1300°C for 2 hours, ii) an intermediate layer formed by dip-coating alumina sol and calcination at 600°C for 3 hours, iii) a top layer of formed by dip-coating Full Zr *or* TiZr 5050 *or* Full Ti, and calcination at 400°C for 3 hours.

The experiments performed by using a membrane composed of:

- a support prepared from alumina with 15% starch addition and partially sintering at 1300°C for 2 hours,
- an intermediate layer formed by dip-coating alumina sol and calcination at 600°C for 3 hours,
- a top layer of formed by dip-coating TiZr 5050 (10 sec.) (600°C / 2 h),
    - TiZr 5050 (5 sec.) (600°C / 2 h).
    - TiZr 5050 (1:1 diluted) (5 sec.) (600°C/2h)

resulted almost no retention of sugar supporting the idea that the pore forming agent (starch) after decomposition forms huge pores which could not be filled by dip-coating with alumina sol for 10 seconds. Probably the sol was sucked into these huge pores but was still not able to fill them and form a smooth homogeneous surface to coat with nano

particles. The permeate flux in this experiment decreased below 5 L / m^2 h for the membrane prepared with multiple dip-coating – calcination cycles but there was almost no sugar retention (Figure 142). Therefore, the intermediate layer preparation should be improved.

The retention capacity of the membranes were also analysed by using solutions of PEG (polyethylene glycol) (MW: 1000, ~10 g / L) of which MW is greater than sugar (MW: 342). The membrane used in this experiment was prepared consisting of a support (with 10% starch mix., 1300°C / 2 h), dip-coated and calcined alumina sol (10 sec., 600 °C for 3 h) and TiZr 5050 sol which was dip-coated first then poured on the membrane to be sure the surface was totally coated with sufficient amount of sol and heat treated at 600°C for 2 h. The permeate flux was over 10 L / m^2 h and the PEG 1000 retention was 60% as shown in Figure 143. Besides the permeate flux was higher although the amount of pore forming agent was decreased from 15% to 10%. This decrement probably resulted less suction of alumina sol and a better intermediate layer (i.e. with less pinholes) formation.

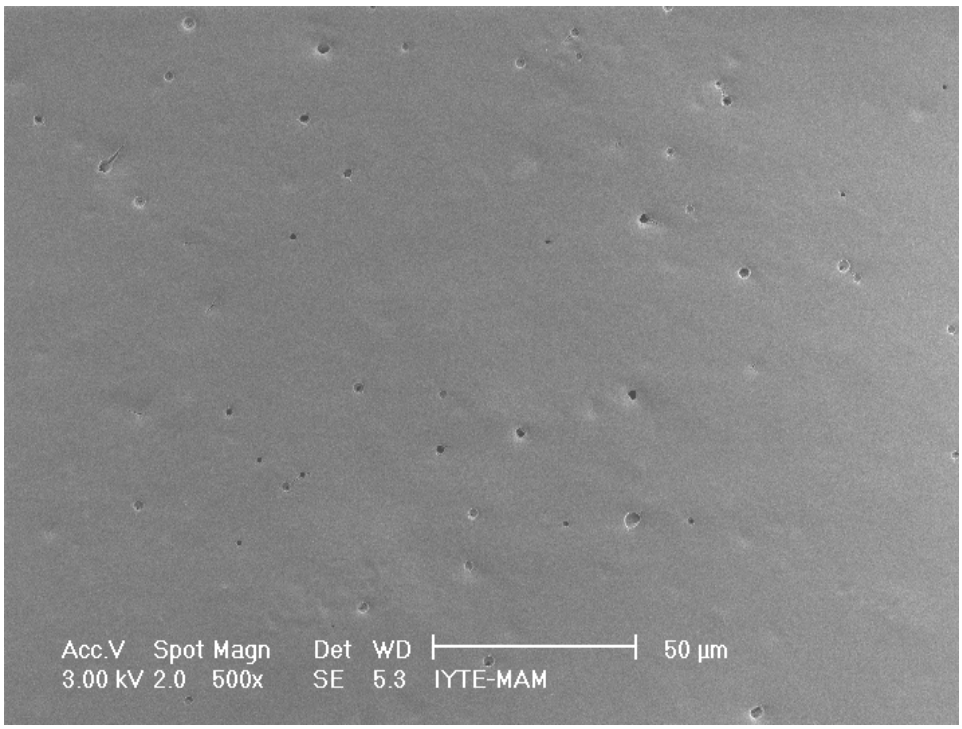

Figure 140. The SEM micrograph of intermediate layer formed by dip-coating alumina sol and calcining at 600°C on the support (11% starch, 1300°C / 2 hours) showing the presence of pinholes.

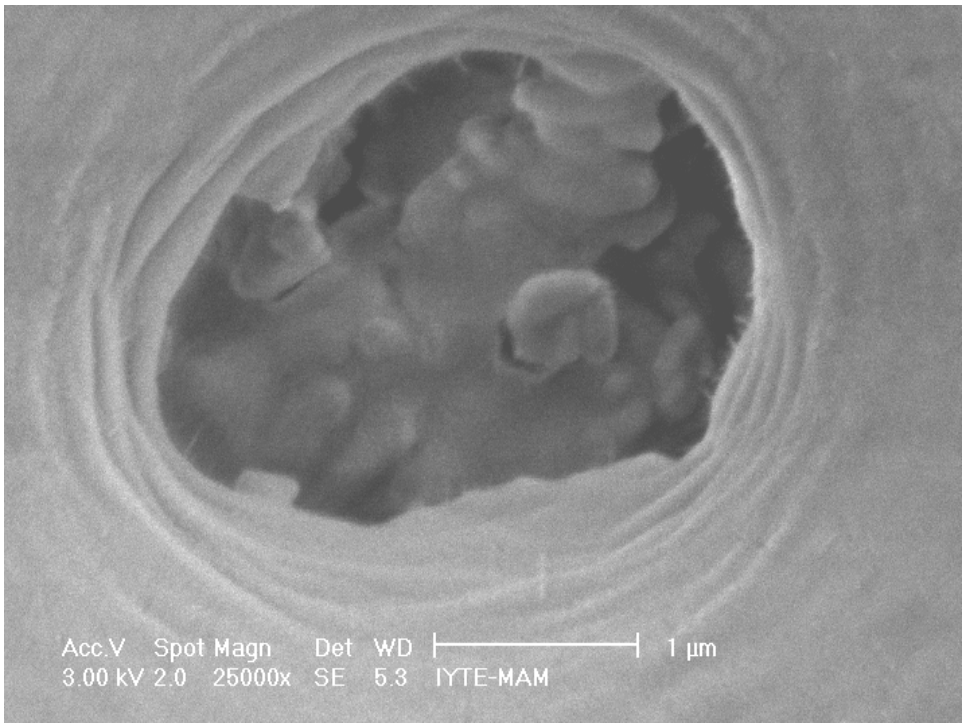

Figure 141. The SEM micrograph of one of the pinholes in Figure 140.

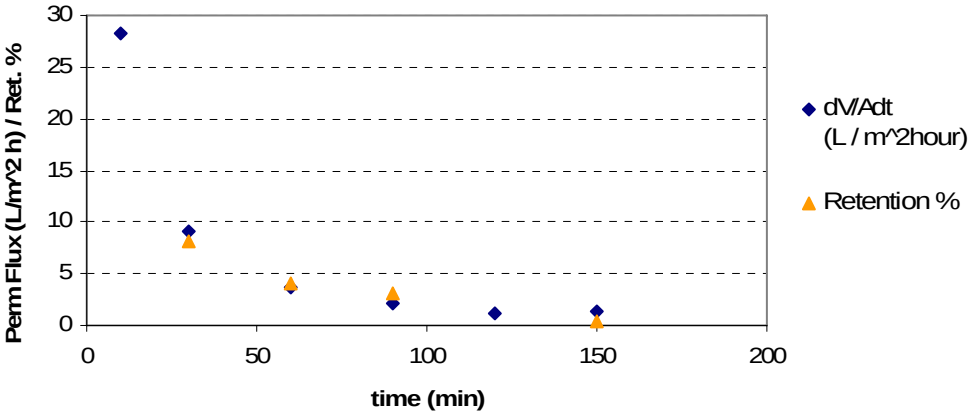

Figure 142. The permeate flux (L / m^2 h) and sugar retention (%) values for the membrane composed of i) a support prepared from alumina with 15% starch addition and partially sintering at 1300°C for 2 hours, ii) an intermediate layer formed by dip-coating alumina sol and calcination at 600°C for 3 hours, iii) a top layer of formed by multiple dip-coating by using TiZr 5050 and calcination at 600°C for 2 hours.

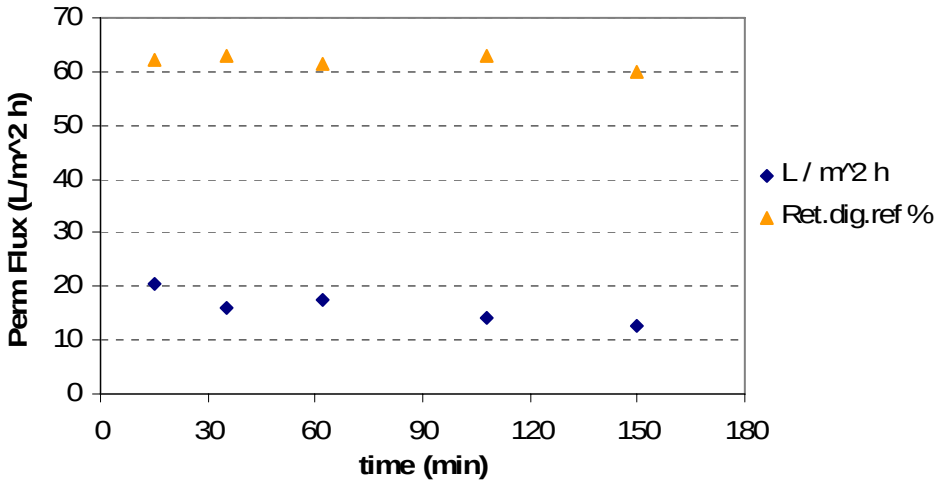

Figure 143. The permeate flux (L / m^2 h) and sugar retention (%) values for the membrane composed of i) a support prepared from alumina with 10% starch (mix.) addition and partially sintering at 1300°C for 2 hours, ii) an intermediate layer formed by dip-coating alumina sol and calcination at 600°C for 3 hours, iii) a top layer of formed by dip & pour-coating by using TiZr 5050 and calcination at 600°C for 2 hours.

The coating thickness of intermediate layer formed by dip-coating of alumina sol for 10 seconds and calcination at 600° C for 3 hours on a support prepared from alumina with 7% starch addition and partially sintering at 1300°C for 2 hours was ~2 µ as can be seen in Figure 144. This thickness should be sufficient if the support surface was homogeneously smooth and free of pinholes. Since the main reason of the pinholes might be the huge pores formed by decomposition of starch and the presence of air bubbles

in the slip of support, forming a layer on the support without bubbles and pore forming additives should result a smoother surface. Such a surface could be prepared by forming a thin layer of ceramic suspension (e.g. by dip-coating) on the support. For this purpose first intermediate layer was prepared by using AKP-50 (alumina) or TZ-3Y (zirconia) suspensions. The thickness of this layer should be kept as thin as possible for not to increase the resistance to fluid flow. The SEM image of the intersection of a membrane prepared by dip-coating an alumina support (11% starch, 1300°C / 2 hours) using 10 volume % AKP-50 for 10 seconds and heat-treating at 1100°C for 2 hours is given in Figure 145. The dip-coating procedure resulted in a layer of 60-70µ thick and free of huge pores.

The (first) intermediate layer to prevent suction of sol which forms second intermediate layer and to form a smoother surface for further coatings were also prepared by using zirconia (TZ-3Y) powder suspensions. The Alcoa alumina support was prepared by addition of 10 % pure wheat starch (instead of 50% wheat and 50% potato starch) which has a significantly smaller particle size and partial sintering at

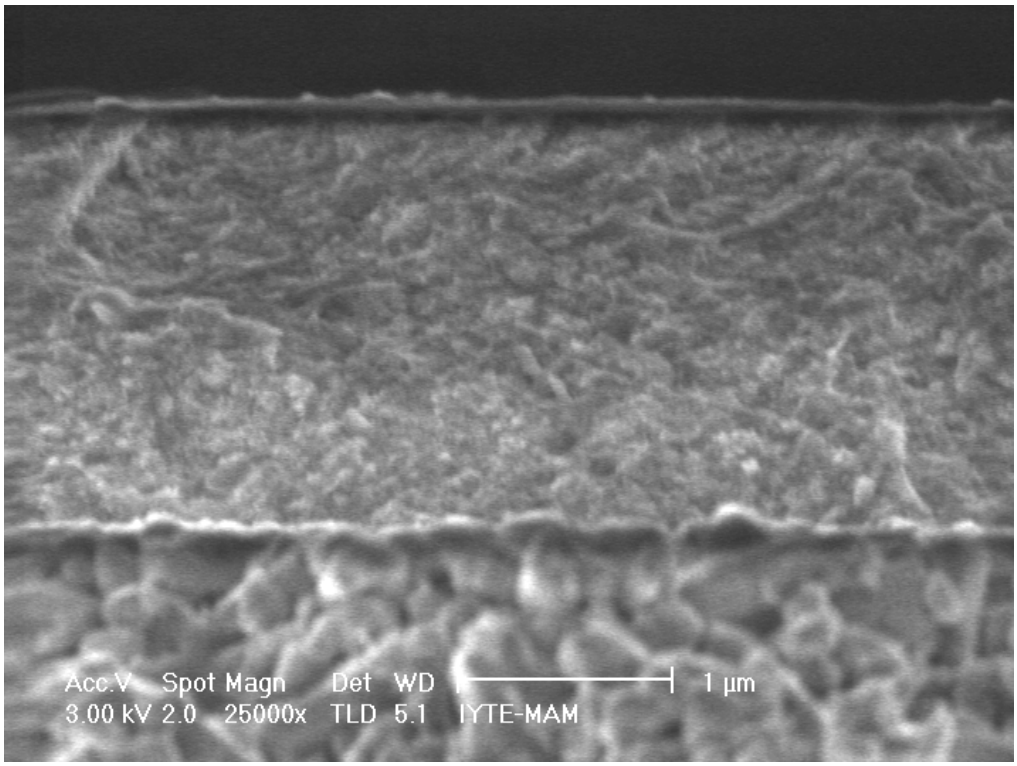

Figure 144. The SEM micrograph of cross-section of a membrane consisting of i) a support prepared from alumina with 7% starch addition and partially sintering at 1300°C for 2 hours, ii) an intermediate layer formed by dip-coating alumina sol and calcination at 600°C for 3 hours, iii) a top layer of formed by dip-coating TiZr 2575 and calcinations at 500°C for 3 hours.

1300° C for 2 hours. The aim was to decrease the size of the pores obtained by decomposition of the starch and reduce the volume resulting suction of the coated material and have a smoother surface. This support was coated by using 1 vol. % TZ-3Y zirconia suspension and heat treated at 1100° C for 2 hours. Then top layer was formed by dip-coating the TiZr 5050 sol for 10 seconds and calcination at 500° C for 2 hours. The top layer coating and calcination were repeated one more time. The retention capacity of this membrane was determined by using PEG (polyethylene glycol) (MW:

1000) solution. There were no considerable PEG retention but the permeate fluxes were relatively higher probably due to better wetting properties of zirconia.

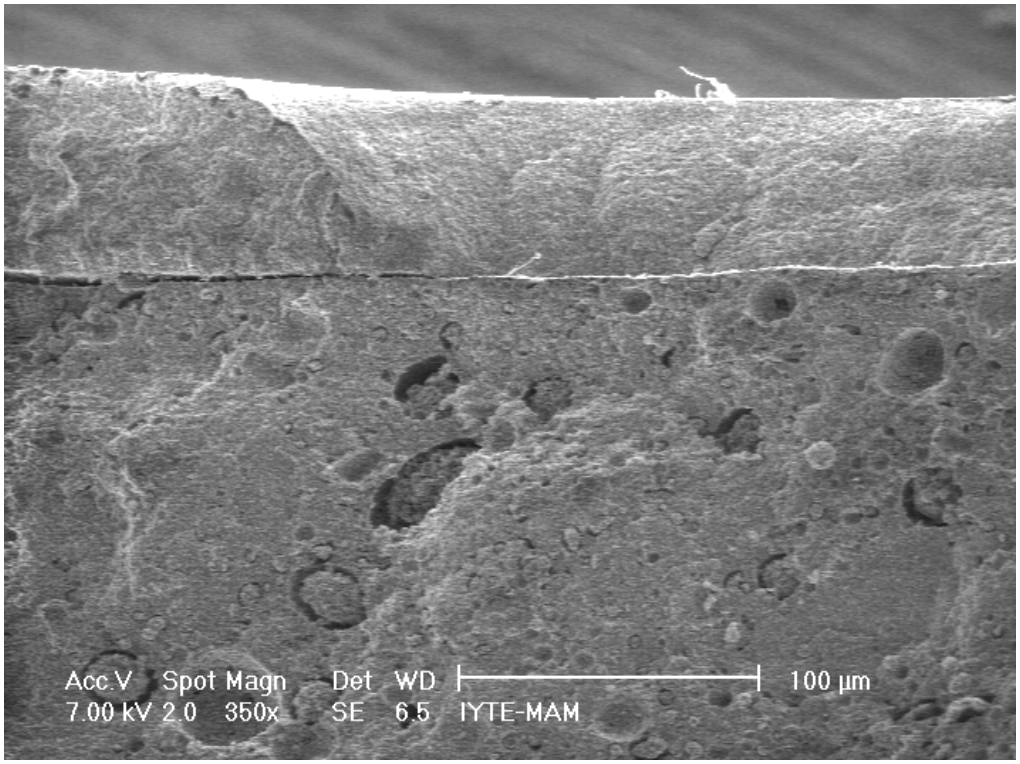

Figure 145. The SEM micrograph of cross-section of a membrane consisting of i) a support prepared from alumina with 11% starch addition and partially sintering at 1300°C for 2 hours, ii) an intermediate layer formed by dip-coating 10 vol. % AKP-50 and heat treatment at 1100°C for 2 hours, iii) an intermediate layer formed by dip-coating 1 % alumina sol and heat treatment at 600°C for 3 hours iv)a top layer of formed by dip-coating TiZr 5050 and calcination at 400°C for 3 hours.

6.2.2.1.1. The effect of modification of sols by ethylene glycol (EG) addition

The low retention values were mainly attributed to absence of a continuous top layer free of defects. This was due to the suction of sol into the porous microstructure of the support. The viscosity of the sol was regulated by introducing some ethylene glycol (EG) into the sol recipe (25-33 vol. %), which resulted an increase of viscosity from 2

cp to higher values (3.2-3.7 cp) that hindered the suction of sol as was reported for pure propanol-EG binary system by Pal and Sharma (1998) plotted in Figure 146. The relatively lower vapour pressure of EG also decreased the drying speed of the sol coated which would result in a more crack-free layer after drying.

The EG added sols were aged at room temperature (RT) (or in an oven at 39° C). Their average particle sizes were determined in time. Supports prepared by using suspensions with relatively higher alumina content (50-57.5 vol. %) were dip-coated (d-c) via these aged sols with varying average particle sizes (ave. PS).

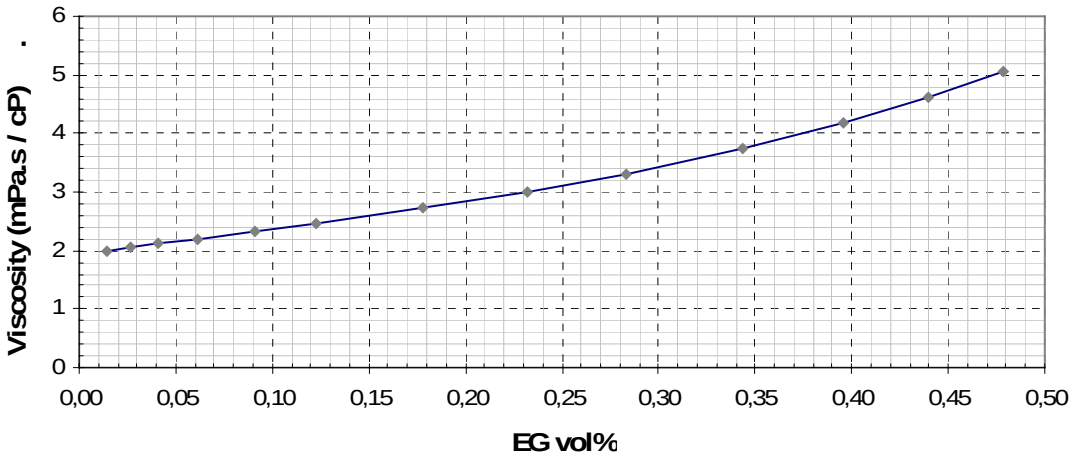

Figure 146. The viscosity values for propanol–ethylene glycol binary system at 25° C plotted from data excerpted from Pal & Sharma (1998).

It was determined that under certain values of ave. PS it was not possible to form a layer although the support surface was relatively denser and the viscosity of the sol was relatively higher. This result was achieved via SEM analysis of supports coated with sols (10 sec. d-c) with varying aging times (i.e. varying ave. PS) and heat treated at similar conditions (400° C / 1 h, with heating and cooling rate of 0.5° C / min.). The SEM micrographs of supports coated via sols with ave. PS of 1.9, 6.7, 20 and 31.5 nm are given in Figure 147, 148, 149, 150 (and 151), respectively. There was no layer formation for sols with smaller ave. PS (i.e. all sol was sucked into the porous support), while there was a layer formed via sol with ave. PS of 31.5 nm, unfortunately with some cracks.

The simplest method for discriminating supports with such a layer was found to be examining the presence of colourfulness on the surface. If the surface was colourful this was due to the layer formed. But it was not possible to determine the presence / absence of cracks and their intensity by such a visual examination. The surfaces of only a number of selected membranes were possible to investigate via SEM for better evaluation. The final evaluation was performed via filtration tests.

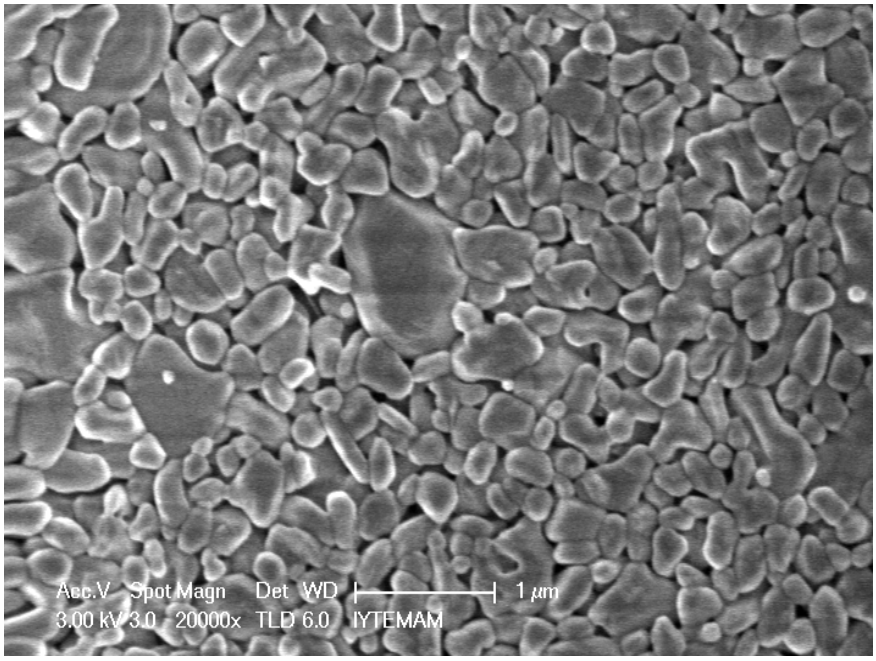

Figure 147. The SEM micrograph of the surface of an Alcoa support prepared via a 53 vol.% suspension ht at 1300° C / 2h and dip-coated (10 sec.) via 0.5 wt.% Full Zr + EG (25 vol. %) sol with ave. PS of 1.9 nm (and ht at 400° C / 1h with 0.5° C / min heating / cooling rates).

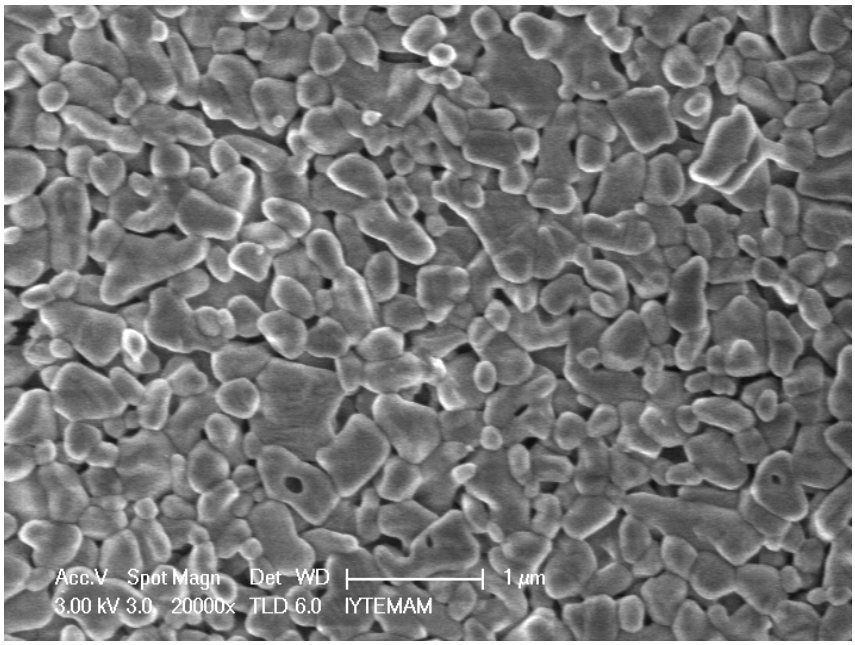

Figure 148. The SEM micrograph of the surface of an Alcoa support prepared via a 53 vol.% suspension ht at 1300° C / 2h and dip-coated (10 sec.) via 0.5 wt.% Full Zr + EG (25 vol. %) sol with ave. PS of 6.7 nm (and ht at 400° C / 1h with 0.5° C / min heating / cooling rates).

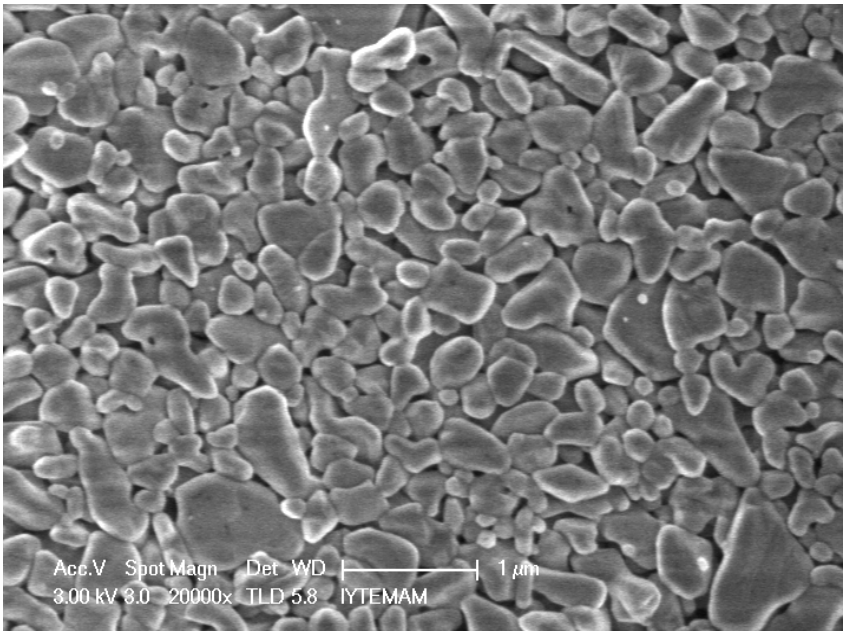

Figure 149. The SEM micrograph of the surface of an Alcoa support prepared via a 53 vol.% suspension ht at 1300° C / 2h and dip-coated (10 sec.) via 1 wt.% T2575 + EG (25 vol. %) sol with ave. PS of 20 nm (and ht at 400° C / 1h with 0.5° C / min heating / cooling rates).

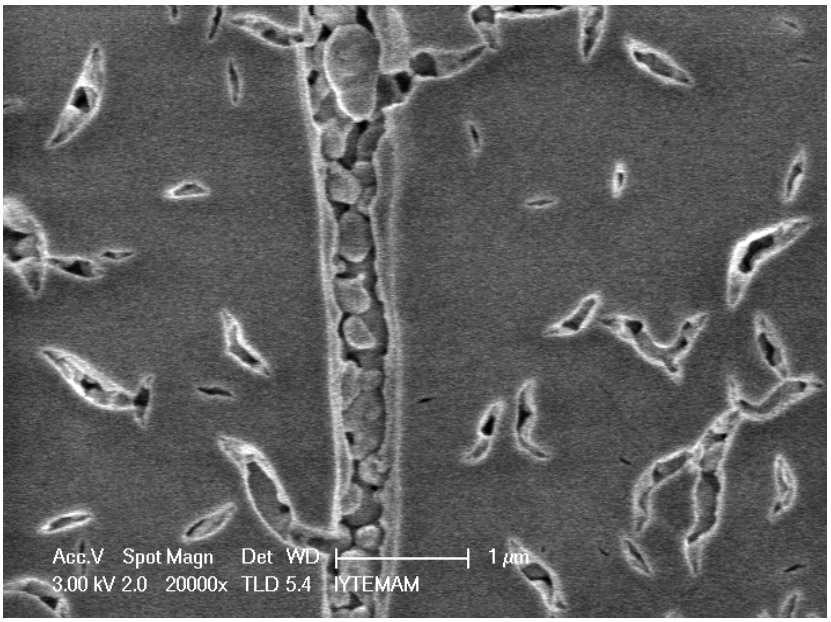

Figure 150. The SEM micrograph of the surface of an Alcoa support prepared via a 53 vol.% suspension ht at 1300° C / 2h and dip-coated (5 sec.) via 1 wt.% Full Zr + EG (25 vol. %) sol with ave. PS of 31.5 nm (and ht at 400° C / 1h with 0.5° C / min heating / cooling rates).

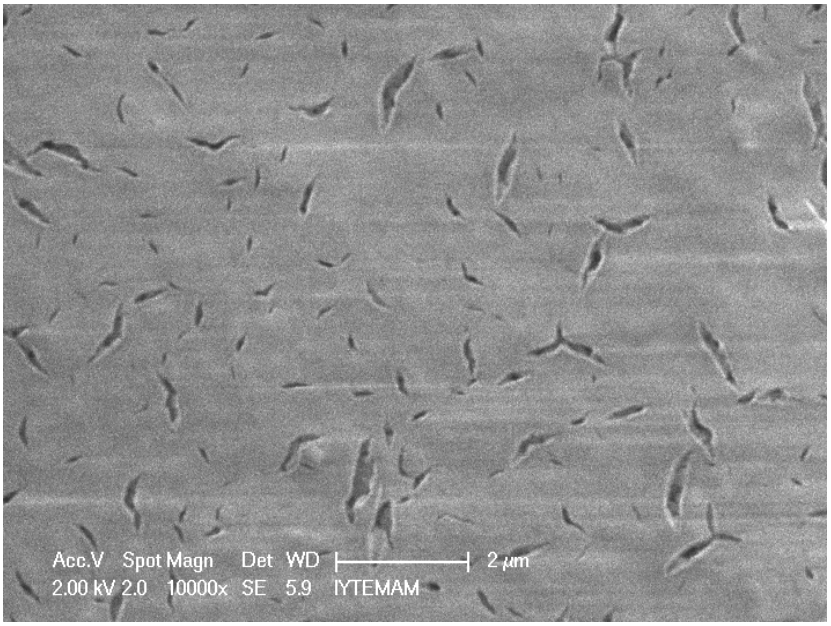

Figure 151. The SEM micrograph of the surface of an Alcoa support prepared via a 53 vol.% suspension ht at 1300° C / 2h and dip-coated (5 sec.) via 1 wt.% Full Zr + EG (25 vol. %) sol with ave. PS of 31.5 nm (and ht at 400° C / 1h with 0.5° C / min heating / cooling rates).

Sugar retention tests were performed via membranes coated EG added sols and aged for different durations to have different ave. PS. The summary of the supports and coatings used were given in Table 13. The sugar retention values for membranes prepared via sols with relatively smaller ave. PS were almost zero while there were small retention values for membranes prepared via sols with higher ave. PS as shown in Figure 152. The permeate fluxes of these membranes are also given in Figure 152 which were 20-50 L / m^2 h. (The feed fluxes were 5 L / min for all and the trans membrane pressure values were 5 bars except for 23.8.9-32d which was 3 bars.)

Table 13. The membranes prepared via sols with EG addition (25 vol. %) with varying ave PS.

Membrane Code	***23.8.9-29a***	***23.8.9-32d***	***4.9.9-15d***	***5.9.9-12d***
Support	53 vol% Alcoa 1300° C / 2h	53 vol% Alcoa 1300° C / 2h	53 vol% Alcoa 1300° C / 2h	53 vol%Alcoa 1300° C / 2h
Coating 1	1wt% Full Ti+EG, V: **3 nm**, 5sec dc, 400° C / 1h (0.5° C / min) 11.9.9	0.5 wt% TiZr5050+EG, V:**1.9nm**, 10sec d-c, 400° C / 1h (0.5° C / min) 11.9.9	0.5 wt% TiZr5050+EG, V:**17.3nm**, 10 sec d-c, 400° C / 1h (0.5° C / min)	0.5 wt% TiZr2575+EG, 5.9.9 P-1, 10 sec d-c (23.9.9), 400° C / 2h (0.5° C / min) 25.9.9

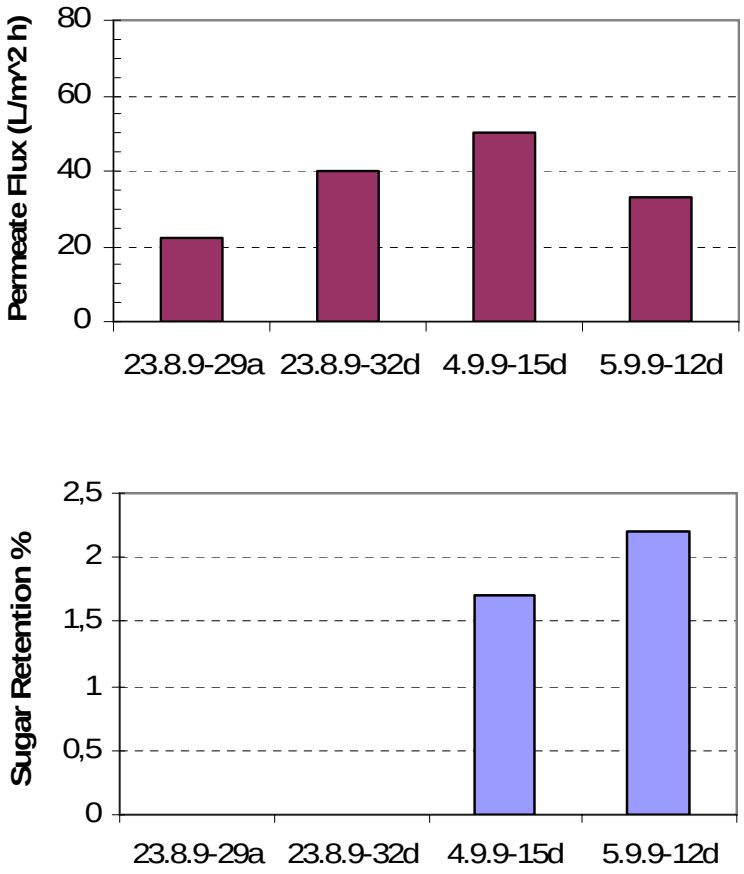

Figure 152. The permeate flux and sugar retention values for membranes prepared via sols with varying ave. PS (+ 25 vol. % EG).

The EG added sols were also coated on supports with previously formed intermediate layers of which preparation procedure was summarized in Table 14. The permeate fluxes and sugar retention values of these membranes are given in Figure 152. The sugar retention was highest (~10%) for the membrane with an intermediate layer heat treated (ht) relatively at higher temperatures for longer periods. The permeate flux was lowest for this membrane (29.7.9-5ü) probably similarly due to ht. In general the membranes with intermediate layer had comparable or higher sugar retention capabilities but lower permeate fluxes with respect to supports without intermediate layer as can be compared via Figures 152 and 153.

Table 14. The membranes prepared via sols with EG addition (25 vol. %) coating on supports with intermediate layers.

Membrane Code	***29.7.9-15ü***	***29.7.9-2ü***	***29.7.9-5ü***
Support	50 vol% Alcoa 1300° C / 2h	50 vol% Alcoa 1300° C / 2h	50 vol% Alcoa 1300° C / 2h
Coating 1	4 vol% ***AKP-50***, 10 sec d-c, 1000° C / 30 min	4 vol% ***AKP-50*** +EG, 10 sec d-c, 1000° C / 30 min	4 vol% ***AKP-50*** +EG, 10 sec d-c, 1100° C / 120min
Coating 2	4 vol% ***AKP-50***, 10 sec d-c, 1100° C / 60 min	4 vol% ***AKP-50*** +EG, 10 sec d-c, 1100° C / 60min,	4 vol% ***AKP-50*** +EG, 10 sec d-c, 1100° C / 120min
Coating 3	Zr Sol NOR (1:1), 50 sec d-c, *CLEANED after ht*	ZrSol NOR 1:4d ,5 sec d-c, 400° C / 2h, *CLEANED after ht*	ZrSol NOR (1:1) , 5 sec d-c, 400° C / 2h, *CLEANED after ht*
Coating 4	0.25 wt% FullZr +EG, 18.9.9, 10sec dc (23.9.9), 400° C / 2h (0.5° C / min) (25.9.9)	0.1 wt% Zr+EG, 10 sec d-c, 400° C / 2h, 0.5° C / min	0.1 wt% Zr+EG, 5 sec d-c , 400° C / 2h, 0.5° C / min
Coating 5		0.1 wt% Zr+EG, 10 sec d-c, 400° C / 2h, 0.5° C / min	0.25 wt% Zr+EG, 10 sec d-c, 400° C / 2h, 0.5° C / min
Coating 6		0.1 wt% Zr+EG, 5 sec d-c, 400° C / 2h, 0.5° C / min	0.1 wt% Zr+EG, 5 sec d-c , 400° C / 2h, 0.5° C / min

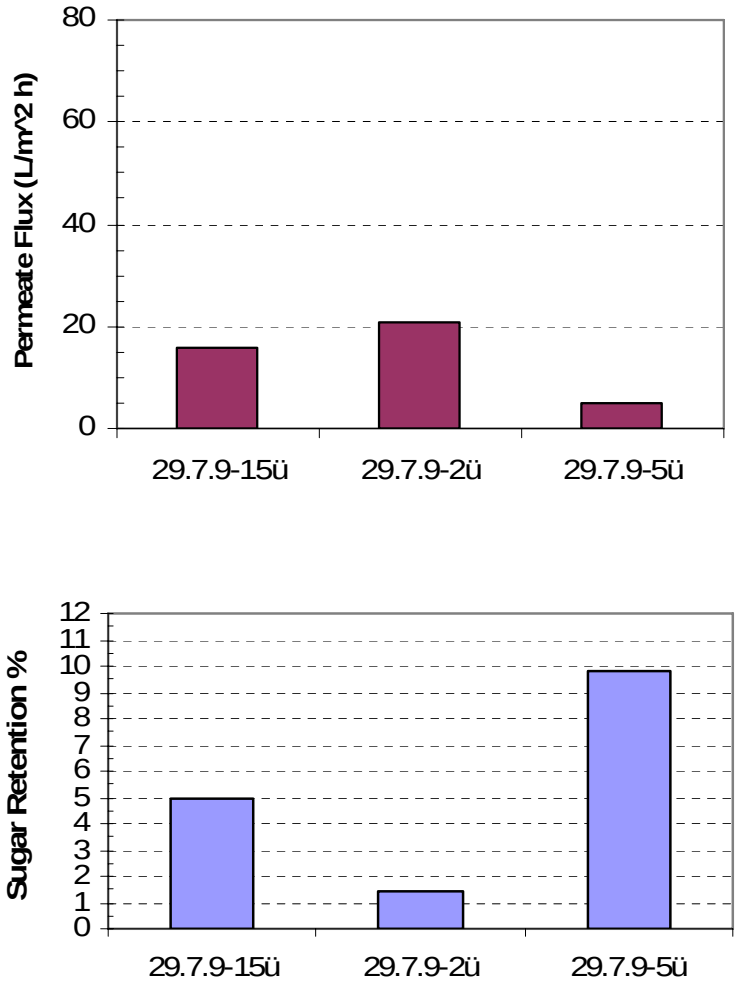

Figure 153. The permeate flux and sugar retention values for membranes prepared via sols with 25 vol. % EG on supports with intermediate layers.

The PEG 4000 retention tests of membranes prepared with sols EG added and aged. The summary of preparation of these membranes are given in Table 15. The PEG 4000 retention values and permeate fluxes for these membranes are given in Figure 154.

The retention value for the membrane coded 17.7.9-2 was almost zero although it has an intermediate layer and coated twice with sols (~1 wt %) and EG containing for the second coating. The main reason for the absence of retention different than the other membranes was the difference in heat treatment. The heating and cooling rate for this membrane was 3° C / min. while it was modified to 0.5° C / min. for the others. This modification resulted in considerable decrease in shrinkage and peeling due to the thermal expansion coefficient difference of support material (alumina) and coated layer (titania-zirconia) which was very deteriorative effect on membrane layers. The shrinked

top layer formed after relatively faster calcination semi-peeled out even taking some particulates from the support or intermediate layer with it. Therefore, the slower ht (calcination) of the top layers were beneficial on membrane integrity and filtration performance.

There were small retention values for membranes formed via sols with relatively smaller ave. PS (0.5-1.9 nm). These membranes were ht at 400° C only for one hour that there were some Carbon residues which were also detected via SEM-EDX analysis. These Carbon residues might result in another resistance to PEG 4000 permeation through the membranes (e.g. via hydrophobic interactions).

There were relatively higher PEG 4000 retentions for membranes which were double coated and calcined slowly. The membrane coded 4.9.9-17ü was first coated via 0.5 wt. % TiZr 5050 (ave. PS: 29.5nm) and then via 0.5 wt. % Full Zr (ave. PS: 39 nm) sols both containing EG for 10 seconds resulted in a 5 % PEG 4000 retention, while the other combination on almost similar support 4.9.9-29d composed of 1 wt. % Full Zr (ave. PS: 6.6 nm) and 0.5 wt. % Full Zr (ave. PS~37 nm), with EG, d-c for 10 seconds, calcined slowly resulted in a retention value of 19%. The permeate flux of the later (30 L / m^2 h) was a little lower than the former (36 L / m^2 h).

These results are indicating a further optimization should be done for top layer coatings composed of multi-layers. The high amount of sol coated on the support or intermediate layer was found to inversely affect the membrane integrity (i.e. keeping the solid content of the sol or coating duration result in formation of thicker layers which are prone to crack and peel. The severity of this effect increases as the porosity of the support or intermediate layer decreases (i.e. the amount of coated material can be hold via support or intermediate layer decreases as the porosity of the support or intermediate layer decreases, which was observed for supports prepared from suspensions with higher solid content and intermediate layers which were prepared via supernatants of fine ceramic powders resulting in denser surfaces).

Table 15. The membranes prepared via sols with EG addition (25 vol. %) with varying ave PS.

Membrane Code	***17.7.9-2***	***23.8.9-29a***	***4.9.9-11d***	***23.8.9-32d***	***4.9.9-17ü***	***4.9.9-29d***
Support	0% starch, 1300° C / 2h	53 vol.% Alcoa 1300° C / 2h	53 vol.% Alcoa 1300° C / 2h	53 vol.% Alcoa 1300° C / 2h	53 vol.% Alcoa 1300° C / 2h	53 vol.% Alcoa 1300° C / 2h
Coating 1	slip-cast via 1.5 mL 2.5 vol% AKP-50 (3%PVA), 1000° C / 30 min	1wt% FullTi+EG (25 vol.%), **V:3nm**, 5sec dc, 400° C / 1h (0.5° C / min) 11.9.9	1wt% TiZr 7525 +EG, **V:0.5 nm**, 5sec dc, 400° C / 1h (0.5° C / min) 11.9.9	0.5wt% TiZr 5050 +EG, **V:1.9nm**, 10sec dc, 400° C / 1h (0.5 C/min) 11.9.9	0.5 wt% TiZr5050 +EG, 5.9.9 P-1 **V:29.5nm**, 10sec dc, 400° C / 1h (0.5° C / min) 11.9.9	1wt% Zr +EG, **V:6.6nm**, 10sec dc, 400° C / 1h (0.5° C / min)
Coating 2	1.75 mL of 1.25 vol.% AKP-50 suspension (3% PVA), - 1000° C / 30 min				0.5 wt% FullZr +EG, 5.9.9 P-2 **V:39nm**, 10sec dc, 400° C / 2h (0.5° C / min)	0.5wt% FullZr +EG, 5.9.9 P-1 **V~37nm**, 10sec dc, 400° C / 2h (0.5° C / min)
Coating 3	2mL ZrSolNOR 1:4d + 2mL propanol, heat surface and dip-coat 5sec , dried					
Coating 4	2mL ZrSolNOR 1:4d + 2mL ethylene glycol 5 sec d-c, 400° C / 2h					

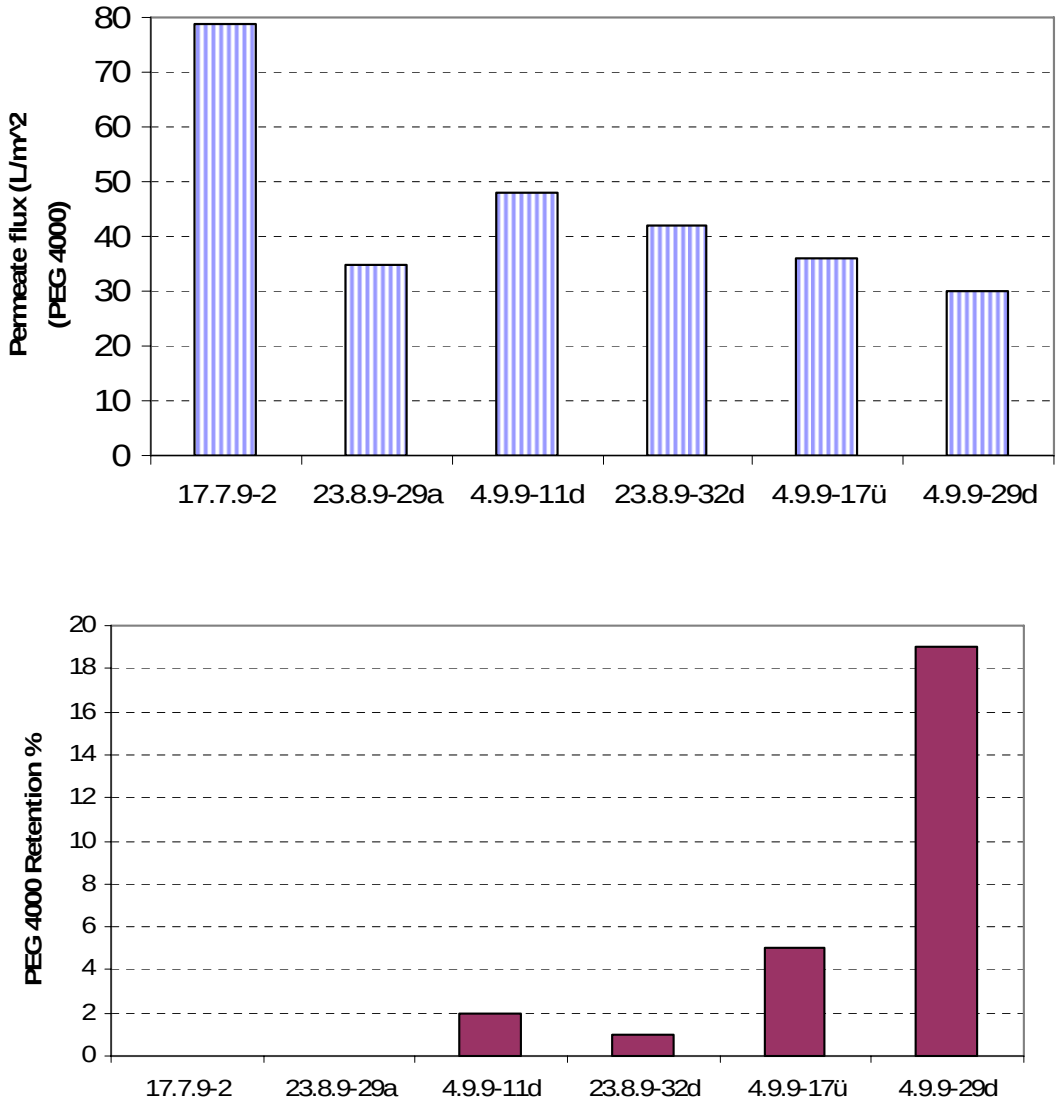

Figure 154. The permeate flux and PEG 4000 retention values for membranes prepared via sols with 25 vol. % EG.

CHAPTER 7

CONCLUSIONS AND RECOMMENDATIONS

Ceramic multi-layer composite membranes were prepared. The support which is mainly responsible from mechanical integrity was prepared with or without pore former (starch) addition. The changes in porosities, CWP values and mechanical stability were determined with respect to changing amounts of pore forming additive and heat treatment temperature. 1300°C was chosen since the mechanical stability was relatively higher. Supports with higher CWP could be prepared via addition of starch (extracted from potato, wheat, corn). The decomposition of these organics form extra pores mimicking the original particle morphology and size. The other important pore former was the air bubbles formed during preparation of ceramic suspensions and these should be eliminated to prevent uncontrolled suction of the coating material into these large pores.

The intermediate layer which enhanced the membrane performance was prepared via a colloidal sol or aged polymeric sol with layer formation capability or a suspension of fine ceramic powders which had a smaller average particle size than the powder used in support preparation. These suspensions of fine alumina or zirconia with varying concentrations were either dip-coated (d-c), wet-coated (w-c) or spin-coated (s-c) on the support and heat treated for mechanical stability. The crack formation on the layer formed could be hindered by using a drying control chemical additive (DCCA) (e.g. PVA (polyvinyl alcohol), EG (ethylene glycol). Dip-coating (d-c) resulted in the formation of more homogeneous layers, but it should be applied more than once for decreasing the number of defects mainly due to the presence of large pores in the close to the support surface.

Intermediate layers were also formed by using colloidal sols which form γ-alumina or zirconia or EG-added and aged polymeric sols forming titania, zirconia or their mixtures. Excess water was used during sol preparation and was peptized to form colloidal sols with average particle sizes of about 50 nm. The alumina sol was more effective than the zirconia sol in the formation of a dip-coated layer. It is formed from

flake like particles which results in easy coating of the surface unlike zirconia sol which has a high thermal shrinkage (~40%) forming gaps in the coating. The resulting layer was γ-alumina since the heat treatment was performed at relatively lower temperatures (500-600° C) and was not as resistant as α-alumina or titania or zirconia. The zirconia intermediate layer should be preferred since it has higher chemical stability / durability at low and high pH values while γ-alumina is susceptible to these harsh conditions. The coating – calcination procedure should be repeated to heal the gaps in the layer formed during heat treatment.

The third (top) layer was prepared by dip-coating polymeric sols forming zirconia and / or titania with average particle sizes of 3-30 nanometers. These sols were dip-coated and calcined on the supports or intermediate layers. The top layer is the surface which mainly determines the retention capacity of the membrane. Its pore size and its physicochemical properties are effective on the membrane performance when the defects in other layers are eliminated. The surface charges of mixed oxides (titania-zirconia), effective in Donnan exclusion, were determined changing with the molar ratios of Ti:Zr and also with the heat treatment conditions. The effect of calcination temperature was significant for pure titania. The zeta potential of titania calcined at 600° C was measured (at initial ph of 8.4) as around -10 mV, although it was measured around -30mV for samples calcined at 400° and 500° C, which may probably be related to anatase (A) to rutile (R) phase transformation. There was a tetragonal (T) to monoclinic (M) phase transformation for zirconia at elevated calcination temperatures which may similarly be effective on the surface charge variation. The *tailor-made* membrane with desired surface characteristics can be prepared by choosing the appropriate Ti:Zr ratio and calcination temperature from the data presented.

The other way of modification of surface charge of the membrane was introducing some elements into the sol (e.g. B, Fe). The isoelectric point (IP) of the zirconia was reduced via addition of both boron and iron (0.2 mol per mol of Zr). The membranes prepared via these sols can have catalytic effects and may present other functionalities for different applications.

The coating capability of the sol can be enhanced by addition of EG (ethylene glycol) increasing sol viscosity and decreasing vapour pressure. The EG containing sol was hardly infiltrated into the porous surface and it dried more slowly that there was less crack formation.

The integrity of the layers formed via dip-coating are susceptible to heat treatment parameters. The temperature increment steps in heating and cooling regime should be selected as small as possible to prevent cracking / peeling of the layers formed (e.g. 0.5° C / minute instead of 3° C / minute).

The filtration experiments showed that there are different routes to prepare membranes with different number of layers, different heat treatment procedures, using different materials and coating procedures. There are a number of parameters to be optimized in preparation of the multi-layer membrane with desired properties. The effects of these numerous parameters were investigated both on formation of microstructure and on filtration performance. The CWP values of the supports increased by increasing pore forming additive, but the mechanical strength decreased. The retention values for sugar, PEG 1000 and PEG 4000 were 10%, 60% and 20% at most with different multilayer membranes. The retention performance of the membranes can be enhanced further by eliminating the pinholes and cracks in the intermediate / top layers. The repetition of coating cycles may be beneficial. The concentration and viscosity of the coated materials (sol, suspension), coating duration, heat treatment regime should be further optimized in order to enhance the membrane performance.

REFERENCES

Agoudjil, N., Benmouhoub, N., Larbot, A., 2005. Synthesis and characterization of inorganic membranes and applications. *Desalination* 184: 65-69.

Ahmad, A. L., Idrus, N. F., Othman, M. R., 2005. Preparation of perovskite alumina ceramic membrane using sol-gel method. *Journal of Membrane Science* 262: 129-137.

Alves, A.M.B., Morao, A., Cardoso, J. P., 2002. Isolation of antibiotics from industrial fermentation broths using membrane technology. *Desalination* 148 181-186, 2002.

Aust, U., Benfer, S., Dietze, M., Rost, A., Tomandl, G., 2006. Development of microporous ceramic membranes in the TiO_2/ZrO_2 system. *Journal of Membrane Science* 281(1-2):463-471.

Benfer, S., Popp, U., Richter, H., Siewert, C., Tomandl, G., 2001. Development and characterization of ceramic nanofiltration membranes. *Separation and Purification Technology*, 22-23: 231-237.

Brinker, C. J., Scherer, G. W., 1990. *Sol-Gel Science: The Physics and Chemistry of Sol-Gel Processing*. Academics Press, Inc.

Cheryan, M., 1998. *Ultrafiltration and Microfiltration Handbook*. Technomic Publishing Company, Inc.

Cot, L., Ayral, A., Durand, J., Guizard, C., Hovnanian, N., Julbe, A., Larbot, A., 2000. Inorganic membranes and solid state science. *Solid State Sciences* 2: 313-324.

Duke, M. C., Mee,S., da Costa, J.C.D, 2007. Performance of porous inorganic membranes in non-osmotic desalination. *Water Research* 41: 3998-4004.

Duran, N., Rosa, M. A., D'Annibale, A., Gianfreda, L., 2002. Applications of laccases and tyrosinases (phenoloxidases) immobilized on different supports: a review. *Enzyme and Microbial Technology*. 31: 907-931.

Durante, D., Casadio, R., Martelli, L., Tasco, G., Portaccio, M., De Luca, P., Bencivenga, U., Rossi, S., Di Martino, S., Grano, V., Diano, N., Mita, D.G., 2004. Isothermal and non-isothermal bioreactors in the detoxification of waste waters polluted by aromatic compounds by means of immobilized laccase from *Rhus vernicifera*. *Journal of Molecular Catalysis B: Enzymatic* 27: 191-206.

Edwards, W., Leukes, W. D., Rose, P.D., Burton, S.G., 1999. Immobilization of polyphenol oxidase on chitosan-coated polysulphone capillary membranes for improved phenolic effluent bioremediation. *Enzyme and Microbial Technology* 25: 769-773.

Ensuncho, L., Alvarez-Cuenca, M., Legge, R. L., 2005. Removal of aqueous phenol using immobilized enzymes in a bench scale and pilot scale three-phase fluidized bed reactor. *Bioprocess Biosystem Engineering* 27: 185-191.

Erdem, İ., 2002. *Preparation of Ultrafiltration / Microfiltration Ceramic Composite Membranes for Biotechnology Applications.* MSc. Thesis, Biotechnology and Bioengineering MSc. Program, İzmir Institute of Technology.

Erdem, İ., Çiftçioğlu, M., Harsa, Ş., 2006. Separation of whey components by using ceramic composite membranes. *Desalination* 189: 87-91.

Finley, J., 2005. Ceramic membranes: a robust filtration alternative. *Filtration + Separation* November: 34-37.

Freger, V., Arnot, T. C., Howell, J. A., 2000. Separation of concentrated organic/inorganic salt mixtures by nanofiltration. *Journal of Membrane Science* 178: 185-193.

Galassi, C., 2006. Processing of porous ceramics: piezoelectric materials. *Journal of the European Ceramic Society* 26(14): 2951-2958.

Gaudon, M., Laberty-Robert, Ch., Ansart, F., Stevens, P., 2006. Thick YSZ films prepared via a modified sol-gel route: Thickness control (8-80 μm). *Journal of European Ceramic Society* 26 (15): 3153-3160.

Gazagnes, L., Cerneaux, S., Persin, M., Prouzet, E., Larbot, A., 2007. Desalination of sodium chloride solutions and seawater with hydrophobic ceramic membranes. *Desalination* 217: 260-266.

Gregorova, E., Pabst, W., 2007. Porosity and pore size control in starch consolidation casting of oxide ceramics-Achievements and problems. *Journal of the European Ceramic Society* 27: 669-672.

Guendez, G., Kallithraka, S., Makris, D. P., Kefalas, P., 2005. Determination of low molecular weight polyphenolic constituents in grape seed extracts-correlation with antiradical activity. *Food Chemistry* 89: 1-9.

Gustafsson, J., Mikkola, P., Jokinen, M., Rosenholm, J. B., 2000. The influence of pH and NaCl on the zeta potential and rheology of anatase dispersions. *Colloids and Surfaces A: Physicochemical and Engineering Aspects* 175: 349-359.

Hao, Y., Li, J., Yang, X., Wang, Lu, L., 2004. Preparation of ZrO_2-Al_2O_3 composite membranes by sol-gel process and their characterization. *Material Science and Engineering A*, 367: 243-267.

Joglekar, H.G., Rahman, I., Babu, S., Kulkarni, B. D., Joshi, A., 2006. Comparative assessment of downstream processing options for lactic acid. *Separation and Purification Technology* 52: 1-17.

Kurniawati, S., Nicell, J. A., 2005. Kinetic model of laccase-catalyzed oxidation of aqueous phenol. *Biotechnology and Bioengineering* 91 (1): 114-123.

Labarbe, B., Cheynier, V., Brossaud, F., Souquet, J.-M., Moutounet, M., 1999. Quantitative Fractionation of Grape Proanthocyanidins According to Their Degree of Polymerization. *Journal of Agricultural Food Chemistry* 47: 2719-2723.

Lante, A., Crapisi, A., Krastanov, A., Spettoli, A., 2000. Biodegradation of phenols by laccase immobilised in a membrane reactor. *Process Biochemistry* 36: 51-58.

Magnan, E., Catarino, I., Paolucci-Jeanjean, D., Preziosi-Belloy, L., Belleville, M.P., 2004. Immobilization of lipase on a ceramic membrane: activity and stability. *Journal of Membrane Science* 241: 161-166.

Malvern Co. (UK) 2009. The measurement of zeta potential by using an auto-titrator: effect of conductivity.
http://www.malvern.com/malvern/kbase.nsf/allbyno/KB000054/$file/Measurement_of_zeta_potential_using_an_Autotitrator_-_Effect_of_conductivity_MRK379-01-Low_Res.pdf (accessed October 13, 2009)

Milcent, S. and Carrere, H., 2001. Clarification of lactic acid fermentation broths. *Separation and Purification Technology* 22-23: 393-401.

Narong, P. and James, A.E., 2006. Sodium chloride rejection by a UF ceramic membrane in relation to its surface electrical properties. *Separation and Purification Technology* 49: 122-129.

Osmonics, 2009. Filtration and separation spectrum. http://www.osmolabstore.com /documents/filtspec-s.pdf (accessed October 13, 2009).

Pal, A.and Sharma, S., 1998. Excess molar volumes and viscosities of 1-propanol + ethylene glycol, + ethylene glycol monomethyl, + ethylene glycol dimethyl, + diethylene glycol dimethyl, + triethylene glycol dimethyl, + diethylene glycol diethyl, and + diethylene glycol dibutyl ethers at 288.15 K. *Journal of Chemical Engineering Data* 43: 532-536.

Pierre, A. C., 1998. *Introduction to Sol-Gel Processing*. Kluwer Academic Publishers.

Rubia, T. de la, Lucas, M., Martinez,J., 2008. Controversial role of fungal laccases in decreasing the antibacterial effect of olive mill waste-water. *Bioresource Technology* 99: 1018-1025.

Sakka, Y. Tang, F., Fudouzi, H., Uchikoshi, T., 2005. Fabrication of porous ceramics with controlled pore size by colloidal processing. *Science and Technology of Advanced Materials* 6 (8): 915-92.

Santamaria, G., Salazar, B., Beltran, S., Cabezas, J. L., 2002. Membrane sequences for fractionation of polyphenolic extracts from defatted milled grape seeds. *Desalination* 148: 103-109.

Sarrade, S.J., Rios, G.M., Carles, M., 1998. Supercritical CO_2 extraction coupled with nanofiltration separation Application to natural products. *Separation and Purification Technology* 14: 19-25.

Skluzacek, J. M., Teodor, M. I., Anderson, M. A., 2006. An iron-modified silica nanofiltration membrane: Effect of solution composition on salt rejection. *Microporous and Mesoporous Materials* 94: 288-294.

Tessier, L., Bouchard, P., Rahni, M., 2005. Separation and purification of benzylpenicillin produced by fermentation using coupled ultrafiltration and nanofiltration technologies. *Journal of Biotechnology* 116: 79-89.

Tsuru, T., 2001. Inorganic porous membranes for liquid phase separations. *Separation and Purification Technology* 30 (2): 191-220.

Vacassy, R., Guizard, C., Palmeri, J., Cot, L., 1998. Influence of the interface on the filtration performance of nanostructured zirconia ceramic, *Nano Structured Materials* 10(1): 77-88.

Van Gestel, T., Vandecasteele, C., Buekenhoudt, A., Dotremont, C., Luyten, J., Leysen R., Van der Bruggen, B., Maes, G., 2002. Alumina and titania multilayer membranes for nanofiltration: preparation, characterization and chemical stability. *Journal of Membrane Science* 207: 73-89.

Van Gestel, T., Kruidhof, H., Blank, D. H. A., Bouwmeester, H. J: M., 2006. ZrO_2 and TiO_2 membranes for nanofiltration and pervaporation *Journal of Membrane Science* 284(1-2): 128-136.

Xia, C., Zha, S., Yang, W., Peng, R., Peng, D., Meng, G., 2000. Preparation of yittria stabilized zirconia membranes on porous substrates by a dip-coating process. *Solid State Ionics* 133: 287-294.

Weber, R., Chmiel, H., Mavrov, V., 2003. Characteristics and application of new ceramic nanofiltration membranes. *Desalination* 157: 113-125.

Winkler, B. H. and Baltus, R. U., 2003. Modification of surface characteristics of anodic alumina membranes using sol-gel precursor chemistry. *Journal of Membrane Science* 226: 75-84.

VITA

İLKER ERDEM

İlker Erdem was born in Kayseri in 1977. He took his BSc. degree in Food Engineering at Ege University in 1999. He got his MSc. degree from Biotechnology and Bioengineering Program at İzmir Institute of Technology with the dissertation entitled "Preparation of Ultrafiltration / Microfiltration Ceramic Composite Membranes for Biotechnological Applications" in 2002. He wrote two articles cited by Science Citation Index:

- Erdem, I., Ciftcioglu, M., Harsa, S., "Separation of Whey Components by Using Ceramic Composite Membranes", Desalination, Vol.189, 87-91, 2006.
- Erdem, I., Ciftcioglu, M., Harsa, S., "Preparation of Ceramic Composite Membranes for Protein Separation", Key Engineering Materials, Euro Ceramics VIII, 2251-2254, 2004.

He has worked as a research assistant in İzmir Institute of Technology (1999-2009) and he has been a member of Chamber of Food Engineers (Union of Chambers of Turkish Engineers and Architects) since 1999. He attended a research project in European Membrane Institute (EMI) (University of Montpellier II, Montpellier, France) as an Erasmus Student Exchange Program scholar during fall semester of 2007-2008.